Exploiting bacterial transporters for the design of novel antibacterial agents

Christopher Thomas Carrick

Ph D

University of York
Chemistry

March 2014

Abstract

The alarming increase in the occurrence of antimicrobial resistance has led to a situation whereby some strains are untreatable by known antimicrobials. The Trojan horse strategy is one methodology with the potential to overcome the rising tide of resistance.

Work was undertaken to synthesise two different Trojan horses. One based on an analogue of the *Bacillus* siderophore petrobactin, the other a novel compound prepared using the Ugi four component condensation. Both contained a fluoroquinolone antimicrobial; ciprofloxacin. Additionally a series of bis-catecholate ligands were prepared for use as iron chelating antimicrobial agents.

The Trojan horse based on the Ugi four component condensation was screened against wild type *E. coli* and was found to have antibacterial activity, but at a lower level than the parent drug ciprofloxacin. The mechanism of action was determined by performing a DNA gyrase assay, which confirmed the conjugate was inhibiting *E. coli* DNA gyrase activity.

A set of three glycosylated fluoroquinolones was screened, to assess the extent to which they were actively transported. Experiments were performed using glucose and galactose as carbon sources, with *E. coli* strains deficient in galactose transport. Further experiments with outer membrane porins (OMPs) mutants were also performed. The results suggested that the conjugates were not actively transported, but were gaining access to the cells via the OMPs. Studies were undertaken on the bis-catecholate ligands to assess their suitability as potential antimicrobial agents. However, stability studies showed that one set of ligands was highly unstable due to hydrolysis and oxidation, and therefore not viable for use. The asymmetric ligand showed promising activity *in vitro* however electrochemical studies indicated it was susceptible to oxidation. Consequently, the active species could not be reliably determined. Further study is required to establish its identity.

Table of contents

Figures

Schemes

Tables

Acknowledgements

I would like to thank a number of people for their help in the completion of this work. First and foremost I wish to thank my supervisors; Dr Anne Routledge, Dr Anne-Kathrin Duhme-Klair, and Dr Gavin Thomas for giving me the opportunity to work with them, for their helpful suggestions and ideas, and for their patience and support when things weren't going to plan. I would also like to thank my IPM Dr Victor Chechik for his support and advice throughout my time here. In addition to this I wish to thank the EPSRC for funding this research.

I wish to thank all the academics and technicians within the department for their assistance. In particular I'd like to thank Ms. Heather Fish for her assistance with NMR, and for running the variable temperature NMR experiments, Dr Karl Heaton and Helen Robinson for mass spectrometry experiments, Dr Graeme McAllister for CHN analysis and for training me in the safe use of the hazard lab, Rob Smith for his help with HPLC, and Dr Alison Parkin for her assistance with my electrochemical and spectroelectrochemical experiments I would also like to thank Mrs Judith Hawkhead for her assistance with my early screening work in the biology department. Additionally, special thanks to Dr Ryan Mewis for assisting me in the formatting of my thesis master document, it made a world of difference.

I would also like to thank my colleagues in the lab both past and present, in particular Dr Sian Hudson and Dr Stephen Milner for their assistance in getting me started and helping me to settle in. Also the members of the Routledge, Duhme-Klair and Thomas research groups for helping make life in the lab enjoyable: Dan Raines, Thomas Sanderson, Abeda Jamadar, Mariah Leigh, and Ellis Wilde. I'd also like to thank the other researchers on E block ground floor for providing a pleasant working environment in my final year.

Finally I would like to thank my Friends from the university concert band for providing me with some amazing memories and some relief from the pressures of the lab; especially the members of “Team Four”.

My parents and sisters for their continued support and encouragement, and last but not least my partner Cherise Rostron for her continued support, love and seemingly unwavering belief in me

Dedication

I would like to dedicate this thesis to the memory of my partner's younger brother Ryan Joseph Rostron, who tragically lost his life on the 12th May 2013. Rest in peace Ryan, you are deeply missed.

Declaration

I declare that this work is entirely my own except where specifically acknowledged. The citation for the jointly authored paper upon which Chapter 5 is based is given below:

Variable temperature ^{1}H NMR was performed by Ms Heather Fish

LC-MS analysis was performed by Dr Karl Heaton.

S. J. Milner, C. T. Carrick, K. G. Kerr, A. M. Snelling, G. H. Thomas, A.-K. Duhme-Klair and A. Routledge, *ChemBioChem* **2014**, *15*, 466-471.

1. Introduction

1.1. Antibiotic resistance

1.1.1. Overview

The increasing occurrence of antibiotic resistance was described in 2013 as a very real threat, which could potentially make otherwise routine medical procedures high risk operations[1]. It is conceivable that unless the situation improves rapidly there will come a point where common infections cannot be prevented or effectively treated[2]. While cases of the well known pathogen methicillin resistant *Staphylococcus aureus* (*S. aureus*) (MRSA), a bacterial strain first reported in the 1960s[3], have reduced in the UK and Europe in the past decade[4], MRSA is still endemic in a number of places such as Romania, Malta Argentina where more than 50% of clinical *S. aureus* isolates are methicillin resistant[5]. Additionally, *S. aureus* strains have been found that display resistance to a broad spectrum of antimicrobial agents in addition to methicillin. Clinically resistant bacterial strains are known for the majority of antimicrobial agents currently in clinical use[6]. Furthermore, in 2011 a bacterial strain was isolated in India which carried a new gene for carbapenem resistance[7-8], a class of antimicrobials that was thought to be reliable in treating most antimicrobial resistant infections. While resistance is most commonly observed where there is a high level of antimicrobial use, particularly where antimicrobials are self-prescribed and administered. Failure to complete a course of antibiotics presents the opportunity for bacteria to develop resistance and subsequently survive and reproduce. The overuse of antimicrobials in both human and veterinary medicine has also contributed to the rise of resistance[9]. There is a comprehensive online database which extensively details antibiotic resistance including data on resistant strains, mechanisms of the resistance and the genes encoding the resistance[10].

The evolution of antimicrobial resistance at the cellular level has occurred largely due to two key factors. The first is intrinsic resistance, micro-organisms which produce antimicrobial agents also carry a corresponding resistance gene, and this gives them a selective advantage over competing microorganisms. The second factor is acquired resistance via horizontal gene transfer. This process is the exchange of DNA between a bacteria and its immediate extracellular environment. Horizontal transfer occurs through several mechanisms: transduction, where new genetic material is delivered into the cell from a virus; transformation, whereby a bacterium takes in genetic material from its extracellular environment; and conjugation whereby transfer of genetic material is initiated by cellular contact[6]. The described mechanisms allow acquired resistance to evolve and spread. These phenomena, coupled with the overuse of antibiotics have resulted in an increase in the number and variety of multi-drug resistant bacterial strains[6]. The evolution of acquired resistance has also occurred due to accumulation of mutations in bacteria[9]. Additionally it has been postulated by Zhang *et al.* that humans are born with antimicrobial resistant bacteria present within their gut flora[11]. Their experiments analysed samples from infants and found that there were high populations of microbes resistant to several antimicrobials present. This was observed with subjects just 1 week of age, even without exposure to antimicrobial agents. They suggest that both environmental and maternal microbes have a significant impact on the development of antibiotic resistance in the gut flora.

The manner of evolution can also vary; Toprak *et al.* studied *Escherichia coli*, culturing the bacterium in real time, using dynamically regulated drug concentrations[12]. Using chloramphenicol, doxycycline and trimethoprim they observed key mutations in target systems for all three antimicrobials. Curiously, they also observed that while the bacteria displayed a “smooth” evolution of resistance to chloramphenicol and doxycycline, which was gradually increasing due to combined mutations, in the case of trimethoprim, the bacteria appeared to evolve in a stepwise fashion, with parallel

populations displaying similar mutations acquired in a similar order, rather than randomly[12]. This suggests that the evolution of antimicrobial resistance under selection pressure depends on the target of the antimicrobial used. In this case the protein synthesis inhibitors appeared to induce gradual random evolution within several genes, and the dehydrofolate reductase inhibitor an ordered stepwise evolution, within a specific gene.

1.2. Mechanisms of resistance

1.2.1. Overview

In spite of the wide variety of genes which encode antimicrobial resistance, the range of basic mechanisms of resistance is surprisingly limited[6]. There are four primary mechanisms of resistance that are commonly observed (**Figure 1.1**). These mechanisms include reduced uptake, increased efflux, target alteration and drug alteration/deactivation. Mutations which reduce the uptake of drug molecules are the key focus of this project, although gyrase mutations are an alternative mechanism of resistance, which will be discussed later (**Section1.4.3.**)

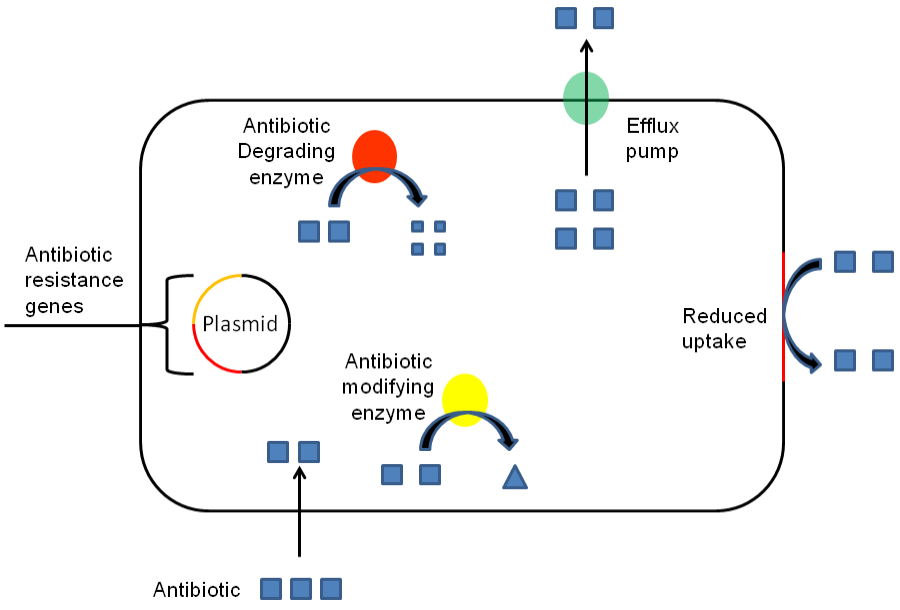

Figure 1.1: Schematic overview of antimicrobial resistance mechanisms (**section 1.2.2**) based on Levy and Marshall

1.2.2. Deactivation of antimicrobial compounds

1.2.2.1. Deactivation of the antimicrobial moiety.

Drug deactivation is a comprehensively studied form of resistance, which involves either degrading or altering an antimicrobial to compromise its antimicrobial activity[13]. A key example of drug degradation is observed in β-lactam resistance[14]. Antimicrobials such as penicillin **1-1** are rendered inactive by β-lactamases enzymatically cleaving open the β-lactam ring (**Scheme 1.1**). β-Lactam antibiotics function by binding to penicillin binding proteins (PBPs), blocking the active site and consequently inhibiting peptidoglycan synthesis. The inhibition of this process results in disruption of the bacterial cell wall integrity. The β-lactam ring is critical to the function of the antimicrobial. Without the ring structure the antimicrobials are unable to bind to the PBPs and consequently no longer exert a bactericidal effect[15].

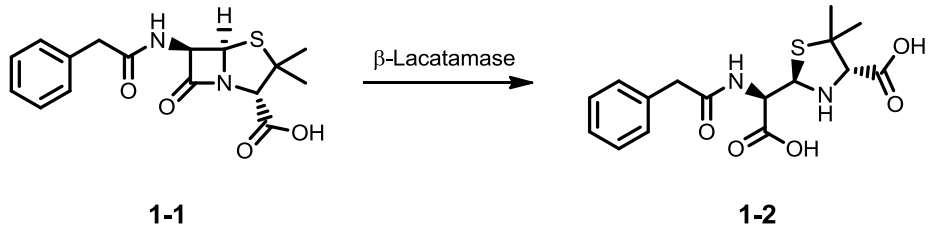

1-1 **1-2**

Scheme 1.1: Cleavage of the β-lactam ring of penicillin

β-Lactamase resistance is extremely wide-spread, to the extent that there are now bacterial strains of *Enterobactericeae* which are resistant to all currently available treatments for Gram-negative bacteria[8]. The situation has been exacerbated by the recent emergence of carbapenemases. Carbapenems were able to resist rapid hydrolysis by β-lactamases due to their *trans* stereochemistry across the lactam ring and containing an α-hydroxy ethyl group instead of a β-amide at carbon 6 (**Figure 1.2**)[13]. However, carbapenemase proteins have been identified with specific adaptations in their active site including a disulfide bridge and additional threonine and histidine residues. *Klebsiella pneumoniae* (*K. pneumoniae*)

carbapenemases (KBCs) are a serious problem as the genes conferring resistance are found on mobile genetic elements, allowing the spread of resistance to other bacteria[13].

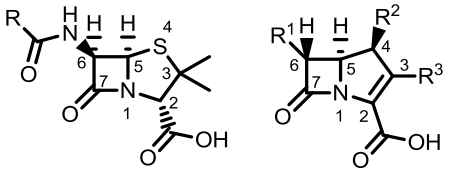

Figure 1.2: Core structure of penicillins (left) and carbapenems (right)

Antimicrobials can also be deactivated by modification of the antimicrobial. Several examples have been observed including the modification of aminoglycosides and lincosamides by phosphorylation and ADP ribosylation of rifampin[13]. The number of different mechanisms of modifying antimicrobials highlights the variety found within the bacterial resistome.

1.2.2.2. Reduction in intracellular drug concentration

Bacteria utilise two different mechanisms to reduce the intracellular concentration of antimicrobial compounds. The first of these is a reduction in membrane permeability. Antimicrobials often gain access through the outer cell membrane via porins, trimeric β-barrel proteins. By down-regulating the expression of these proteins, bacteria can reduce the amount of antimicrobial that enters the cell[16]. A variation of this is the formation of biofilms. Biofilms are aggregates of bacterial cells that form on surfaces in response to environmental stresses[17]. As most antimicrobials are designed to attack planktonic cells, they are ineffective against biofilms as they are unable to penetrate beyond the first layer of cells. In addition, as biofilms are communities of cells, there may be several different resistance mechanisms at work within a biofilm[18]. Consequently biofilms are persistent, and a common feature in chronic infections.

The second method that bacteria have evolved to reduce intracellular drug concentration is the over-expression of active efflux pumps. There are several super-families of efflux pumps including ATP binding cassette (ABC), resistance nodulation-cell division (RND) and multidrug and toxic compound extrusion (MATE)[19]. There are examples of both specific and non-specific antimicrobial efflux pumps. The MacAB-TolC efflux pump specifically transports macrolide antibiotics, whereas ArcAB-TolC transports a broad spectrum of antimicrobials including chloramphenicol and tetracycline[20].

1.2.2.3. Modification and protection of the antimicrobial target

An alternative form of resistance in bacteria is to alter or protect the intracellular target of an antimicrobial. This removes the need to reduce the active concentration or to break down an antimicrobial. Resistance has been observed to tetracyclines through the production of ribosomal protecting proteins[21]. Proteins have also been indentified in some *P. aeruginosa* strains that incorporate an additional methyl group into the 30S subunit of bacterial ribosomes, resulting in resistance to aminoglycosides. The proteins show a high degree of similarity to 16S rRNA methyl transferase proteins found in aminoglycoside producing acetomytes[22]. Occurrences like this are examples of the transfer of intrinsic resistance to a strain which would normally be susceptible to an antimicrobial. An additional mode of target protection is to over-express the antimicrobial target, or a protein mimic of the target. The consequence of over-expression is the antimicrobial being sequestered from the intracellular medium by the excess target, leaving additional target molecules uninhibited and able to carry out their function[20].

1.3. Counteracting antimicrobial resistance

1.3.1.1. Developing novel antimicrobial compounds

The most obvious strategy for counteracting the growing number of antimicrobial resistant strains is to identify or develop novel antimicrobial compounds. A current challenge in this is a lack of funding in antimicrobial

research. A recent report found that; since 1997, from £2.6 billion of investment in infectious disease research in the UK, only 3.9% (£102 million) was spent on antimicrobial research[23]. In addition, there is a lack of interest from large pharmaceutical companies due to the low financial returns on offer in the antimicrobial market. Considering the rate at which resistance is increasing, this seems a worrying situation. In the last few decades only two new classes of antimicrobials have been developed. The first is a class of protein synthesis inhibitors which target bacterial ribosomes, the oxazolidinones (**Figure 1.3**)[24-26]. The second class is lipopeptides which disrupt bacterial membranes in Gram-positive bacteria

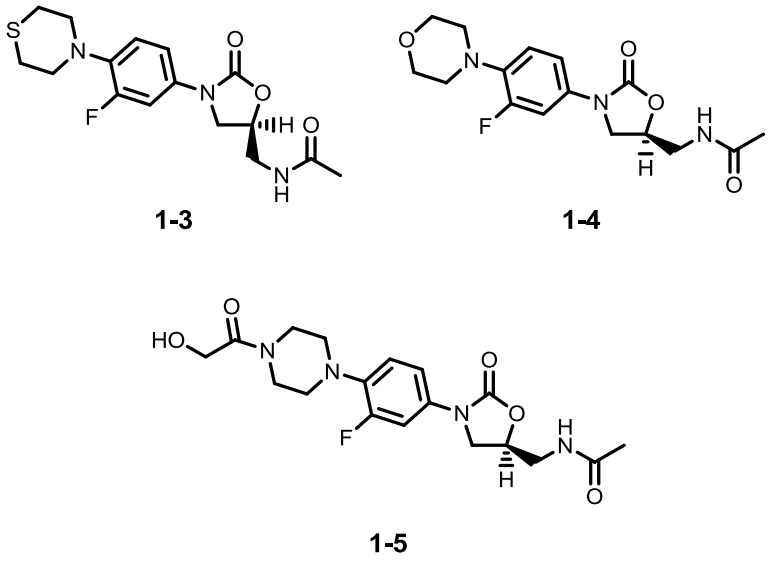

Figure 1.3: Structures of oxazolidinones synthesised by Zurenko *et al.*

In 2000, Tally and DeBruin reported the development of the lipopeptide Daptomycin **1-6** (**Figure 1.4**), New examples of lipopeptides have recently been found in both *Citrobacter* and *Enterobacter* species[27].

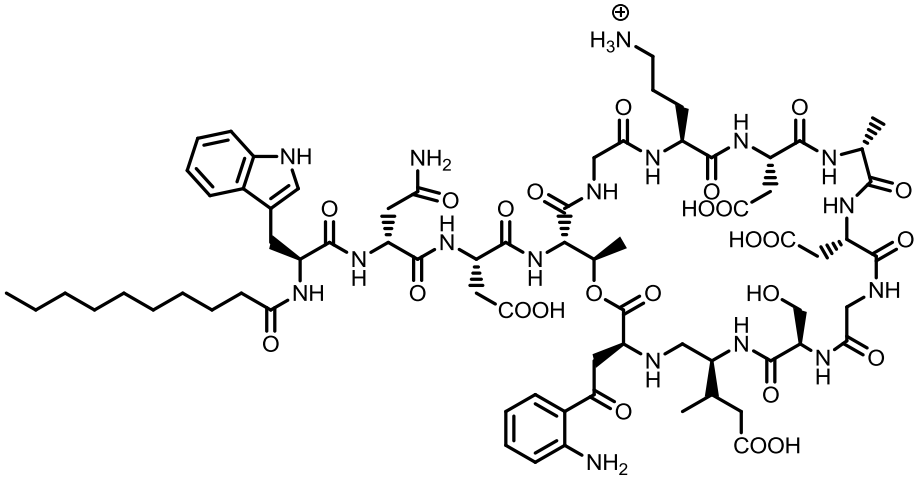

1-6

Figure 1.4: Structure of the lipopeptide antimicrobial Daptomycin

A more recent attempt at developing novel antimicrobial agents has been made by Wright *et al*., by analysing the genomes of bacterial species to identify strains which carry genes for inherent bacterial resistance. The logic behind this is that bacteria which naturally carry resistance genes are likely to be producers of antimicrobial compounds. Using this approach they discovered a glycopeptide antimicrobial, pekiskomycin **1-7**, which had a novel peptide scaffold not previously observed in antimicrobials (**Figure 1.5**)[28].

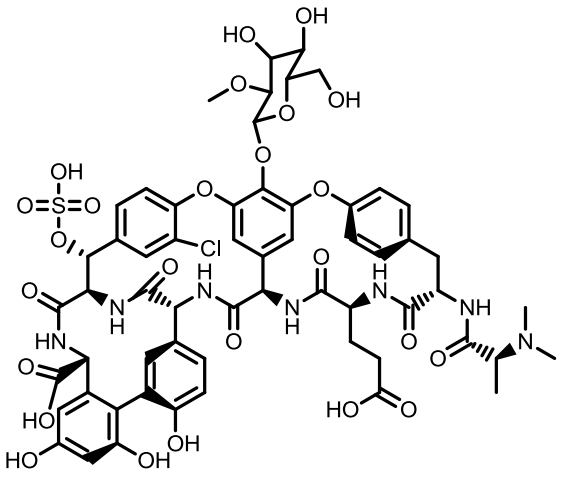

1-7

Figure 1.5: Structure of the glycopeptide antimicrobial pekiskomycin

While identifying and developing novel pharmacophores is the ideal method of counteracting resistance, in 2011 there were 40 different drugs in clinical trials[29], it is a time consuming and highly costly process. The cost of developing an antimicrobial compound from initial lead to a marketable product is over £400 million. When coupled with the length of time required, it is not perceived as a profitable process for pharmaceutical companies. Consequently there has been a significant decline in the amount of money invested in antimicrobial research. However, as the number of drugs in clinical trials indicates, work is still being undertaken, including on the synthetic fluoroquinolone drug class.

1.3.1.2. Alternative approaches to combat bacterial resistance

In situations where the mechanism of resistance to a specific antimicrobial is known, it is possible to utilise a secondary agent to counteract resistance. In the case of β-lactams, where the antibiotic is degraded by a β-lactamase enzyme, the solution is to co-administer a β-lactamase inhibitor, such as tazobactam **1-8** (**Figure 1.6**) in addition to the antimicrobial[13]. Recently, research has been undertaken to achieve a similar result with aminoglycoside resistant bacteria. Aminoglycosides target

bacterial ribosomes, interfering with bacterial replication. They are deactivated by bacterial kinases, which phosphorylate the antimicrobial species, rendering it unable to bind its target[30]. Wright *et al*. have used structure-guided optimisation to develop new inhibitors of bacterial protein kinases, in an effort to counteract aminoglycoside resistance. They successfully managed to synthesise compounds based on a pyrazolopyrimidine scaffold **1-9** which restored antimicrobial susceptibility to an aminoglycoside resistant *E. coli* strain [31].

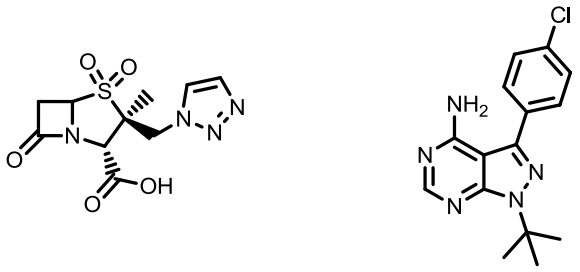

1-8 **1-9**

Figure 1.6: Tazobactam **1-8**, a β-lactamase inhibitor and PP2 **1-9**, an aminoglycoside phosphotransferase inhibitor

A simpler version of combination therapy is to utilise two different classes of antimicrobial simultaneously. Combination therapy is already used to treat MRSA and vancomycin resistant *S. aureus,* using a combination of two streptogramins: dalfopristin **1-10** and quinupristin **1-11.** (**Figure 1.7**). However, this method is flawed as it is costly, and doesn't tackle the problem of bacteria developing resistance[14]. Buckling *et al.* have demonstrated that using a variation of combination therapy, sequential therapy, can be more effective. By administering antimicrobials in a specific order, the development of multidrug resistant strains can be attenuated[32]. If acquiring resistance to the first antimicrobial administered comes at a high cost to the bacteria, the chance of multidrug resistance occurring is minimised.

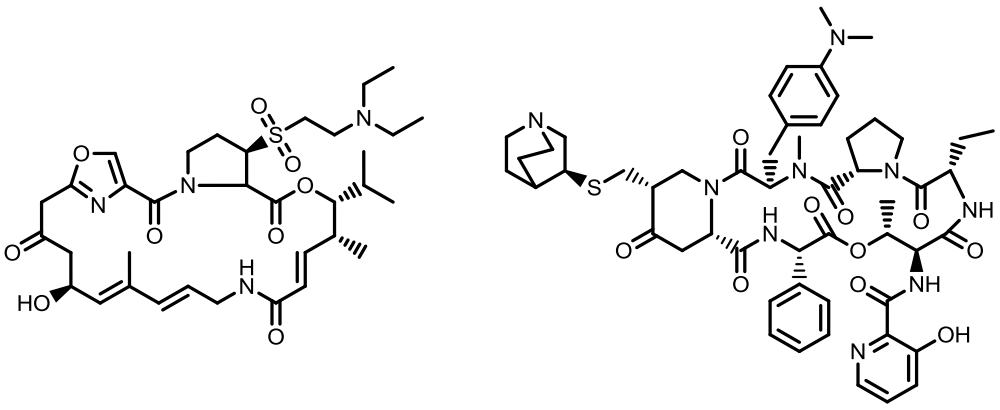

1-10 **1-11**

Figure 1.7: Structures of streptogramin drugs dalfopristin **1-10** and quinupristin **1-11**

Hybrid antimicrobials have also been developed. Two antimicrobials where resistance has been observed are combined in order to overcome resistance. Gordeev *et al.* synthesised oxazolidinone-quinolone hybrids (**Figure 1.8**). The compounds showed activity against both ciprofloxacin **1-18** and linezolid **1-3** resistant bacterial strains[33].

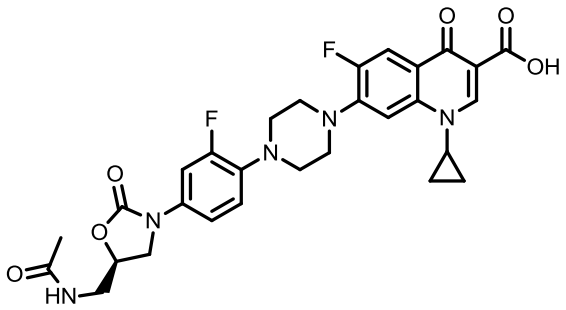

1-12

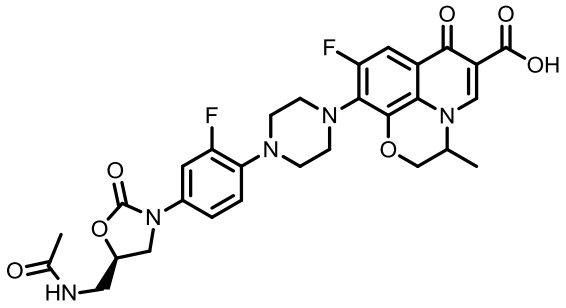

1-13

Figure 1.8: Structures of two quinolone-oxazolidinone hybrids using linezolid **1-3** as the oxazolidinone component and ciprofloxacin, conjugate **1-12**, and levofloxacin, conjugate **1-13**, as the fluoroquinolone components.

While combination therapy and hybrid antimicrobials have proven to be effective, they are only a short term solution as strains eventually evolve resistance to both drugs contained within a hybrid/combination. What is required is the development of novel, preferably synthetic antimicrobials, where innate resistance does not exist, or is at least absent from the bacterial resistome of pathogenic bacteria. The focus of the research in this thesis is on one such class of antimicrobials: the fluoroquinolones.

1.4. Fluoroquinolones

1.4.1. Introduction to fluoroquinolones

The fluoroquinolones are a synthetic class of antimicrobials that have gone through several generations since they were first identified[10]. The first of the quinolone drugs, nalidixic acid **1-16**, was discovered in 1962, when it

was isolated as a by-product of chloroquine **1-14** synthesis (**Error! eference source not found.**)[34].

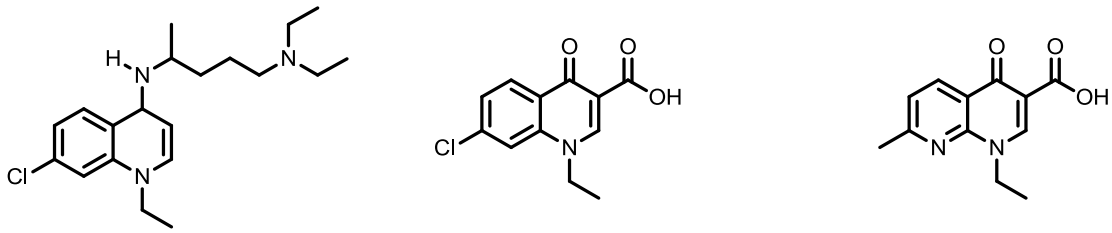

1-14 **1-15** **1-16**

Figure 1.9: Structures of chloroquine 1-14, the antibacterial by-product **1-15**, and the first quinolone nalidixic acid **1-16**.

Lesher observed that a by-product **1-15** displayed antimicrobial activity against a series of Gram-negative pathogens including *Escherichia coli* and *Staphylococcus aureus,* but was largely ineffective against Gram-positive strains[34]. Initial attempts at broadening the spectrum of activity were largely unsuccessful, with nalidixic acid **1-16** having limited applications beyond treating urinary tract infections[35]. The next significant breakthrough in the development of the fluoroquinolones came in 1980, when Koga *et al.* reported a drug with an enhanced spectrum of Gram-negative activity, and increased Gram-positive activity[36].

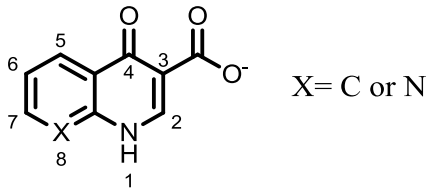

Figure 1.10: The basic pharmacophore of the quinolones with substitution positions labelled

This drug featured a fluorine atom at position 6 and a piperazinyl ring at position 7 (**Figure 1.11**), whilst maintaining the β-diketone system observed in nalidixic acid **1-16**, and became known as norfloxacin **1-17**. While norfloxacin **1-17** was an effective antimicrobial, it had poor bioavailability,

meaning higher doses were required for a clinically relevant bactericidal effect[35]. In an attempt to improve the efficacy of the fluoroquinolone pharmacophore, studies have analysed the effect of modifications to various points on the central skeleton of the molecule (**Figure 1.10**). A study by Koga *et al.* in 1980 found that fluorinating the quinolone pharmacophore at position 6 appeared to reduce the rate at which resistance was acquired, and that a piperazinyl moiety at position 7 produced an increase in activity[36].

A study by Murphy *et al.* built on this research and produced a series of nitrile containing fluoroquinolones. They found that adding a nitrile to the piperazinyl ring on position 7 enhanced activity. They also found that modifications at 5, 6 and 8 did not compromise activity[37]. Modifications at positions 3 and 4 are not possible, as these disrupt the planar β-diketone system, which is critical to quinolone function. Modifications at position 2 would also be unfavourable, as any additional steric bulk could have a detrimental effect on binding to the target protein[35]. Subsequently, in 1983, a new fluoroquinolone was produced: Bay09867[38]. Bay09867 retained the piperazinyl ring and fluorine atom present in norfloxacin **1-17**, but exhibited a cyclopropyl ring at **N**1. This compound was ciprofloxacin **1-18** , and is still in clinical use today[35]. More recent developments include antimicrobials such as levofloxacin **1-19** and moxifloxacin **1-20** (**Figure 1.11**)[39], with variations in specific positions around the pharmacophore. These variations effect key antimicrobial properties including bioavailability, spectrum of activity and half life.

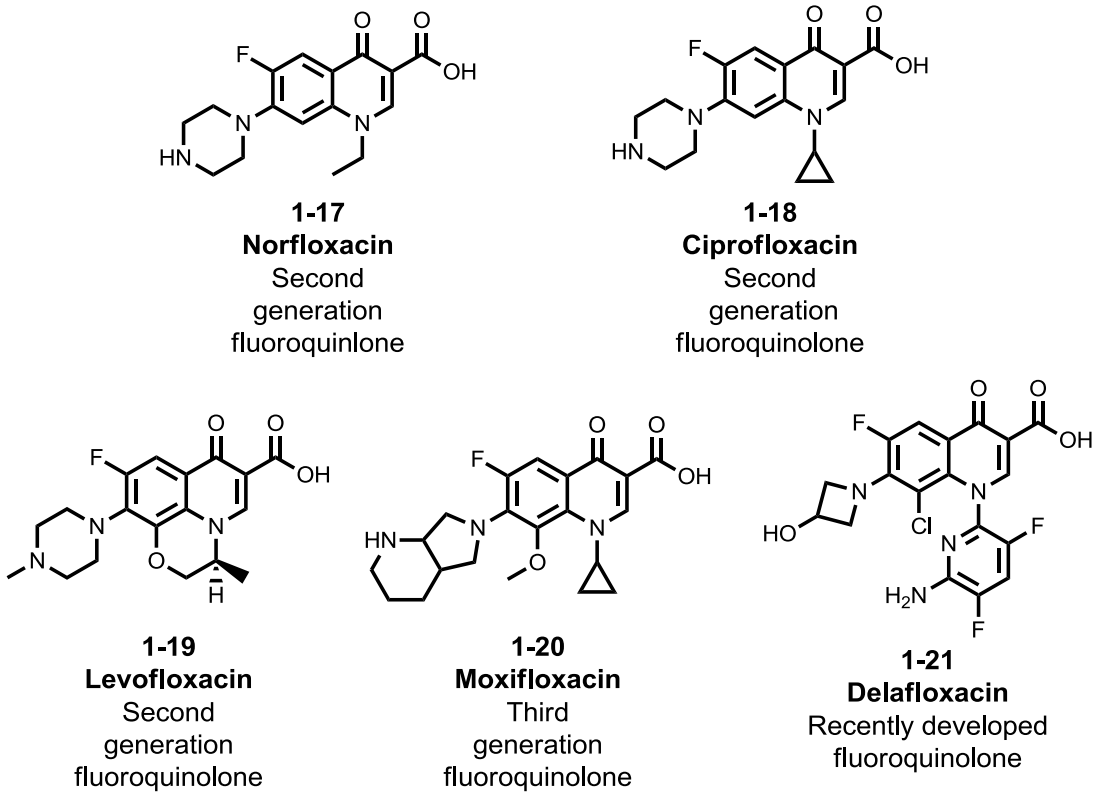

Figure 1.11: Structures of second and third generation fluoroquinolones and the recently developed fluoroquinolone delafloxacin **1-21**

In 2006 Barnes *et al.* reported the synthesis of a new fluoroquinolone antimicrobial, ABT-492[40]. The structure was unusual for a fluoroquinolone due to chlorination at **C**8 and a substituted pyridine ring at **N**1 (**Figure 1.10**, **Figure 1.11**). A key feature is that delafloxacin **1-21** is anionic, allowing it to exert an antimicrobial effect at acidic pHs which zwitterionic fluoroquinolones are incapable of[41]. Lemair *et al.* examined the properties of delafloxacin under acidic conditions, using moxifloxacin **1-20** as a control. Their findings suggested that the uptake of delafloxacin **1-21** increased significantly under acidic conditions[41]. Furthermore Lemair postulated that the nature of delafloxacin **1-21** would allow it to diffuse more readily than a zwitterionic fluoroquinolone under acidic conditions, but once inside the cell the increase in pH would de-protonate the drug, reducing the likelihood of passive diffusion back into the extracellular environment[41]. The drug also displayed

good levels of activity against fluoroquinolone resistant strains and at the time of writing has been granted status as a qualified infectious disease product (QIDP) by the food and drug administration (FDA).

1.4.2. Mechanism of action

The fluoroquinolone drugs function by targeting the DNA replication pathway in bacteria, specifically the two stabilising proteins DNA gyrase (in Gram-negative strains) and topoisomerase IV (in Gram-positive strains)[35, 42]. These proteins are both type II topoisomerases, so called because they introduce temporary strand breaks in double stranded DNA as opposed to type I topoisomerases which make temporary strand breaks in single stranded DNA. DNA gyrase catalytically introduces negative supercoils in bacterial DNA to relieve torsional strain during DNA replication[43]. Topoisomerase IV is a homologue of DNA gyrase, both are tetrameric proteins, which use double stranded passage as a mode of action[42]. During the process two strands cross over, and as the top strand moves along the amount of strain increases. The topoisomerase catalyses a double strand break in the lower strand, allowing the top strand to pass through the gap made. The break is then ligated to repair the broken strand, resulting in a stable supercoil[35].

The mode of binding of the fluoroquinolones is via a ternary complex. The earliest theory was of a “Viking helmet” conformation postulated by Mitscher *et al.* Their hypothesis focused on a cooperative binding model involving four quinolone molecules[44] (**Figure 1.12**). A more recent study by Laponogov *et al*. agrees that the model is cooperative. However, they successfully co-crystallised DNA gyrase with moxifloxacin **1-20** and demonstrated that the complex only involves two fluoroquinolone molecules[45]. There is also evidence that magnesium ions play a key role in stabilising the ternary complex[46]. Each fluoroquinolone molecule binds to one strand of DNA, in a sequence dependent manner. The presence of magnesium ions encourages tighter binding[47]. The binding of

fluoroquinolones to the DNA-gyrase complex blocks the ligation of the double strand break. This stabilises the DNA in a supercoiled state. Consequently the release of DNA from the complex is blocked, triggering the apoptosis pathway and resulting in cell death[35].

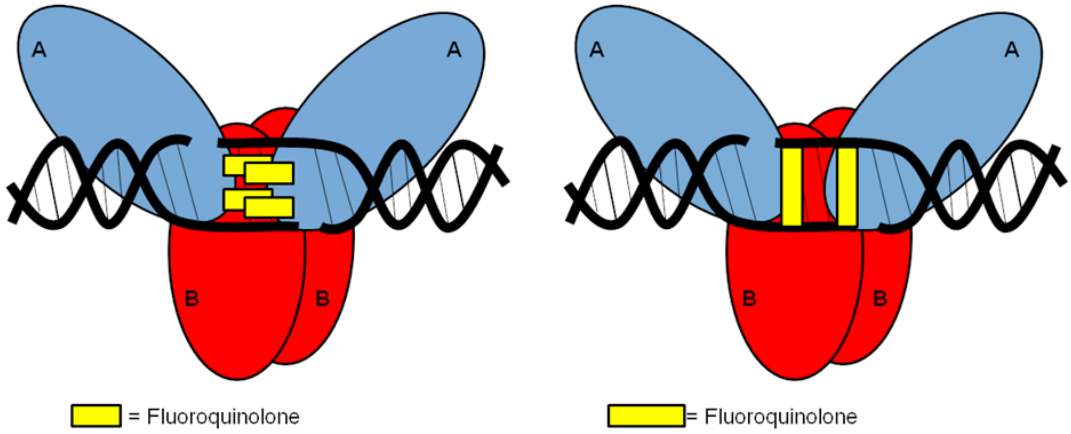

Figure 1.12: Proposed binding modes of fluoroquinolone antimicrobials detailing the initial four molecule "Viking helmet" configuration [44] and the recently identified 2 fluoroquinolone binding mode[45].

1.4.3. Mechanism of resistance

Bacterial resistance to the quinolones and fluoroquinolones manifests itself using several mechanisms of resistance: reduced accumulation, target alteration, target protection, and drug modification/degradation[48].

1.4.3.1. Reduction of intracellular fluoroquinolone concentration

As the main uptake pathway of fluoroquinolone drugs is through the porins situated on the outer membrane of bacteria, reduced accumulation is a key resistance mechanism[35]. In Gram negative bacteria, studies have shown that a reduction in the expression of outer membrane porins (OMPs) in a bacteria's plasma membrane drastically reduces its susceptibility to the fluoroquinolones[48-49]. Furthermore, genes have been identified in bacteria which down regulate the expression of outer membrane porins. These strains exhibit resistance to both ciprofloxacin **1-18** and norfloxacin **1-17**[50].This reduction in the number of porins can also result in resistance to other drug

classes including tetracyclines[51]. A second method of reducing accumulation is the over-expression of efflux pumps, which is observed in both Gram-positive and negative strains. Over-expression of efflux pumps increases the export of drug molecules back into the extracellular environment, preventing the intracellular concentration of the antimicrobial reaching toxic levels[51]. Efflux pump mediated resistance to quinolones has been reviewed in detail[52-53]. There have been several examples of specific fluoroquinolone exporting pumps identified in several species including both *E. coli* and *S. aureus*. The transporters QepA1 and QacBIII are both proton dependent efflux pumps from the major facilitator superfamily (MFS). These two pumps transport hydrophilic fluoroquinolones, QacBIII having a high specificity for norfloxacin and ciprofloxacin[52]. The best characterised efflux pump is the NorA pump from *S. aureus.* NorA is also targeted to transporting hydrophilic fluoroquinolones, however it can also transport other antimicrobials such as chloramphenicol[48]. While efflux pumps are a useful tool for bacteria in evolving resistance to fluoroquinolones, they do not confer total resistance. As with other transferable mechanisms of quinolone resistance (TMQRs), they have an additive effect. The consequence of the additive effect is that initial over-expression of efflux pumps can raise the MIC of a fluoroquinolone against the bacterial strain in question, facilitating the development of further resistance mechanisms[52].

1.4.3.2. Mutation and protection of fluoroquinolone targets

There are examples of mutations in DNA gyrase and topoisomerase IV resulting in resistance in bacteria. One recent study indicated that amino acid substitutions at positions 87 and 91 of DNA gyrase A in *Helicobacter pylori* confer antibiotic resistance[54]. A further study by Yokoyama *et al.* found that substitutions at position 95 of DNA gyrase A conferred resistance in *Mycobacterium leprae*[55]. Proteins have also been identified that shield the DNA-gyrase complex, these have been dubbed quinolone resistance proteins (Qnr)[56]. The structure of one of these proteins, QnrB1 was recently elucidated. It is a penta-peptide repeat protein (PRP) with a quadrilateral β-

helix structure. The dimer is asymmetric, and confers a degree of quinolone resistance[57].

1.4.3.3. Modification and degradation of fluoroquinolones

While modification and degradation of fluoroquinolones isn't common, there is some evidence of organisms producing chemicals that are capable of modifying and degrading fluoroquinolones. Degradation has been observed in wood rotting fungi[58]. An enzyme has also been observed that can acetylate the piperazinyl nitrogen of ciprofloxacin **1-18**, it is a variant of an aminoglycoside acetyl transferase. The modification results in a small reduction in activity[59]. While this modification does not disrupt the β-diketo system, and consequently does not confer significant resistance, if this type of resistance was acquired by a bacterial strain which also possessed genes to express Qnr proteins, a significant clinically resistant strain could arise.

1.5. Siderophores

1.5.1. Iron bioavailability and introduction to siderophores

Iron is a vital element in biology. It is required by most life forms for survival, due to its key role in metalloproteins and their functions within an organism[60]. Consequently, it is crucial that organisms evolve ways of sequestering the iron they require. In theory this should not be too problematic as iron is the fourth most abundant element in the earth's crust. However, in the environment, ferric iron (Fe(III)) exists mainly as insoluble iron hydroxides and oxides, such as haematite (Fe_2O_3)[61]. Under physiological conditions, the concentration of free Fe(III) ranges from 10^{-9}-10^{-18} M[62]. In a mammalian system, proteins such as transferrin remove iron from the bloodstream meaning the *in vivo* concentration of ferric iron is reduced to approximately 10^{-24} M. This is an important defence mechanism as it further reduces the amount of iron available to invading pathogens[62].

To counteract this lack of iron, bacteria have evolved to synthesise low molecular weight iron chelators known as siderophores. These iron chelators

allow bacteria to compete with the mammalian host for iron, in some cases removing bound iron from transferrin[63]. There are several classes of siderophore (**Figure 1.13**) produced by a wide variety of bacteria, as well as some fungi and plants[64]. The main classes of siderophore are catecholate, carboxylate (α-hydroxycarboxylate) and hydroxamate, although there are three less common classes which are: hydroxyphenyloxazolone, α-amino carboxylate, α-hydroxyimidazole.

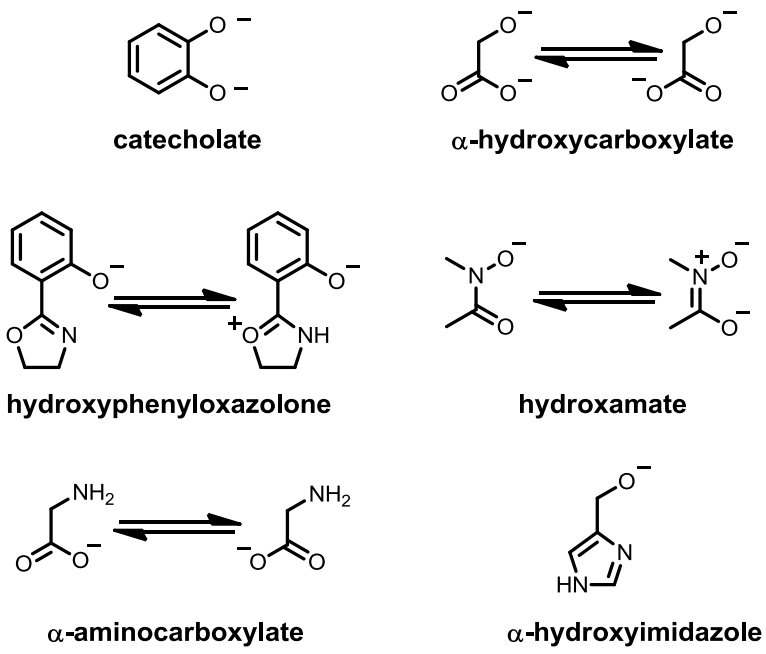

Figure 1.13: Structure of six different classes of siderophore binding groups, including resonance forms, from Hider and Kong 2010

The iron binding units outlined above are all bi-dentate, however in siderophores two or three of these binding groups are linked together via a backbone to form tetradentate and hexadentate ligands respectively[64]. The donor atoms in siderophores are generally hard donors such as oxygen. However, in some cases, such as the mycobactins and the *Yersinia pestis* siderophore yersiniabactin **1-40** (**Figure 1.18**)[61, 65]; heterocyclic nitrogen atoms are used in addition to carboxylate and alkoxide binding sites to sequester iron. The co-ordination geometry is influenced by both the denticity

and the nature of the binding groups in the siderophore. The preference for an octahedral geometry is a factor behind the high prevalence of hexadentate siderophores[61]. Hexadentate siderophore iron complexes are less dependent on the free ligand concentration (**Equation 1)**, and have higher overall formation constants.

There is also a correlation between formation constants and the Fe(II)/Fe(III) redox potential of the iron complexes siderophores. The higher the formation constant, the more negative the redox potential. The large negative redox potential prevents redox cycling of iron within the iron-siderophore complex. For most siderophores and mammalian iron binding proteins, the Fe(II)/Fe(III) redox potential is below -0.2 V[66].

$$\text{Bidentate: } Fe + 3L \rightleftarrows FeL_3 \quad \beta_3 = \frac{[FeL_3]}{[Fe^{3+}][L]^3} \quad \text{(i)}$$

$$\text{Tetradentate: } 2Fe + 3L \rightleftarrows Fe_2L_3 \quad \beta_2 = \frac{[Fe_2L_3]}{[Fe]^2[L]^3} \quad \text{(ii)}$$

$$\text{Hexadentate: } Fe + L \rightleftarrows FeL \quad K_f = \frac{[FeL]}{[Fe][L]} \quad \text{(iii)}$$

Equation 1: Equations of overall formation constants for bidentate (i), tetradentate (ii) and hexadentate (iii) siderophore complexes (charges omitted for clarity). $\beta_2 = K_1 \times K_2$, $\beta_3 = K_1 \times K_2 \times K_3$, where K_1, K_2, and K_3 are the stepwise equilibrium constants for the sequential addition of multiple ligands for bidentate and tetradentate ligands.

The siderophore that gives rise to the lowest Fe(II)/Fe(III) redox potential is the hexadentate (tris-didentate) catecholate siderophore enterobactin **1-34**[64]. Complex formation by siderophores is also promoted by the chelate effect, which lowers the entropic cost of forming 1:1 complexes with Fe(III) and consequently makes such complexes more thermodynamically favourable.

It should be noted that formation constants of iron-siderophore complexes are conditional and vary depending on the pH of their environment. At pHs

above the pKa value of the donating oxygen atoms, the pFe^{3+} values are very high, as the deprotonated oxygen carries a high charge density, and consequently a high affinity for cations. As the pH is lowered, the oxygen donor atoms become protonated, reducing the charge density on the donor atoms and consequently lowering their affinity for cations in solution. Consequently siderophores with donor atoms that have low pKa values are more effective at acidic pHs, whereas those with high pHs, like the catecholate siderophores are far more effective at alkaline pHs[67].

1.5.2. Hydroxamate siderophores

Hydroxamate siderophores are commonly produced by fungi, for example ferrichrome **1-24 (Figure 1.14)** and coprogen are both known to be produced by the fungus *Suillus granulatus* (*S. granulatus*), as well as streptomycetes[61, 64, 68]. There are a number of examples of hydroxamates known in the literature. The best known are the ferrichromes and ferrioxamines, which differ in the nature of their backbone while utilising the same chelating groups. Ferrichromes exhibit cyclic backbones, whereas ferrioxamines have linear backbones[64]. Hydroxamate siderophores have also been identified in marine bacteria, putrebactin **1-23** is a cyclic hydroxamate isolated from a Gram-negative pathogen; *Shewanella putrefaciens* (*S. putrefaciens*). There are also examples of mixed ligand, hydroxamate-containing siderophores, such as arthrobactin **1-25**.

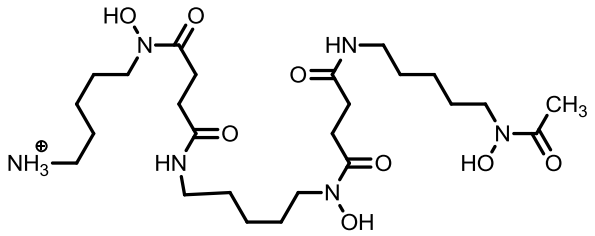

1-22
Desferrioxamine B

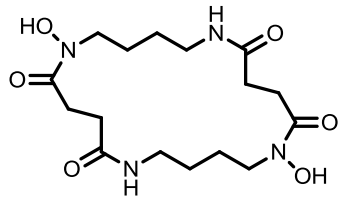

1-23
Putrebactin

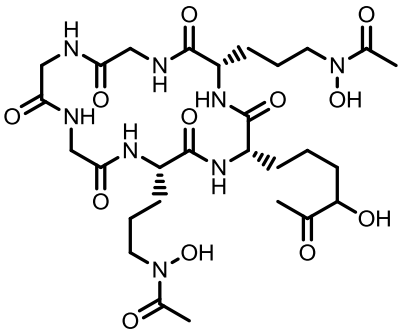

1-24
Ferrichrome

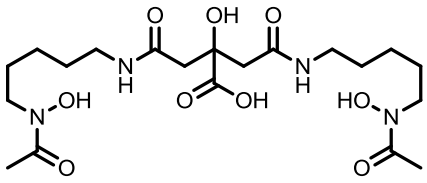

1-25
Arthrobactin

Figure 1.14: Some examples of known hydroxamate siderophores: desferrioxamine B **1-22**, putrebactin **1-23**, ferrichrome **1-24** and arthrobactin **1-25**

The hydroxamate siderophore desferrioxamine B **1-22** is also versatile, it can also coordinate to Mn(II) and Mn(III) as well as Fe(III)[70]. It has been found that some hydroxamate siderophores, specifically the albomycins (**Figure 1.23**), display innate antimicrobial activity, these are a natural example of a "Trojan horse" and will be discussed later in this chapter[61].

1.5.3. Carboxylate siderophores

Carboxylate siderophores are more recently documented phenomena[61]. Siderophores in this class tend to be bis-tridentate ligands containing citrate moieties. However, there are exceptions to this rule such as rhizobactin **1-28**, which uses individual carboxylic acids as ligand groups[71]. Citric acid **1-26** can also act as an exogeneous siderophore which can bind iron and is actively transported by certain species of enteric bacteria. However, citrate is not secreted by bacteria for this purpose[72]. Carboxylates also appear in

mixed ligand siderophores, like the previously shown arthrobactin **1-25** and petrobactin **1-30**[73-74].

While carboxylate siderophores are common, they are relatively weak chelators when compared with the hydroxamate and catecholate siderophores. This is despite the high pKa of the hydroxyl component giving them a high affinity for Fe(III)[75]. Siderophore affinities can be compared using pFe values. Rhizoferrin **1-29** has a pFe(III) of 20.0, compared with a value of 35 for enterobactin **1-34**. A siderophore's pFe is defined as the negative log of the concentration of free Fe(III) under a fixed set of conditions (10 μM of ligand and 1 μM of Fe(III) at pH 7.4).

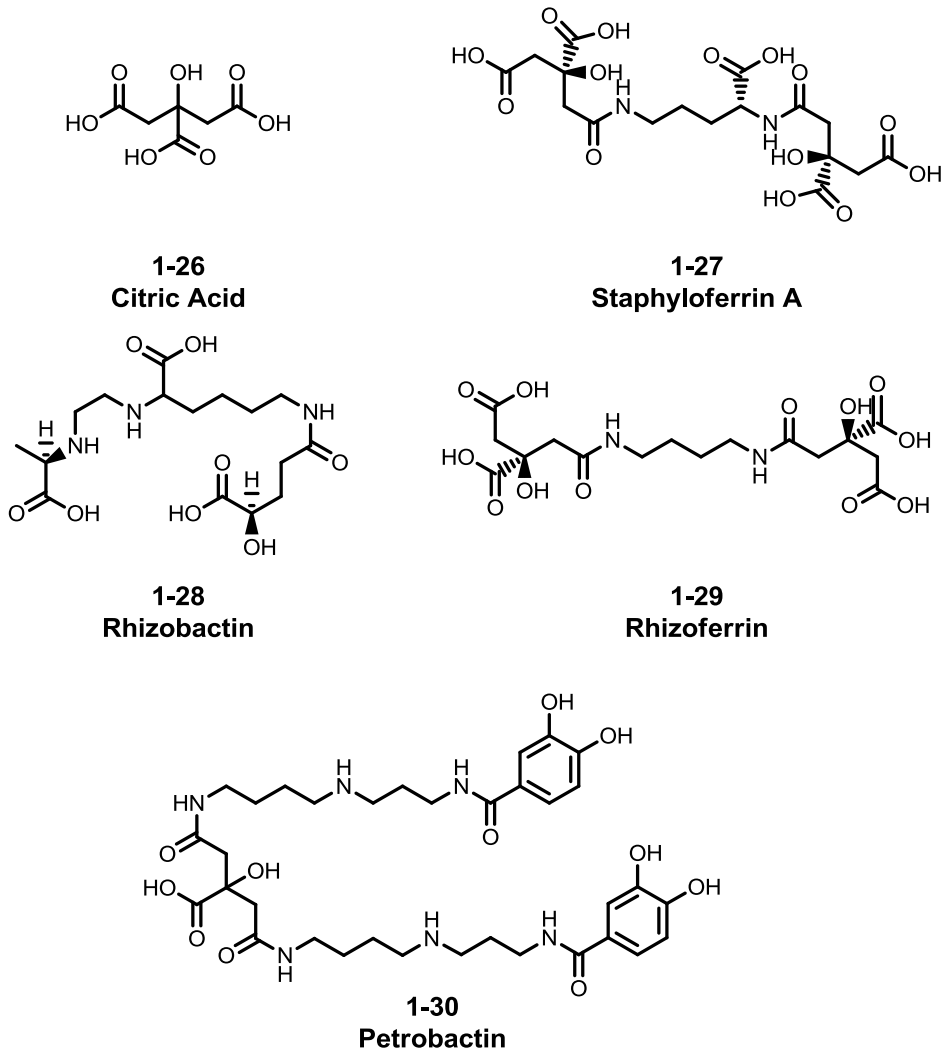

Figure 1.15: Examples of carboxylate siderophores including carboxylate only and mixed ligand siderophores.

Citrate siderophores are less effective compared to the catecholate and hydroxamate siderophores at physiological pH but become more competitive at acidic pHs. As citrate siderophores remain deprotonated at lower pHs than hydroxamate or catecholate siderophores, they have been shown to show optimum iron binding and transport at pH 4.5[75]. This is a logical situation, as citrate siderophores desferrioxamine B **1-22** and rhizoferrin **1-29** are both fungal siderophores. The optimum pH for the growth of the Rhizobium fungi that produce rhizoferrin is pH 4.0, significantly lower than physiological pH and consequently siderophores that are effective at lower pHs are well suited

to a fungal environment. A more recently discovered citrate siderophore is vibrioferrin **1-31** (**Figure 1.16**). Vibrioferrin has a more intriguing structure than the previously described citrate based siderophores, as it contains a cyclic amide and only has five chelating groups. Vibrioferrin **1-31** still forms 1:1 complexes with Fe(III), the complex is stabilised by a co-ordinating H_2O completing the co-ordination sphere. However vibrioferrin **1-31** is also a weaker iron chelator than other citrate siderophores.

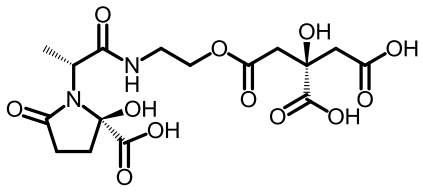

1-31
Vibrioferrin

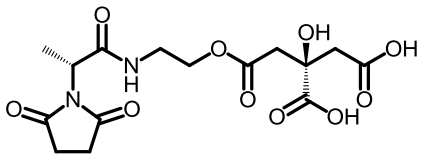

1-32
Proposed vibrioferrin photoproduct

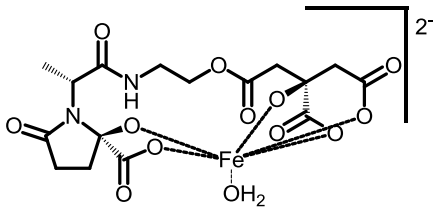

1-33
Vibrioferrin-Fe complex

Figure 1.16: Structures of vibrioferrin **1-31**, proposed vibrioferrin photoproduct **1-32** and the vibrioferrin-Fe(III) complex **1-33**

The studies on the siderophore also suggest that like a number of marine siderophores, it is photoreactive, which may aid it's iron delivery as iron can be released by photoreduction[76].

1.5.4. Catecholate siderophores

The catecholate class of siderophores, which also includes the phenolates, is the main focus of the research described in this thesis. The catecholate class contains one of the strongest binding siderophores,

enterobactin **1-34**, with a pFe(III) value of 35.5[64]. The formation constant has been reported as 10^{52} dm^3 mol^{-1}[60]. Part of the reason for this high affinity is the chelate effect. A second reason is linked to its structure (**Figure 1.17**). The catechol amides allow each of enterobactin's three binding groups to bind iron in a salicylate type configuration, before rotating and bringing the iron into the centre of the siderophore where it is chelated by the remaining ligand groups[77]. Enterobactin **1-34** was the first catecholate siderophore to be identified, by Pollack and Neilands in 1970.

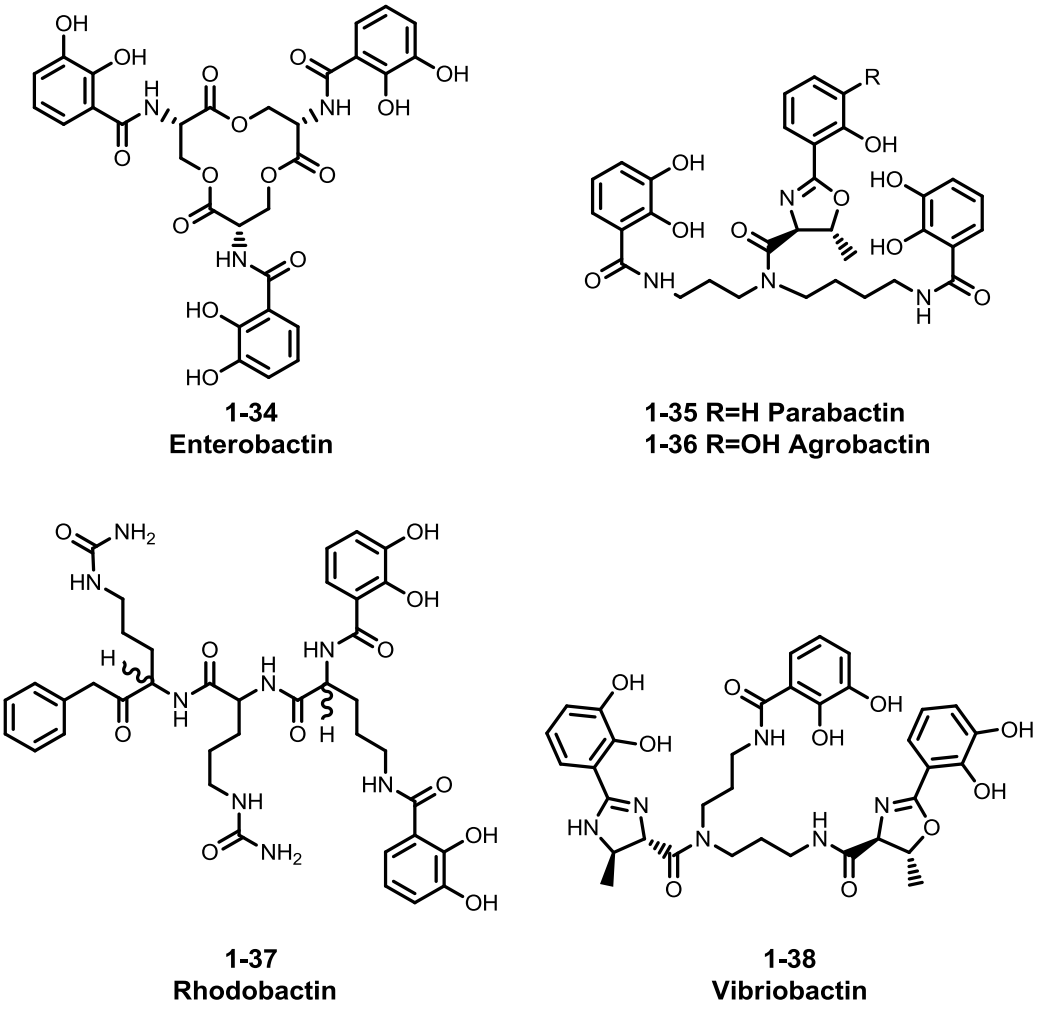

Figure 1.17: Structures of five catecholate siderophores; enterobactin **1-34** parabactin **1-35**, agrobactin **1-36,** rhodobactin **1-37** and vibriobactin **1-38**.

As a representative of the catecholate class, enterobactin **1-34** is rather atypical. It is one of only two characterised catecholate siderophores with a cyclic backbone. The other cyclic catecholate siderophore is the *Bacillus* siderophore bacillibactin **2-3** (**Figure 2.1**). The majority of catecholate siderophores have linear backbones. It is also apparent that this class of siderophores generally contains tris-bidentate (hexadentate) ligands, as well as very similar backbones. Parabactin **1-35** and agrobactin **1-36** differ only in that one of the ligand groups in parabactin is a phenolate rather than a catecholate binding group[79]. Vibriobactin **1-38** is also similar, with the two differences being a shorter backbone, and an additional oxazoline ring[80]. The best known phenolate examples within this class of siderophores exhibit a different kind of structure. They still exhibit linear backbones; however their denticity is not the usual tris-bidentate configuration (**Figure 1.17**). The mycobactins **1-41**, a series of siderophores from *Mycobacterium tuberculosis* exhibit hydroxyphenyloxazolone ligands. Pyochelin **1-39** and yersiniabactin **1-40** exhibit a similar structure, but with thiazoline rings as opposed to oxazoline rings adjacent to the phenol.

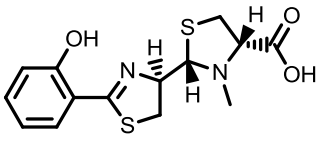

1-39
Pyochelin

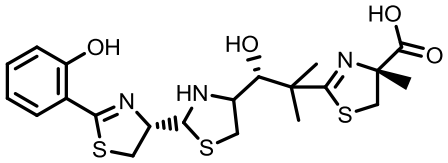

1-40
Yersiniabactin

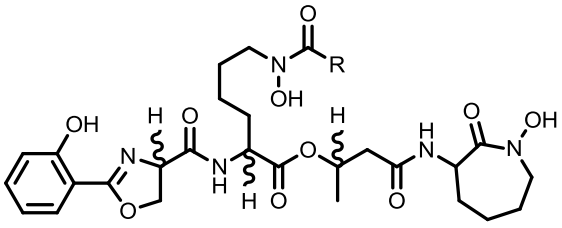

1-41
Mycobactin

Figure 1.18: Examples of phenolate siderophores; pyochelin **1-39**, yersiniabactin **1-40** and mycobactin **1-41**.

The phenolate groups allow iron binding in these siderophores. Examining the structures shows that this class of ligands display structural diversity. They have been isolated from a broad range of species including enteric bacteria, *Mycobacteirum*, *Yersinia,* and *Pseudomonas* species, as well as some marine organisms. It is this diversity of species that produce and recognise the siderophores that makes them an ideal siderophore for use in a "Trojan horse" strategy.

1.5.5. Siderophore uptake mechanisms

Whilst the ligand geometry and backbone structure of siderophores can vary substantially, the general mechanisms for uptake into bacterial cells are relatively uniform. In Gram-negative bacteria, the siderophore-iron complex is recognised by a binding protein on the outer cell membrane, once in the periplasm it binds to a periplasmic binding protein (PerBP), which hands it over to the inner membrane transporter complex, which carries it across the inner membrane into the cytoplasm[81]. *E.coli* is capable of transporting a multitude of different siderophores from its environment in order to obtain the iron it requires.

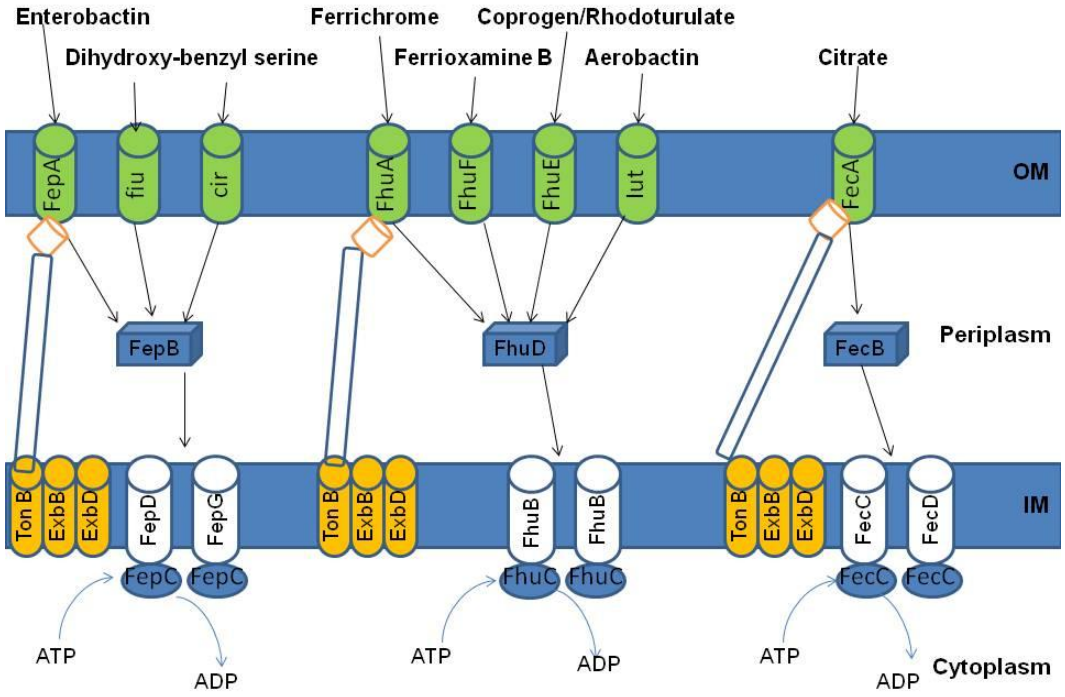

Figure 1.19: Schematic overview of siderophore uptake in *E.coli* redrawn from Liang *et al*.[81] OM = outer membrane IM = inner membrane. Reproduced from X. Y. Liang, D. J. Campopiano and P. J. Sadler, *Chem. Soc. Rev.* **2007**, *36*, 968-992 with permission from The Royal Society of Chemistry.

The energy for active siderophore-Fe(III) complex uptake is produced by ABC proteins. In this case, this is a protein complex comprised of three proteins: ExbB, ExbD and TonB. These proteins are in a 7:2:1 ratio (ExbB: ExbD: TonB). The Exb proteins are ATPases which generate the energy for transporting the siderophore complex across the inner membrane[62, 81]. TonB has a more important role in this process. It is TonB which interacts with the receptor proteins on the surface of the outer membrane[82]. This interaction occurs via an N-terminal region on the receptor proteins referred to as the TonB box, this is a highly conserved motif which always contains aspartic acid and valine residues[82]. The interaction between TonB and siderophore transporters has been demonstrated by Moeck *et al*, among others, by cross linking TonB to the ferric hydroxamate transporter FhuA[83]. The siderophore

transporters all have a broadly similar tertiary structure (**Figure 1.20**). This is composed of a 22 stranded β barrel, and an N-terminal chain (approximately 150 residues) which folds inside the barrel as a plug domain[62, 81]. When TonB interacts with the "TonB box" it induces a conformational change which removes the plug domain from the barrel, allowing the siderophore iron complex to pass through the receptor and into the periplasm[81].

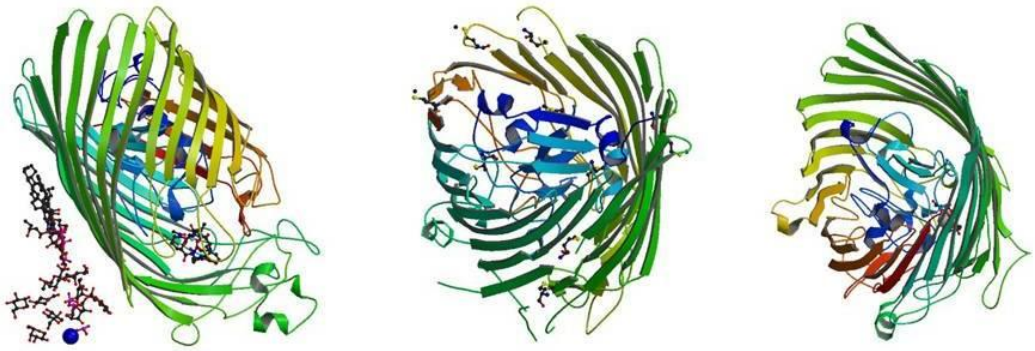

Figure 1.20: Crystal structures of FhuA (left), FepA (centre) and FecA (right) all with bound ligands [84-86]. Structures from the Protein Data Bank: FhuA image came from RCSB PDB (www.RCSB.org) of PBD ID 2FCP (Ferguson, A.D. Hoffman, E. Coulton, J.W. Diederichs, K. Welte, W.(1998) Siderophore-mediate iron transport: crystal structure of FhuA with bound liposaccharide Science. 282:2215-2220). FepA image came from RCSB PDB (www.RCSB.org) of PBD ID 1FEP (Buchanan, S.K. Smith, B.S. Venkatramani, L. Xia, D. Esser, L. Palnitkar, M. Chakraborty, R. van der Helm, D. Deisenhofer, J.(1999) Crystal structure of the outer membrane active transporter FepA Nat. Struct. Biol. 6: 56-63). FecA image came from RCSB PDB (www.RCSB.org) of PBD ID 1PNZ (Yue, W.W. Grizot, S. Buchanan, S.K.(2003) Structural evidence for iron free and ferric citrate binding to the TonB-dependent outer membrane transporter FecA J. Mol. Biol. 332: 353-368).

It should be noted however, that not all siderophore transporters rely on this interaction. LbtU, a receptor for the *Legionella pneumophila* siderophore legiobactin, was recently found to be TonB independent. This conclusion is based on the fact that while the bacterium produces siderophores, and siderophore transporters, there is no gene encoding TonB within its genome[87].

1.5.6. Mammalian defence against siderophores

While siderophores are a triumph of evolution from bacteria, in terms of allowing them to scavenge sufficient iron to survive from the minimal amount available in their host, mammals have evolved mechanisms of preventing siderophores from doing their job. Mammals have evolved proteins known as siderocalins, which bind siderophores and preclude them from scavenging iron. These proteins have a highly conserved structure with an 8 stranded β-barrel, with α- and 3_{10} helices. The β-barrel encloses a cup shaped binding site[88].

Siderocalin is unlike most of the lipocalins (the family of proteins to which it belongs) due to the nature of its binding site. While the lipocalins possess hydrophobic binding pockets, siderocalin has a series of positively charged residues. The binding pocket contains arginine and lysine residues[88]. The nature of this binding pocket allows it to bind a range of catecholate siderophore complexes including those of enterobactin **1-34**, bacillibactin and parabactin. Additionally, siderocalin was found to bind the siderophore-Fe(III) complex of the mixed catecholate/hydroxamate siderophore carboxymycobactins from *Mycobacterium*. The siderocalin protein binds catecholate siderophores and their Fe(III) complexes by positioning the positively charged arginine and lysine residues of the binding pocket between the three catecholate rings. The protein-siderophore complex is secured by a combination of ionic and cation-π interactions[89], resulting in strong binding of siderocalin's siderophore targets. It has been found to bind ferric enterobactin **1-34** with a K_D of 0.4 nM[88].

The combination of ionic and cation-π interactions allows siderocalin to bind multiple types of siderophore. However, as in the long running arms race between bacteria and antibiotics, bacteria are also raising the stakes in the battle for iron. Siderophores are being identified that can evade sequestration by the siderocalin protein. Petrobactin **1-30** (**Figure 1.15**) has evolved with an alternative catechol configuration which alters the

conformation of its iron complex sufficiently to prevent it being bound by siderocalin[90]. Additionally it has been found that bacteria have evolved to glycosylate their siderophores[91].

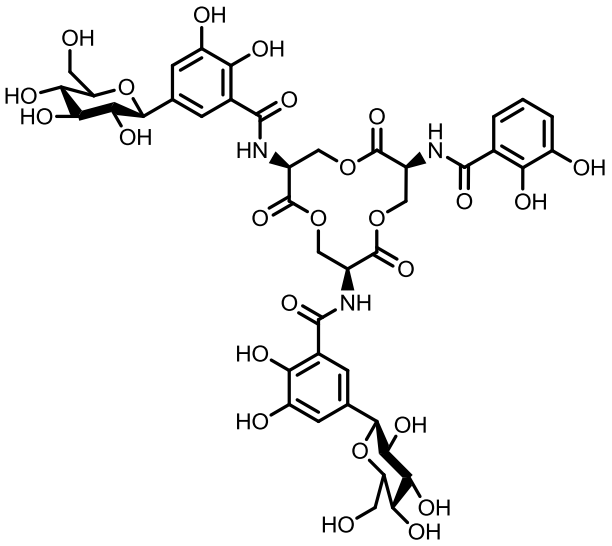

1-42

Figure 1.21: Salmochelin S4, a glycosylated analogue of enterobactin

The glycosylation generates sufficient steric hindrance to have a negative effect on the binding by siderocalin[92]. In designing our siderophore-antimicrobial conjugates, we need to bear in mind the presence of siderocalin, and amend the target structures accordingly. The methods employed by bacteria can be used to generate siderophore analogue-antimicrobial conjugates, which siderocalin will not bind, but will bind iron and be recognised by bacteria. This ability to evade a host's immune system is potentially useful in the design of siderophore based Trojan horses. If the siderophore component is not recognised by mammalian siderocalins, it minimises the risk of the Trojan horse being removed from the host before it can act on its target bacteria.

1.6. Trojan horse strategy

1.6.1. The basic concept

In biological terms the aim is to mask a drug or other toxic moiety as harmless or preferably essential to a bacterial species. In this project, the essential component is iron, which as previously described is essential for bacteria to function and grow. By exploiting bacterial iron uptake, it could be possible to bypass drug access related resistance mechanisms (**Figure 1.22**), specifically the mechanisms by which bacteria reduce the intracellular concentration of antimicrobials: reduced uptake and efflux pumps[48]. Research on outer membrane porin (OMP) mutants has shown that a reduction in the number of OMPs can convey resistance by decreasing accumulation[49]. A study on *Acinetobacter* showed an emphasis on the efflux of antimicrobials in its resistance profile[93], whilst Speciale *et al.* observed that *P. aeruginosa* develops resistance by modifying its outer membrane[94]. Consequently, reduced accumulation is a significant mechanism to target when attempting to eliminate antimicrobial resistance. By exploiting the uptake of a key nutrient, in the case of this research iron, it makes the development of resistance by reduced uptake or active efflux evolutionarily unfavourable. If a bacterium evolves to reduce the uptake of a conjugate, or actively removes it from the cell, it will also reduce its ability to obtain iron from its extracellular environment. Such mutations would reduce the likelihood of bacteria to survive and would ultimately result in attenuated growth or cell death.

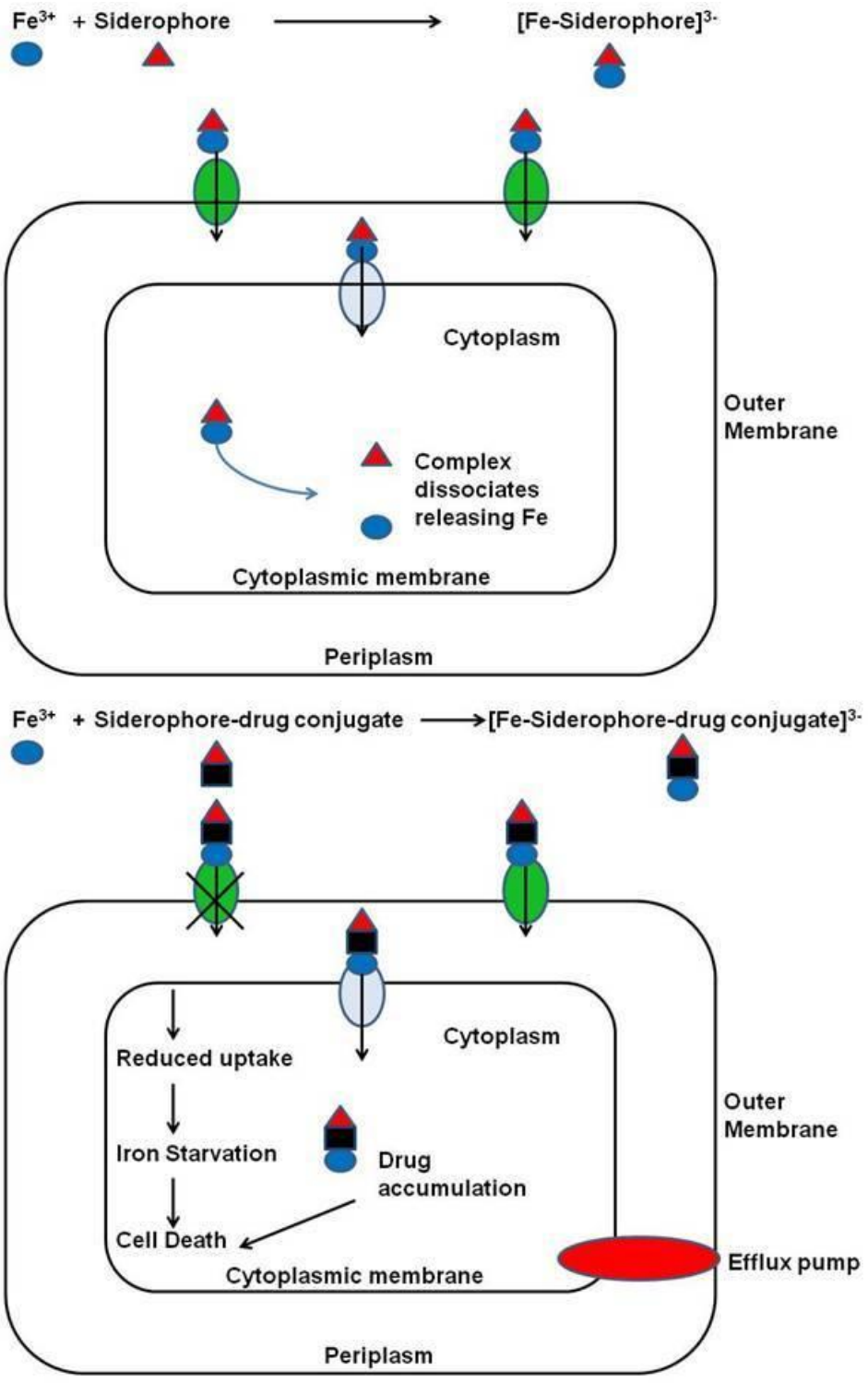

Figure 1.22: Schematic overview of bacterial iron transport (top) and the concept of the Trojan horse strategy (bottom)

1.6.2. Natural examples of Trojan horses

The idea of "Trojan horses" for antibiotics is based on a natural precedent, as bacteria evolved their own Trojan horses, the sideromycins. These are based on a number of siderophores including enterobactin **1-34** and microcins[6]. The two best known are salmycin **1-46** and the albomycins **1-43−1-45** (**Figure 1.23**). Natural Trojan horses are structurally diverse, but their overall composition is the same. They contain a siderophore component to chelate and transport iron, and an antimicrobial component to induce cell death. The albomycins comprise of a nucleotide analogue and a thioribosyl pyrimidine component, conjugated to a tripeptide siderophore[95]. A third example Ferrimycin A **1-47** is based on the siderophore ferrioxamine B, with an antimicrobial moiety conjugated via its terminal hydroxamate[96]. The salmycins use danoxamine as their siderophore component. The antimicrobial component is an aminoglycoside[97].

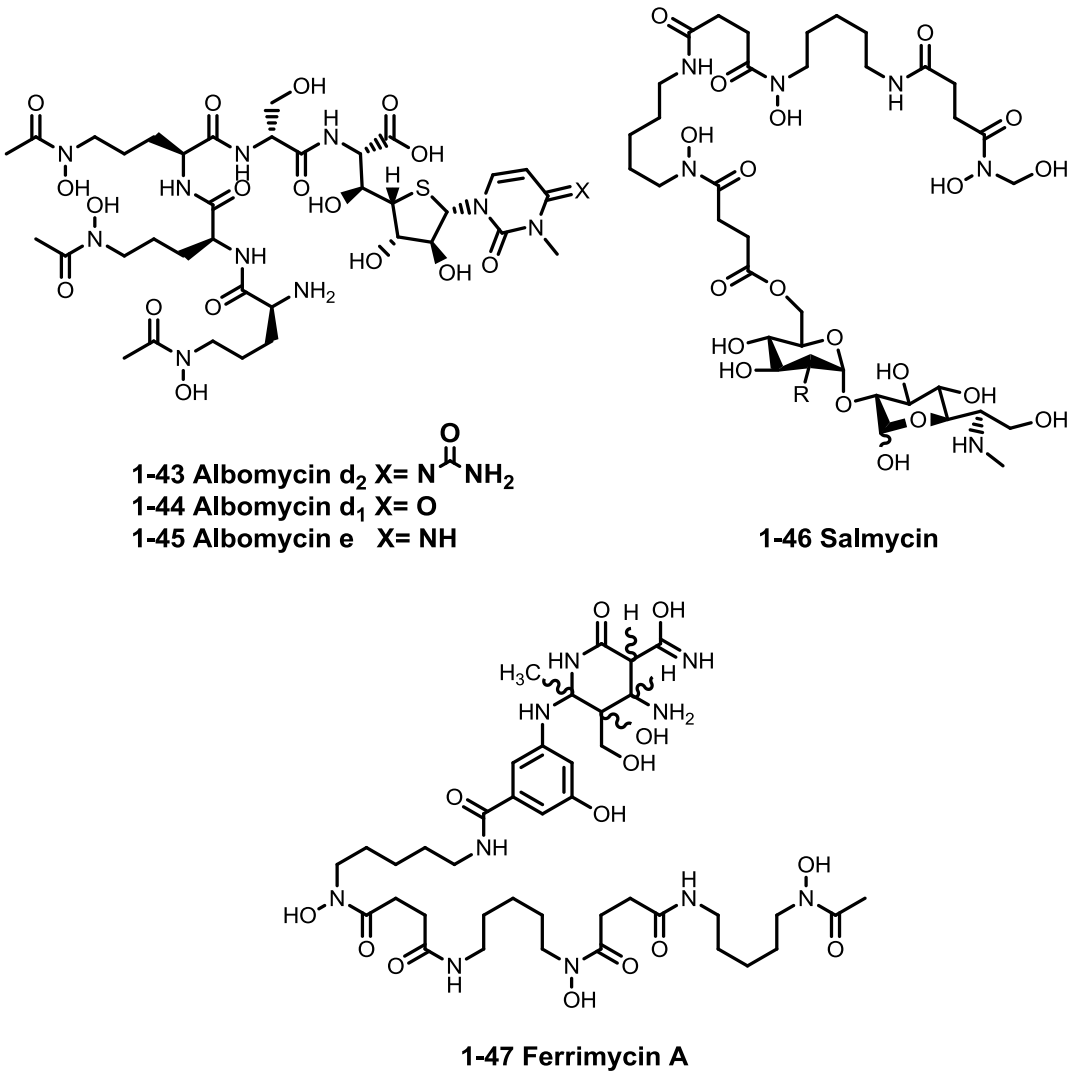

Figure 1.23: Examples of naturally occurring Trojan horses; albomycin **1-43−1-45**[95] , salmycin **1-46**[97], and Ferrimycin A **1-47**[98]

There are other naturally occurring examples including the nannochelins and myxochelin, identified by Kunze *et al*[99-100]*.* There is also a more recent example published by Nolan *et al.*, a microcin based on enterobactin **1-34**. The microcin is an 84 amino acid ribosomal protein linked to enterobactin by a sugar residue[101]. Siderophore mimicking Trojan horses are not the only natural form produced by bacteria. An alternative Trojan horse strategy is the production of bacteriocins, which target competing

bacteria, and gain access by exploiting the TonB and TolB active uptake systems[102].

1.6.3. Synthetic examples of Trojan horses

There have been two main approaches to preparing synthetic "Trojan Horses", either through conjugation of a known antimicrobial agent to a natural siderophore, or conjugation of a known antimicrobial agent to a novel iron chelator[103-104]. The earliest work began in the 1970s and focused on antimicrobials whose chemistry was well established, namely; sulfonamides, cephalosporins and β-lactams[62]. The second advantage of these particular antimicrobials is that they have periplasmic targets, and consequently the "Trojan horse" only needed to penetrate the outer membrane and not the cytoplasmic membrane.

The first example of a synthetic "Trojan horse" was published by Zähner *et al.* in 1977. The work utilised sulfonamide antimicrobials, and prepared two conjugates using two hydroxamate siderophores: ferrichrome **1-23** (**1-48**) and ferrioxamine **1-21** (**1-49**) (**Figure 1.24**)[105]. The compounds were prepared by conjugating the antimicrobial to the siderophores via a nicotinic acid linker, in the case of ferrichrome the conjugation was via the hydroxyl group of a serine residue in the backbone. For the ferrioxamine conjugate **1-49**, a primary amine was used as the point of attachment[105]. Antimicrobial screening showed the ferrichrome conjugate **1-48** to have similar levels of activity against *S. aureus* to the parent sulfonamide. The ferrioxamine conjugate **1-49** showed no activity, this raised the question of whether the antimicrobials needed to be released once inside the cell, or whether longer linkers were needed to ensure activity was retained[105].

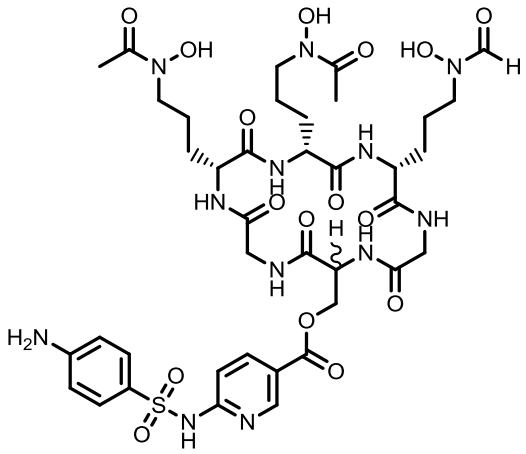

1-48

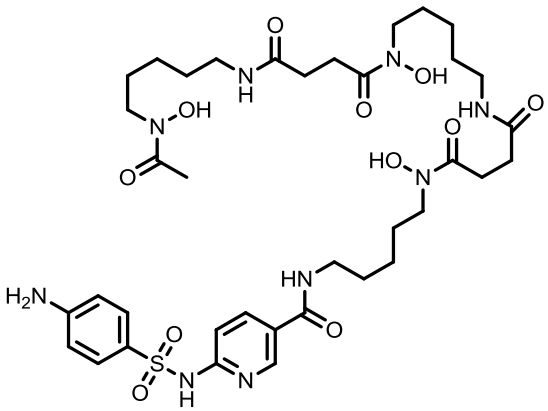

1-49

Figure 1.24: Sulfonamide Trojan horses utilising ferrichrome **1-24** (**1-48**) and ferrioxamine **1-22** (**1-49)**[105]

1.6.3.1. Catecholate siderophore Trojan horses

A significant proportion of the work undertaken on Trojan horses has focused on utilising catecholate siderophores and novel catechol based ligands as the iron binding component. Throughout the 80's and 90's several groups reported catechol based Trojan horses, with a variety of β-lactam antibiotics including aminopenicillins and cephalosporins. Watanabe produced a conjugate designated E0702, **1-50**. This contained a phenolate binding group and a 6,7-dihydroxy-4-hydro-chromen-4-one moiety as the iron binding groups (**1-50, Figure 1.25**)[106], conjugated to the antimicrobial via an amide bond. This conjugate exhibited good levels of activity with MIC values that were significantly lower than well established antibiotics including ampicillin, tetracycline and several cephalosporins. This was observed across a series of *E. coli* strains. Curiously, when mutants with resistance were observed, the mutation wasn't mapped to the target or a specific transporter, but to the TonB protein[106]. As TonB is essential for the iron transport system[81], it was clear that the conjugate was successfully working as a Trojan horse and exploiting the bacteria's iron transport system. This

was further confirmed by its high level of efficacy against iron starved bacteria[106].

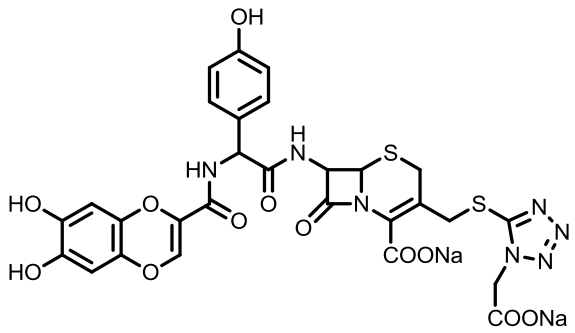

1-50

Figure 1.25: Structure of a cephalosporin based Trojan horse using phenolate/catecholate binding groups **1-50**

A disadvantage of the Trojan horse approach is that the additional steric bulk created by conjugating an antimicrobial molecule to a natural or synthetic siderophore, may reduce or completely prevent uptake of the complex by bacteria. This is not necessarily the case, as evidenced by a catechol siderophore conjugate containing the high molecular weight macrolide vancomycin, prepared by Ghosh and Miller (**1-51**, **Figure 1.26**)[107].

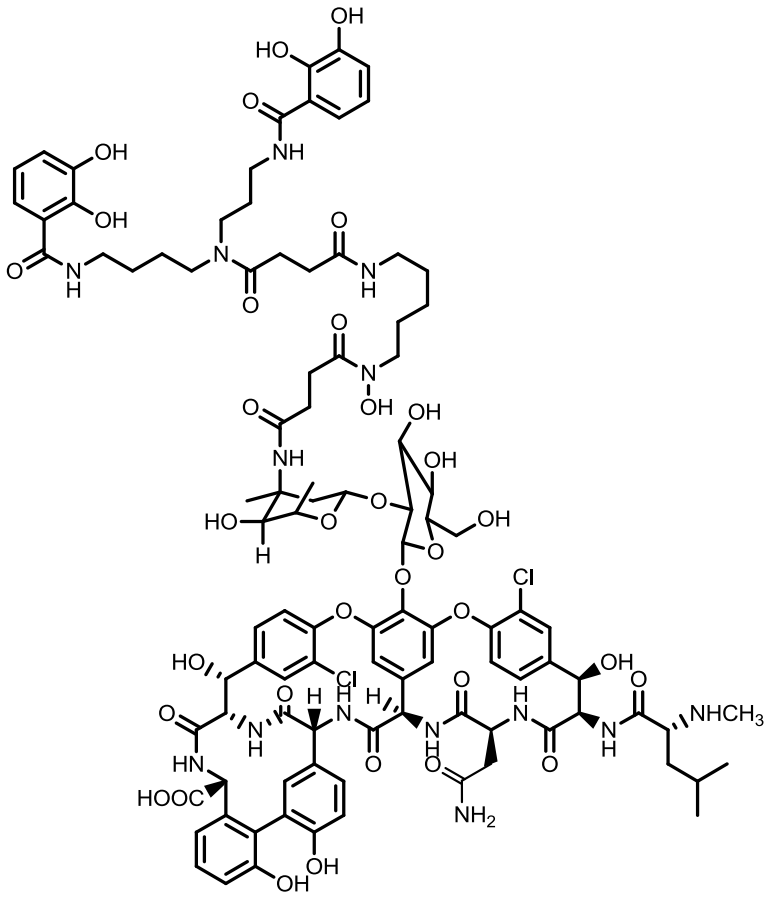

1-51

Figure 1.26: Structure of a vancomycin-pyoverdin conjugate **1-51** produced by Ghosh and Miller[107]. This showed increased activity against *Pseudomonas aeruginosa*.

The Pyoverdin component is a bis-catecholate/hydroxamate mixed ligand siderophore. The conjugate **1-51** displays a 4-8 fold increase in activity when compared to vancomycin when tested against bacteria in iron deficient conditions. As iron is tightly regulated in a mammalian host and is present only at yoctomolar concentrations[62], this conjugate could be highly effective *in vivo*.

As the bacterial iron transport system is designed to bind and transport specific siderophores (e.g. FepA transporting enterobactin)[81], siderophore-antimicrobial conjugates could also be targeted at specific transporters, using known siderophores, or analogues with similar structures. As there are

known natural siderophores with mixed ligands, Trojan Horses can be prepared using natural mixed ligand siderophores, or mixed ligand iron chelators. As long as the iron binding regions of the siderophores are not disrupted, this is a realistic possibility. Schobert *et al.* employed this theory to produce new synthetic Trojan horses (**1-52**, **Figure 1.27**), using β-lactams as the antimicrobial moiety[108].

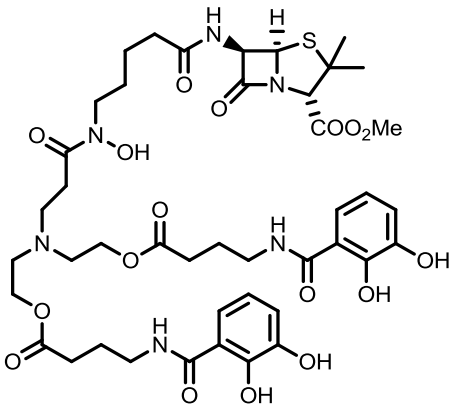

1-52

Figure 1.27: A mixed ligand (catecholate/hydroxamate) siderophore-β-lactam conjugate synthesised by Schobert *et al.*[108]

Schobert *et al.* used 6-aminopenicillanate as the antimicrobial moiety, and prepared a variety of conjugates including bis-catecholate hydroxamates and tris-catecholate conjugates. They established the conjugates were acting as siderophores by using antibiotic-free siderophores and analysing the promotion of growth in siderophore deficient *E.coli*. These experiments suggested that the synthetic siderophores **1-52** (**Figure 1.27**) and similar conjugates they prepared were being actively transported[108]. Additionally, Schobert *et al.* highlighted the importance of the iron binding ligands. They observed that removing a single key atom from the iron binding groups removed the siderophore activity of the conjugates[108].

More recently Heinisch *et al.* and Wittmann *et al.* both reported catechol based Trojan horses. Like Schobert they utilised aminopenicillins as the

antimicrobial component, conjugated to via an amide bond (**Figure 1.28**)[109-110].

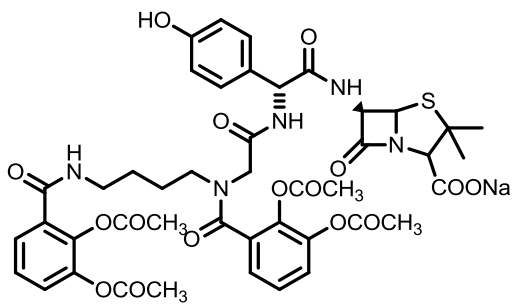

1-53

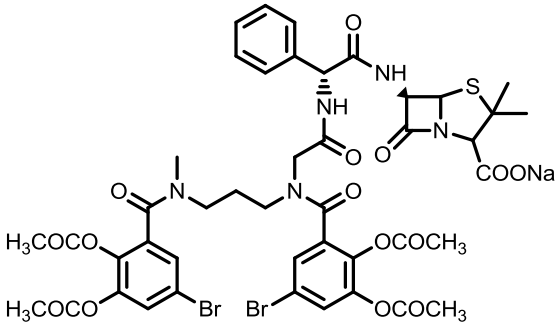

1-54

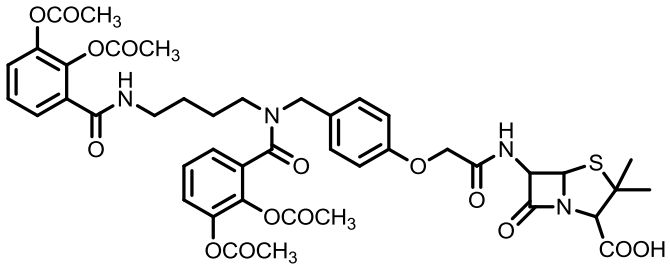

1-55

Figure 1.28: Structures of catecholate siderophore-β-lactam pro-drugs synthesised by Heinisch *et al.*[110]

These conjugates **1-53** and **1-54** (**Figure 1.28**) proved to be successful *in vitro* with the amide coupled conjugates displaying MIC values as low as 1 mg/L against wild type *Pseudomonas aeruginosa*. This value is one hundred fold lower than the MIC of ampicillin against the same strain. The ether linked compound **1-55** was substantially less active. It exhibited an MIC of 50 mg/L. However, when compared with the MIC of ampicillin this was still a significant improvement[109, 111]. This difference in activity suggests that the lability of the siderophore component is key to the success of the conjugate. This was further explored by Miller *et al.* with their desferrioxamine-ciprofloxacin

conjugates (**section 1.6.3.2**)[112]. Heinisch *et al*. also attempted to investigate the mechanism of uptake, and the efficacy of the conjugates as siderophores. The activity of the conjugates was diminished when they were tested against strains which were deficient in key catecholate transporters, suggesting that the conjugates were binding iron and being actively transported via the iron uptake system to reach their intracellular target as opposed to accessing the cell via a porin[109].

1.6.3.2. Quinolone and fluoroquinolone based Trojan horses

In recent years there have been several Trojan horses reported that use fluoroquinolones as the parent antimicrobial[104]. Miller *et al.* used nalidixic acid and prepared conjugates with desferrioxamine B **1-22**. Their experiments found that the conjugates could perform DNA cleavage *in vitro*, but only in the presence of Fe(II) ascorbate and H_2O_2 as reducing agents. However the conjugate did show significant anti-malarial activity[113]. Mislin *et al.* did work using norfloxacin **1-17** and the *Psuedomonas* siderophore pyochelin (**Figure 1.29**). They focused not only on whether the conjugate would function as a siderophore, but whether the nature of the linker between siderophore and antimicrobial would influence the function of the conjugate as an antibiotic[114]. They observed that the conjugate with a bio-labile linker retained the antimicrobial activity, but the conjugate with a non-labile linker had no activity. This suggests that either the presence of the siderophore prevents the antimicrobial binding to its target or that the antimicrobial prevents the siderophore from being recognised and subsequently transported into the cell[114]. A more recent study by Miller *et al.* examined salmycins and desferridanoxamine-antibiotic conjugates to elucidate the importance of drug release. After synthesising a series of conjugates with both labile and non-labile linkers, they found that the conjugates with labile linkers often displayed equal or greater activity than the free antimicrobial, but those with non-labile linkers had reduced activity[115].

A)

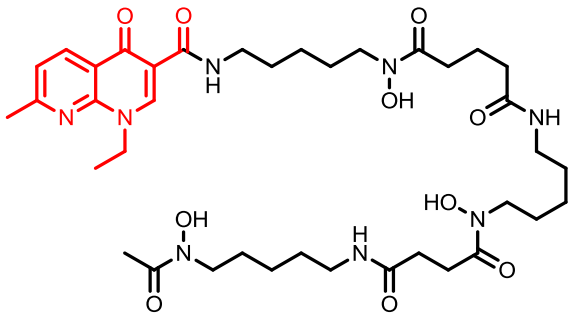

1-56

B)

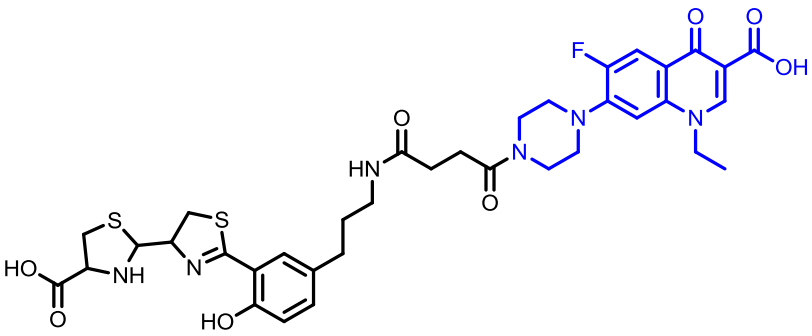

1-57

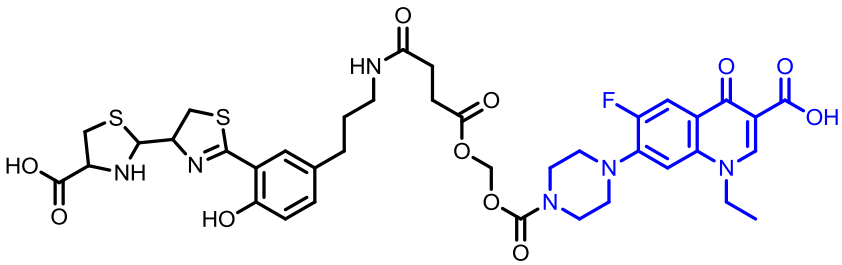

1-58

Figure 1.29: A) Conjugate **1-56** synthesised by Miller *et al*. using desferrioxamine **1-22**/nalidixic acid **1-16**. B) Conjugates **1-57** and **1-58** synthesised by Mislin *et al.* using pyochelin **1-39**/norfloxacin **1-17**. Fluoroquinolones are coloured, nalidixic acid **1-16**: red, norfloxacin **1-17**: blue

In addition to these conjugates, there are also several recent examples of fluoroquinolone based Trojan horses using ciprofloxacin **1-18**. Mislin *et al.* built on their earlier work with fluoroquinolone-pyochelin conjugates (**Figure 1.30B**). In these conjugates, the fluoroquinolone was linked to an N3' functionalised version of pyochelin rather than via the aromatic ring as in conjugates **1-57** and **1-58**. However, the same stable and cleavable linkers

were used. Miller *et al* built on their work on Desferrioxamine B conjugates. Like Mislin they used ciprofloxacin as the fluoroquinolone component. Miller used "trimethyl-lock" based linkers, designed to release the antimicrobial agent via cleavage by an esterase or phosphatase[112].

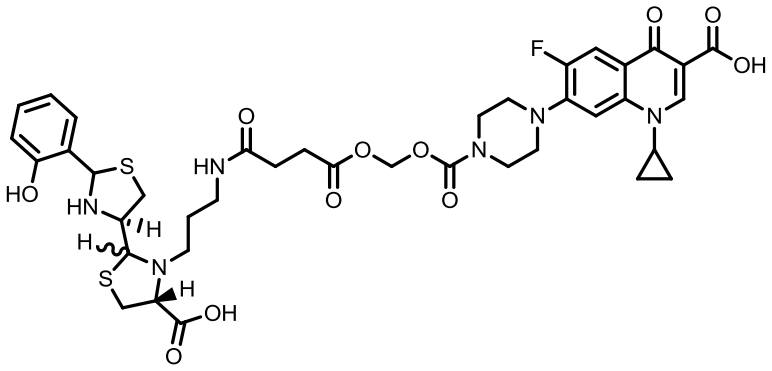

1-59

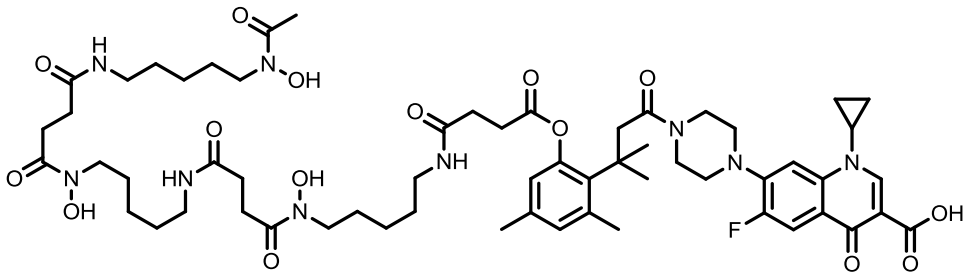

1-60

Figure 1.30: Structures of a pyochelin ciprofloxacin conjugate **1-58** and an esterase sensitive desferrioxamine-ciprofloxacin conjugate **1-59**[112].

Mislin *et al.* found that their conjugates **1-57** and **1-58** displayed weaker activity than the free fluoroquinolones. However, they attributed this to low solubility and potential hydrolysis of the labile linkers in aqueous media, preventing the active uptake of the antibiotic[116]. Miller observed that the esterase sensitive conjugate **1-60** had good antimicrobial activity against desferrioxamine-utilising bacteria, however the conjugates designed to be phosphatise sensitive were inactive against the same panel of strains[112].

Two additional examples of Trojan horses using ciprofloxacin **1-18** have been reported by the Duhme-Klair/Routledge research group[117-118]. They used α-carboxylate siderophores as the iron binding component (**Figure 1.31**). They reported two conjugates with a single citrate as the iron binding moiety **1-61** and **1-62**[117], and subsequently reported a ciprofloxacin conjugate with the *Staphylococcus aureus* siderophore staphyloferrin A as the iron binding component **1-63** [118].

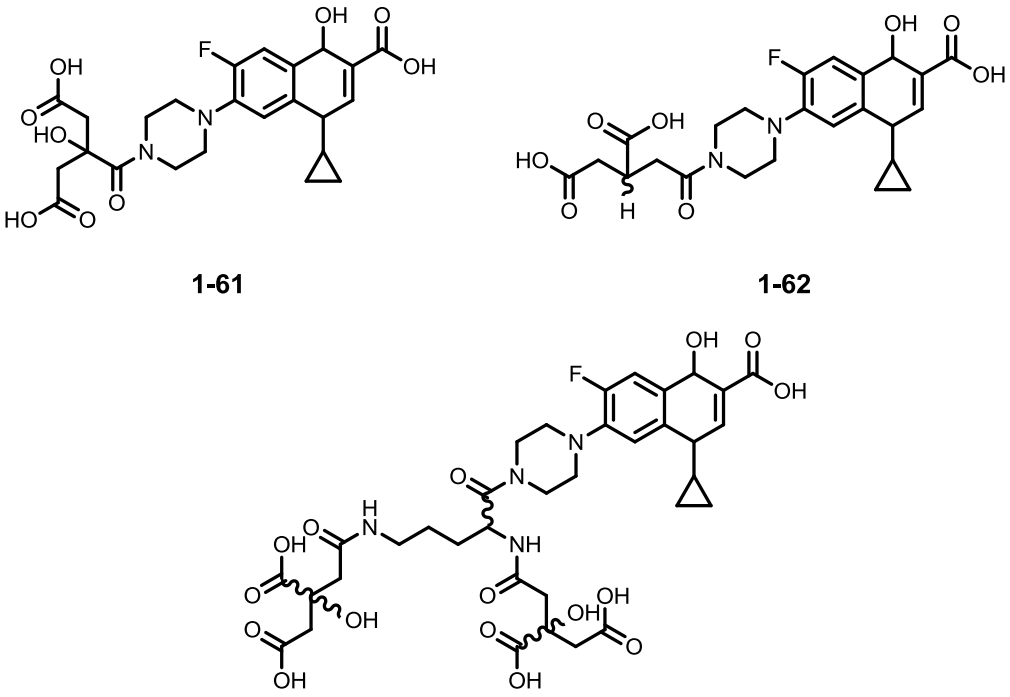

1-61 **1-62**

1-63

Figure 1.31: Structures of carboxylate siderophore-ciprofloxacin conjugates reported by the Duhme-Klair/Routledge group

The carboxylate-ciprofloxacin conjugates (**Figure 1.31**) showed activity against a range of pathogenic bacteria, however the activity was significantly attenuated compared to that of the parent antimicrobial ciprofloxacin **1-18**[117-118]. The decrease in activity was determined to be due to reduced inhibitory activity against DNA gyrase.

1.6.3.3. Recent successes with Trojan horse antimicrobials

There have been some significant discoveries in the field of Trojan horses in recent years. Miller *et al*. prepared artemisinin-mycobactin conjugates to target *Mycobacterium tuberculosis* as well as malaria. (**Figure 1.32**)[119]. The antimicrobial component artemisinin has no anti-mycobacterial activity. However, it is known to be an effective antimalarial drug.

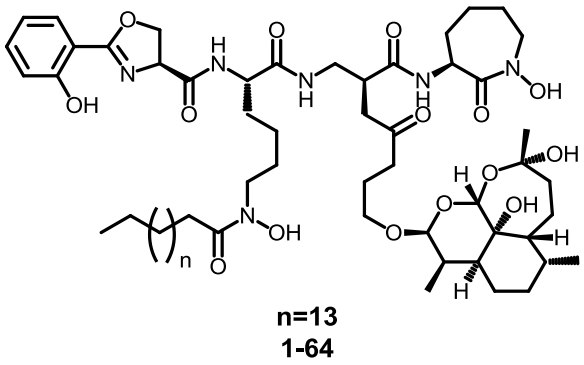

Figure 1.32: Structure of an artemesinin-mycobactin conjugate **1-64** produced by Miller *et al.*[119]

Miller *et al.* found that their conjugate **1-64** (**Figure 1.32**) possessed good activity and as expected was highly specific for *Mycobacterium tuberculosis,* including activity against multi-drug resistant strains[119]*.* Furthermore, artemisinin retained its activity against *Plasmodium* falciparum. The high affinity of the conjugate for one specific bacteria suggests that it may be possible to use the Trojan horse strategy to design bacteria specific delivery agents[103]. Recently, in our research group a ciprofloxacin **1-18** based siderophore was produced using staphyloferrin A (**1-63**, **Figure 1.31**) as the siderophore component, which showed antimicrobial activity against a range of strains, albeit reduced when compared to the parent antimicrobial ciprofloxacin **1-18**[118].

A significant success in the field of Trojan horses has recently been achieved at Basilea Pharmaceutica. The Trojan horse antimicrobial Bal30072 is currently in phase 1 clinical trials (**Figure 1.33**)[104, 120]. The conjugate

contains a monosulfactam antimicrobial with a dihydropyridone as an iron binding group. Bal30072 **1-65** shows a good spectrum of activity against gram negative bacteria, including several multi-drug resistant strains[120].

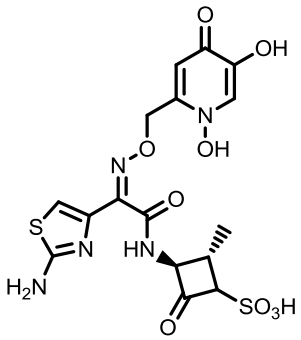

1-65

Figure 1.33: Structure of Bal 30072, a siderophore-monosulfactam drug currently in clinical trials

The variety of conjugates that have been prepared using different siderophore and antimicrobial components demonstrates how powerful a tool the Trojan horse strategy could be against antimicrobial resistance. The versatility of the strategy allows the synthesis of a diverse range of compounds possess both iron chelating and antimicrobial activity. By investigating natural and synthetic iron chelators with existing antimicrobials it may be possible to overcome certain forms of resistance, specifically mechanisms linked to reduced uptake and efflux of antibiotics.

1.7. Overall project aims

This thesis details the development of novel catechol based Trojan horse antimicrobials, specifically the attempted synthesis and characterisation of a Trojan horse based on the *Bacillus* siderophore petrobactin and the fluoroquinolone antimicrobial ciprofloxacin. Furthermore, this thesis details the development of a novel Trojan horse antimicrobial using the Ugi four component condensation. The compounds produce will then undergo biological evaluation to determine if they possess similar

bactericidal activity to the parent antimicrobial. If this is not the case, further experimentation will be performed to elucidate the reason for any observed decrease or increase in activity. It is possible that catechol based Trojan horses may be able to target bacteria which rely on catecholate siderophores such as *Bacillus* species and *E. coli.*

Additionally, the potential of catechol based ligands as metal delivery agents, and as antimicrobials in their own right, will be investigated. Simple ligands will be synthesised and subjected to biological evaluation to establish if they possess bactericidal activity, and the mechanism by which they may be acting.

Additionally, experiments will be undertaken to probe the viability of using carbohydrate transport for the Trojan horse strategy. Several carbohydrate based Trojan horses will be screened under specific carbon limiting conditions to determine whether or not they are taken into bacterial cells via active transport or via a passive uptake mechanism.

2. Studies towards the synthesis of a siderophore-ciprofloxacin conjugate based on petrobactin

2.1. Aims

The aim of the research in this chapter was the synthesis of a Trojan horse conjugate, using ciprofloxacin **1-18** as the antimicrobial component, and an analogue of the *Bacillus* siderophore petrobactin **1-30** as the iron-binding component. The conjugate was designed to incorporate the key iron binding groups of the native siderophore structure, with the ciprofloxacin moiety conjugated via the carboxylic acid of the central citrate.

2.2. Introduction

2.2.1. The stealth siderophore: Petrobactin

Petrobactin **1-30** is a mixed ligand siderophore, containing two catechols and a central citrate. The siderophore was originally isolated from the marine bacteria *Marinobacter hydrocarbonoclasticus* by Butler *et al.* in 2002[74]. Based on NMR analysis of the siderophore, they predicted a bis-catecholate structure with 2,3-configuration around the aromatic ring, linked via a bis-spermidine backbone with a central citrate. They observed that the petrobactin-Fe(III) complex **2-1** can undergo a photolytic ligand to metal charge transfer, this results in decarboxylation of the ligand, followed by oxidation which resulted in the formation of a keto group (**Scheme 2.1**). Butler *et al.* had previously demonstrated that aquachelin, another marine siderophore, was important for iron cycling. They had found that photolysis of the aquachelin Fe(III) complex by UV light resulted in reduction of Fe(III) to Fe(II)[74, 121]. It is possible that bacterial uptake of iron via petrobactin **1-30** utilises the same mechanism to release bound iron into the intracellular medium. The siderophore aerobactin, a siderophore produced by numerous bacterial species, has also been shown to be photoreactive.

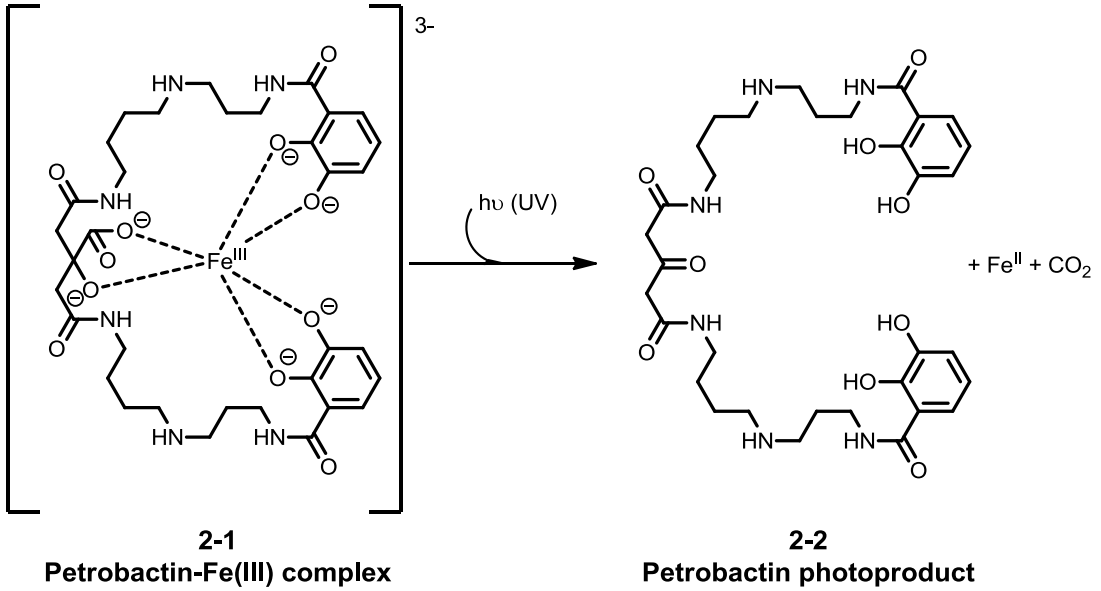

2-1
Petrobactin-Fe(III) complex

2-2
Petrobactin photoproduct

Scheme 2.1: Schematic representation of the photolysis of the petrobactin-Fe(III) complex proposed by Butler *et al*.[74] Based on the originally accepted structure of petrobactin.

Butler *et al.* subsequently found that the structure they initially published for petrobactin **1-30** was incorrect. They synthesised petrobactin with both 2,3-dihydroxy and 3,4-dihydroxybenzamide moieties, and found that the NMR data of the 3,4-configured petrobactin matched the previously published NMR data[122]. While the siderophore was initially isolated from a marine bacterium, in 2005 Ruggiero *et al.* identified it as a key siderophore of the anthrax pathogen *Bacillus anthracis*[123]. This was the first example of petrobactin **1-30** observed in a pathogenic species, although the presence of 3,4-dihydroxybenzamide moieties had previously been observed in *B. anthracis* siderophores[124].

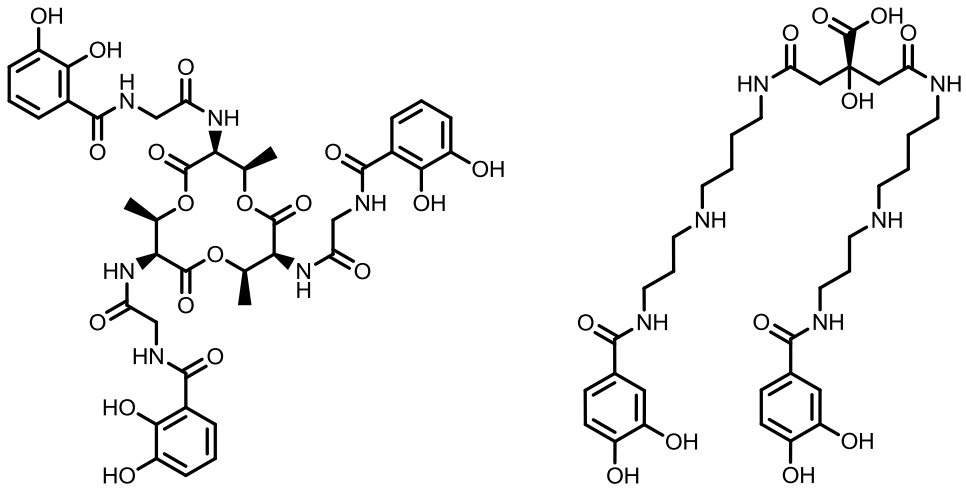

2-3
Bacillibactin

1-30
Petrobactin

Figure 2.1: Structure of *Bacillus* siderophores bacillibactin **2-3** and petrobactin **1-30**

It was found that *Bacillus cereus* also produced petrobactin **1-30**, but *Bacillus thuringiensis* did not[125]. They did however find that all *Bacillus* species they tested produced bacillibactin (**Figure 2.1**) Studies on the siderophores in *B. anthracis* have demonstrated that petrobactin is required for the virulence of the bacterium[126]. The study also found that in low iron media, petrobactin was secreted several hours before the bacterium started producing bacillibactin. A recent investigation into the impact of iron and O_2 concentration on petrobactin and bacillibactin production, demonstrated a repression of bacillibactin production in high iron concentrations[127]. However, they found petrobactin was still produced even at iron concentrations of 20 μM, suggesting that other factors were involved in the regulation of petrobactin biosynthesis. They went on to demonstrate that petrobactin biosynthesis was also regulated by the amount of oxygen available. They observed that accumulation of petrobactin in the extracellular medium was higher in an oxygen rich atmosphere than an atmosphere with low oxygen levels.[127] Additionally they found that high levels of oxygen delayed the repression of petrobactin biosynthesis by iron.

The iron binding properties of petrobactin have been investigated by Raymond *et al.* and Butler *et al.* Both groups observed a p*M* value of approximately 23 at physiological pH[63, 128]. Raymond determined that the photoproduct of petrobactin **2-2** had a higher affinity for iron, with a p*M* of 24.1 at physiological pH. Byers had previously established that *B. anthracis* could scavenge iron that was bound by transferrin, as well as hemoproteins and heterologous siderophores[124]. Raymond investigated the rate at which petrobactin **1-30** could remove iron from transferrin. They found that the k_{max} for the process was $12.3x10^{-2}$ min^{-1}, this was six times the published k_{max} for enterobactin **1-34** ($2.1x10^{-2}$ min^{-1}) by Harris *et al.* in 1979[63, 129]. The efficiency with which petrobactin **1-30** removes iron from transferrin suggests transferrin-bound iron is the primary iron source utilised by *Bacillus* species during initial stages of infection[63].

2.2.2. Biosynthesis of petrobactin

The use of 3,4-dihydroxybenzoic acid in petrobactin **1-30**, raised questions about the biosynthetic pathway of the siderophore. Hanna *et al*. first identified the importance of six genes to the virulence of *B. anthracis; AsbABCDEF*[130]. Several studies have elucidated the individual roles of the proteins encoded by the gene cluster. Challis *et al.* demonstrated that the AsbA protein catalysed the ATP dependent condensation of spermidine to the central citrate of the siderophore[131]. They subsequently found that AsbB protein fulfilled a similar role, catalysing the condensation of a second spermidine moiety onto the central citrate (**Scheme 2.2**)[132].

The AsbC, AsbD and AsbE proteins work in a pathway to catalyse the condensation of 3,4-dihydroxybenzoic acid moiety **2-7** onto the N^8- N^8- bis-spermidyl citrate.

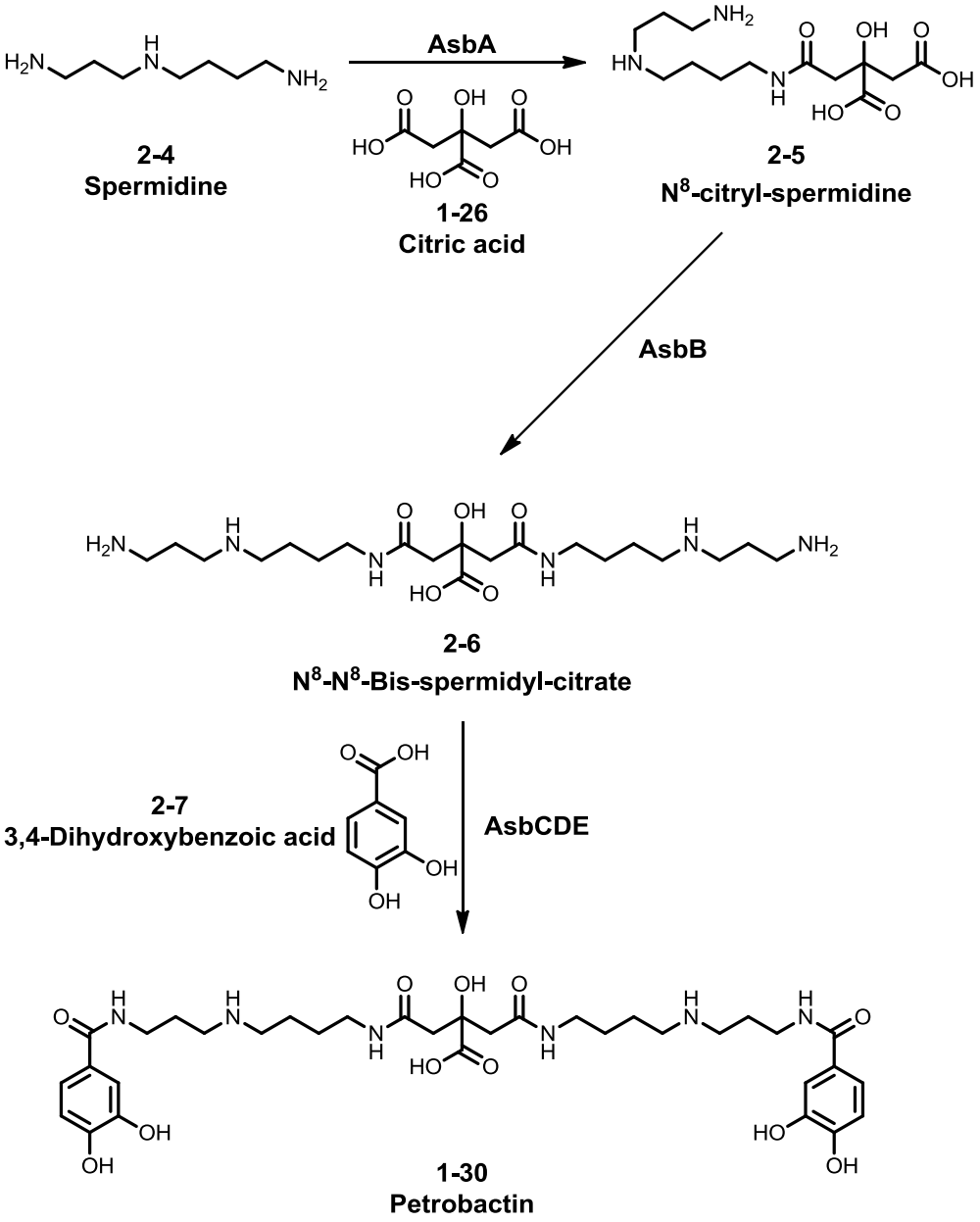

Scheme 2.2: Biosynthesis of petrobactin proposed by Challis *et al*.

The AsbF protein is responsible for the formation of the 3,4-dihydroxybenzoic acid moiety. The gene encoding AsbF had previously been observed in bacteria that produced 3,4-dihydroxybenzoic acid[124-125]. Koppisch *et al*. postulated that the 3,4-dihydroxybenzoic acid moiety was a by-product of the shikimate pathway[133]. Further research into the role of

AsbF by Koppisch *et al.* and Pfleger *et al*. determined that the protein is a 3-dihydroshikimate dehydratase[134-135].

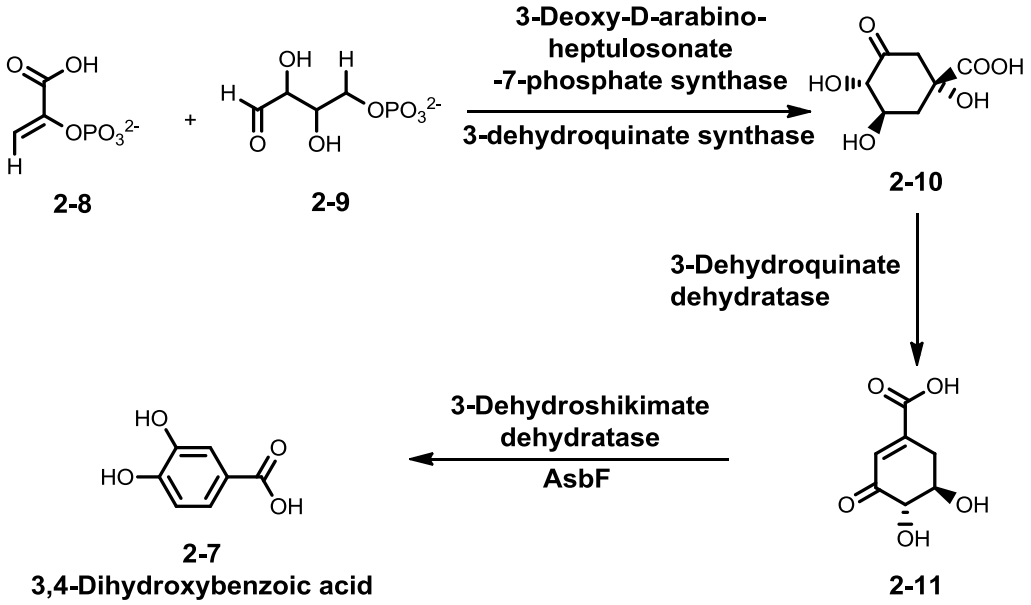

Scheme 2.3: Proposed biosynthetic pathway to 3,4-dihydroxybenzoic acid from Koppisch *et al.*, showing the roles of several enzymes including the proposed role of the key AsbF protein (3-dehydroshikimate dehydratase)

2.2.3. Total synthesis of petrobactin

The total synthesis has been achieved by several research groups[122, 136-137]. The syntheses all used a fragment based approach, synthesising the individual building blocks before systematically coupling them together to form the complete siderophore.

2.2.3.1. Synthesis of the catechol subunit

To prepare the catechol groups, the hydroxyls were benzyl protected. Butler used the method of Rastetter *et al.* reacting 3,4-dihydroxybenzaldehyde with benzyl chloride and K_2CO_3 in EtOH[122, 138]. Phanstiel used a similar method, utilising benzyl bromide instead of benzyl chloride[137]. Low took an alternative approach, reacting 3,4-dihydroxybenzoic

acid with MeOH to generate a methyl ester, then performing the benzyl protection using benzyl bromide and K_2CO_3 in DMF[136]

2.2.3.2. Coupling and deprotection of the petrobactin backbone

To generate the full siderophore backbone, several methods have been employed. The initial step in the published total syntheses is the formation of a *tert*-butyl protected citrate. All three reported total syntheses achieved this using a procedure published by Milewska *et al.*, where 1,5-dimethyl citrate was trans-esterified using *tert*-butyl acetate[139]. The second step was to couple the catechol unit to the spermidine linker. Butler and Phanstiel both achieved this by activating the benzylated catechol. 3,4-bis(benzyloxy)benzoic acid was reacted with oxalyl chloride to yield 3,4-bis(benzyloxy)benzoyl chloride. The acid chloride was then reacted with the free amine of spermidine to generate the catechol-spermidine moiety. Low *et al.* used an alternative method, whereby the methyl ester of 3,4-bis(benzyloxy)benzoic acid was reacted with the spermidine linker by ester-amide exchange[136]. To assemble the back bone, the spermidine catechol moiety was coupled to the central citrate (**Scheme 2.4**). Phanstiel and Low both achieved this by generating a disuccinimidyl ester of the *tert*-butyl citrate, and reacting it with the catecholate-spermidine moiety in triethylamine, dioxane and DCM[136-137, 139]. Butler also used an activated form of the citrate moiety, utilising a method originally published by Miller *et al*. they generated a di-nitrophenol ester, which they subsequently reacted with the catecholate-spermidine moiety using DIPEA in MeCN[122, 140]. The final stage of the total synthesis was the removal of the *tert*-butyl and benzyl ether protecting groups. Butler and Low both removed the ester via TFA mediated hydrolysis in DCM, Phanstiel utilised an HCl mediated hydrolysis in acetone. All three published syntheses removed the benzyl ether protecting groups by hydrogenolysis with a Pd/C catalyst, with Butler and Low performing the deprotection in acetic acid, and Phanstiel using EtOH. In terms of reaction economy, the synthesis published by Butler *et al.* was the most efficient, with the highest overall yield (25%) and smallest number of

reaction steps (7 steps)[122]. While the synthesis by Phanstiel was less efficient, they were able to use it to generate several homologues of petrobactin in addition to the native structure[137].

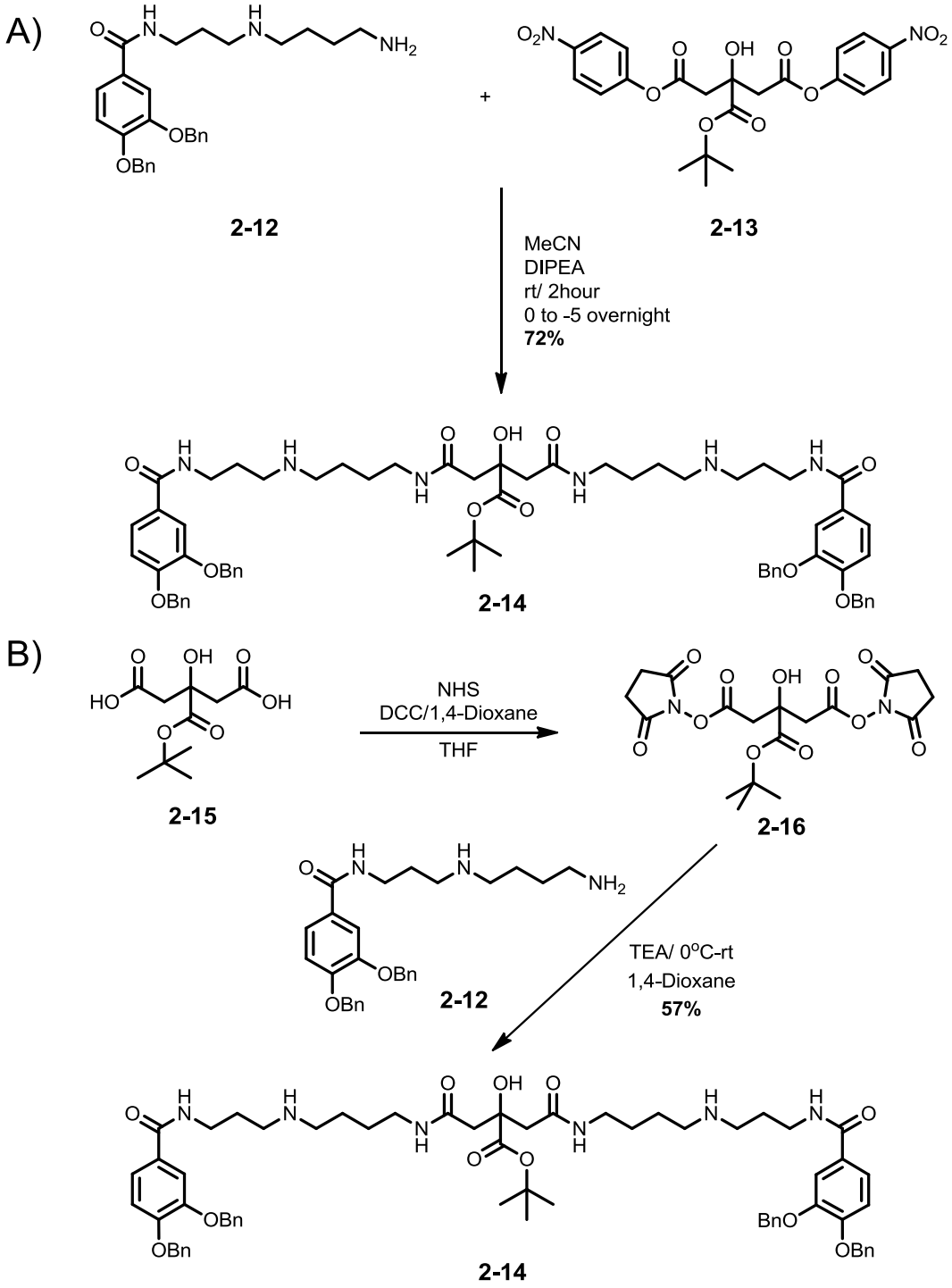

Scheme 2.4: Assembly of the petrobactin backbone by **A)** Butler *et al.* and **B)** Gardner *et al.*/Low *et al*.

2.2.4. Transport of petrobactin

The uptake mechanism for petrobactin **1-30** is similar to other siderophores, using TonB dependent uptake, with the energy provided by ATP hydrolysis[141]. The first receptors were identified and characterised by Raymond *et al.* in 2009. They identified two binding proteins in *Bacillus cereus*, named FatB and FpuA. FatB showed a broad range of binding, including to the 3,4-dihydroxybenzyl moiety and the petrobactin iron complex photoproduct. However, FpuA showed a high level of specificity, only binding to free petrobactin and the iron complex[142]. They also identified a further binding protein from *Bacillus subtilis*: YclQ, which has similar properties to FatB, in that it binds selectively to both iron free and ferric petrobactin, 3,4-dihydroxybenzoic acid and the ferric complex photoproduct. The crystal structure demonstrated that YclQ was capable of binding for petrobactin[143]. YclQ was subsequently renamed FpiA after Oberthür *et al.* used synthetic petrobactin ligands to confirm the binding of the protein to petrobactin, and subsequently demonstrated that it was essential for petrobactin transport in *Bacillus subtilis*[144].

Recent research has examined transport of petrobactin in *Bacillus anthracis*, as it has been established that petrobactin is essential for virulence in the pathogen[92, 145-146]. Analysis of the FatB and FpuA proteins by Hanna *et al.* demonstrated that FatB was not required for petrobactin transport in *B. anthracis*[147], despite being able to bind petrobactin[142]. FpuA however was found to be essential for petrobactin uptake, as growth was attenuated in iron depleted conditions, even with purified petrobactin added. In a later study, they were able to elucidate more details about the overall uptake mechanism, describing two permeases and three ATPases that were required for petrobactin transport[141]. It was found that only one of the two permeases, FpuB or FatCD, was required. However if the ATPase corresponding to that permease was missing, attenuation of growth in iron limited conditions was observed.

2.3. Results and discussion

2.3.1. Towards the synthesis of a ciprofloxacin-petrobactin analogue conjugate

The analogue designed in this research will retain the key binding groups, the central citrate and two catechol units. The analogue will use a 2,3-dihydroxybenzoic acid moiety for the catechol groups, and the length of the backbone will be decreased. Both modifications could influence the iron binding ability of the siderophore. The conjugation of ciprofloxacin may also influence iron binding and bacterial uptake, as conjugation will be to one of the chelating groups within the siderophore structure, the citrate unit. The synthesis of the 2,3-configured petrobactin analogue was chosen as the catechol chemistry is well established[148].

2.3.1.1. Components of the target molecule

In order to establish a synthetic route to the target molecule **2-17**, it was disconnected to individual components (**Figure 2.2**) to give a fragment-based synthetic scheme, similar to that employed in total synthesis of the full petrobactin siderophore[122, 136-137]. The target molecule is composed of four key fragments: 2,3-dihydroxybenzaldehyde **2-14**, 1,2-diaminoethane **2-15**, citric acid **1-23** and the antimicrobial component: ciprofloxacin **1-18**. The structure was subsequently revised to include a butyl linked backbone, as the chemistry to prepare the catechol-amine unit using 1,4-diamino butane and 2,3-bis(benzyloxy)benzoic acid was already established. Additionally, a glycine spacer was added to ciprofloxacin **1-18** to generate a primary amine and allow a more efficient coupling to the analogue backbone (**section 2.3.2.8.).**

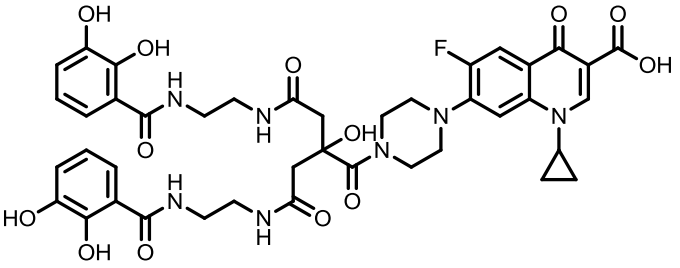

2-17

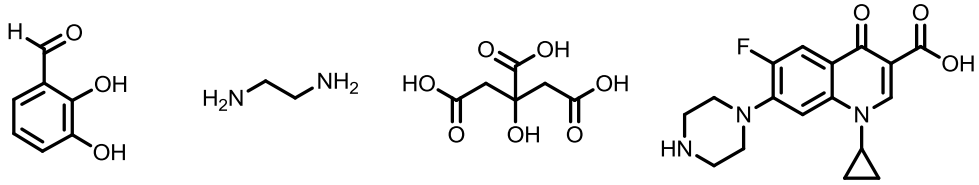

2,3- Dihydroxy benzaldehyde 2-18

1,2-Diamino ethane 2-19

Citric acid 1-26

Ciprofloxacin 1-18

Figure 2.2: Structure and initial components of the target petrobactin analogue-ciprofloxacin conjugate **2-13**

The synthesis of homologues of petrobactin and the total synthesis of petrobactin **1-30** has also been achieved by several groups[122, 136-137]. The chemistry employed in these investigations was the basis of the synthesis of the target molecule **2-17**[122, 136-137].

*2.3.1.2. Protection of ciprofloxacin **1-18** by esterification*

The first step in the synthesis of the proposed petrobactin analogue **2-17** was the protection of the drug component, ciprofloxacin **1-18**. Ciprofloxacin has zwitterionic character at neutral pH, consequently it has limited solubility in both aqueous and organic solvents; therefore protection of one of these groups was undertaken to increase the solubility of the compound in organic solvents. In addition, as the β-keto acid system is required for antimicrobial activity[35], carboxylic acid protection was used to protect the β-keto acid from unwanted side reactions. To protect the carboxylic acid, the methyl ester of ciprofloxacin **1-18** was synthesised[117].

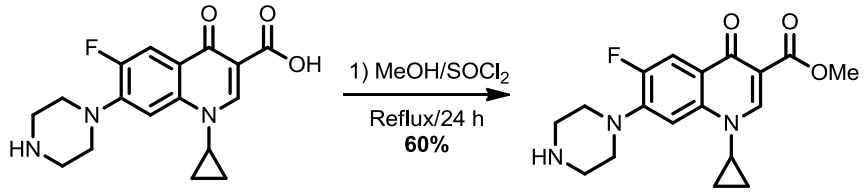

1-18 **2-20**

Scheme 2.5: Synthesis of the methyl ester of ciprofloxacin **2-16** using thionyl chloride

The reaction was carried out as shown by refluxing ciprofloxacin **1-18** in MeOH with thionyl chloride (**Scheme 2.5**). After work up, **2-20** was isolated in 60% yield. Formation of the product was supported by ^{1}H NMR spectroscopy, with a singlet with a relative integration of three at 3.89 ppm corresponding to the methyl ester evident in the spectra. ESI mass spectrometric analysis gave a peak with *m/z* 346.16, corresponding to the $[M+H]^{+}$ form of **2-20**.

2.3.1.3. Preparation of the central citrate moiety

As the citric acid has three carboxylic acid groups, the central carboxylic acid required protection prior to being incorporated in the synthesis (**Scheme 2.6**). This ensures that after the backbone is synthesised, the central carboxylic acid can be deprotected, so it is available for chemical conjugation to the methyl ester of ciprofloxacin **2-20**.

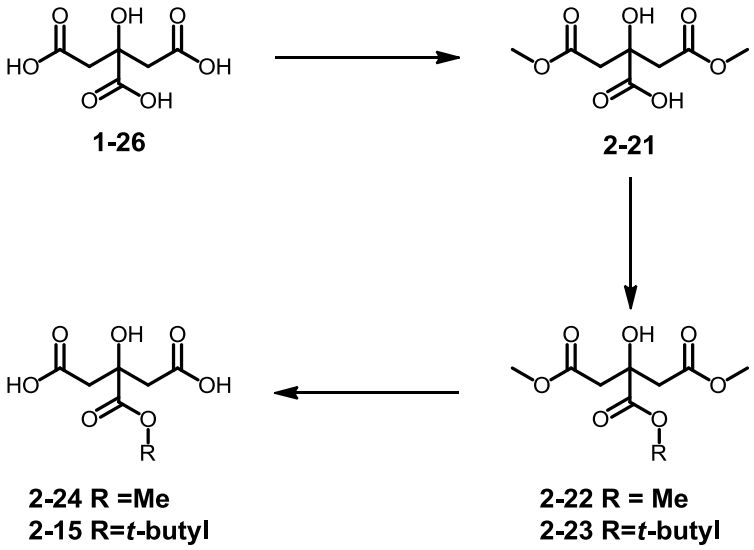

Scheme 2.6: Protecting group strategy to give mono-protected citrate

The synthesis of 1,5-dimethyl citrate **2-21** was achieved by refluxing citric acid **1-26** in MeOH with H_2SO_4 (**Scheme 2.7**)[149-150].

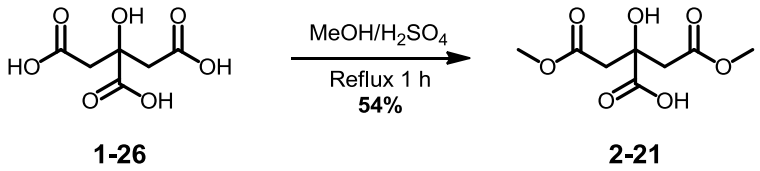

Scheme 2.7: Synthesis of 1,5-dimethyl citrate by acid catalysed esterification of citric acid

To isolate **2-21** a hybrid purification process of two published procedures was used. The first stage of the purification used the method of Hirota *et al.*[149]. The solution was neutralised using $Ca(OH)_2$, the resultant precipitate filtered off, and the filtrate concentrated *in vacuo*[149]. The remainder of the purification used the procedure of Guo *et al*.[150]. This involved sonicating the solid from concentration of the filtrate in H_2O and the removal of insoluble material The filtrate was acidified to pH zero using conc. HCl and the precipitate isolated by filtration. The precipitate was then redissolved using $NaHCO_{3(aq)}$ and extracted using $CHCl_3$. The aqueous

phase was then reacidified to pH zero using conc. HCl, resulting in precipitation of the product as a white solid. After purification, 1,5-dimethyl citrate **2-21** was isolated in 54% yield. The successful synthesis of the product was supported by ^{1}H NMR spectroscopy with a singlet at 3.64 ppm with a relative integration of six due to the terminal methyl groups present in the spectrum. ESI mass spectrometric analysis showed peaks with *m/z* 221.06 and 243.04, corresponding to the $[M+H]^+$ and $[M+Na]^+$ ions of the required product **2-21**. A by-product of the reaction was 1,3,5-trimethyl citrate, which was isolated in 15% yield [151].

Protection of the secondary carboxylic acid group used the method of Deacon *et al.* reacting 1,5-dimethyl citrate with *tert*-butyl acetate in the presence of 70 % perchloric acid (**Scheme 2.8**)[150].

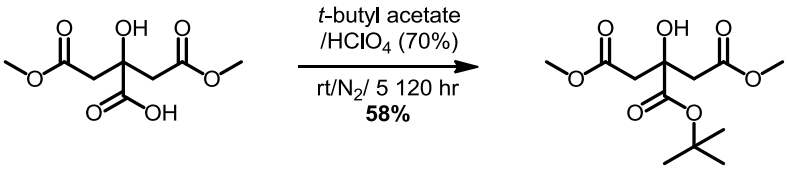

2-21 **2-23**

Scheme 2.8: Synthesis of 3-*tert*-butyl-1,5-dimethyl citrate **2-23** using the method of Deacon *et al.*

Initially a procedure by Phanstiel *et al.* was followed, this utilised a 10:1 (*t*-butyl acetate: 1,5-dimethyl citrate) molar ratio[150], ^{1}H NMR spectroscopy of **2-23** showed a singlet resonance at 1.49 ppm with relative integration nine corresponding to the *t*-butyl group present in the spectra. ESI mass spectrometry gave a peak with *m/z* of 299.11, corresponding to the $[M+Na]^+$ ion of the product **2-23**. However, the ESI mass spectrometric analysis also gave a peak with *m/z* of 221.06, suggesting the presence of unreacted 1,5-dimethyl citrate **2-21**. Subsequently a method by Deacon *et al.* was attempted[152]. This method used a greater excess of *tert*-butyl acetate (~15:1, *t*-butyl acetate: 1,5-dimethyl citrate molar ratio). The product **2-23**

was isolated as pale yellow oil, in 58% yield. ^{1}H NMR and ESI mass spectrometric data was obtained. The peak with *m/z* of 299.11 corresponding to the $[M+Na]^+$ of **2-23** was observed in the ESI mass spectrum, but no peak with mass corresponding to **2-21** was observed, suggesting a pure product. In the ^{1}H NMR spectrum the ratio of the integrations of the *t*-butyl group and the methyl esters was 9:6, as expected for the product **2-23**.

To deprotect 1,5-dimethyl-3-*tert*-butyl citrate **2-23**, the method by Phanstiel *et al.* was used (**Scheme 2.9**)[150].

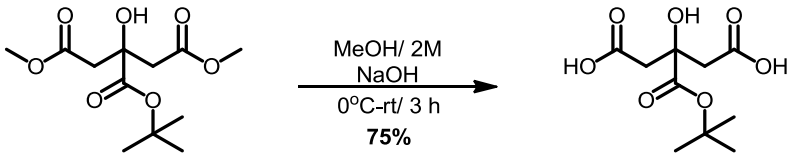

2-23 **2-15**

Scheme 2.9: NaOH mediated deprotection of 3-*tert*-butyl 1,5-dimethyl citrate **2-23**

The reaction gave **2-15** as a white solid in 75% yield. ^{1}H NMR spectroscopic analysis supported successful formation that the product **2-15** with the loss of a singlet at 3.64 ppm with relative integration of six corresponding to the two terminal methyl esters. In addition, ESI mass spectrometric analysis gave two peaks with *m/z* 249.10 and 271.08, corresponding to the $[M+H]^+$ and $[M+Na]^+$ ions of the product **2-15** respectively.

A drawback of this synthetic step was the five day reaction time required. Additionally the reaction was unreliable, giving variable yields and purity as unreacted 1,5-dimethyl citrate **2-21** was often observed. The *tert*-butyl ester was also found later to be an unsuitable protecting group (Section *2.3.1.4*), as the benzyl ethers used in the protection of the catechol units did not survive a HCl-mediated deprotection and consequently would be unlikely to survive the required TFA mediated deprotection of the *t*-butyl ester[122, 137].

An alternative strategy was adopted[149], 3-monomethyl citrate **2-24** was prepared (**Scheme 2.10**)[149]. The process involved taking the previously synthesised 1,5-dimethyl citrate **2-21** and performing an additional esterification to produce 1,3,5-trimethyl citrate **2-22**. This was then deprotected to produce 3-monomethyl citrate **2-24**.

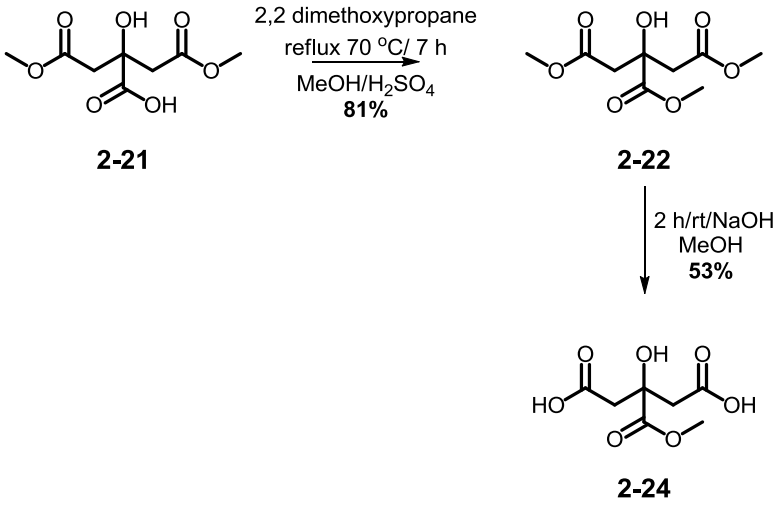

Scheme 2.10: Preparation of 3-monomethyl citrate **2-24** in two steps from 1,5-dimethyl citrate.

1,3,5-trimethyl citrate **2-22** was deprotected using a variation of the method published of Hirota *et al*.[149]. Commercially available 1,3,5-trimethyl citrate **2-22** (Fluka) was used, and the reaction gave **2-24** as a white crystalline solid in 53% yield. Presence of the product was supported by ^{1}H NMR spectroscopic analysis with a singlet at 3.61 ppm with a relative integration of three for the central methyl ester present, and the loss of the six proton singlet corresponding to the terminal methyl esters. ESI mass spectrometric analysis gave two peaks with *m/z* 207.05 and 229.03 corresponding to the $[M+H]^+$ and $[M+Na]^+$ ions of the required product **2-24**. Due to the prohibitive cost of purchasing 1,3,5-trimethyl citrate **2-22** from a commercial source, it was necessary synthesise 1,3,5-trimethyl citrate **2-22** from 1,5-dimethyl citrate **2-21**. To produce the 1,3,5-trimethyl citrate **2-22**, esterification of 1,5-dimethyl citrate was performed using an acid catalysed

esterification with 2,2-dimethoxypropane. After work up, the product **2-18** was isolated in 81% yield. This successful synthesis was supported by the presence of two singlets in the ^{1}H NMR spectrum at 3.83 ppm, with a relative integration of three, and 3.69 ppm, with a relative integration of six, corresponding to the central and terminal methyl groups respectively. ESI mass spectrometric analysis gave two peaks with *m/z* 235.08 and 257.06 corresponding to the $[M+H]^+$ and $[M+Na]^+$ ions of the required product **2-22** respectively.

2.3.1.4. Preparation of the catechol subunit

The catechol subunit is an integral part of the target molecule and while petrobactin contains a 3,4-dihydroxybenzamide moiety, it was decided to initially synthesise analogues based upon 2,3-dihydroxybenzamide acid moieties as procedures for these reactions were well established (**Scheme 2.11**)[138, 153-154]. Additionally, due to the salicylate binding mode, 2,3-configured catechol amides have a higher iron affinity[77, 155-156]. Furthermore, due to intramolecular hydrogen bonding, 2,3-configured catechols are less susceptible to oxidation.

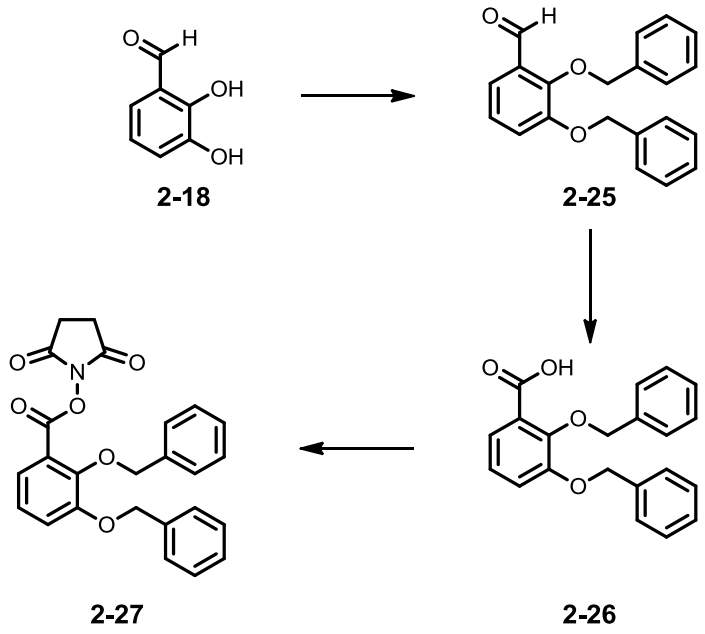

Scheme 2.11: The proposed synthetic route from 2,3-dihydroxybenzaldehyde to the activated ester of the protected benzoic acid

The first step was to protect the hydroxyl groups at the 2- and 3-positions of the dihydroxybenzaldehyde (**Scheme 2.12**). This was required to protect the hydroxyl groups from unwanted side reactions, specifically oxidation of the catechols to the corresponding quinone. To protect 2,3-dihydroxybenzaldehyde **2-18,** it was refluxed in dry EtOH with benzyl chloride. After purification **2-25** was isolated in 92% yield. ESI mass spectrometric analysis gave three peaks with *m/z* 319.13 and 336.16 and 341.12. These corresponded to the $[M+H]^+$, $[M+NH_4]^+$ and $[M+Na]^+$ ions of the required product **2-25**. ^{1}H NMR spectroscopy also supported successful formation of **2-25.**A 10 H multiplet in the aromatic region from 7.38-7.21 ppm due to additional benzyl rings was observed in addition to two singlets with relative integration two at 5.26 and 5.17ppm corresponding to the benzyl CH_2 groups observed.

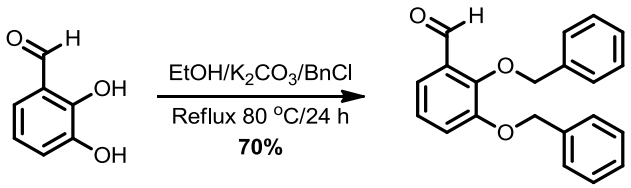

2-18 **2-25**

Scheme 2.12: Protection of 2,3-dihydroxybenzaldehyde

However, there was evidence of impurities in the ^{1}H NMR spectrum suggesting that the initial method of purification by partitioning between EtOAc/H_2O was insufficient. Consequently, the procedure was modified in subsequent reactions, the reaction solution was filtered, and the filtrate evaporated to dryness *in vacuo*. The resultant yellow solid was then recrystallised from hot methanol and isolated as a pale brown crystalline solid in 70% yield.

The next step in the synthesis of the catechol unit was a sodium chlorite mediated oxidation of **2-25** to the corresponding carboxylic acid **2-26**, a variation of the method used by Chimiak *et al*.[153] was used. 2,3-bis (benzyloxy)benzaldehyde **2-25** was reacted with alternating portions of sulfamic acid and sodium chlorite. (**Scheme 2.13**). After reaction **2-26** was isolated in 90% yield.

ESI mass spectrometry confirmed the presence of a molecular ion with an *m/z* value of 335.12 corresponding to the $[M+H]^+$ ion of the required product **2-26**. ^{1}H NMR spectrometry confirmed the identity of **2-26**.

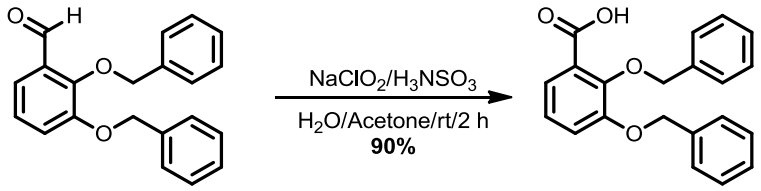

2-25 **2-26**

Scheme 2.13: Oxidation of the protected aldehyde to the corresponding carboxylic acid.

2,3-bis(benzyloxy)benzoic acid **2-26** was then converted to a succinimidyl ester, to allow rapid coupling to the diamine when assembling the siderophore backbone. The reaction was performed using DCC as a coupling agent[153]. 2,3-bis(benzyloxy)benzoic acid was dissolved in 1,4-dioxane with *N*-hydroxysuccinimide and DCC (**Scheme 2.14**)

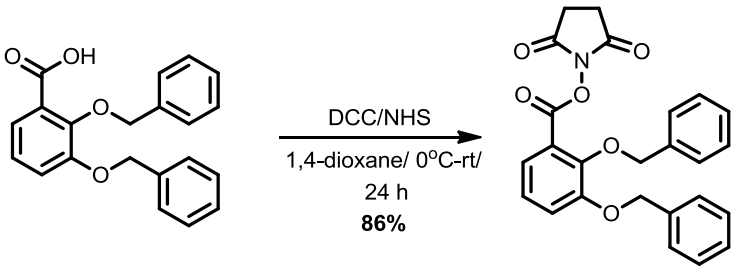

2-26 **2-27**

Scheme 2.14: Preparation of activated ester of the bis(benzyloxy)benzoic acid using the method of Chimiak *et al*.

After workup **2-27** was isolated as a white crystalline solid in 86% yield. The presence of a broad singlet in the ^{1}H NMR spectrum at 2.8 ppm with a relative integration of four indicated the presence of the succinimidyl CH_2. A signal at 169.2 ppm in the ^{13}C NMR spectrum confirmed the presence of the carbonyl (C=O) groups of the succinimidyl ring. ESI mass spectrometric analysis gave three peaks with *m/z* 432.14, 449.17 and 454.13 corresponding to the $[M+H]^+$, $[M+NH_4]^+$ and $[M+Na]^+$ ions of the required product **2-27**.

2.3.1.5. Assembly of the siderophore backbone:

With the central citrate **2-24** and terminal catecholate subunits **2-27** prepared, the two catechol units were ready to link via the citrate using an alkyl diamine backbone. Rather than using the bis-spermidine linker found in native petrobactin[122], a shorter 1,2-diaminoethane linker **2-19** was used, to create a smaller, more compact siderophore (**Scheme 2.15**). The advantage of this is a reduction in molecular weight, which should aid uptake through outer membrane porins (OMPs) if the conjugate isn't actively transported. Additionally, a shorter linker reduces the entropic cost of chelating Fe(III) in solution. One disadvantage is that a petrobactin analogue with a significantly shorter linker may not be recognised for active transport.

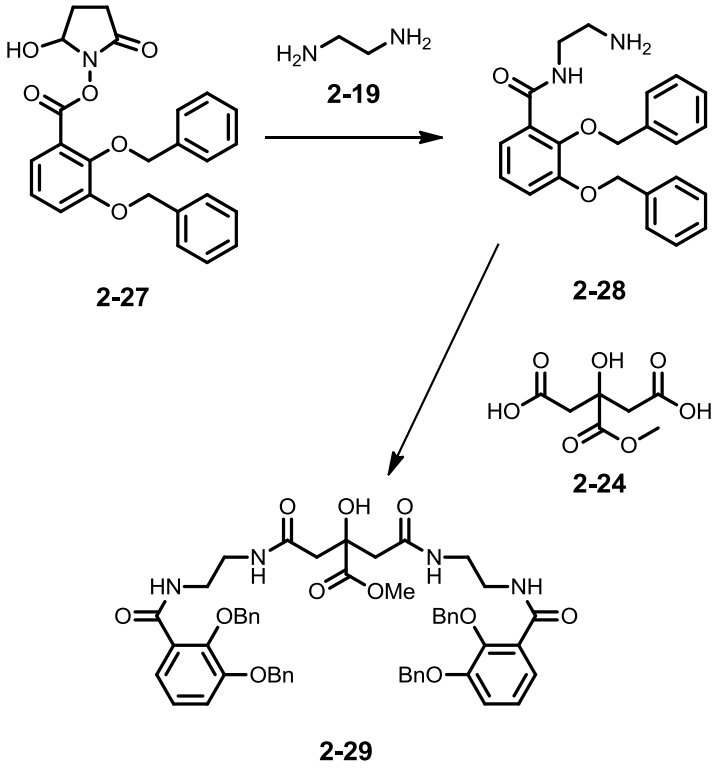

Scheme 2.15: Route to petrobactin analogue with ethyl linked backbone

To enable the coupling of the diamine component to the catechol moiety, it was necessary to protect one of the amine groups of the 1,2-diaminoethane using a *tert*-butyloxycarbonyl (Boc) protecting group, to

prevent the formation of dimers. The method of Keillor *et al.* was followed for the synthesis[157]. A solution of Boc_2O in DCM was added dropwise to an excess (10 equivalents) of 1,2–diaminoethane **2-19**.

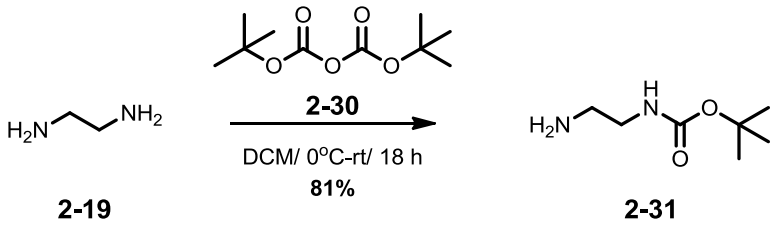

Scheme 2.16: Boc protection of 1,2-diaminoethane using a combination of the methods published by Keillor *et al.* and Saari *et al.*

The product **2-31** was purified using the method of Saari *et al*.[158] to give the product **2-31** in 81% yield. ^{1}H NMR analysis showed a singlet at 1.5 ppm with a relative integration of nine, indicating the presence of the *tert*-butyl group. ESI mass spectrometric analysis gave a peak at *m/z* 161.13 corresponding to the $[M+H]^+$ ion of the required product **2-31**.

The protected diamine was then conjugated to the benzyl protected catechol unit (**Scheme 2.17**).

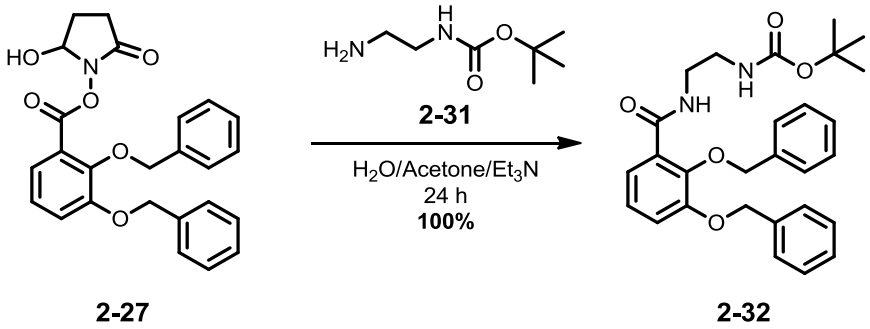

Scheme 2.17: Coupling of the Boc protected 1,2-diaminoethane **2-32** to the activated ester of the catechol moiety

To ensure full conversion of the activated ester **2-27**, a slight excess of the Boc protected diamine **2-31** was used (1.1: 1 molar ratio) and the product

2-32 was isolated in quantitative yield. ESI mass spectrometry showed two peaks at *m/z* 477.24 and 499.22 corresponding to the $[M+H]^+$ and $[M+Na]^+$ ions of the product **2-32**. In addition ^1H NMR analysis showed a triplet resonance at 7.99 ppm, corresponding to the amide proton adjacent to the catechol unit.

The next stage of the synthesis was the removal of the Boc protecting group to allow conjugation of the catechol unit to the central citrate. The deprotection was first attempted by using a procedure by Han *et al.*[159].

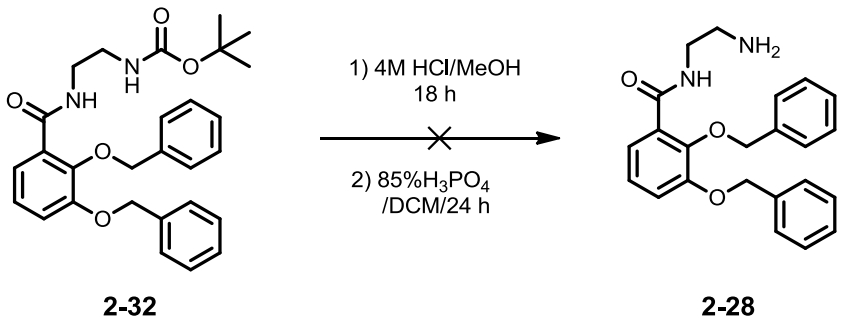

2-32 **2-28**

Scheme 2.18: Attempted deprotection of the Boc protected catechol amine using two methods of acid hydrolysis.

After reaction with 4 M HCl in MeOH, ^1H NMR spectroscopy showed that the resonance at 1.5 ppm of relative integration 9 was absent from the spectrum. However, the two singlet resonances of relative integration two at 5.0 ppm and the multiplet with a relative integration of ten in the aromatic region were also absent from the spectrum. This indicated that the acidic conditions had removed both the Boc protecting group, and the benzyl ethers.

The reaction was repeated using a reduced reaction time. ESI mass spectrometry indicated that the required product **2-28** was present with a peak of *m/z* 377.18. However, the main molecular ion appeared with an *m/z* of 287.14, consistent with one benzyl ether removed, **2-33** and **2-34**. An *m/z*

of 197.09 consistent with a fully deprotected product was also present. This suggested a mixture of products had been formed (**Figure 2.3**).

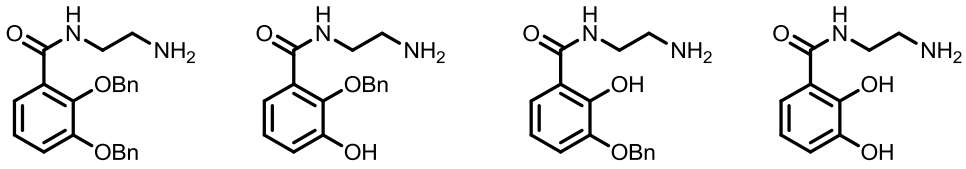

2-28 **2-33** **2-34** **2-35**

Figure 2.3: Compounds formed from the attempted acid-mediated removal of the Boc protecting group

As the benzyl protecting groups on the catechol subunit were sensitive to 4 M HCl, a milder set of conditions by Li *et al*. was used[160]. This method used 85% H_3PO_4 for the deprotection (**Scheme 2.18**). After three hours, TLC analysis of the reaction mixture suggested successful deprotection of the amine. After workup ESI mass spectrometry showed formation of **2-28** as a peak with *m/z* 377.18 was observed in the spectrum. However, an *m/z* of 499.22 consistent with the $[M+Na]^+$ ion of the starting material was also present, ^{1}H NMR analysis showed a singlet at 1.34 ppm with a relative integration of nine, confirming that the Boc protecting group was still present. The reaction was repeated, extending the reaction time to 24 h. However, the result of the reaction was the same.

A procedure by Duhme *et al.*[161] coupled the 2,3-bis(benzyloxy)benzoic acid unit **2-26** directly to a diamine (**Scheme 2.19**). As this procedure utilised 1,4-diaminobutane **2-39**, the design of the target molecule was altered accordingly to incorporate this change (**Figure 2.4**).

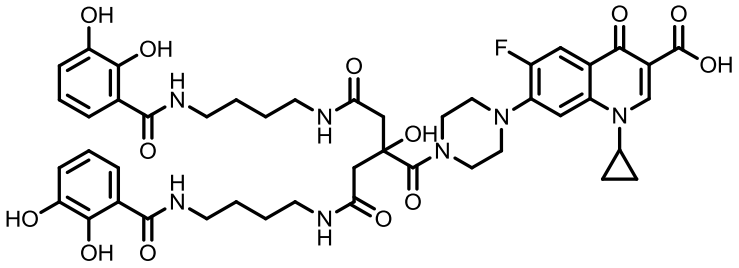

2-36

Figure 2.4: Updated target structure incorporating 1,4-diamino butane linker

N,N'-carbonyldiimidazole mediated coupling was used and after work up **2-40** was isolated as a white precipitate in 54% yield. Successful formation of the product was confirmed by the presence of a peak with *m/z* 405.21 in the ESI mass spectrum corresponding to the $[M+H]^+$ ion of **2-40**. Further confirmation was provided by the presence of a triplet with a relative integration of one at chemical shift 8.25 ppm, corresponding to the amide proton in the ^1H NMR spectrum.

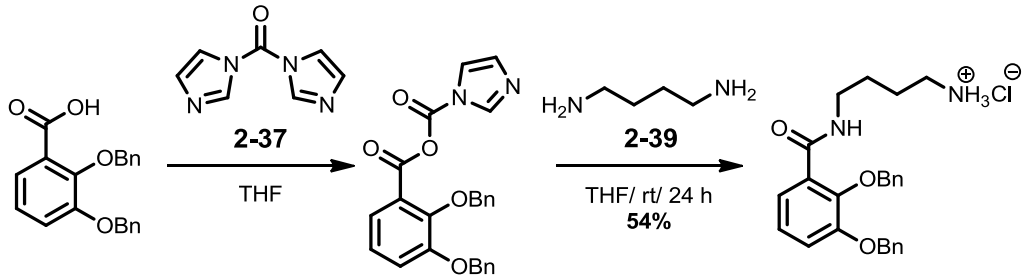

2-26 **2-38** **2-40**

Scheme 2.19: Synthesis of benzyl protected aminochelin using the synthesis published by Duhme *et al.*[161]

2.3.2. Synthesis of a protected petrobactin analogue

2.3.2.1. Attempts at coupling using existing literature procedures

To prepare the backbone of the analogue, it was decided to use the method published by Gardner et al. and Low *et al.*, generating a

disuccinimidyl ester of the protected citrate and reacting this with benzyl protected aminochelin **2-40** (**Scheme 2.4**) The reaction was performed as described in the literature, on a larger scale[136-137].

The first stage of the reaction proceeded as described in the literature, with a precipitate of urea being observed. The second phase of the reaction was stirred for 24 hours. The reaction mixture was then worked up and purified according to the literature procedure[137]. However, analysis by ESI mass spectrometry showed that the molecular ion of the expected product at *m/z* = 979.4 was not present. ^{1}H NMR analysis also showed a mixture of compounds as there were multiple resonances in the range 4.9-5.2 ppm, where there should only have been two resonances, with relative integration four corresponding to the benzyl CH_2 groups.

2.3.2.2. Coupling with HBTU

The use of HBTU as the coupling agent was investigated (**Scheme 2.20**). Formation of **2-41** was confirmed by ^{1}H NMR spectroscopy due to the presence of a triplet resonance at 6.84 ppm, with a relative integrations of two, corresponding to the amide protons adjacent to the central citrate. The loss of a broad signal at 8.07 ppm corresponding to the NH_2 group of aminochelin was also observed. In the ESI mass spectrometric analysis, peaks with *m/z* 979.44 and 1001.42 were identified, corresponding to the $[M+H]^+$ and $[M+Na]^+$ ions of **2-41**. However, there was a problem with the synthesis. Although initially promising, close inspection of the ^{1}H NMR spectrum showed there was also a singlet resonance at 2.80 ppm which did not correspond to anything in the structure of **2-41**. Integration of this resonance gave a relative integration of twelve, which suggested the impurity was a by-product of HBTU, tetramethyl urea[162]. The suggested methods for removal of the impurity were washing with H_2O or toluene[163]. Unfortunately, the product was also toluene soluble, rendering this method unsuitable. It was also attempted to remove the impurity by sonicating the product in H_2O,

however while this reduced the amount of tetramethyl urea present, it did not remove it entirely.

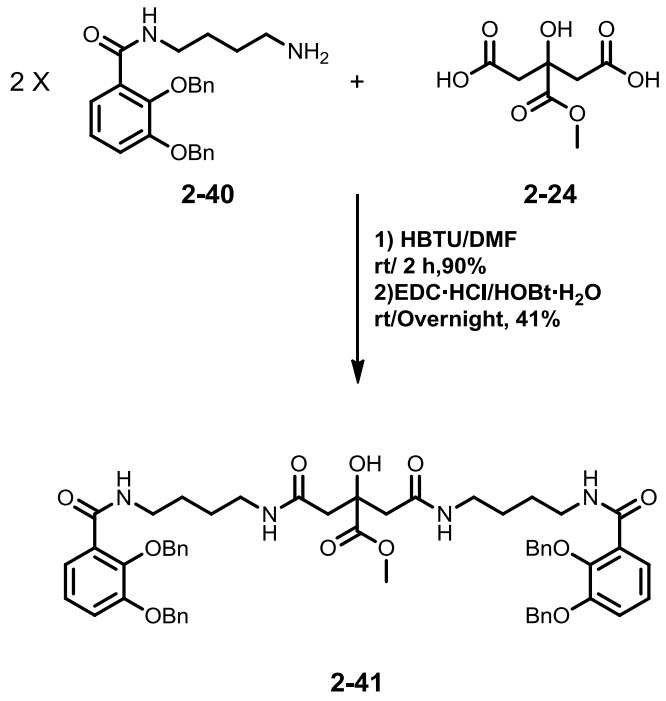

2-41

Scheme 2.20: Formation of the protected petrobactin analogue **2-41** via a 1) HBTU mediated coupling, 2) EDC·HCl mediated coupling

2.3.2.3. Coupling with EDC·HCl and HOBt·H_2O

Due to the difficulties in removing tetramethyl urea from **2-41**, an alternative method using EDC·HCl/HOBt·H_2O was investigated. After reaction and workup successful formation of the product **2-41** was confirmed by ESI mass spectrometry and ^{1}H NMR spectroscopy. The disadvantage of using EDC·HCl and HOBt·H_2O is a longer reaction time, and a lower yield of 41%, however, a pure product was obtained (**Scheme 2.20**).

*2.3.2.4. NaOH mediated deprotection of **2-41***

The methyl ester of the analogue backbone **2-41** was deprotected using the method of Theodorou *et al*.[164]. The protected analogue **2-41** was

dissolved in a 9:1 mixture of DCM: MeOH and the solution adjusted to pH 12 by the addition of 2 M methanolic NaOH (**Scheme 2.21**).

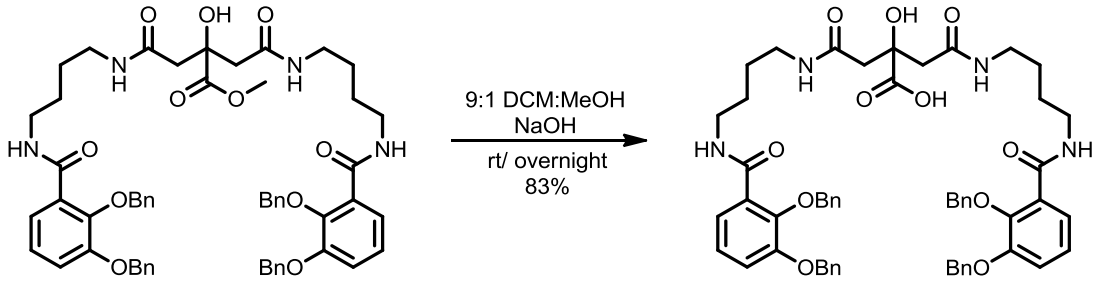

2-41 **2-42**

Scheme 2.21: Deprotection of the methyl ester on the petrobactin analogue backbone using methanolic NaOH in 9:1 DCM: MeOH

After reaction and workup ESI mass spectrometry confirmed successful formation of the product. Peaks with *m/z* 965.43 and 987.41 corresponding to the $[M+H]^+$ and $[M+Na]^+$ ions of **2-42** were observed in the spectrum. However, there was also a peak at *m/z* 947.42, which did not correspond to **2-42**. Analysis by ^{1}H NMR spectroscopy showed that the signal with relative integration three corresponding to the methyl ester in the protected precursor was absent. However, the roofed doublets observed in the protected analogue **2-41** at 2.8 ppm with a relative integration of four were no longer symmetrical. This suggested that the central citrate had cyclised via one of the amide bonds to form the cyclic succinimide **2-43**. Phanstiel *et al.* and Butler *et al.* reported an imide by-product in their total syntheses of petrobactin[122, 137]. However, in the published syntheses, the deprotection of the central citrate was an acid catalysed (TFA or HCl) hydrolysis, as opposed to base catalysed; therefore it was unlikely the basic conditions (pH 12.0) used in the reaction induced the cyclization.

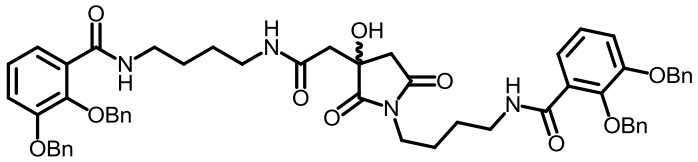

2-43

Figure 2.5: Structure of the succinimide by-product of the petrobactin analogue backbone deprotection.

It is proposed that the cyclization took place during flash chromatography purification, due to the acidic nature of the silica and the use of formic acid in the solvent system. The reaction was repeated, without the use of flash chromatography for product purification. This produced **2-42** as a white solid in 83% yield. The ^{1}H NMR spectrum showed successful formation of the product with no imide present, confirmed by the symmetrical doublet resonances at 2.7 ppm with relative integration four, corresponding to the enantiotopic citrate protons. ESI mass spectrometric analysis showed no peak with *m/z* 947.42 corresponding to the succinimide **2-43**.

*2.3.2.5. Hydrogenolysis of protected analogue backbone to give petrobactin the analogue **2-44***

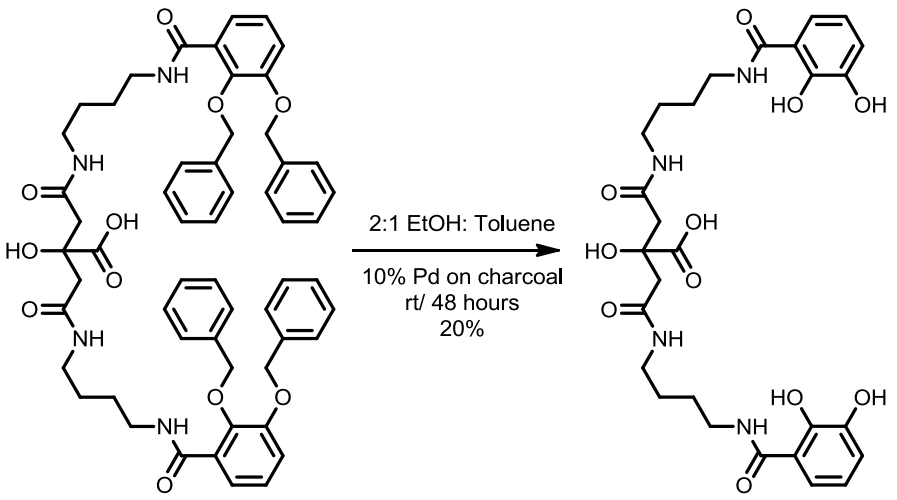

2-42 **2-44**

Scheme 2.22: Hydrogenation of the petrobactin analogue backbone.

The protected siderophore **2-42** was subjected to hydrogenolysis over Pd on carbon to remove the benzyl protecting groups. After 24 hours TLC analysis showed the reaction was only partially complete. A small amount of additional catalyst was added and the reaction was continued. After a further 24 hours, TLC analysis showed the reaction had reached completion, as only one UV active spot was visible. The deprotected product **2-44** was isolated in 20% yield. Successful formation of **2-44** was confirmed by ESI mass spectrometric analysis, where peaks with *m/z* of 605.24 and 627.22 were observed. These corresponded to the $[M+H]^+$ and $[M+Na]^+$ ions of the required product **2-44** respectively. ^{1}H NMR spectroscopy showed the loss of two signals with relative integration 4 at 5.26 and 5.17 ppm and the loss of a multiplet in the aromatic region, confirming removal of the benzyl groups. The low yield for the deprotection is most likely due to adsorption of **2-44** onto the charcoal component of the catalyst. Charcoal has a high affinity for compounds containing aromatic rings[148].

2.3.2.6. Coupling of the methyl ester of ciprofloxacin to the analogue backbone

The next stage of the synthesis was to couple the methyl ester of ciprofloxacin **2-20** to the benzyl protected analogue backbone **2-42**. This was performed using an HBTU-mediated coupling (**Scheme 2.23**). In this case the required product **2-45** was recovered as an oil in 65% yield. The successful formation of **2-45** was supported by ESI mass spectrometry and ^{1}H NMR spectroscopy. In the mass spectrum a peak with *m/z* 1292.49 was observed, corresponding to the $[M+H]^{+}$ ion of **2-45**. ^{1}H NMR spectroscopy showed the loss of a broad singlet with relative integration one at 1.95 ppm, corresponding to the loss of the piperazinyl nitrogen proton. This provided supportive evidence for successful coupling to the analogue backbone.

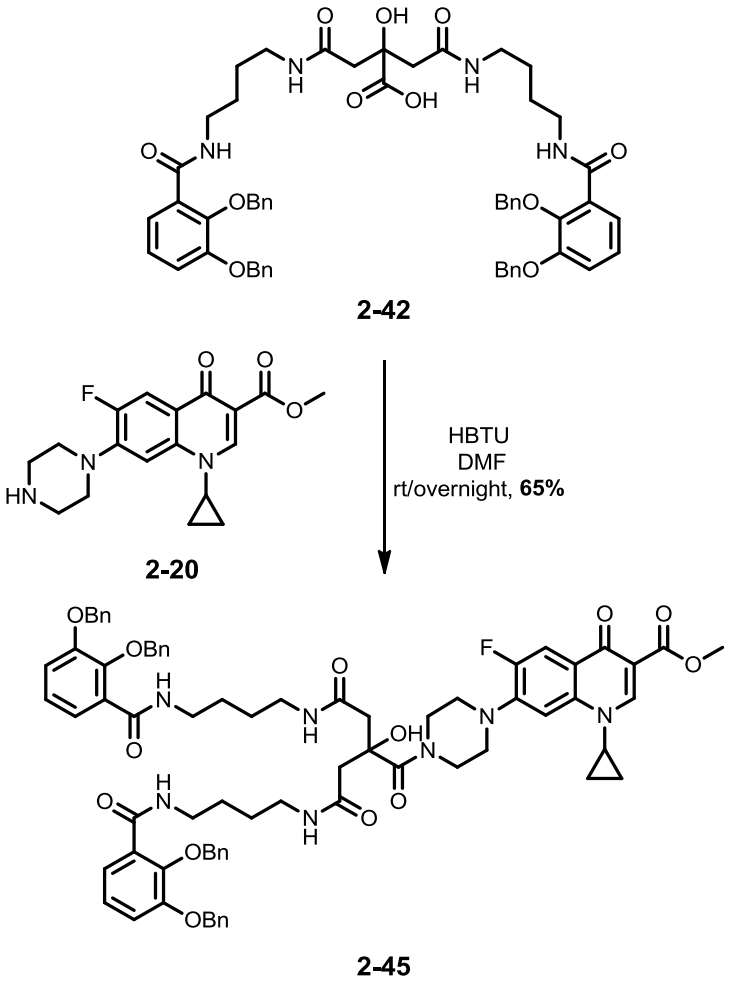

2-42

2-20

2-45

Scheme 2.23: Synthesis of the protected petrobactin-ciprofloxacin conjugate using an HBTU mediated coupling

2.3.2.7. Attempted NaOH mediated deprotection of the ciprofloxacin methyl ester

With the conjugate **2-45** synthesised in protected form, deprotection was required in order to give **2-46.** As the hydroxyl groups in the catechols are highly sensitive to oxidation at basic pH, the methyl ester needed to be removed first. The conjugate **2-45** was dissolved in 9:1 DCM: MeOH and the pH of the solution adjusted to 12 by addition of methanolic NaOH. After reaction and workup ESI mass spectrometric analysis of the reaction mixture showed that a peak with an *m/z* of 1278.5 corresponding to the molecular ion

of **2-46** was not evident**.** However, peaks with *m/z* 965.0 and 346.4 corresponding to the molecular ion of the analogue backbone **2-42** and the methyl ester of ciprofloxacin **2-20** were present.

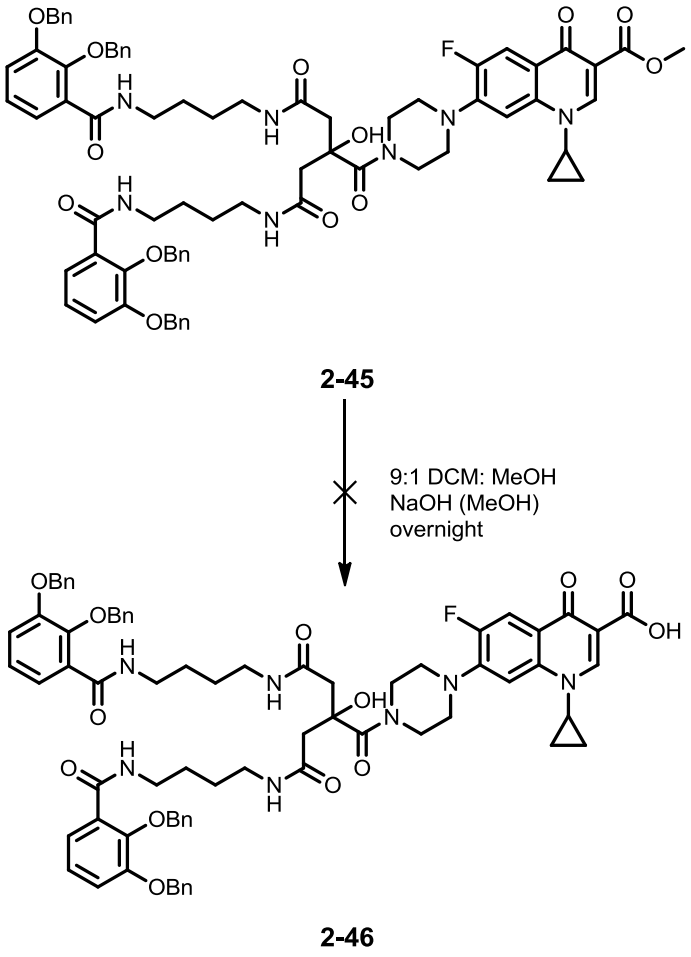

Scheme 2.24: Attempted NaOH mediated deprotection of the analogue-ciprofloxacin conjugate **2-45**

^{1}H NMR spectroscopy also suggested that the amide bond in the product **2-46** had been cleaved to give **2-42** and **2-20**, as a resonance at 1.95 ppm consistent with the piperazinyl amine of the methyl ester of ciprofloxacin **2-20** was present. The reason for the breakdown of the product was acid hydrolysis. It has been reported that some tertiary amide bonds can be susceptible to hydrolysis[165]. As the product was purified by flash

chromatography in 9:1:0.1 $CHCl_3$: MeOH: CHOOH, it is likely that the amide bond was cleaved by the formic acid used during purification.

2.3.2.8. Modification of the ciprofloxacin moiety

In an attempt to increase the yield of the coupling reaction between the petrobactin analogue **2-42** and the methyl ester of ciprofloxacin **2-20**, it was decided to add a glycine spacer to the methyl ester of ciprofloxacin. This would provide a primary amine for the coupling reaction with the analogue backbone **2-42**, which was expected to react more readily than the secondary amine in the piperazinyl ring of ciprofloxacin **1-20**. Additionally, the glycine introduces more space between the antimicrobial and iron binding components of the conjugate. The glycine spacer was introduced by coupling the methyl ester of ciprofloxacin **2-20** to Boc protected glycine. This required compound was synthesised using a EDC·HCl/HOBt·H_2O mediated amide coupling[117]. After reaction and workup **2-48** was isolated in 68% yield (**Scheme 2.25**).

ESI mass spectrometric analysis of the product showed two peaks at *m/z* 503.23 and 525.21, corresponding to the $[M+H]^+$ and $[M+Na]^+$ ions of **2-48**. Additionally, ^1H NMR spectroscopy showed a singlet resonance at 1.45 ppm with a relative integration of nine, corresponding to the Boc group, and an apparent doublet at 4.33 ppm with a relative integration of two corresponding to the CH_2 group of glycine. Furthermore, the loss of the resonance at 1.95 ppm corresponding to the piperazinyl nitrogen proton of ciprofloxacin **1-20** was observed, supporting successful conjugation of the linker to form the product **2-48**.

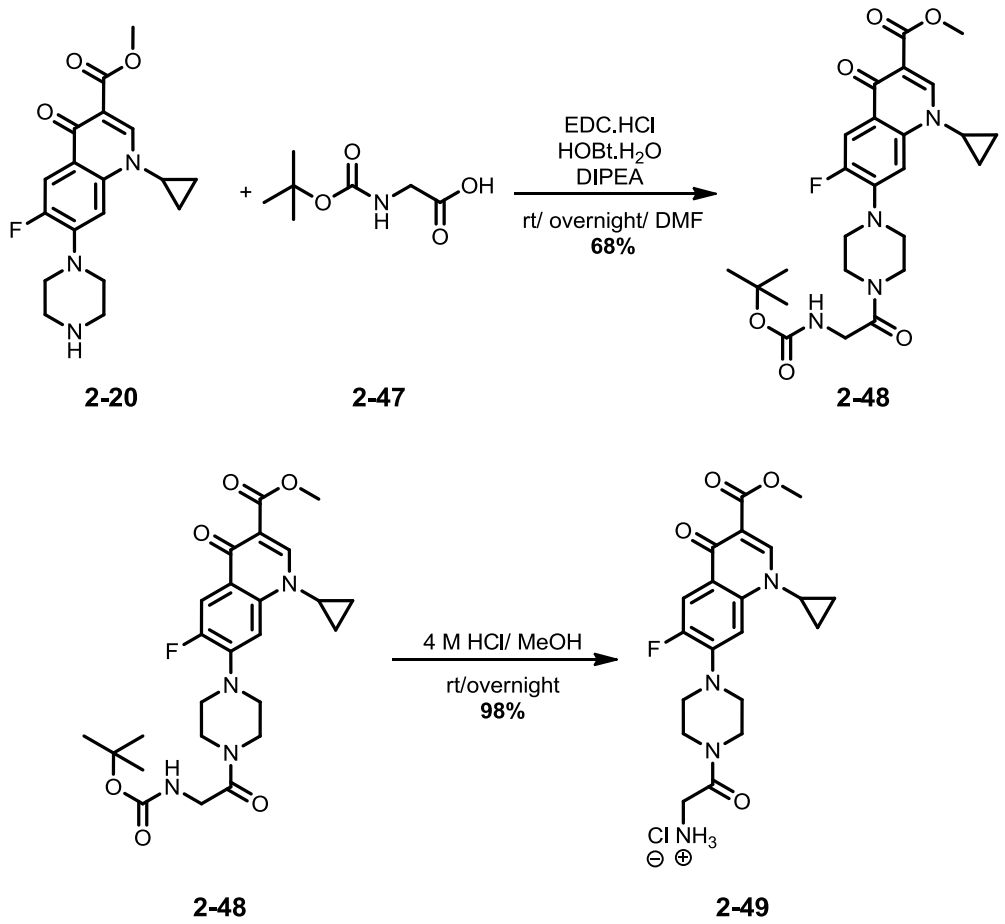

2-20 **2-47** **2-48**

2-48 **2-49**

Scheme 2.25: Preparation of the ciprofloxacin-glycine moiety

To prepare the primary amine salt **2-49**, the Boc protecting group was removed using acid-mediated hydrolysis, 4 M HCl in MeOH (**Scheme 2.25**).The reaction gave **2-49** in 98% yield. The ESI mass spectrum showed peaks with *m/z* of 403.17 and 425.15 corresponding to the $[M+H]^+$ and $[M+Na]^+$ adducts of **2-49**. Hydrolysis was confirmed by the loss of the resonance with relative integration 9 at 1.45 in the ^1H NMR spectrum corresponding to the *tert*-butyl group. As a consequence of this modification, the structure of target compound was modified accordingly (**Figure 2.6**)

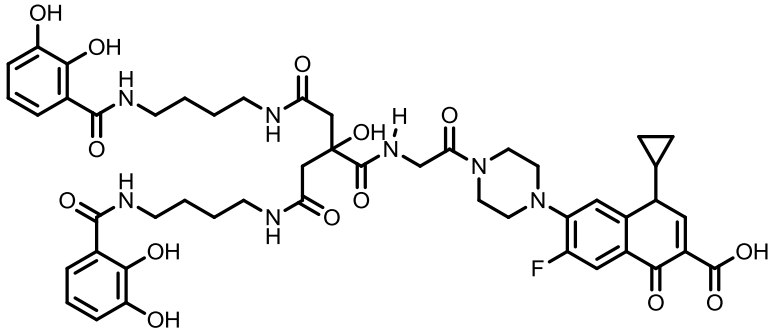

2-50

Figure 2.6: Modified petrobactin analogue-ciprofloxacin conjugate with glycine linker

*2.3.2.9. Coupling of ciprofloxacin-glycine **2-49** to the petrobactin analogue backbone **2-42***

The free amine **2-49** was coupled to the backbone **2-43** using the previously described EDC·HCl/HOBt·H_2O mediated coupling. After purification the product **2-51** was isolated in 45% yield (**Scheme 2.26**)

Successful formation of the product was confirmed by ESI mass spectrometry, where peaks with *m/z* 1371.57, corresponding to the $[M+Na]^+$ ion, and 697.28, corresponding to the $[M+2Na]^{2+}$ ion were observed in the spectrum. Further evidence was provided by ^1H NMR spectroscopy where a triplet resonance with a relative integration of one at 6.77 ppm, corresponding to the amide proton, was observed. This strongly supported successful coupling of the amine to the free carboxylic acid on the backbone.

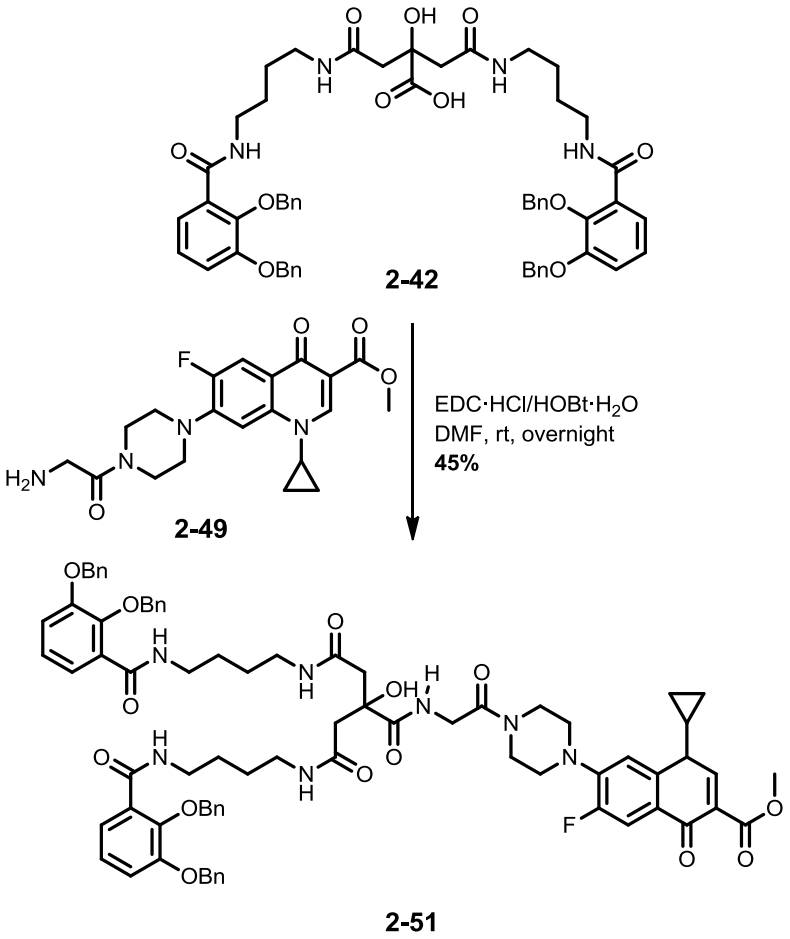

Scheme 2.26: Coupling of cpf-gly **2-49** to the analogue backbone using EDC·HCl and HOBt·H_2O

*2.3.2.10. NaOH mediated deprotection of the petrobactin analogue-glycine-ciprofloxacin conjugate **2-51***

With the fully protected conjugate **2-51** synthesised, the next step was to remove the methyl ester on the carboxylic acid of ciprofloxacin. After stirring in 9:1 DCM: MeOH at pH 12.0 overnight, the pH of the solution was adjusted to 5.5 using 2 M pyruvic acid in MeOH, before evaporating to dryness *in vacuo*.

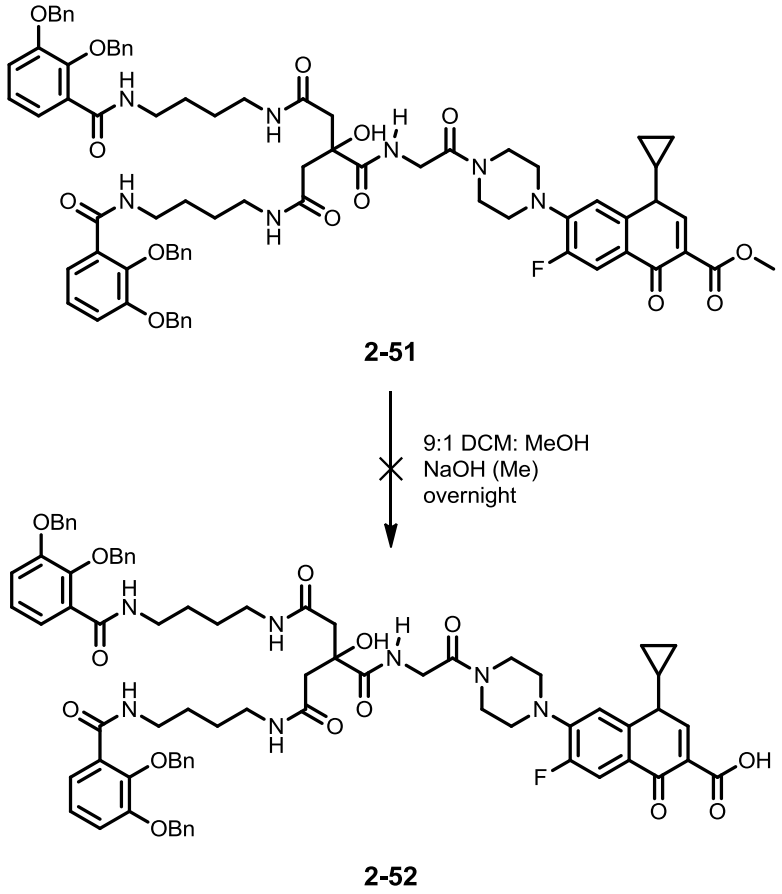

Scheme 2.27: Attempted NaOH mediated deprotection of conjugate **2-50** using 9:1 DCM: MeOH

ESI mass spectrometric analysis supported successful formation of **2-52**. A peak at *m/z* = 1357.55 corresponding to the $[M+Na]^+$ adduct of the required product was observed. However, an additional peak at *m/z* = 987.39 corresponding to the $[M+Na]^+$ ion of the free acid backbone **2-42** was also observed. This suggested that the amide bond between the glycine linker and the central citrate had been partially cleaved, resulting in the regeneration of the free acid backbone and the ciprofloxacin-glycine. The mechanism of this cleavage is likely to be via a cyclisation, as observed with the deprotection of the analogue backbone **2-41**. The cyclisation of the backbone results in the cleavage of the amide bond and release of ciprofloxacin glycine. Upon treatment with base during the work up, the

succinimidyl ring reopens to form the sodium salt form of the analogue backbone.

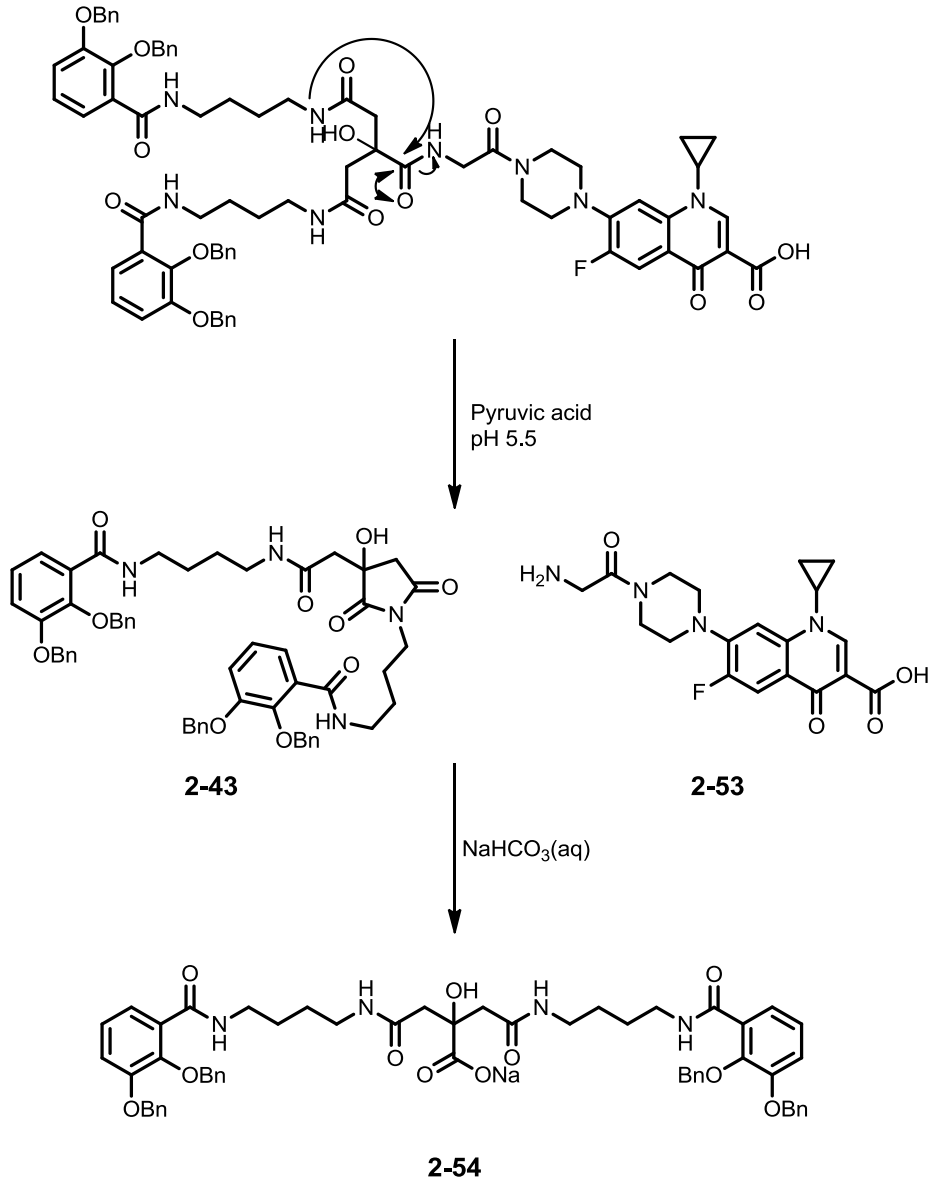

2-43 **2-53**

2-54

Scheme 2.28: Likely mechanism of the cleavage of the citrate amide bond via cyclisation and subsequent ring opening to reform the sodium salt of the analogue backbone

This cleavage of the amide bond between the central citrate and glycine has resulted in the failure to isolate the required compound **2-52** and

consequently the failure to obtain the required petrobactin analogue-ciprofloxacin conjugate **2-50**.

2.4. Conclusions and future work

In this chapter, the synthesis of a fully protected precursor to a siderophore fluoroquinolone Trojan horse has been reported. A procedure has been established for the synthesis of a petrobactin-analogue with 2,3-configured catechols and a shortened backbone. The precursor has been prepared both with and without a linker between ciprofloxacin **1-20** and the analogue backbone. This precursor has been fully characterised using ESI mass spectrometry, ^{1}H NMR, ^{13}C NMR, and IR spectroscopy.

Attempts to deprotect the conjugate have proved unsuccessful. It has been demonstrated, in agreement with previous work performed in the group[151], that the conjugate is unstable in the presence of strong acids. The bond to the central carboxylic acid of the citrate moiety cleaves, giving free ciprofloxacin **1-20** and the sodium salt of the analogue backbone **2-54**.

Future work in this area could involve the deprotection of the conjugate to yield the final Trojan horse compound with both its antimicrobial activity (via the β-keto acid of ciprofloxacin) and iron binding capacity (via the catechol groups) restored. For this to be possible a new protection strategy would be required, possibly using a benzyl ether protecting group on ciprofloxacin instead of a methyl group, allowing a universal deprotection instead of a two step deprotection. In addition, a variety of analogues could be prepared. Possibilities include using 3,4-configured catechols to more closely mimic the native structure of petrobactin, and varying the length of the linker between the central citrate and the catechol amide groups. There is also potential to make analogues using alternative fluoroquinolones such as norfloxacin.

Future work should also include the biological evaluation of the Trojan horse compound and any analogues prepared. This would involve both disc

diffusion assays to determine the general efficacy of the compound against specific strains of bacteria, and DNA gyrase assay to determine if the compound acts by the same mechanism as the isolated fluoroquinolone component. An important aspect of any future work will be determining the MIC of the compounds to ascertain if they are active at a clinically useful level.

3. Investigation into the application of the Ugi multicomponent condensation to the Trojan Horse strategy

3.1. Aims

The aim of the research outlined in this chapter was to enable the synthesis of Trojan horse conjugates using the Ugi four component condensation, and create a set of building blocks which would form the basis of a potential library of Trojan horse conjugates using the fluoroquinolone ciprofloxacin.

3.2. Overview

3.2.1. Multicomponent reactions

Synthesising natural products, such as siderophores, can be a complex process. The biosynthesis of these compounds is the result of a long evolutionary process and involves pathways under enzymatic control. While the total chemical synthesis of selected siderophores and other natural products has been achieved[122, 166-169], these often involve complex multistep syntheses, especially when stereocentres are present in the target molecule. Multicomponent condensation (MCC) reactions enable the synthesis of complex molecules in a single step. Three or more components are combined in a "one pot reaction" to produce a single product. There are two key advantages to this approach. The first is multistep syntheses can result in low overall yields of the target molecule if each step in the synthesis only gives a moderate yield. The second is that using a multicomponent reaction allows the rapid synthesis of structurally related compounds in a short space of time by varying one or more of the components, an approach exploited in combinatorial libraries[170]. A multicomponent condensation reaction (MCR) approach would allow the rapid synthesis of structurally related siderophore-fluoroquinolone conjugates in a minimal number of steps. To demonstrate the

application of this methodology, conjugate **3-1** was designed (**Figure 3.1**), incorporating ciprofloxacin **1-18** and a model "siderophore like" component.

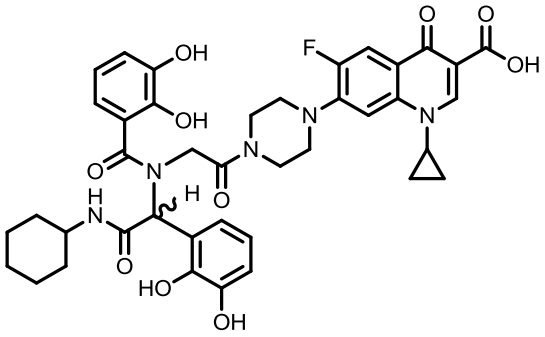

3-1

Figure 3.1: Structure of the target compound **3-1**

3.2.2. Multicomponent condensation reactions

MCC reactions have been known for at least 160 years. The Strecker synthesis, which generates α-amino acids from α-amino cyanides, was reported in 1850[171]. The use of isocyanides in MCC reactions was first published in 1921 by Passerini (**Scheme 3.1**). This reaction is a three component condensation (M-3CR), using an isocyanide **3-4**, a carbonyl **3-3** and an organic acid **3-2**[172]. This reaction provided a one pot synthesis of α-acyloxycarboxamides.

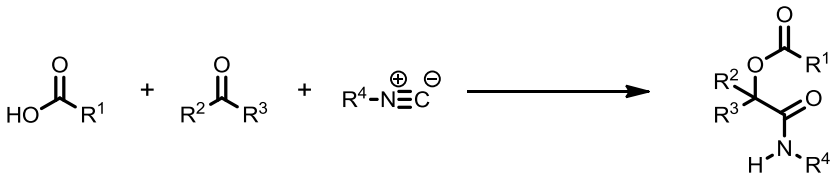

3-2 **3-3** **3-4** **3-5**

Scheme 3.1: Overview of the Passerini reaction

3.2.3. The Ugi condensation

The Ugi condensation was first published in 1959 by Ivar Karl Ugi[173]. The reaction was similar to the Passerini reaction, but with an additional amine component, giving α-aminoacyl amides. The Ugi condensation is a stepwise reaction that goes through several intermediates before the final α-aminoacyl amide compound is formed (**Scheme 3.2**). The first reversible step is an imine formation between the aldehyde and amine component, which is then protonated by the organic acid to form an iminium ion.

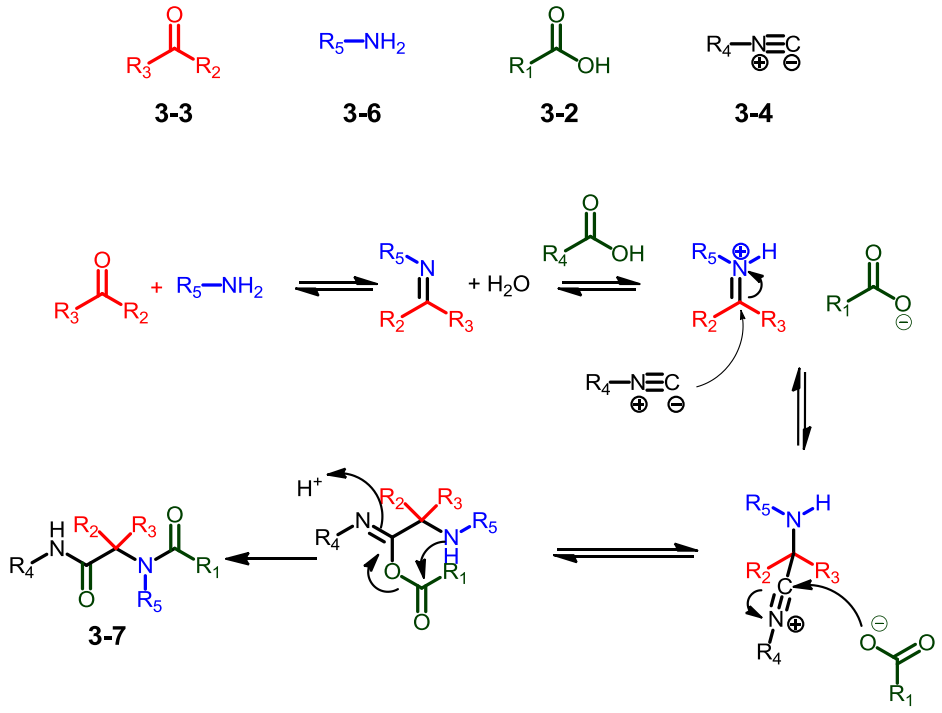

Scheme 3.2: Components and mechanism of the Ugi four component condensation

Once the iminium ion is formed, the isocyanide attacks the electron deficient carbon of the imine to form a new nitrilium containing intermediate. The deprotonated acid can then attack the carbon of the isocyanide moiety to form the final intermediate. This adduct then undergoes an intramolecular 1,3(O-N) acyl transfer, known as a Mumm rearrangement (**Scheme 3.2**). This final step is irreversible and gives the Ugi condensation product. A recent study by Neto *et al*. has suggested this step is also rate determining

within the reaction. They also determined that the rearrangement is less likely to occur in aprotic solvents[174]. Studies have shown that there are a number of different factors that influence the Ugi reaction. One key factor is the nucleophilicity of the amine, with amines that have reduced nucleophilicity resulting in low yields. Ugi condensation reactions have been reported in a variety of solvents[175]. The key elements in selecting a solvent are the solubility of reagents, polarity and insolubility of the Ugi product[175]. It has also been shown that the use of microwave irradiation can facilitate the reaction, particularly when the reaction is performed using a polymer supported isocyanide[176]. In 2012 Ostaszewski *et al*. published studies on an enzyme catalysed version of the three component variation of the Ugi condensation[177]. There is also scope for added diversity in the Ugi condensation, Armstrong and Keating developed a "universal" isocyanide **3-8** which participates in the Ugi condensation, but can subsequently be reacted further using a nucleophile (**Figure 3.2**)[178].

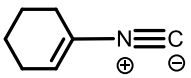

3-8

Figure 3.2: A universal isocyanide developed by Armstrong and Keating

3.2.4. Use of MCCs in the synthesis of bioactive molecules

In recent years there have been a number of applications of MCCs to prepare biologically relevant molecules. The use of MCCs for biological applications has been reviewed in detail by Dömling *et al*. and focuses on the use of MCCs to synthesise molecules to target a variety of protein targets[170]. This is often done by combining the Ugi condensation in a cascade with other reactions e.g. Ugi-Smiles or Ugi-Michael-aza Michael[179].

3.2.4.1. The use of MCCs in the synthesis of compounds targeting proteins

A significant area of research using MCCs is protein inhibitors and there are numerous examples of this in the literature, with a variety of different protein classes targeted[170]. One example is the synthesis of hydantoin based compounds (**Figure 3.3**)[180]. Torroba *et al.* synthesised a complex hydantoin based structure **3-9** using an Ugi/cyclisation/Ugi sequence. Such compounds are useful as hydantoins have shown activity as anti-convulsants, anti-tumor agents and anti-arthritic drugs[181]. Vacca *et al*. used the Ugi condensation to prepare spiropiperidine iminohydantoins as inhibitors of the protein β-secretase[182].

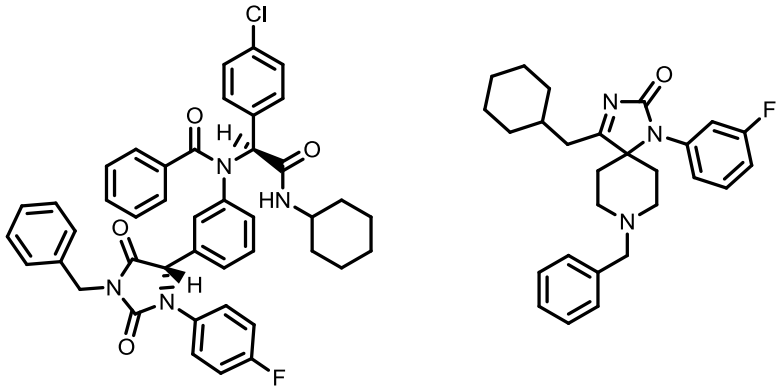

3-9 **3-10**

Figure 3.3: Structure of a hydantoin containing structure synthesised by Torroba *et al.***3-9** and a spiropiperidine iminohydantoin by Vacca *et al*. **3-10.**

Multicomponent condensations have also been used to synthesise bioactive peptidomimetics through the use of specific building blocks and post condensation reactions[183-186]. Cai *et al.* utilised an Ugi/click reaction to generate triazole modified peptidomimetics (**Scheme 3.3**)[186].

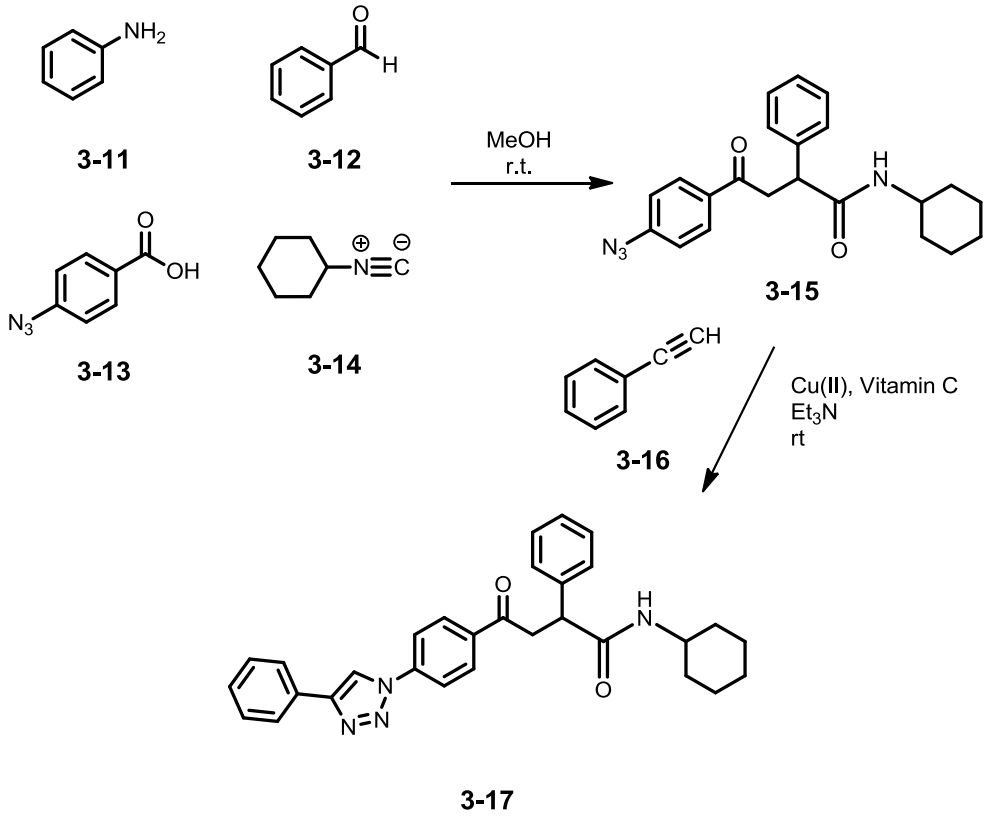

Scheme 3.3: Synthesis of a triazole functionalised Ugi product by Cai *et al.* using a tandem Ugi/click reaction[186].

An alternative method was used by Lesma *et al*. they synthesised tryptophan-based peptidomimetics using an Ugi/Pictet-Spengler reaction[183]. The synthesis of peptidomimetics in this fashion creates core structures which can be further derivatised to generate ligands for different proteins (**Scheme 3.4**).

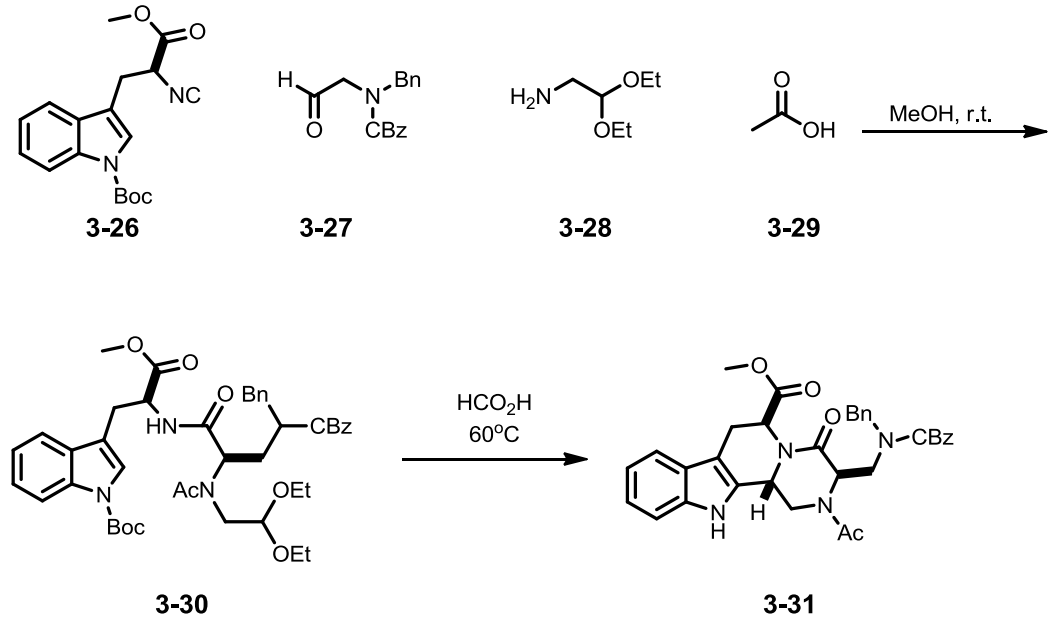

3-26 **3-27** **3-28** **3-29**

3-30 **3-31**

Scheme 3.4: Protected tryptophan-based peptidomimetics synthesised by Lesma *et al.* using an Ugi/Pictet-Spengler reaction

3.2.4.2. The use of MCC reactions in the synthesis of antimicrobial compounds

The use of MCC reactions in synthesising antimicrobial compounds is less well explored than its applications for the synthesis compounds for protein based drug targets. Sureshbabu *et al.* utilised an Ugi condensation to prepare β-lactams, using chiral N^{β}-Fmoc amino alkyl isonitriles[185]. Additionally, they utilised amino acids to incorporate both the amine and carboxylic acid functionalities in a single component.

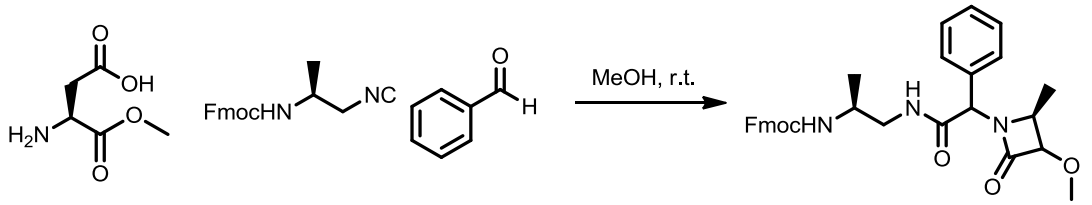

3-32 **3-33** **3-34** **3-35**

Scheme 3.5: Example of a β-lactam synthesised utilising the Ugi condensation

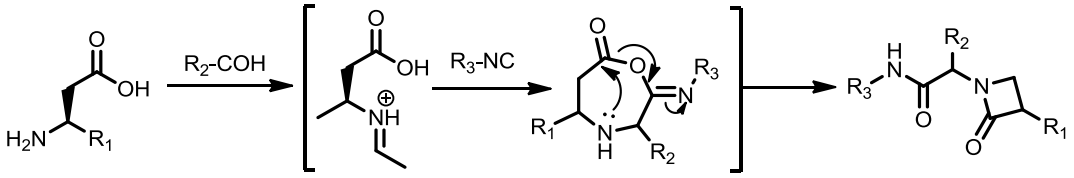

3-36 **3-37**

Scheme 3.6: General mechanism for the formation of β-lactams using the Ugi condensation

Shiskin *et al.* used an azido-Ugi condensation, followed by cyclization to form spyrocyclic γ-lactams. This particular methodology utilises an oxo ester and as the aldehyde component and an azide in place of the carboxylic acid (**Figure 3.4**)[187].

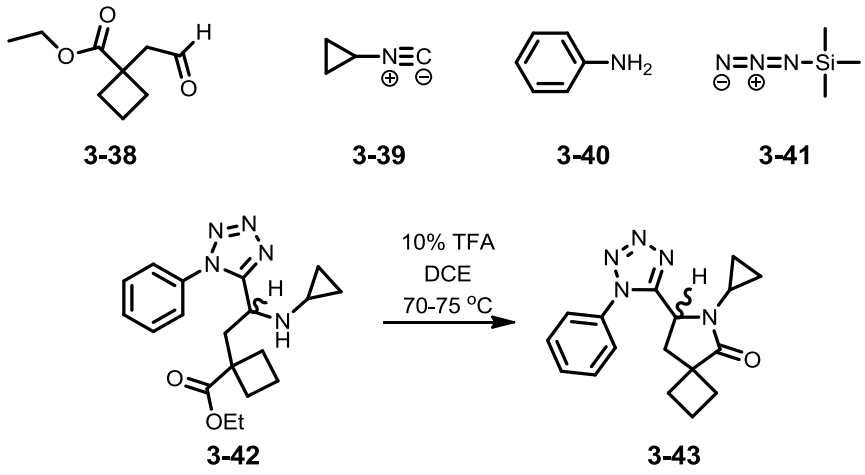

3-38 **3-39** **3-40** **3-41**

3-42 **3-43**

Figure 3.4: Example of a tetrazole substituted spirocyclic γ-lactam **3-43** synthesised by Shiskin *et al*.

MCC reactions have also been successfully used to synthesise peptide containing antibiotics. Ichikawa *et al.* used an Ugi MCC to synthesise the antimicrobial pacidamycin **3-44** and its 3'-hydroxy analogue **3-45** (**Figure 3.5**).

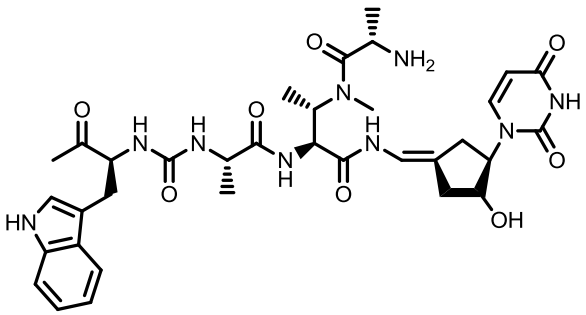

3-44

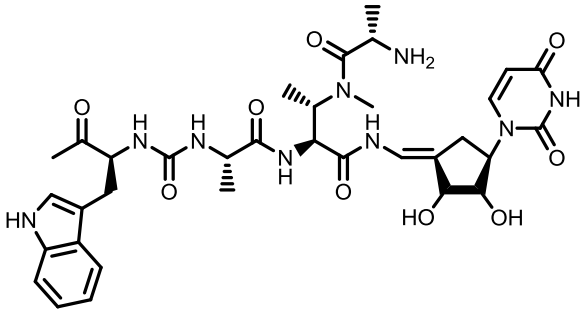

3-45

Figure 3.5: Pacidamycin (**3-44**) and its 3'-hydroxyl analogue (**3-45**) synthesised by Ichikawa *et al.*

The use of MCC reactions to generate compounds which target specific proteins also has applications in generating antimicrobials. Larhed *et al*. synthesised 3-aminoimidazo[1,2-a]pyridines as glutamine synthetase inhibitors[188] (**Figure 3.6**). Nenajdenko *et al*. published N-acetyl cysteine and glutathione compounds synthesised using the Ugi condensation. These compounds could have potential use as inhibitors of the bacterial malonyl CoA transferase[189].

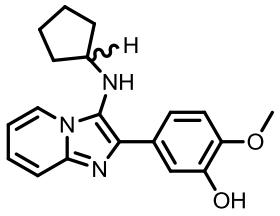

3-46

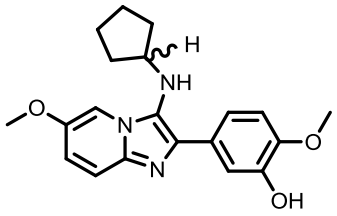

3-47

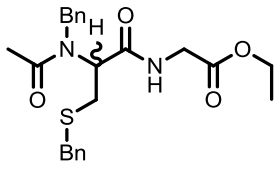

3-48

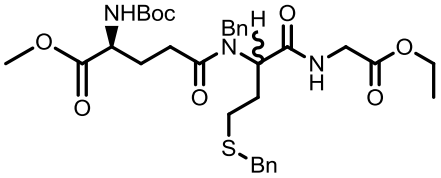

3-49

Figure 3.6: 3-Aminoimidazo[1,2-α]pyridines (**3-46** and **3-47**) synthesised by Larhed *et al.*[188] and N-acetyl cysteine **3-48** and glutathione **3-49** derivatives synthesised by Nenajdenko *et al.*[189]

A similar use of MCC reactions in medicine is in the synthesis of anti-viral compounds and anti-parasitical compounds. Torrence *et al*. published a series of nucleoside derivatives prepared using the Ugi reaction, with the intention of developing antivirals for the smallpox virus (**Figure 3.7**). A number showed promising activity against the parasite *Leishmania donovani*[190].

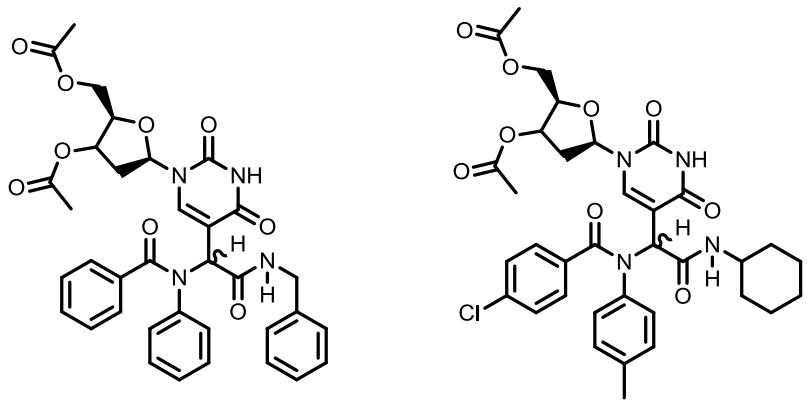

3-50 **3-51**

Figure 3.7: Nucleoside (5-formyl-2'-deoxyuridine-3',5'-diacetate) derivates formed using the Ugi condensation by Torrence *et al.*[190]

Chibale *et al.* have also exploited multicomponent condensations to develop anti-parasitic compounds, specifically anti-malarial drugs. Using the Ugi condensation they were able to develop novel 4-aminoquinoline compounds with activity against both chloroquine susceptible and resistant strains of *Plasmodium falciparum*[191].

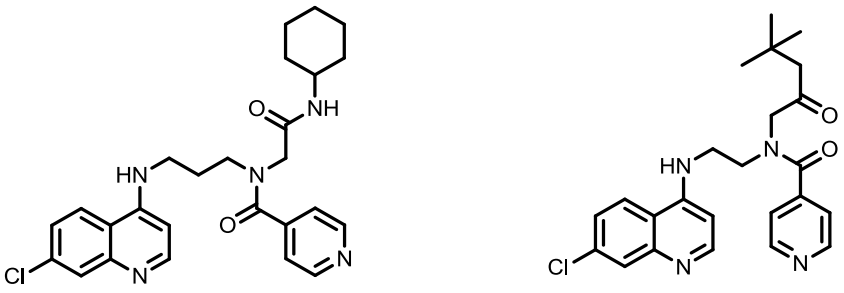

3-52 **3-53**

Figure 3.8: Examples of 4-aminoquinoline compounds synthesised by Chibale *et al.*[191]

Although there are several examples of the Ugi condensation being used to synthesise antimicrobial compounds, as of yet there is no precedent for using multicomponent condensations in the synthesis of Trojan horses.

This research seeks to establish the principle of synthesising Trojan horses in a multicomponent reaction by using a known antimicrobial as one of the reaction components.

.

3.3. Results and discussion

3.3.1. Synthesis of the protected conjugate 3-56 using the Ugi condensation

The Ugi condensation requires an amine component and ciprofloxacin was a logical choice due to the secondary amine in the piperazinyl ring. However, as a primary amine could be expected to be more reactive, it was decided to introduce a primary amine via glycine linked ciprofloxacin **3-56**[151].

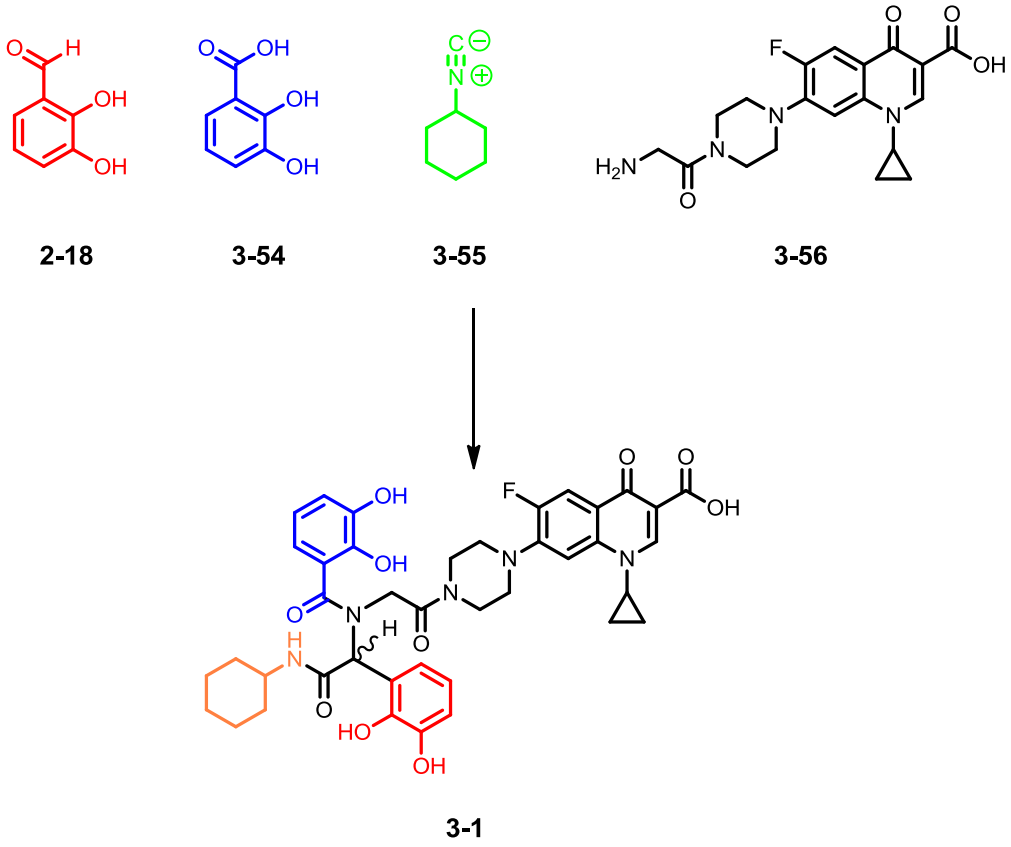

Scheme 3.7: Components and structure of the target Ugi conjugate **3-1**.

Commercially available cyclohexylisocyanide **3-55** was used as the isocyanide component, 2,3-dihydroxybenzaldehyde **2-18** (chapter 2) and 2,3-dihydroxy benzoic acid **3-54** were selected as the aldehyde and acid components, respectively. The ciprofloxacin glycine moiety **2-49** was synthesised as previously described (chapter 2).

The reaction was initially performed using 2,3-bis(benzyloxy)benzaldehyde **2-25**, 2,3-bis(benzyloxy)benzoic acid **2-26**, cyclohexyl isocyanide **3-55**, and the methyl ester of glycine-ciprofloxacin **2-49,** following the method of Marcacinni and Torroba[175]. This involved reacting **2-25** with **2-49**, then once the imine had formed adding **2-26** and **3-54** in quick succession. After 24 hours the reaction mixture was evaporated to dryness *in vacuo.* The residual solid was analysed by ESI mass spectrometry and ^{1}H NMR spectroscopy, which suggested that some product was present.

The imine formation did not appear to be proceeding efficiently in the reaction. The synthesis was subsequently modified to isolate the imine intermediate **3-57** (**Scheme 3.8**). 2,3-bis(Benzyloxy)benzaldehyde **2-25** was reacted with the hydrochloride salt of **2-49** in MeOH. Two equivalents of DIPEA were added and after 18 hours **3-57** was isolated by filtration in 71% yield.

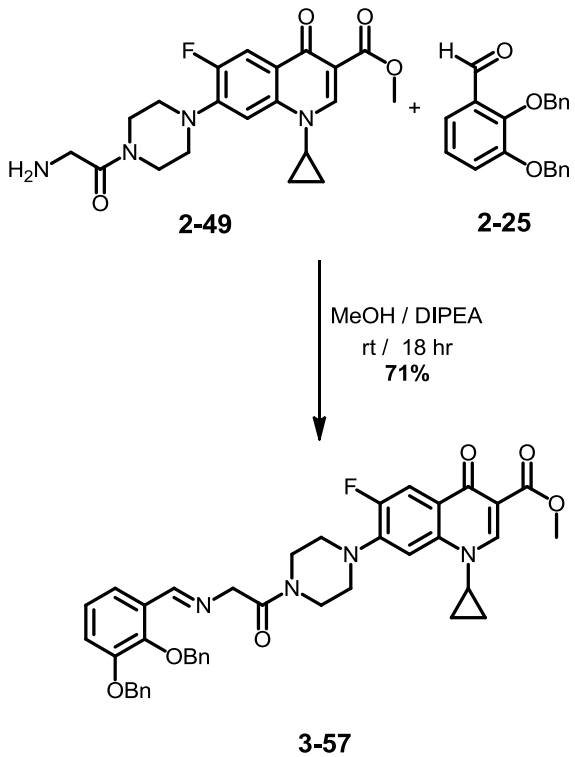

Scheme 3.8: Synthesis of the imine intermediate **3-57** for the Ugi condensation using ciprofloxacin glycine **2-49** and 2,3-bis(benzyloxy)benzaldehyde **2-25** in MeOH

^{1}H NMR spectroscopic analysis supported the successful formation of **3-57** with a singlet with a relative integration of one at 8.59 ppm, present in the spectrum. This signal corresponded to the imine proton in **3-57**. ESI mass spectrometric analysis showed a peak with *m/z* of 703.29 corresponding to the $[M+H]^+$ ion of **3-57**. Peaks corresponding to starting materials were also observed in the ESI mass spectrum. However, there were no signals corresponding to the free amine of **2-49** or the aldehyde proton of **2-25** in the ^{1}H NMR, which suggests that any unreacted starting materials were present at a level below NMR detection limits.

Having successfully prepared imine **3-57**, it was then reacted with 2,3-bis(benzyloxy)benzoic acid **2-26** and cyclohexylisocyanide **3-54**. After 30 hours at room temperature the formation of a precipitate was observed, which was isolated by filtration. Analysis of the precipitate by ESI mass spectrometry confirmed the presence of the product, as a peak with *m/z* of 1146.50 corresponding to the $[M+H]^+$ ion of **3-58** was observed in the spectrum However, ^{1}H NMR spectroscopic analysis showed a significant number of impurities.

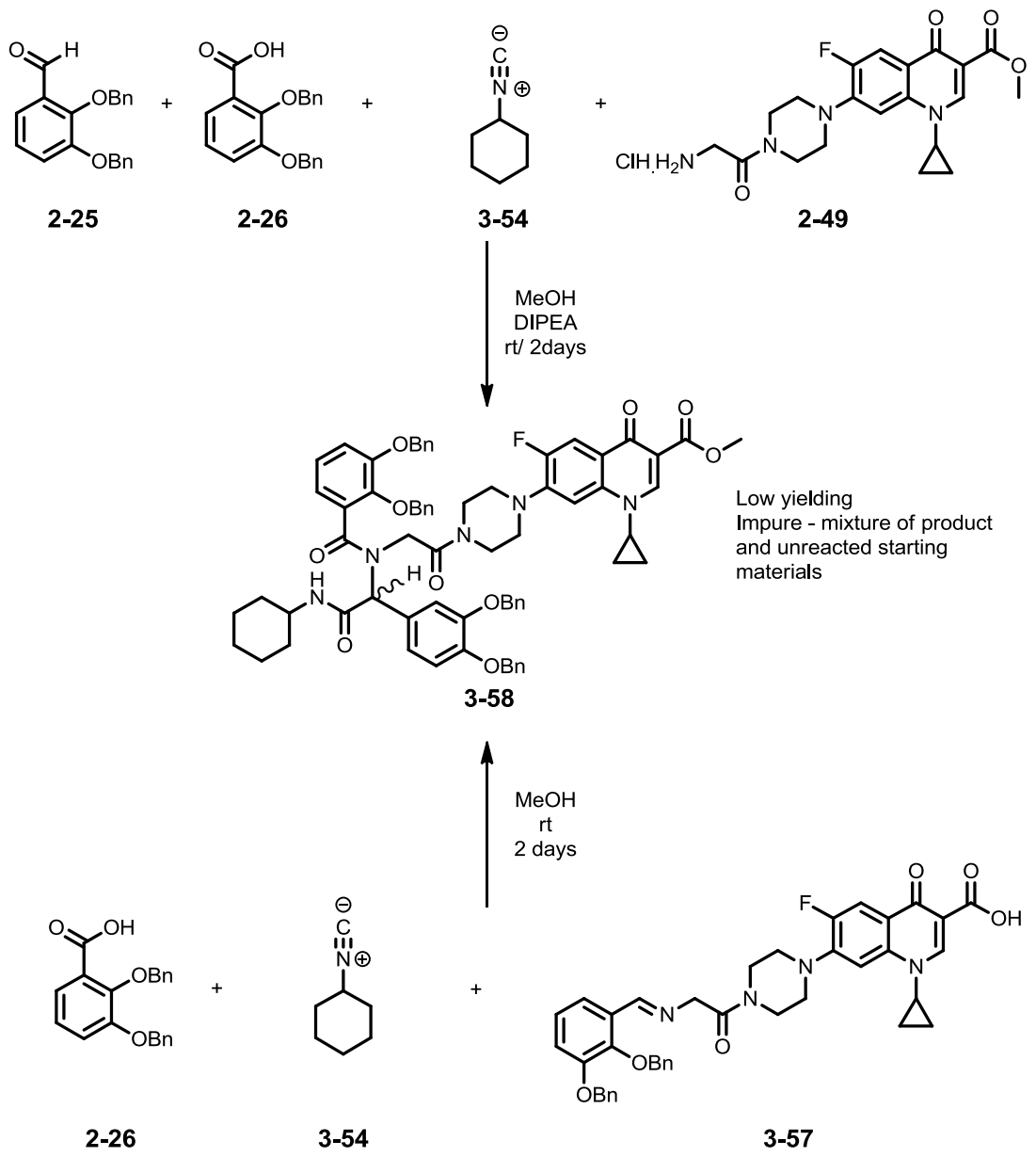

Scheme 3.9: Comparison of the initial attempts at synthesising Ugi conjugate **3-58,** generating the imine intermediate *in situ*, and generating and isolating the imine before proceeding with the reaction.

It was apparent that the Ugi reactions were not proceeding efficiently to the final product, with only a limited amount of product that had undergone the irreversible Mumm rearrangement detected[172, 175, 192]. Both methods (**Scheme 3.9**) resulted in a mixture of **3-58** and unreacted starting material. It was therefore decided to attempt the synthesis using microwave irradiation. Barreto *et al.* established that multicomponent reactions can be performed

under microwave irradiation, applying the technology to both the Ugi[193] and Passerini[194] reactions. Andreana and Santra have also demonstrated the use of microwave-assisted synthesis in Ugi condensation chemistry[195].

The microwave conditions used for our Ugi chemistry were a temperature of 90 °C at 50 W for 60 min. Using microwave irradiation appeared to improve the crude yield of **3-58**, with an increase from 60% to 80% observed. Column chromatography in 12:1 DCM was used to purify **3-58**. This resulted in the successful isolation of pure **3-58** in 38% yield. Mass spectrometric analysis showed an *m/z* peak of 1146.50, corresponding to the $[M+H]^+$ ion of **3-58**. However the ^{1}H NMR spectrum was more complex than expected (**Figure 3.9**).

^{1}H NMR analysis suggested multiple species were present in solution. For example, where there should be four singlet resonances with relative integration two at approximately 5 ppm, corresponding to four sets of benzyl CH_2 groups, there is a convoluted multiplet, suggesting several species. The resonance at 4.03 ppm in the spectrum of **2-49**, which corresponds to the glycine CH_2 group, appeared as a pair of roofed doublets instead of a singlet, suggesting that those protons were now diastereotopic.

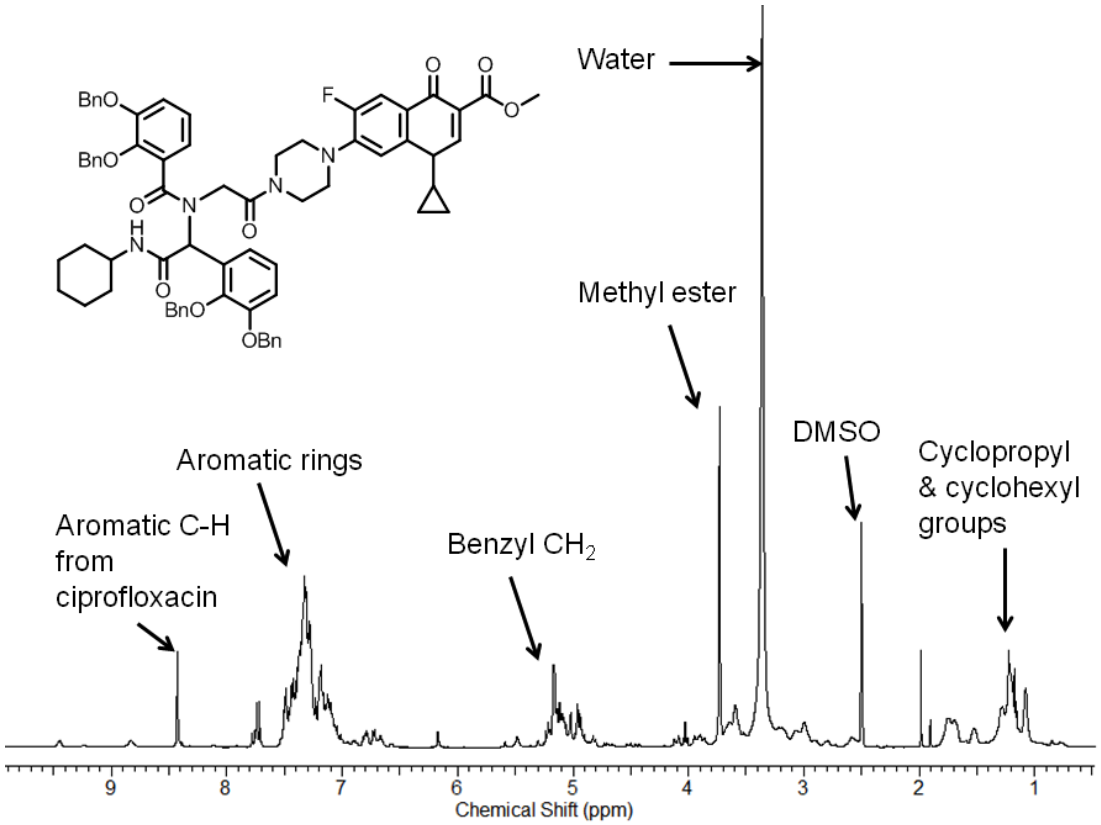

Figure 3.9: H NMR spectrum of **3-58** with key signals identified

In order to analyse why the ^{1}H NMR spectrum of **3-58** was complex, a 3D structure was generated using Chemdraw 3D pro 7.0. Examination of the 3D structure of suggested that the complex ^{1}H NMR spectra could be due to rotamers about the amide bonds within the structure. ^{1}H NMR analysis suggested multiple species were present in solution. Additionally, the 3D structure showed that the close proximity of the benzyl protecting groups to the cyclohexyl groups could result in hindered rotation.

In order to investigate if rotamers were responsible for the complex NMR spectrum, **3-58** was dissolved in d_6-DMSO and variable temperature 500 MHz ^{1}H NMRs were recorded at 298 K, then heating to 383 K, and lowering the temperature back to 298 K. (**Figure 3.10**). In the high temperature spectrum the resonances in the aromatic region and the CH_2 resonances due to the benzyl groups became more resolved.

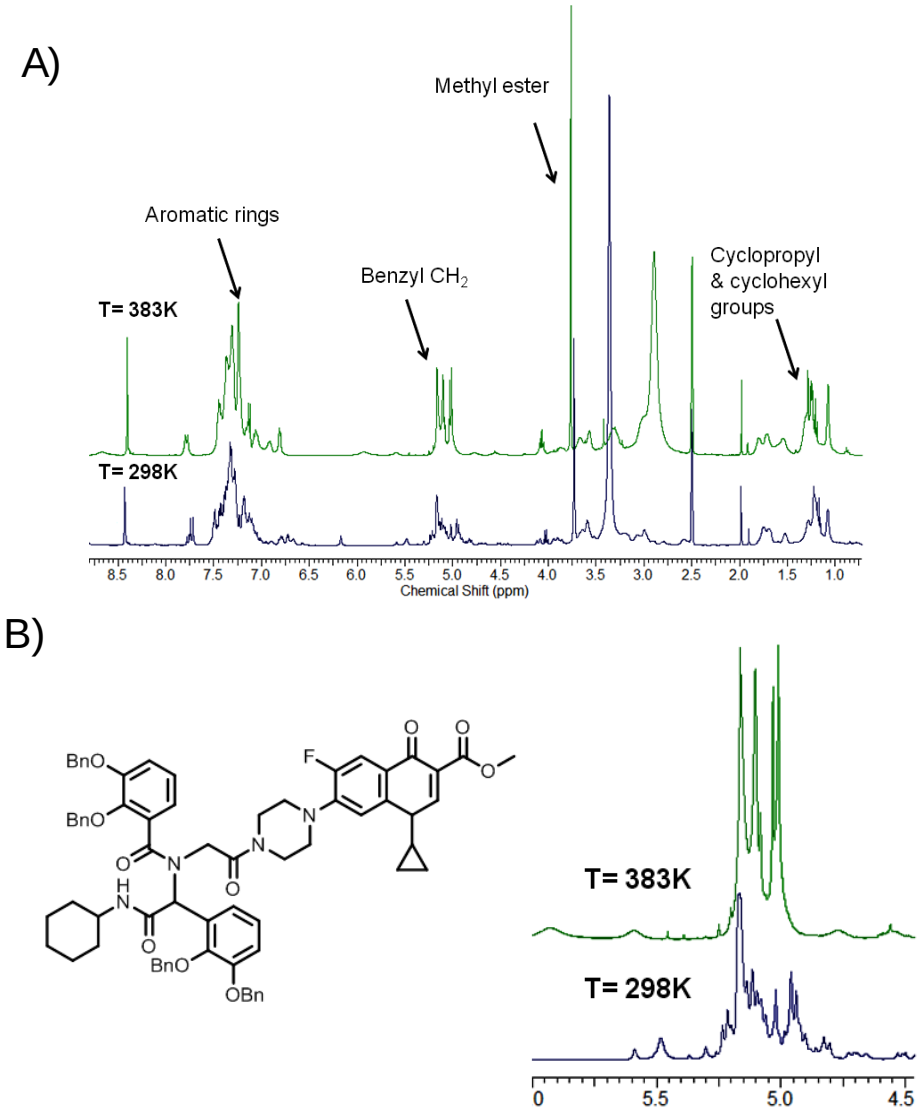

Figure 3.10: Variable temperature ^{1}H NMR spectra **A)** full spectrum **B)** resonances corresponding to the benzyl CH_2 groups of **3-58**. Blue spectra T=298 K, Green spectra T= 383 K

These spectra support the theory that rotamers are present in **3-58**, providing evidence that, in spite of a complex ^{1}H NMR spectrum, the Ugi reaction was successful.

3.3.2. Hydroxide-mediated deprotection of the conjugate 3-58

With the protected conjugate **3-58** in hand deprotection of the carboxylate functionality was investigated. The protected conjugate **3-58** was insoluble in hydrophilic solvents: therefore our established hydroxide-

mediated deprotection was not viable. A deprotection strategy which utilised a two phase system was investigated[164]. Conjugate **3-58** was dissolved in a 9:1 DCM: MeOH and three molar equivalents of methanolic NaOH were added (**Scheme 3.10**). After 18 hours the reaction mixture was evaporated to dryness *in vacuo.* Analysis of the crude residue by TLC and ESI mass spectrometry confirmed the presence of the free carboxylate **3-59**. This was further supported by ^{1}H NMR, as the 3H singlet at 3.76 ppm due to the methyl ester was absent from the spectrum.

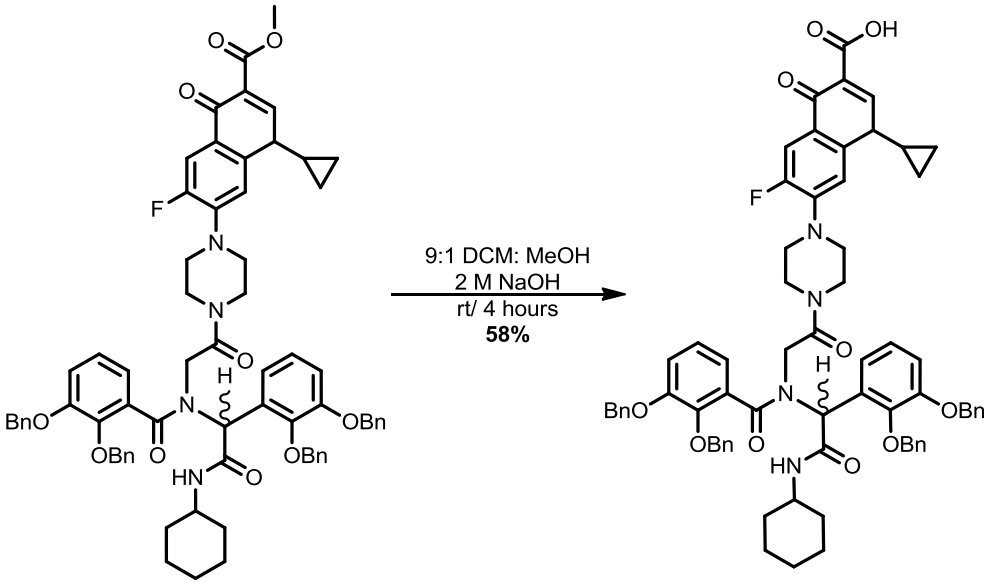

3-58 **3-59**

Scheme 3.10: Hydrolysis of the methyl ester using the method of Theodorou *et al.*[164]

The reaction was repeated, followed by an acidification to pH 5 to ensure the free acid of **3-59** was obtained rather than the sodium salt. The solution was then evaporated to dryness under reduced pressure to yield an orange solid. The solid residue was redissolved in DCM, washed with brine and the organic solvent removed *in vacuo,* yielding **3-59** in 58% yield.

3.3.3. Hydrogenolysis of the conjugate 3-59

The final stage in the synthesis was to remove the benzyl ether protecting groups on the catechol units. This was performed by hydrogenolysis using a palladium catalyst (**Scheme 3.11**).

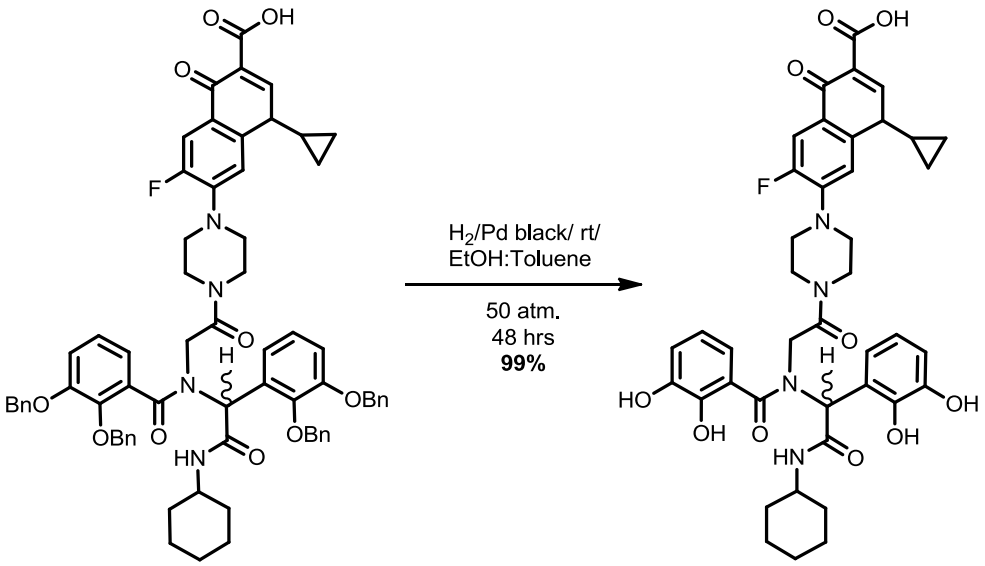

3-59 **3-1**

Scheme 3.11: Removal of the benzyl ether protecting groups by hydrogenation using a palladium black catalyst

The palladium catalyst chosen was palladium black. It had previously been shown that compounds containing ciprofloxacin **1-18** gave low yields and poor mass recovery when deprotected by hydrogenolysis using palladium on charcoal. The poor mass recovery was due to absorption of either the starting material or the product onto the catalyst surface[148]. Conjugate **3-59** was dissolved in DMF and a catalytic amount of palladium black was added. The resultant suspension was stirred under H_2 at 50 atm. After 24 hours the reaction was examined. TLC analysis suggested partial deprotection, as a spot corresponding to a new species was observed along with starting material. Additional catalyst was added, and the reaction stirred under H_2 for a further 24 hours. After work up, **3-1** was isolated in 99% yield. ESI mass spectrometric analysis supported the presence of **3-1** with a peak at *m/z* 772.29 corresponding to the $[M+H]^+$ ion of **3-1,** observed in the spectrum. ^{1}H NMR confirmed the successful removal of the benzyl ethers as the complex resonances at ~5.0 ppm due to the CH_2 groups of the benzyl moieties were absent. However despite the successful hydrogenolysis of **3-1** the ^{1}H NMR spectrum was still complex than expected, suggesting rotamers were still present in **3-1**

LC-MS analysis was performed using a gradient elution and detection at 280 nm. The starting solvent system was 9:1 H_2O:MeCN, increasing to 45:55 H_2O: MeCN after 20 minutes, then to 1:4 H_2O:MeCN after 25 minutes. One strong peak with a small shoulder was observed in the chromatographic trace (**Figure 3.10**). Upon examination of the mass spectrum of each peak, it was found that both main peak and the shoulder region contained MS peaks with *m/z* values that could be assigned to the same chemical species. This suggests that there is still an issue with hindered rotation, even once the product is fully deprotected, and the two overlapping bands observed in the LC trace were rotameric forms of **3-1**.

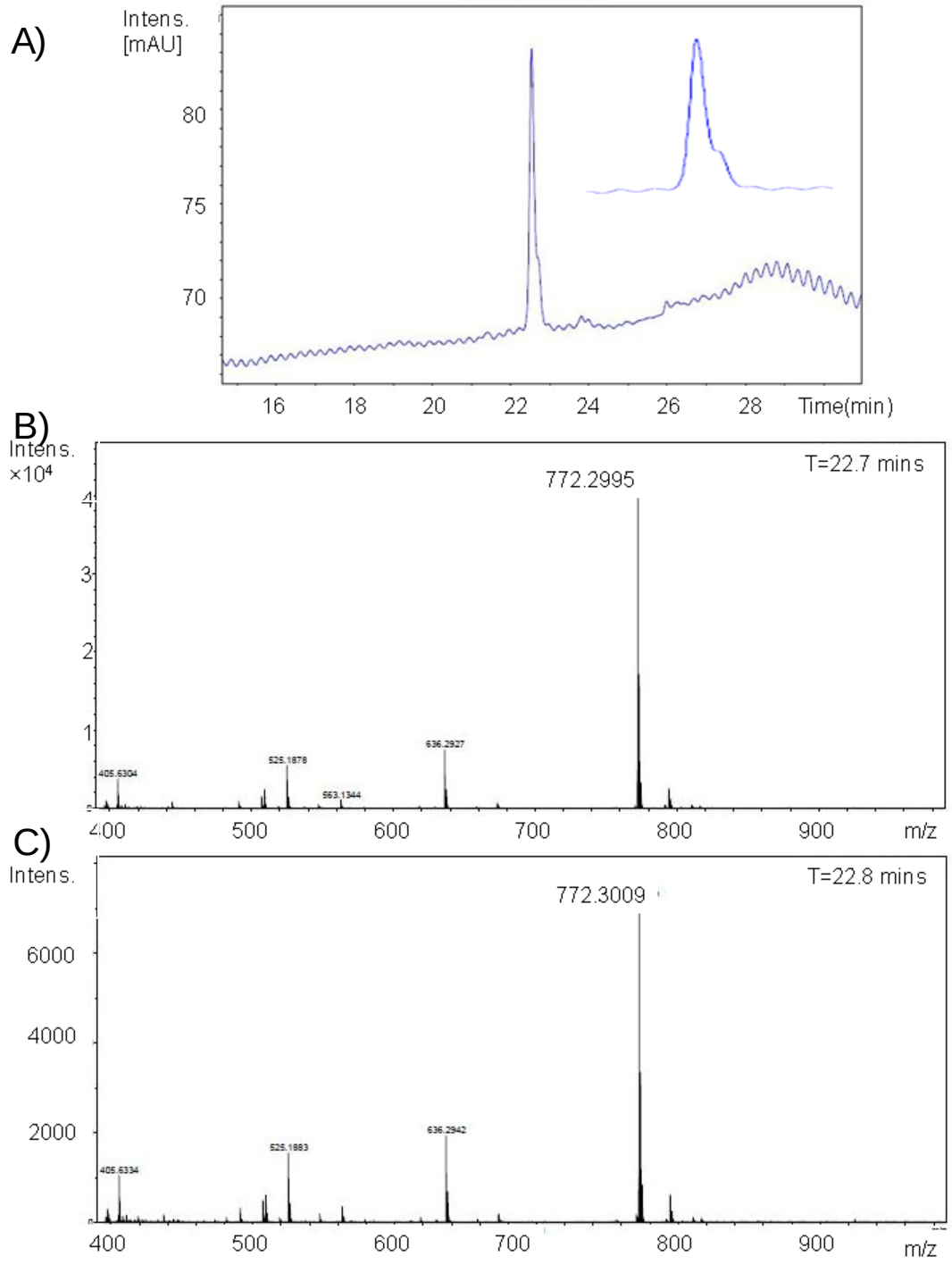

Figure 3.11: A) UV trace (280 nm) from the LC-MS column with expanded view of the detected peak inset, **B)** Mass spectral trace from main peak (taken at 22.7 minutes), **C)** Mass spectral trace from the shoulder (taken at 22.8 minutes)

The purity of the product was assessed by HPLC analysis using a reverse phase column (**Figure 3.12**). The product gave a single elution peak

using a gradient solvent system with MeCN as the organic phase and a phosphate buffer as the aqueous phase[196]. The gradient started with 0.1% organic phase, 99.9% aqueous phase. After five minutes the gradient was gradually increased to 0.5% organic. After a further five minutes, the gradient was increased to reach 20% organic after 20 minutes. After 24 minutes the gradient was set to 50% organic and slowly increased to 80% organic to flush the column. After 20 minutes, the gradient was returned to 0.1% organic phase to re-equilibrate the column.

Compound **3-1** was determined to be 98% pure by HPLC, however the rapid elution, raised questions as to the accuracy of the measurement. However, based on the LC-MS and HPLC results, conjugate **3-1** was sufficiently pure to allow biological screening.

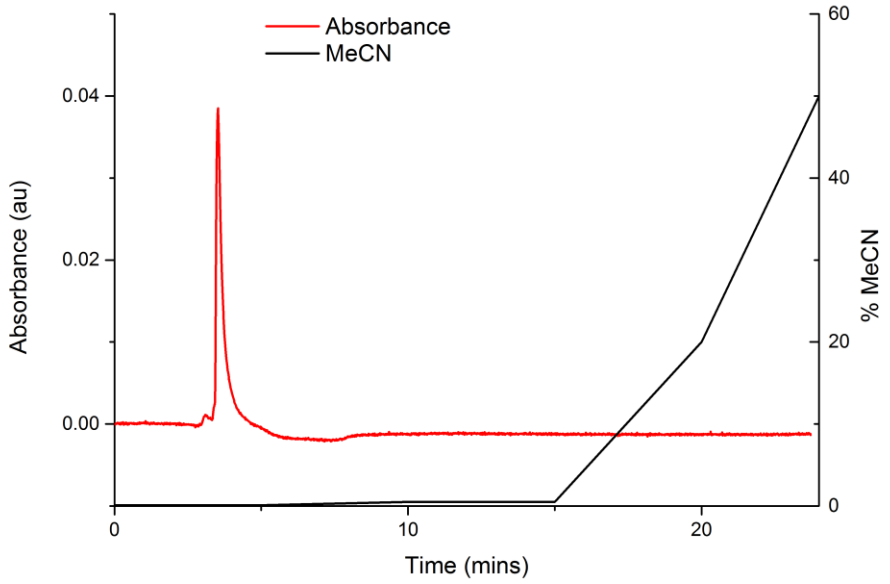

Figure 3.12: HPLC trace of the 2,3-2,3-configured Ugi conjugate **3-1** in aqueous/acetonitrile, detection at 280 nm.

A qualitative solubility screen was undertaken on **3-1.** It was noted that **3-1** had limited solubility in organic solvents including DCM and MeOH. The compound was only readily soluble in DMF. However its solubility was sufficient in DMSO for ^{1}H NMR spectroscopic analysis, and MeCN for HPLC

analysis. The solubility in DMSO was also sufficient to allow biological screening.

3.4. Screening of the Ugi conjugate 3-1

3.4.1. Screening against *E. coli* on LB and M9 agar

The antibacterial activity of the conjugate was assessed using a variation of a disc diffusion assay[118]. The key difference was that rather than using a disc impregnated with the compound, 3 μL of the solution was pipetted directly onto the agar plate. The compound was screened against *E. coli* BW25113 using ciprofloxacin **1-18** as a standard. The highest concentration used was 3.02 mM (equivalent to 1 mg/mL of ciprofloxacin **1-18**), and a 1 in 5 dilution series was prepared with four further concentrations (minimum 4.8 μM). Four plates were run concurrently, two plates using standard LB nutrient agar, and two using an M9 minimal agar (Chapter 7). In each plate both compounds were run in duplicate, allowing for four sets of data for each compound. The plates were spotted with ciprofloxacin **1-18** and conjugate **3-1** and grown overnight at 37°C. The plates were analysed and the radii of the zones of inhibition were measured (**Figure 3.13**). The data indicates that compound **3-1** is active against wild type *E. coli*. However, the antimicrobial efficacy was approximately 50% of that demonstrated by ciprofloxacin **1-18** at the same concentration. This was consistent with other ciprofloxacin conjugates reported[117-118]. It is proposed that a bulky substituent conjugated via the piperazinyl ring of ciprofloxacin **1-18** inhibits the ability of **3-1** to form the required dimer in the DNA replication complex[45-46]. This theory was further explored using a DNA gyrase assay.

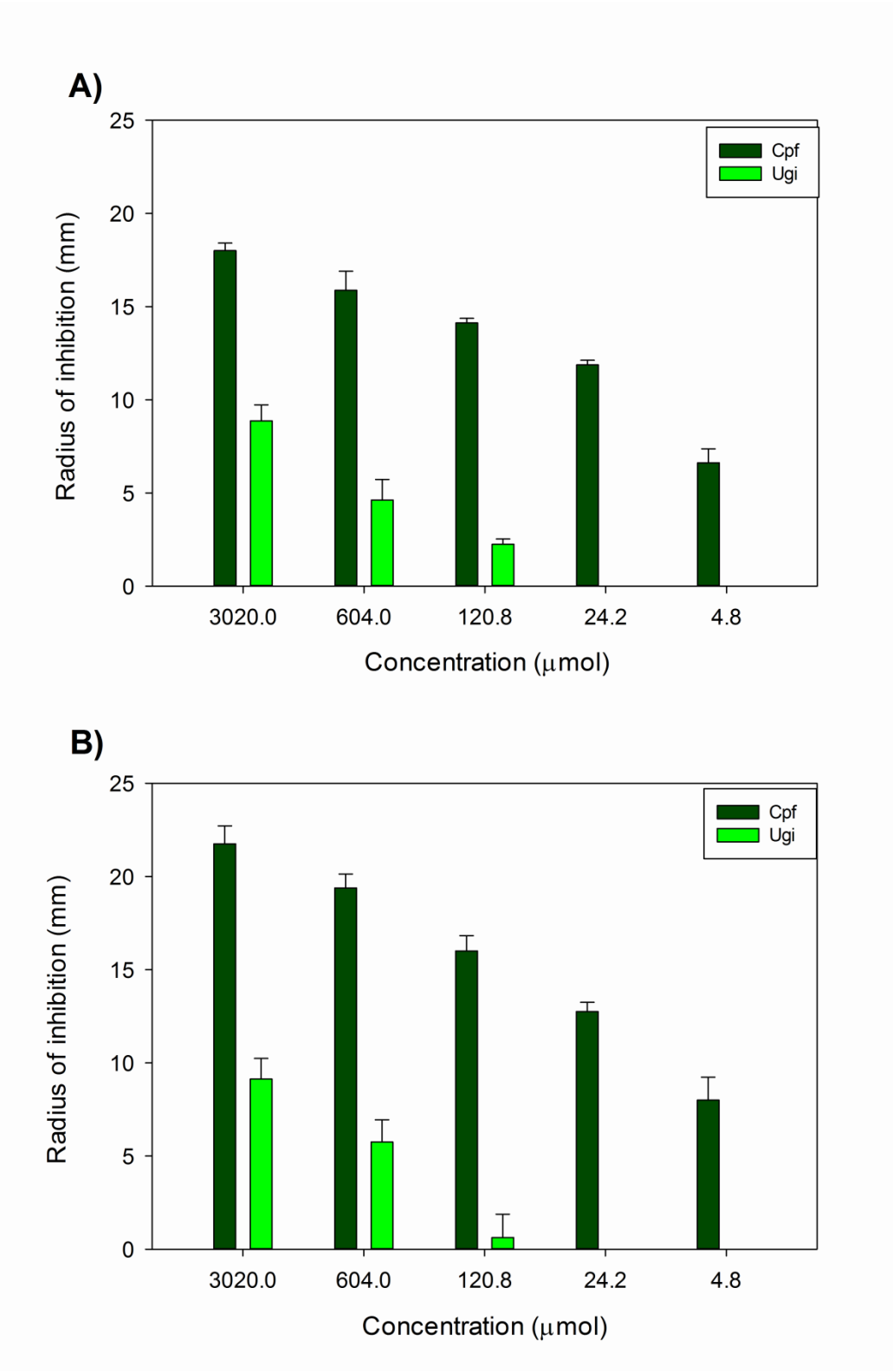

Figure 3.13: Plots of radii of inhibition for the Ugi conjugate **3-1** (light green) with a ciprofloxacin **1-18** control (dark green) on **A)** LB and **B)** M9 media. The experiments were performed in triplicate. Error bars represent ± one standard deviation from the mean.

3.4.2. DNA gyrase assay

While the zone of inhibition assay confirmed that the Ugi Trojan horse conjugate **3-1** was active against wild type *E. coli*, it did not prove that the ciprofloxacin moiety in the compound was the pharmacologically active component. To confirm this, a DNA gyrase assay was performed to ascertain if the compound inhibited the supercoiling of DNA by the gyrase protein. The assay involved incubating relaxed DNA with gyrase and the conjugate, at 37°C for 30 minutes, then separating the samples using electrophoresis on an agarose gel. Supercoiled and relaxed DNA run at different rates on the gel and so can be visualised as two separate bands after staining with ethidium bromide. A compound inhibiting DNA gyrase will give a result that shows high levels of relaxed DNA with relatively little supercoiling. Conversely an inactive compound, or one with lower activity, will show the opposite.

Initially, the assay used ciprofloxacin **1-18** over a range of concentrations ranging from 10 μM-0.1 μM, with two controls (no ciprofloxacin, no gyrase). After electrophoresis, the stained gel indicated a clear decrease in inhibition of DNA gyrase with decreasing concentration. The assay was repeated with both ciprofloxacin and the conjugate **3-1** over the same concentration range (**Figure 3.14**).

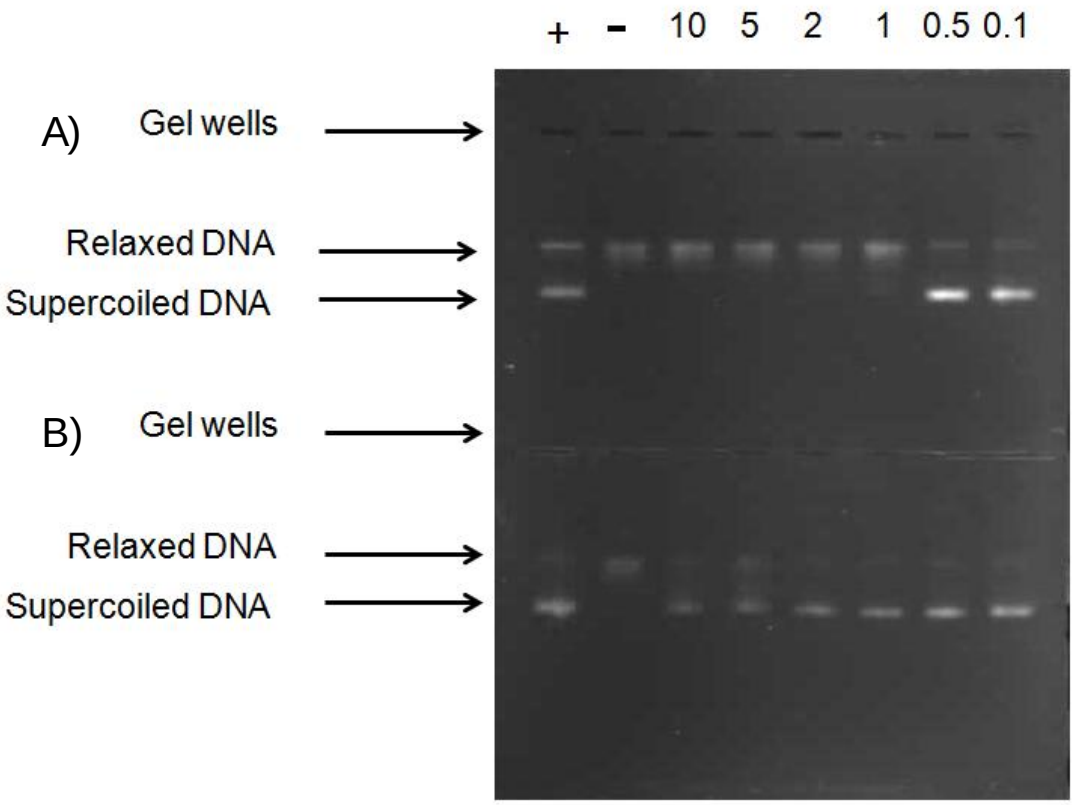

Figure 3.14: DNA gyrase supercoiling assay of **A)** ciprofloxacin **1-18** and **B)** the Ugi conjugate **3-1** with concentrations ranging from 10-0.5 μM. + = positive control, DNA gyrase present without the antimicrobial. − = negative control, no DNA gyrase or antimicrobial.

The assay showed ciprofloxacin acting on the DNA gyrase down to a concentration of 1 μM. This provides a reference point for comparing the activity of **3-1.** At 5 and 10 μM, there is evidence of some relaxed DNA. However, this may be due to the small amount of nicked DNA present in all the samples. A second assay was performed, using the conjugate **3-1** over a wider range of concentrations, from 200-1 μM. The resultant gel indicated that there was significant inhibition of DNA gyrase at higher concentrations (**Figure 3.15**)

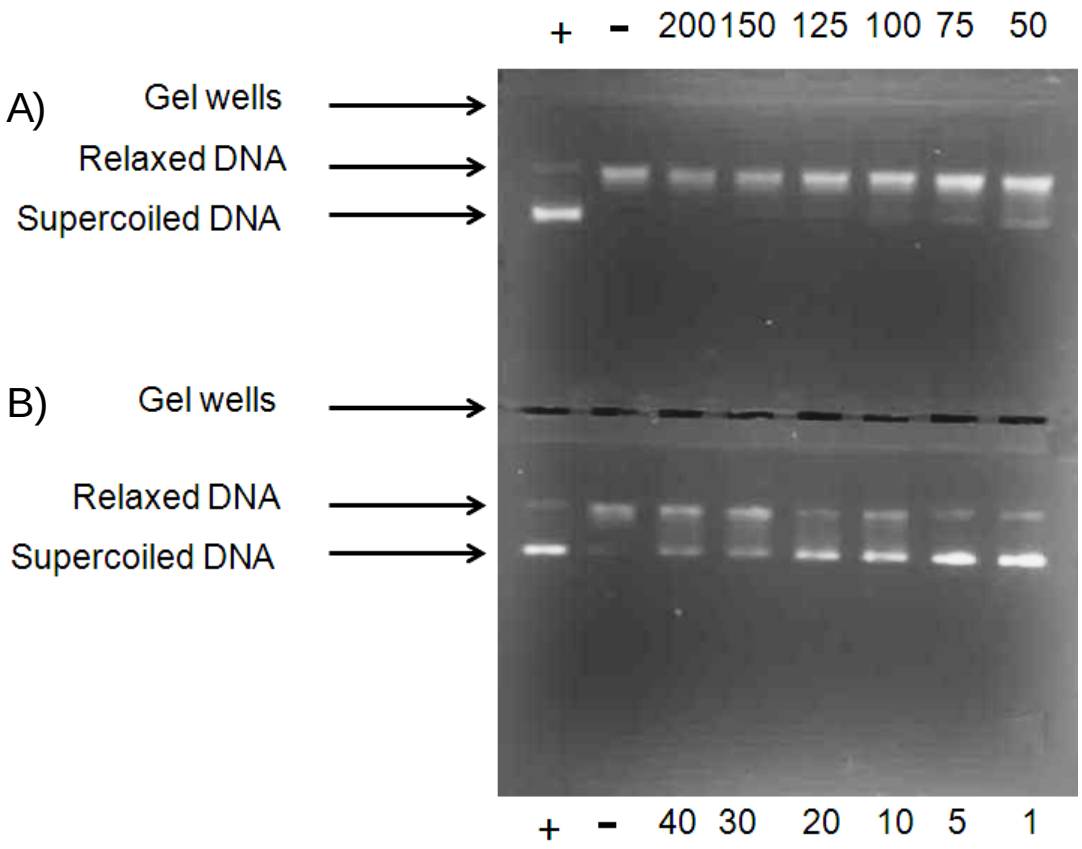

Figure 3.15: DNA supercoiling assay of the Ugi conjugate **3-1** with concentrations ranging from 200-1 μM. + = positive control, DNA gyrase present without the antimicrobial. − = negative control, no DNA gyrase or antimicrobial.

From the assay, an approximate MIC value can be elucidated, with a gradual, visible increase in activity with increasing concentration. The data shows that the MIC required for activity of **3-1** is between 10-20 μM, and the MIC for 100% inhibition is demonstrated to be 100 μM. This data supports the MIC value suggested by the zone of inhibition assay, where the lowest concentration that resulted in killing was 120 μM. The fact that the MIC for partial gyrase inhibition is lower than this value is due to the nature of the two assays. In the zone of inhibition assay the conjugate has to enter the cell and pass both the outer membrane and cytoplasmic membrane to reach its target, whereas in the DNA gyrase assay the compound is delivered directly to the gyrase. In this situation the ability to bind DNA gyrase is the key to activity and subsequently the observed activity is higher than that observed when using live bacterial cells. The biological data demonstrates that the

conjugate **3-1** is active as an antimicrobial compound; however its activity is significantly lower than the parent antimicrobial ciprofloxacin, due to steric hindrance of binding. Additionally it can be concluded from the difference in MIC between the two different assays; that reduced uptake of the conjugate is a factor in the lack of activity relative to the parent drug ciprofloxacin, but not as significant a factor as the inhibition of binding caused by steric hindrance.

3.5. Towards the synthesis of alternative siderophore-ciprofloxacin conjugates using the Ugi MCC

In conjugate **3-1 (Figure 3.16)**, there is only one atom between the two catecholamides, the minimum number of atoms between binding groups required for 1:1 complexation of iron is four, consequently **3-1** theoretically cannot form a 1:1 complex with iron. Chelators with short inflexible linkers favour the formation of binuclear complexes[197].

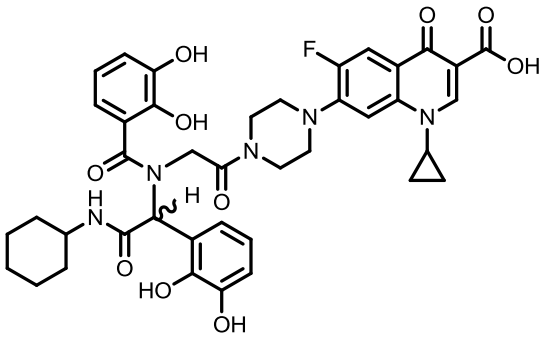

3-1

Figure 3.16: Structure of the Ugi conjugate **3-1**

Consequently, **3-1** is likely to form complexes with a 3:2 ligand:metal stoichiometry or 2:2 dimers. This would be problematic, as dimers and 3:2 complexes of **3-1** would have a molecular weight of over 1500 Daltons. As such, a complex would be more than double the size of a natural siderophore Fe(III) complex. It would be too large for siderophore transporters to accommodate. Consequently new analogues were designed to allow for greater flexibility and an increased distance between the iron binding

catechol groups. In addition, there are also alternative iron binding groups such as carboxylates which could be utilised in this synthesis.

3.5.1. Alternative iron binding groups

There are several examples of catechol siderophores with 2,3-dihydroxybenzoic acid groups such as bacillibactin **2-3** and enterobactin **1-34** (**Figure 1.16** and **figure 2.1**)[125, 198], and also a number of citrate (carboxylate) based siderophores[199-200]. The Ugi condensation allows the use of catechols with different hydroxyl configurations or combining catecholate and citrate binding groups in a single molecule, similar to petrobactin[74] (see chapter 2).

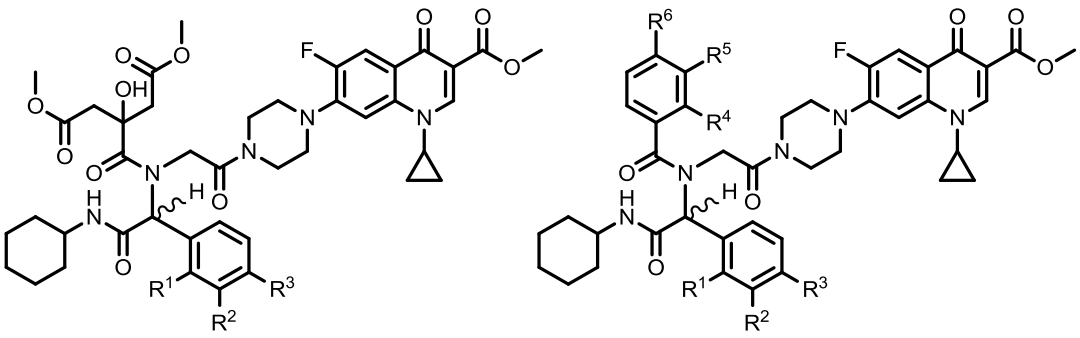

3-60: $R^1 = R^2 = OH$, $R^3 = H$
3-61: $R^1 = H$, $R^2 = R^3 = OH$

3-62: $R^1 = R^6 = H$, $R^2 = R^3 = R^4 = R^5 = OH$
3-63: $R^1 = R^4 = H$, $R^2 = R^3 = R^5 = R^6 = OH$
3-64: $R^3 = R^4 = H$, $R^1 = R^2 = R^5 = R^6 = OH$

Figure 3.17: Structures of potential Ugi conjugates with alternative iron binding groups.

3.5.1.1. Synthesis of alternative iron chelating components

A citrate component had been synthesised in the development of a petrobactin analogue (Chapter 2)[122]. It was decided to also prepare precursors that would allow the incorporation of 3,4-dihydroxybenzoic acid units into an Ugi MCC synthesised conjugate. The protected 3,4-bis(benzyloxy)benzaldehyde **3-65** and benzoic acid **3-66** precursors were prepared using the method of Rastetter *et al*. and Chimiak *et al*.[138, 153] (Chapter 2).

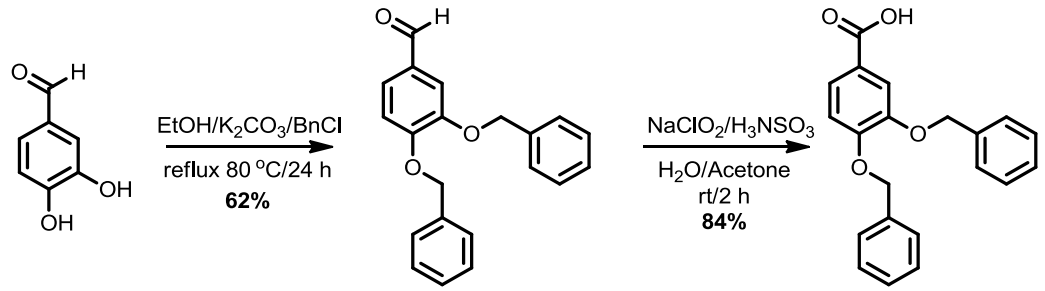

2-7 **3-65** **3-66**

Scheme 3.12: Synthesis of 3,4-bis(benzyloxy)benzaldehyde **3-65** and oxidation to the corresponding benzoic acid **3-66**

In a small scale reaction the aldehyde **3-65** was obtained in 62% yield, and subsequently oxidised to the carboxylic acid **3-66** in 84% yield, (**Scheme 3.12**). The citrate component, 1,5-dimethyl citrate **2-21** was synthesised as previously described (chapter 2) using the method of Hirota *et al*.[149].

3.5.1.2. Acid components with flexible linkers

Introducing a longer flexible linker between the carboxylic acid and the catechol units could modify the acid component of the Ugi MCC. This could also potentially reduce the hindered rotation seen which in **3-58** made analysis by ^{1}H NMR complex.

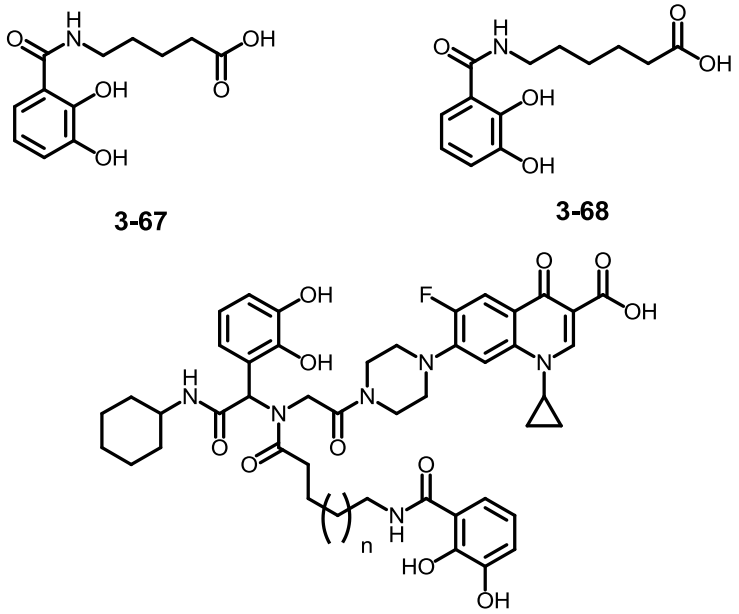

Figure 3.18: Two acid components for the Ugi condensation with pentyl **3-67** and hexyl **3-68** linkers, and the expected final structure of the condensation products **3-69** and **3-70**

It was decided to use two different aminated acids to generate linkers: 5-aminopentanoic acid **3-71**, and 6-aminohexanoic acid (**Figure 3.18**). The carboxylic acid of 5-aminopentanoic acid was protected using the same method used to protect the free carboxylic acid of ciprofloxacin **1-18** (**Scheme 3.13**)[117]. However the purification utilised a protocol specifically for the methyl ester of 5-aminopentanoic acid **3-72**[201], which gave the hydrochloride salt of **3-72** in 99% yield. The identity of the product was confirmed by an *m/z* peak of 132.1 in the ESI mass spectrum, corresponding to the $[M+H]^+$ ion of the required product **3-72**. A resonance at 3.67 ppm with a relative integration of three was present in the ^1H NMR spectrum. This supported the presence of the methyl ester. 6-aminohexanoic acid methyl ester was supplied commercially as the hydrochloride salt **3-73**.

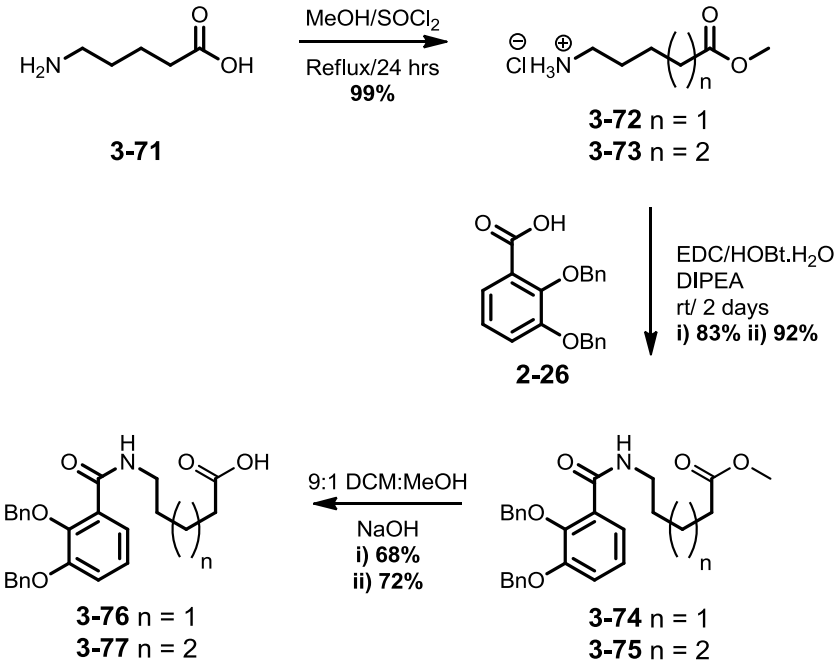

Scheme 3.13: Synthetic route to a catechol based carboxylic acid component with a pentyl linker. The hexyl linker was purchased as the methyl ester.

Both linkers were then coupled to 2,3-bis(benzyloxy)benzoic acid **2-26**. The coupling reaction was performed using the same amide coupling method as previously described[117]. The reactions were followed by TLC analysis. When the starting materials had been consumed, reaction mixtures were concentrated *in vacuo* and purified using flash chromatography. The hexyl linker **3-75** in 5:1 EtOAc: Pet. Ether, the pentyl linker **3-74** in 1:1 EtOAc: Pet. Ether. ESI mass spectrometry supported the successful formation of the pentyl linker **3-74**, as a peak with *m/z* 448.2 corresponding to the $[M+H]^+$ ion of the product **3-74** was observed in the spectrum. The ^1H NMR spectrum showed singlet resonances at 5.16 ppm and 5.09 ppm with relative integration of two corresponding to the benzyl CH_2 groups, a singlet resonance at 3.65 ppm with relative integration of three corresponding to the methyl ester and a triplet resonance at 7.97 ppm with relative integration of one corresponding to the amide proton. Formation of the hexyl linker **3-75** was supported by peaks of *m/z* 462.2 and 484.2 in the ESI mass spectrum, corresponding to the $[M+H]^+$ and $[M+Na]^+$ ions of **3-75** respectively. ^1H NMR analysis of **3-75** revealed the presence of the appropriate resonances at 4.9

and 5.1 ppm (benzyl CH_2 groups) and 3.57 ppm (methyl ester) with relative integrations of two, two and three respectively. This supported the formation of the product **3-75**. The pentyl linked **3-74** was isolated in 83% yield, and the hexyl linked product **3-75** in 92% yield.

The hexyl linker **3-75** was then deprotected to give **3-77** in 72% yield. The successful formation of the product was supported by two peaks with *m/z* of 448.2 and 470.2 in the ESI mass spectrum, corresponding to the $[M+H]^+$ and $[M+Na]^+$ ions of **3-77** respectively. In addition, the resonance of relative integration three at 3.57 ppm corresponding to the methyl ester was absent from the ^{1}H NMR spectrum The pentyl linked compound **3-74** was deprotected to give **3-76** in 68% yield. Successful deprotection was confirmed by ESI mass spectrometry where peaks with *m/z* of 462.25 and 484.21 were observed, corresponding to the proton and sodium adducts of **3-76** respectively. In the ^{1}H NMR spectrum, the singlet resonance with a relative integration of three at 3.65 ppm, corresponding to the methyl ester, was absent.

3.5.1.3. Rearrangement of functional groups

A second approach to prepare more flexible Ugi MCC synthesised conjugates is to alter the spatial arrangement of the components within the conjugate. It was decided to convert the ciprofloxacin amine to an acid component, and one of the catechol binding groups to an amine. (**Figure 3.19**) 2,3-bis(benzyloxy)benzoic acid **2-26** was reacted with 1,4-diaminobutane **2-40** as previously described (Chapter 2) to create the HCl salt of aminochelin **2-41**[161]. The methyl ester of ciprofloxacin was reacted with glutaric anhydride **3-80** to generate an acid functionalised linker **3-78** in 99% yield (**Scheme 3.14**).

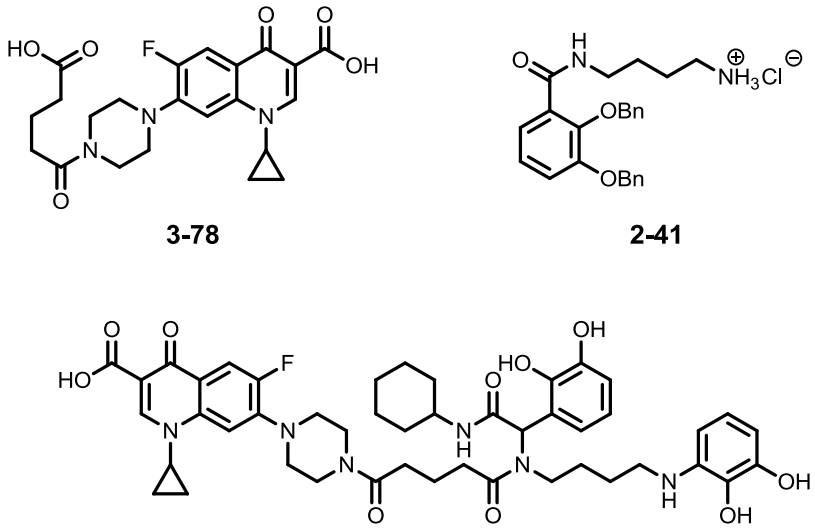

Figure 3.19: Structure of alternative acid and amine components for the Ugi condensation.

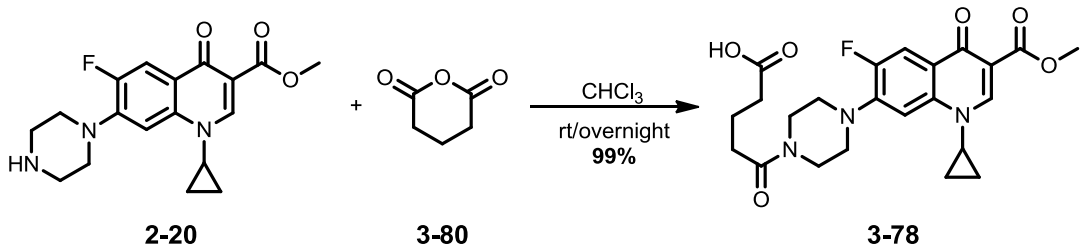

Scheme 3.14: Conjugation of an extended acid functionalised alkyl linker to the piperazinyl nitrogen of the methyl ester of ciprofloxacin

The formation of **3-78** was confirmed by ESI mass spectrometry and ^{1}H NMR spectroscopy. ESI mass spectrometry showed a peak at *m/z* 460.18, corresponding to the $[M+H]^{+}$ molecular ion of **3-78**. The ^{1}H NMR spectrum showed the resonance with a relative integration of one at 1.95 ppm was absent, confirming successful coupling to the piperazinyl nitrogen.

Aminochelin **2-40** was reacted with 2,3-bis(benzyloxy)benzaldehyde **2-25** to produce imine **3-80** (**Scheme 3.15**). Aminochelin **2-40** and 2,3-bis(benzyloxy)benzaldehyde **2-25** were suspended in anhydrous EtOH, and two molar equivalents of DIPEA added. After 18 hours stirring, a white

precipitate was observed. This was isolated by filtration giving **3-80** in 84% yield

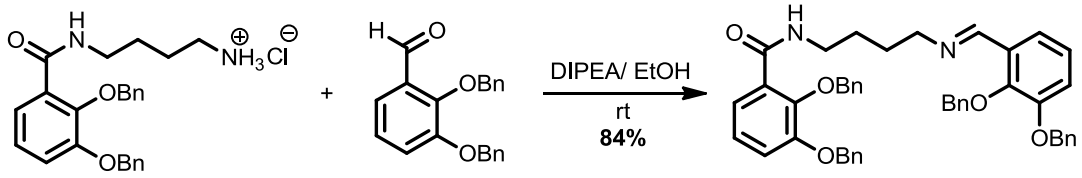

2-40 **2-25** **3-81**

Scheme 3.15: Synthesis of an imine intermediate **3-81** for an Ugi conjugate with a catechol based moiety as the amine component

Product formation was supported by ESI mass spectrometry and ^{1}H NMR analysis. The ESI mass spectrum contained peaks of *m/z* 705.3 and 727.3, corresponding to the $[M+H]^{+}$ and $[M+Na]^{+}$ ions of **3-81** respectively. ^{1}H NMR showed a singlet with relative integration one at 8.42 ppm, corresponding to the CH proton of the imine. A similar reaction was attempted using aminochelin with the protected version of the 3,4-(bis) benzyloxy benzaldehyde **3-66**. However, the reaction only proceeded in 10% yield and was not pursued further. With new building blocks successfully synthesised, future work can now be pursued preparing Ugi MCC conjugates with a variety of binding groups and varying linker lengths.

3.6. Summary, conclusions and future work

In summary, a novel Trojan horse antimicrobial compound has been synthesised from four components using the Ugi condensation. The compound contains two iron chelating groups and ciprofloxacin as the antimicrobial component. The compound has been characterised using ^{1}H NMR, IR spectroscopy and ESI mass spectrometry, with its purity assessed using HPLC. The antimicrobial activity has been assessed using a disc diffusion assay on nutrient rich and minimal media. The compound has been found to possess antimicrobial activity against *E. coli*, albeit at a lower level than the parent antimicrobial ciprofloxacin, which was used as the control. A DNA gyrase binding assay indicated that the compound acts in the same way as ciprofloxacin by inhibiting the action of DNA gyrase.

In addition, a number of building blocks have been synthesised with the potential to give alternative Trojan horse conjugates using the Ugi condensation. These include acid and aldehyde components with alternative iron binding groups, specifically citrate and 3,4-dihydroxybenzoic acid. Components have also been prepared containing alkyl linkers to act as precursors for more flexible Ugi conjugates with greater intramolecular distance between iron binding groups. This was achieved by conjugating amino acids to an existing acid component, and also by using an amine component for an iron binding group and using glutaric anhydride to convert the antimicrobial amine component to an acid component.

Future work in this area could be to see how effectively the proposed precursors can be employed in the Ugi condensation, and how effective the new Trojan horse conjugates are as antimicrobials. The proposed, more flexible, compounds may have limited activity due to their increased size, which may make them less likely to be taken up by bacteria. Additionally, further work could be performed to investigate the limits of the synthesised compound in terms of its spectrum of activity, and investigations could be carried out using iron transport *E. coli* mutants to probe whether or not the compound is actively transported.

4. Synthesis and biological evaluation of tetradentate catechol based ligands

4.1. Aims

The primary aim of the research in this chapter was to prepare a series of tetradentate bis-catecholate ligands with alkyl linkers of varying length. The secondary aim was to assess the stability and biological activity of the ligands with a view to using them as metal-chelating antibacterial agents, or as a means to smuggle cytotoxic metals into bacterial cells.

4.2. Introduction

4.2.1. Tetradentate ligands for the formation of metal complexes

The use of tetradentate ligands as metal chelators has been studied extensively in recent years, specifically their ability to self-assemble supramolecuar structures[202]. Tetradentate ligands, composed of two bidentate ligands joined via a spacer, have been shown to form bi-nuclear helical structures (**Figure 4.1**) with a variety of metal ions including gallium, titanium, copper and molybdenum[197, 203-204].

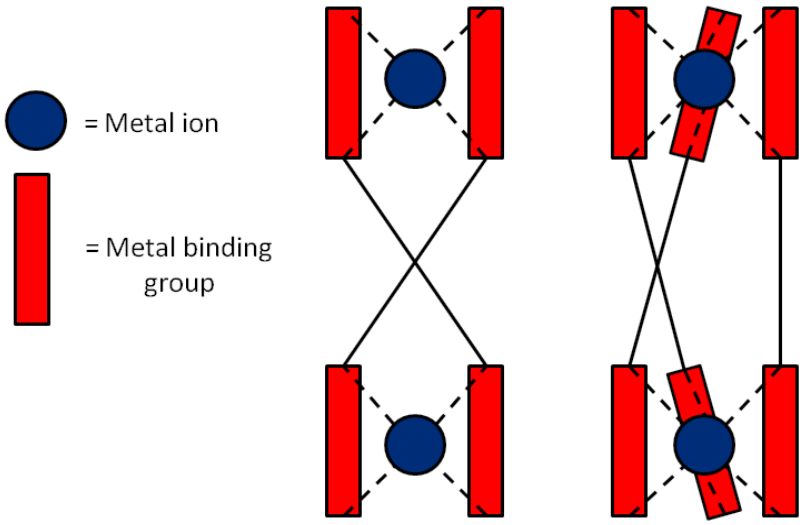

Figure 4.1: Schematic representation of double and triple stranded dinuclear helicates

The earliest example of the formation of helicates using tetradentate ligands was published by Lehn *et al.* They demonstrated the formation of double stranded helicates using a tetradentate bipyridine ligand (**Figure 4.2**)[204] . Subsequent work by Lehn also demonstrated the formation of tri nuclear double and triple stranded helicates using oligobypridine ligands[205].

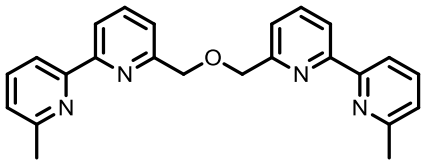

4-1

Figure 4.2: Bipyridine ligand synthesied by Lehn *et al.*

4.2.1.1. Tetradentate catecholamide ligands

The work of Lehn *et al.* has subsequently been built on by several groups to investigate the complexes of bis-catecholate ligands. Raymond *et al.* had already investigated the use of catecholamide based compounds for the sequestration of actinides, which included the early LICAMs (**Figure 4.3**)[206]

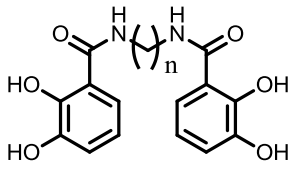

n = 2 **4-2**
n = 4 **4-3**
n = 6 **4-4**

Figure 4.3: Structure of the first LICAM ligands by Raymond.

In subsequent work Raymond produced catecholamide based ligands capable of forming 1:1 complexes with oxovanadium[207]. Duhme *et al*. produced similar mononuclear complexes using analogues of the *Azotobacter vinelandii* siderophore azotochelin (**Figure 4.4**). By mimicking a

natural siderophore they were able to prepare 1:1 complexes of dioxomolybdenum using their ligands[203, 208].

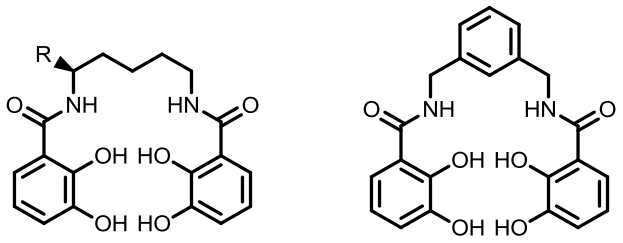

Figure 4.4: Bis-catecholamide ligands based on the *A. vinelandii* siderophore azotochelin (**4-5**)

Stack *et al.* demonstrated the formation of dinuclear complexes and triple helices using simple catecholamide ligands. These were based on alkane linkers, similar to ligands synthesised by Raymond designed for sequestering actinides (**Figure 4.5**)[206, 209-210]

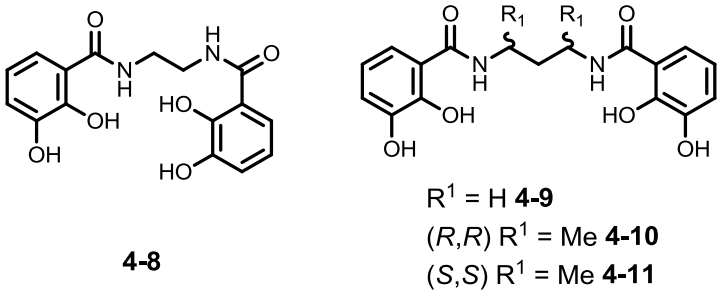

Figure 4.5: Alkyl linked bis-catecholamides synthesised by Stack *et al.* with ethyl **4-8** and propyl **4-9, 4-10** and **4-11** spacers

Stack demonstrated that the ethyl ligand **4-8** could form both dinuclear triple helices and 2:2 complexes with ferric iron. When using gallium with the propyl ligand **4-9** they observed only two species: free ligand and a 3:2 complex. Additionally, by using modified, chiral analogues **4-10** and **4-11**, they found that they could produce helicates stereoselectively. Subsequently Raymond *et al.* designed a series of rigid aryl linked bis-catecholate ligands (**Figure 4.6**), and successfully prepared discrete dinuclear helical complexes

using both gallium and iron[211-213]. Additionally, Raymond *et al* observed that if a mixture of their aryl linked ligands was reacted with Gallium acetylacetonate (Ga acac), rather than obtaining a range of mixed ligand complexes, they obtained three discrete helicates containing only one type of ligand[213]. Another key conclusion that has been drawn from the study of this type of ligand is that linker length is critical in the formation of the ligand-metal complexes. Specifically, a linker length of four atoms or less between the amides prevents the formation of 1:1 complexes and consequently favours the formation of 2:2 dimers, and 3:2 helicates. Duhme *et al.* and Raymond *et al.* both demonstrated that linkers with five atoms or more between the amide functionality were capable of co-ordinating to metal ions in a 1:1 ratio in tetradentate fashion[203, 207].

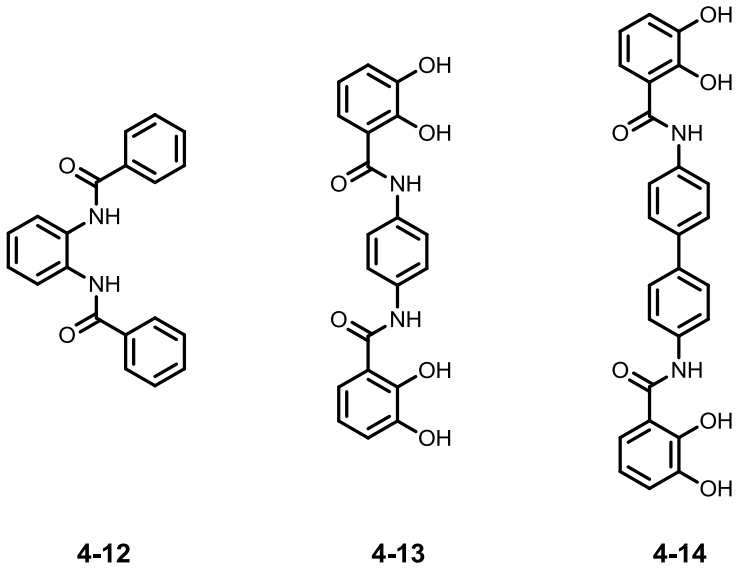

4-12 **4-13** **4-14**

Figure 4.6: Aryl linked bis-catecholamides synthesised by Raymond *et al*.[207]

4.2.1.2. Tetradentate catecholimine ligands

Further work in the field of tetradentate bis-catecholate ligands has also focused on catecholimines. The key advantage to this type of ligands is their easy synthetic availability[214]. Albrecht *et al.* prepared a broad range of catecholimine based ligands utilising both alkyl and aryl linkers (**Figure 4.7**)[214-216]. In their initial work on bis-catecholimine ligands, Albrecht *et al.* found that like bis-catecholamides, their ligands readily formed triple stranded

helicates. They also observed that the orientation of the binding group to the transition metal cation could be modulated using counter-ions. In the solid state the imine nitrogen was on the outside of the helicate (**4-18**), due to repulsion between the lone pairs on the nitrogen and the adjacent catechol hydroxyl oxygen (**Figure 4.8**).However, in solution in the presence of an alkali metal cation, the imine nitrogen faced inwards (**4-19**), adopting a conformation similar to the one observed by Raymond *et al.* with catecholamides (**4-20**)[214, 217].

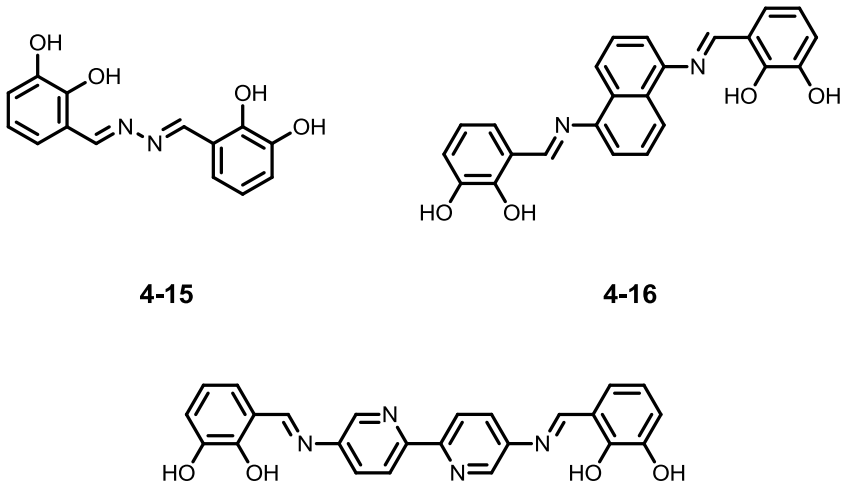

4-15 **4-16**

4-17

Figure 4.7: Examples of catechol imine ligands synthesised by Albrecht *et al*.[214]

4-18 **4-19** **4-20**

Figure 4.8: Binding modes of catecholimines in the absence **4-18** and presence **4-19** of an alkali metal cation, and the binding mode of a catecholamide **4-20**. M = transition metal cation, M' = alkali metal cation.

In later work Albrecht also demonstrated that the nature of the linker between the imine groups was important in the formation of metal helicates, by synthesising bis-catecholimines with sterically bulky backbones. They observed that sterically bulky ligands, while capable of forming triple helicates, also formed both oligomers and polymers, due to the steric bulk of the linkers suppressing binding of the alkali metal counter ions that direct helicate assembly[216].

4.2.2. Use of metal chelators as antimicrobials

Recently, the use of hydroxypyridininone ligands as antimicrobial compounds has been explored. Hydroxypyridinones are isostructural and can be isoelectronic with catecholates. As catechols are a common structural motif in siderophores[64], their iron binding capacity is well documented. As hydroxypyridinones are capable of binding ferric iron, but not mediating iron uptake, they can prevent bacteria from accessing it and consequently have potential as antimicrobial agents. Hider *et al*. have developed hexadentate ligands that demonstrated inhibitory activity (**Figure 4.9**)[218-219]. Activity was observed against both Gram-positive and Gram-negative bacteria.

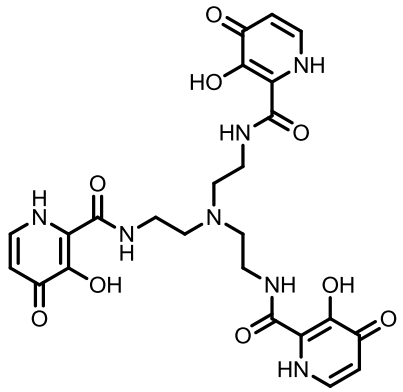

4-21

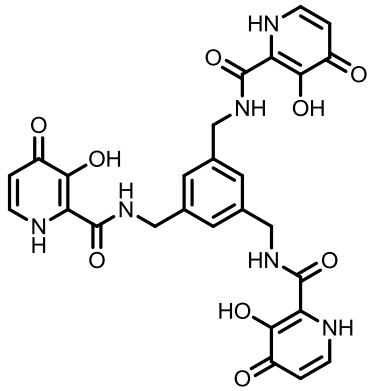

4-22

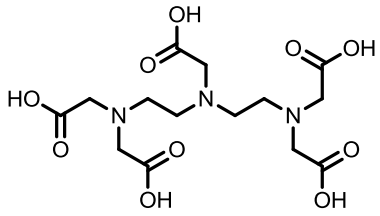

4-23

Figure 4.9: Hexadentate hydroxypyridinone ligands synthesised by Hider *et al*.[219] and DTPA **4-23**, a commercially iron chelator

The MIC values observed for Hider's compounds were comparable to a commercially available chelator: diethylene triamine pentaacetic acid **4-23** (DTPA). Hider observed MIC values as low as 40 μg/ml against *S. aureus;* with one compound (an analogue of **4-21**) displaying an MIC of 16 μg/ml against *E. coli* and *P. aeruginosa.*

The work of Hider demonstrates the potential that iron chelators have as antimicrobial agents. They could be applied as iron chelators to induce iron starvation in bacteria, or as delivery agents for cytotoxic metals such as gallium in the form of metal complexes.

4.3. Results and discussion

4.3.1. Synthesis of ligands

4.3.1.1. Design of ligands

The design of the ligands took into account several factors. The first factor was ease of synthesis. Alkyl linked bis-catecholimine ligands can be rapidly prepared by combining 2,3-dihydroxybenzaldehyde with the desired diamine linker in MeOH[214, 220], and the analogous amines prepared by using 2,3-(bisbenzyloxy)benzaldehyde in the imine condensation and subsequently reducing the imines and cleaving the benzyl ethers in a single step by palladium catalysed hydrogenolysis. Using catecholimines and amines is also advantageous, as it reduces the likelihood of the ligand-Fe(III) complex being recognised as a siderophore and utilised by bacteria as natural catecholate siderophores utilise catechol amides[64]. Catechol groups were used as donors as due to the high electron density of the oxygen atoms [67], they have a high affinity for tri-cations, reducing the risk of the ligands chelating important biologically relevant di-cations such as Zn(II) and Cu(II) *in vivo*[67]. Additionally it has been demonstrated that tetradentate siderophores can also form stable complexes with molybdenum[203, 208], which could provide an additional target against bacteria which rely on molybdate as well as iron for growth. The reason for using tetradentate bis-catecholate ligands is that while their ability to form metal complexes is well established[202, 211], their potential for use as antimicrobial agents has not been explored, with existing work in the literature more focused on bidentate and hexadentate ligands[219].

4.3.1.2. Unsymmetrical ligand

The initial idea for this work came from the synthesis of a component for the Ugi condensation chemistry described in the previous chapter. The Schiff base generated by combining benzyl protected aminochelin **2-37** with 2,3-bis (benzyloxy)benzaldehyde **2-25** provided an ideal precursor for an unsymmetrical bis-catecholate ligand **3-81**. It was decided to reduce the precursor using the same method used to deprotect the Ugi ciprofloxacin

conjugates (**Scheme 4.1**). This had the advantage of removing the benzyl ethers and reducing the imine to a secondary amine in a single step.

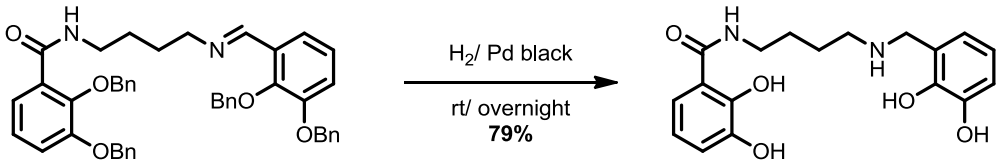

3-81 **4-24**

Scheme 4.1: Conversion of the imine **3-81** to give the unsymmetrical bis-catecholate ligand **4-24**

The precursor **3-81** was prepared using the method described in chapter 3. The deprotection was performed by catalytic hydrogenolysis. As the precursor was not EtOH soluble, a 1:1 mixture of EtOH and toluene was used to dissolve the precursor. Pd black was added as catalyst and the solution was stirred under H_2 at 50 atmospheres. After reaction workup the required product **4-24** was isolated in 79% yield. Product formation was confirmed by the presence of a molecular ion peak with *m/z* 347.16 in the ESI mass spectrum, confirming the removal of all four benzyl ethers and the successful reduction of the imine to a secondary amine. The ^{1}H NMR spectrum provided further confirmation. The resonance at 8.47 ppm with a relative integration of one was replaced by a resonance at 3.83 ppm with a relative integration of two. This confirms the transformation from a CH adjacent to an imine to a CH_2 adjacent to an amine. In addition, the resonances at 5.09 and 5.17 ppm, corresponding to the CH_2 groups of the benzyl ethers were no longer present.

4.3.1.3. Synthesis of bis-imine ligands

It was decided to prepare a series of bis-imine ligands to utilise as a comparison for the unsymmetrical ligand **4-24**. The chemistry for this had already been established by Smith and Winstanley, by reacting 2,3-dihydroxy benzaldehyde **2-18** in a 2:1 ratio with 1,8-diaminooctane in MeOH[220]. A series of compounds was synthesised using a range of linkers (**Scheme 4.2**).

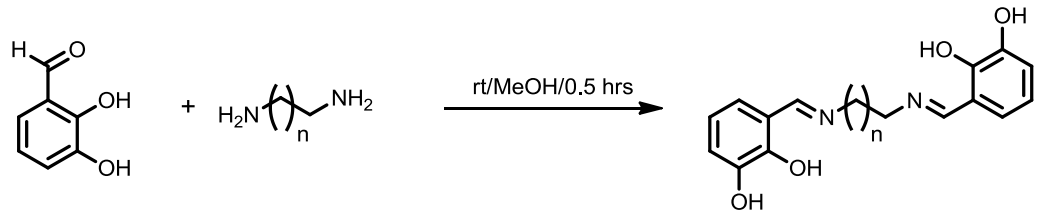

2-18

2-19 - n = 1
4-25 - n = 2
2-40 - n = 3
4-26 - n = 4
4-27 - n = 5
4-28 - n = 6
4-29- n = 11

4-30 - n = 1
4-31 - n = 2
4-32 - n = 3
4-33 - n = 4
4-34 - n = 5
4-35 - n = 6
4-36 - n = 11

Scheme 4.2: Overview of the synthesis of a series of bis-imine ligands

The ligands were all synthesised using a slightly modified method of Smith and Winstanley. In each synthesis 2,3-dihydroxybenzaldehyde **2-18** was dissolved in dry MeOH. 0.5 equivalents of the appropriate diamine were added and the solution stirred. After a brief period of stirring a brightly coloured precipitate, yellow or orange depending on the linker length, of the required imine was observed and isolated by filtration. A purification step was added to the method reported by Smith and Winstanley, the recovered imine was washed with ice cold MeOH to remove any remaining starting material, and yield the pure product. The colour of the product varied depending on the linker length. The yields of each synthesis are summarised in (**Table 4.1**)

Linker	Compound number	Yield (%)
Ethyl	**4-30**	89
Propyl	**4-31**	90
Butyl	**4-32**	100
Pentyl	**4-33**	72
Hexyl	**4-34**	75
Heptyl	**4-35**	100
Dodecyl	**4-36**	80

Table 4.1: Summary of bis-imine ligand syntheses

Successful synthesis was confirmed by ESI mass spectrometry and ^{1}H NMR spectroscopy. Successful formation of all ligands **4-30−4-36** was confirmed by the presence of a singlet resonance of relative integration two in the region 8.45-8.55 ppm. Additionally, there was no resonance corresponding to the starting material **2-18** in the spectra of the purified products.

4.3.1.4. Synthesis of bis-amine ligand precursors

To ascertain the impact of the linker between the catechol moieties and the alkyl backbone, a series of benzyl protected bis-imine ligands was prepared (**Scheme 4.3**). The intention was to hydrogenate these ligands using the same methodology used to convert the imine **3-81** to the amine **4-24**.

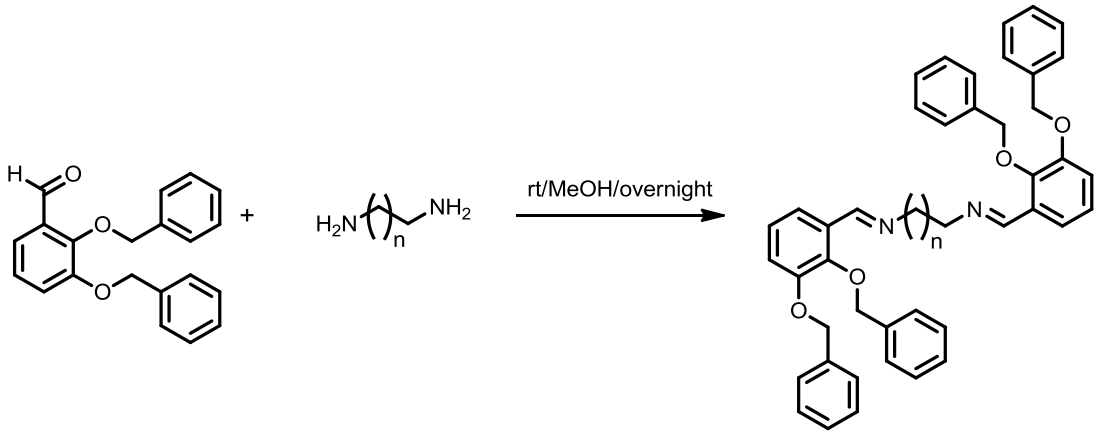

2-25

2-19 - n = 1
4-25 - n = 2
2-40 - n = 3
4-26 - n = 4
4-27 - n = 5
4-28 - n = 6
4-29 - n = 11

4-37 - n = 1
4-38 - n = 2
4-39 - n = 3
4-40 - n = 4
4-41 - n = 5
4-42 - n = 6
4-43 - n = 11

Scheme 4.3: Synthesis of benzyl protected bis-imine ligands

The ligands were prepared using the same method as bis-imines **4-30 – 4-36**. As 2,3-bis(benzyloxy)benzaldehyde **2-25** is significantly less soluble in MeOH than 2,3-dihydroxybenzaldehyde **2-18**, the required reaction time was longer. The yellow suspension was stirred overnight, a white precipitate was observed and isolated by filtration. The resultant white solid was then stirred in hot MeOH and filtered whilst hot to remove unreacted starting material, yielding a white solid as the product. The syntheses are summarised in (**Table 4.2**). Successful synthesis was confirmed by ESI mass spectrometry and ^{1}H NMR spectroscopy. In each ^{1}H NMR spectrum a singlet with relative integration of two was observed at approximately 8.52 ppm.

Linker	Compound number	Yield (%)
Ethyl	**4-37**	89
Propyl	**4-38**	90
Butyl	**4-39**	99
Pentyl	**4-40**	72
Hexyl	**4-41**	75
Heptyl	**4-42**	74
Dodecyl	**4-43**	56

Table 4.2: Summary of benzyl protected bis-imine syntheses

Despite the successful synthesis of the precursors for bis-amine ligands, Smith and Winstanley reported that their octyl bis-amine ligand was highly unstable, and decomposed in the solid state in approximately seven days [220]. It was unfeasible to deprotect, characterise and perform all the necessary tests on the ligands within that time scale and consequently the work on these ligands did not proceed further.

4.3.2. Biological screening of symmetrical bis-imine ligands and gallium

4.3.2.1. Use of gallium as a cytotoxic metal

Gallium was selected for use as a cytotoxic metal as it possesses the same electron configuration as ferric iron, and consequently can be incorporated into proteins which would usually contain iron. However, as it does not possess a variable oxidation state, gallium is incapable of undergoing the redox chemistry required for the function of such protein, and therefore blocks their function. Gallium has been shown to possess bactericidal activity against *P. aeruginosa* and has also been shown to

disrupt biofilm formation[221]. This can be a crucial property in treating more persistent infections. Consequently a treatment involving gallium nitrate entered clinical trials in 2009 for the treatment of *P. aeruginosa* in cystic fibrosis patients[222]. In 2012 a study by Visca *et al*. demonstrated the activity of gallium nitrate ($Ga(NO_3)_3$) against resistant strains of *A. baumannii* with activity observed down to a concentration of 4 μM in a human serum media[223]. Chen *et al*. also demonstrated the efficacy of $Ga(NO_3)_3$ against *A. baumannii,* they demonstrated that in the presence of transferrin $Ga(NO_3)_3$ had a bacteriostatic effect, due to the reduced availability of iron. Additionally Trojan horses using the siderophore desferrioxamine B and gallium have been studied, and found to kill both planktonic and mature biofilms of *P. aeruginosa* [224].

4.3.2.2. Screening of bis-imine ligands on solid media

Initially, it was decided to screen the ligands on solid media, using the same method as previously described (Chapter 3). Solutions (20 mM) were prepared of the propyl **4-31** and butyl **4-32** ligands, and gallium acetyl acetonate in DMSO. In addition, solutions of the propyl and butyl ligands were prepared containing gallium at ratios of 1:1 and 3:2 ligand:metal. A 1 in 5 dilution series was prepared in sterile H_2O, giving a set of solutions with concentrations ranging from 20 mM to 32 μM. The ligands were screened against *E. coli* BW25113 on LB agar. Ciprofloxacin was used as a control compound. After incubation, examination of the plates revealed that bacterial growth had occurred, but there was no sign of inhibition caused by the ligands, or by gallium acac. As gallium is known to have antimicrobial activity[221], this was an unexpected result. A likely explanation is the adsorption of gallium onto the agar, subsequently reducing the bioavailability of the metal and consequently its uptake into the bacterial cells. It was decided to rescreen the ligands and gallium acac in liquid culture.

4.3.2.3. Initial liquid culture screening of ligands

For the liquid cultures, cells were pre-grown in LB media. After overnight incubation at 37 °C the cells were centrifuged at 3500 rpm for three minutes, the supernatant removed, and resuspended in M9 glucose. The

process was then repeated. After the second resuspension, the culture was diluted 1 in 10 into sterilins containing M9 glucose. Each sterilin was then inoculated with 0.5 μM of each test compound (ligand, ligand: gallium or gallium) giving an active concentration of 100 μM in each culture. The cultures were incubated at 37 °C and their optical density at 650 nm (O/D_{650}) was measured after 0.5 hours, 6 hours and after overnight incubation (**Figure 4.10**).

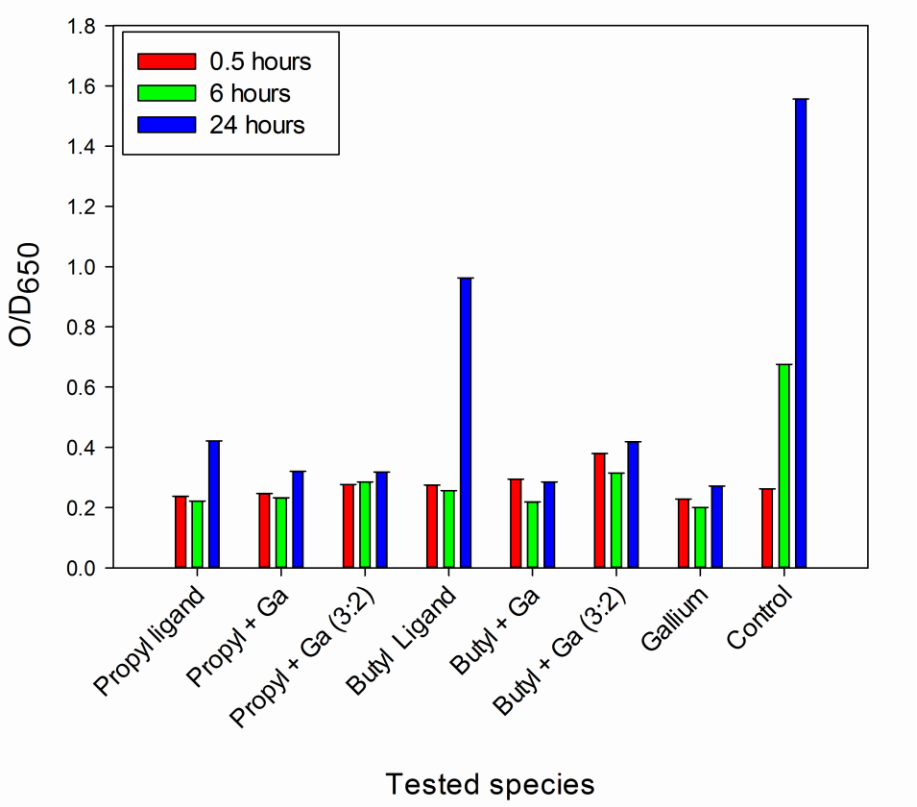

Figure 4.10: Initial liquid culture screening at 100 μM of ligands **4-13, 4-32** and in M9 agar with 0.2% glucose. The experiments were performed in triplicate. Error bars represent ± one standard deviation from the mean.

The results of the test screen were unexpected. All the solutions containing gallium acac exerted an antimicrobial effect: however the solutions containing only ligands **4-31** and **4-32** also showed evidence of growth inhibition. This suggested that the ligands could potentially act as antimicrobial agents in their own right, without the requirement for added gallium. Further investigation into the properties of the ligands was required.

4.3.2.4. Assessment of the impact of gallium on E. coli BW25113

While gallium acac displayed a high level of efficacy in the preliminary screening of the symmetrical ligands, it was decided to switch to gallium nitrate as an alternative gallium salt. The reason for the change was the potential toxicity of acac[225]. Using nitrate would allow certainty that gallium was the species exerting the antimicrobial effect. In addition, nitrate is non toxic and consequently would be safe for use in a drug preparation. A 20 mM solution of gallium nitrate ($Ga(NO_3)_3$) was prepared in DMSO. The *E. coli* cultures were prepared as previously described. The experiment was run in triplicate. Each culture was inoculated with $Ga(NO_3)_3$ solution to a specific concentration ranging from 100 – 0 μM, with six cultures for each concentration. Half of the cultures were also inoculated with 1 equivalent of iron nitrate ($Fe(NO_3)_3$). The cultures were incubated as previously described and their O/D_{650} measured after 0.5 hours, 4 hours and after overnight incubation (**Figure 4.11**). The data showed that over a 24 hour period, $Ga(NO_3)_3$ inhibited the growth of *E. coli*, down to a concentration of 40 μM in the absence of iron, relative to a control solution containing no gallium. However, while the cultures incubated with an equimolar amount of iron present suggested inhibition occurred after 4 hours, after 24 hours the O/D_{650} measurements observed were greater or equal to those observed for the control culture, even at 100 μM. This initial run demonstrated that $Ga(NO_3)_3$ was a suitable salt for use in further screening of the bis-imine ligands **4-30–4-36**. However subsequent assays using gallium nitrate yielded inconsistent results, with some assays showing normal growth of *E. coli*, even in the presence of high $Ga(NO_3)_3$ concentrations. A possible explanation for the lack of reproducibility could be the behaviour of $Ga(NO_3)_3$ in aqueous solutions. Under the assay conditions, the predominant gallium species formed is gallium hydroxide [$Ga(OH)_4^-$], which has poor bioavailability[226]. This could have resulted in lower accumulation of gallium in bacterial cells, and the subsequent lack of a bactericidal effect. Consequently, further experiments using gallium were not pursued as the data would not have been suitably reliable.

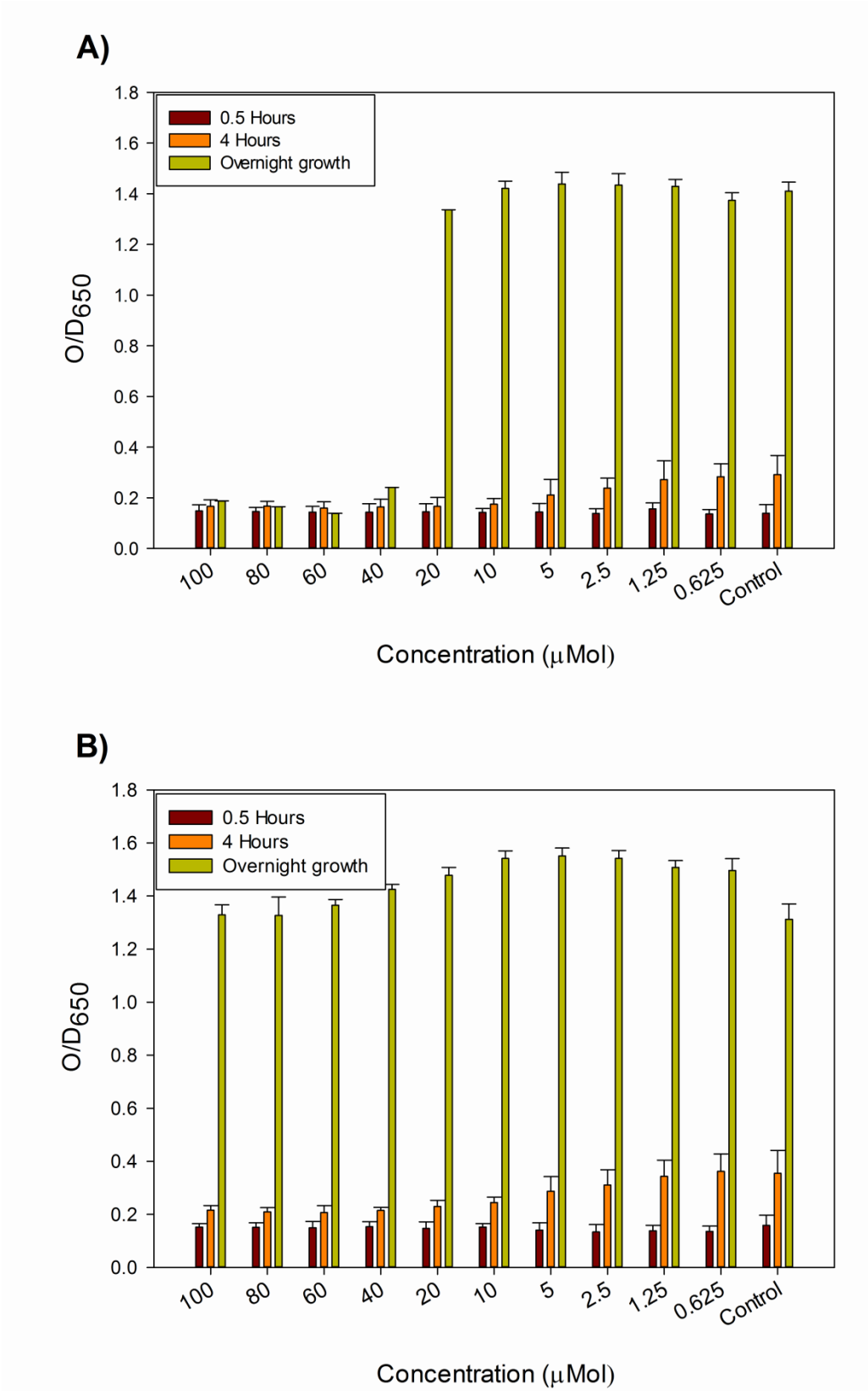

Figure 4.11: Effect of $Ga(NO_3)_3$) on the growth of *E. coli* in the **A)** absence and **B)** presence of one molar equivalent of $Fe(NO_3)_3$. The experiments were performed in triplicate. Error bars represent ± one standard deviation from the mean.

4.3.3. UV analysis of symmetrical bis-imine- ligands

As the small scale test screening on the ethyl and propyl ligands had yielded promising results, it was necessary to assess the stability of the ligands under the conditions used in the assay. Determining the stability would allow conclusions to be drawn about whether the ligands or a breakdown product were exerting the observed bacteriostatic effect.

4.3.3.1. UV analysis of symmetrical bis-imine ligands

To replicate the screening conditions, a buffer was prepared containing a phosphate concentration equivalent to the bacterial growth media (See experimental section). The carbon source and additional salts ($MgSO_4$, NaCl, and NH_4Cl) were omitted. As the ligands are not water soluble, an organic co-solvent was required. Consequently, the solutions for the UV analysis were prepared in a mixture of MeCN and buffer (5:3 ratio). For the experiments, a 2 mM solution (equivalent to 5 mg in 8 mL of the ethyl ligand) of each ligand was prepared in the MeCN: buffer solution. The stock solution of the ligand was then subjected to a 1 in 5 dilution (80 μM). The diluted sample was then analysed over a period of 8 hours with a reading taken every hour (**Figure 4.12**). The dodecyl ligand **4-36** was not subjected to analysis due to poor solubility in the solvent system used. The UV data showed clear variation over the specified time frame, indicating the breakdown of the bis-imine ligands, and the formation of a new species, determined to be 2,3-dihydroxybenzaldehyde **2-18** by comparison with the UV spectrum of the aldehyde. The increase in absorbance over time is attributed to the oxidation of the catechols to the corresponding quinone (**Scheme 4.4**). This was also observable as a colour change over time in the stock solution, as the solution gradually darkened from yellow to brown (**Figure 4.13**).

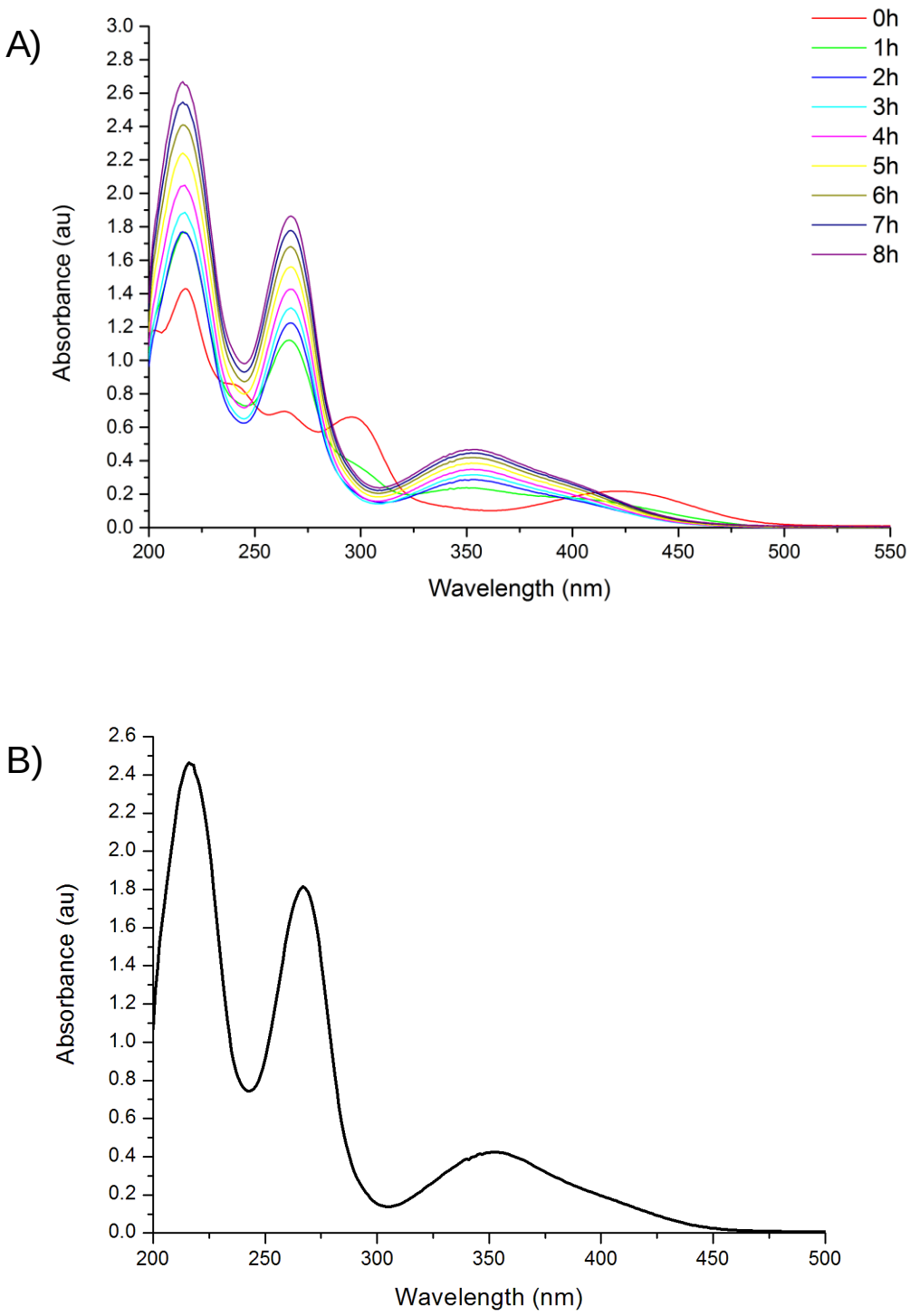

Figure 4.12: A) UV/vis spectra of the ethyl bis-imine ligand **4-30** recorded over 8 hours. B) UV/vis spectrum of 2,3-dihydroxybenzaldehyde **2-18**.

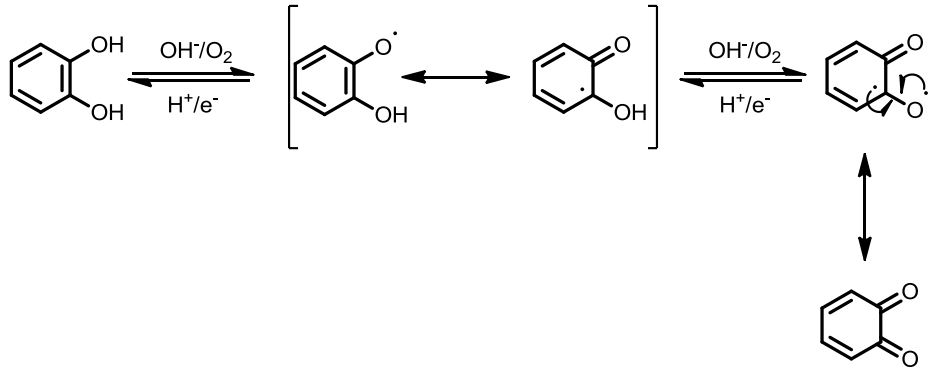

Scheme 4.4: Oxidation of a catechol to a quinone via the radical semiquinone intermediate

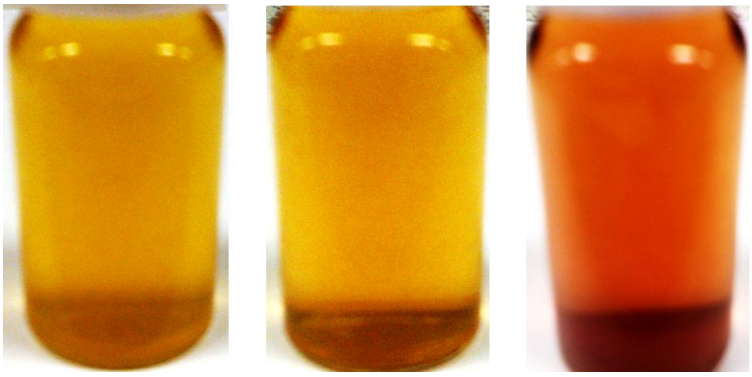

Figure 4.13: Solution of ethyl bis-imine ligand **4-30** in 5:3 MeCN:phosphate buffer at (left to right) T0, 8 hours, 24 hours

It was observed by comparing the UV spectra of the ligands **4-30–4-36**, that the rate at which the ligands decomposed was inversely proportional to the length of the linker between the catechol units. (See appendix 1). As ligands **4-30** and **4-31** decomposed very rapidly, it was decided to analyse their decomposition over a shorter time frame. The short time frame experiments on the two smallest ligands **4-30** and **4-31** confirmed the hypothesis that they were rapidly hydrolysing in aqueous solution. Whilst the remaining ligands **4-32−4-35** showed increasing stability, they were still unstable over the 24 hour time scale utilised for liquid culture biological screening experiments. An additional factor to consider is that the UV/vis experiments were performed at room temperature. As the ligands were unstable in solution at this temperature, it would be logical to presume that the hydrolysis of the ligands

would proceed at a higher rate during a biological assay performed at 37°C. Consequently it was decided not to proceed further with the screening of these ligands.

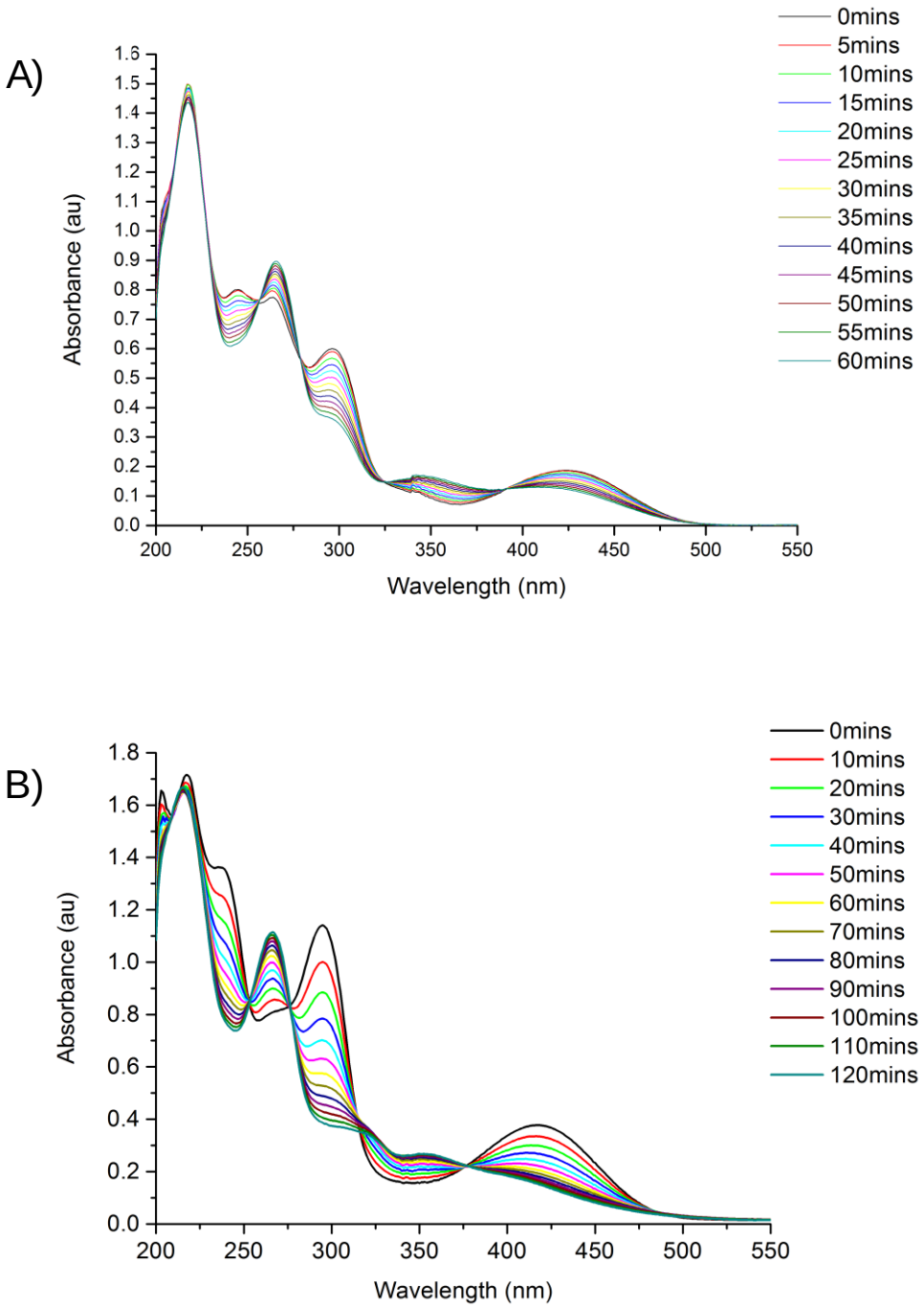

Figure 4.14: Changes in the UV/vis spectra of A) the ethyl bis-imine **4-30** over 1 hour and B) the propyl bis-imine **4-31** over two hours.

4.3.4. Biological screening of unsymmetrical ligand 4-24

4.3.4.1. Wild type screening in liquid culture

As screening of the symmetrical bis-imine ligands on solid media had yielded no useful data due to gallium adsorption onto the agar, the unsymmetrical ligand **4-24** was only screened in liquid culture. The cultures of *E. coli* were prepared and incubated as previously described. A 3 mM solution of the unsymmetrical ligand **4-24** was prepared in DMSO. The experiments were again run in triplicate. The cultures were inoculated with a specific volume of the unsymmetrical ligand **4-24**, using a concentration range from 100–0 μM. The cultures were incubated with shaking at 37°C, and the O/D_{650} was measured after 0.5 hours, 3 hours, 6 hours, and after overnight incubation (**Figure 4.15**). The results obtained indicated that the unsymmetrical ligand **4-24** possessed antimicrobial activity, with statistically significant levels of inhibition observed down to a concentration of 20 μM. In addition, unlike the bis-imines, where normal growth was restored after a period of 24 hours, cell growth was still repressed after the same period by **4-24** relative to the control culture.

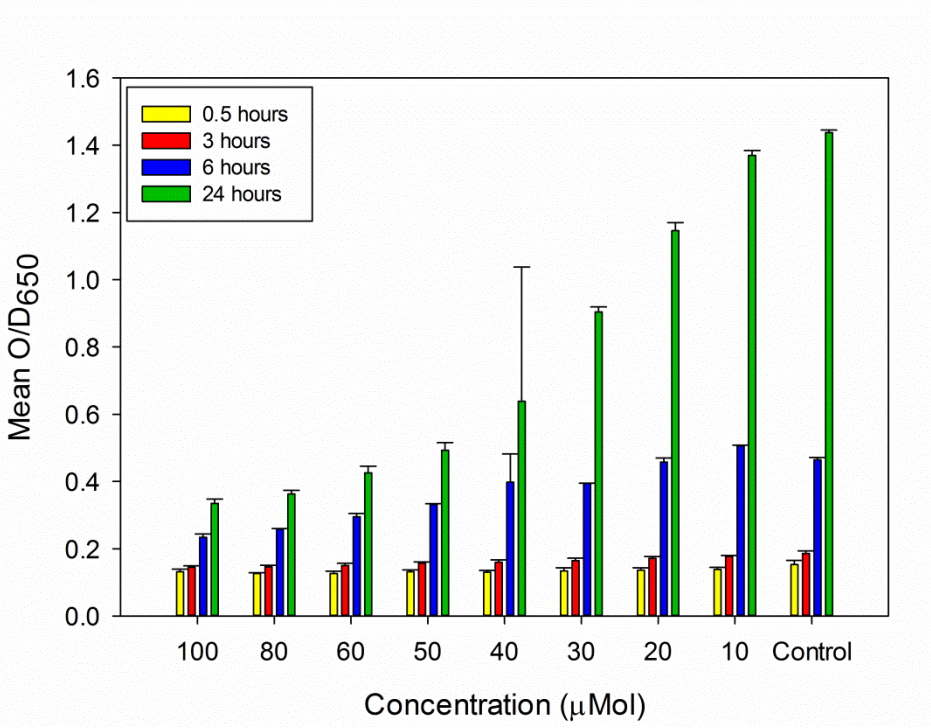

Figure 4.15: Inhibition of growth of E. coli BW25113 in the presence of unsymmetrical ligand **4-24**. The experiments were performed in triplicate. Error bars represent ± one standard deviation from the mean. Control culture solution contains no ligand.

The next step was to ascertain how **4-24** was exerting its bactericidal effect. As the compound **4-24** had been designed as a metal chelator, a potential explanation is that the ligand **4-24** sequesters iron from the culture medium, inhibiting the growth of bacterial cells via iron starvation. To test this hypothesis, the assay was repeated with 1 equivalent of $Fe(NO_3)_3$ added to each culture (**Figure 4.16**)

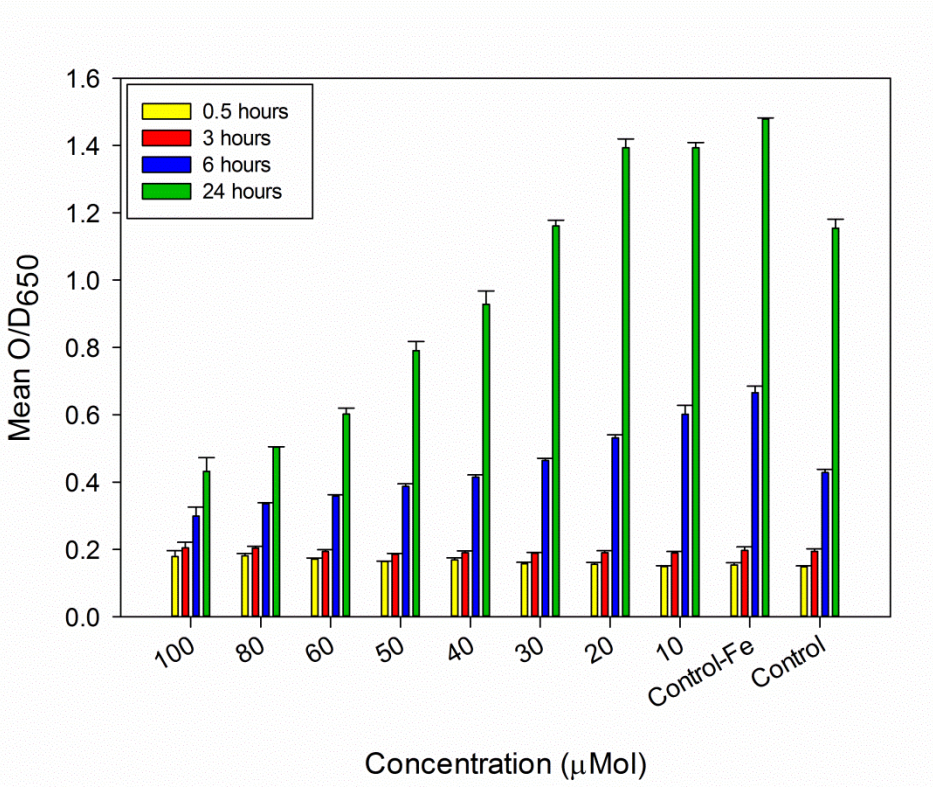

Figure 4.16: Inhibition of growth of *E. coli* BW25113 by unsymmetrical ligand 4-24 in the presence of 1 equivalent of $Fe(NO_3)_3$. The experiments were performed in triplicate. Error bars represent ± one standard deviation from the mean. Control-F culture contains no ligand and 50 μM $Fe(NO_3)_3$. Control contains no ligand or $Fe(NO_3)_3$.

The results of the assay indicated that while the addition of iron to the cultures increased the MIC of **4-24** to approximately 40 μM, there was still significant inhibition observed. This suggests that **4-24** is inhibiting the growth of *E. coli* via a mechanism other than iron starvation. Furthermore, at concentrations below 20 μM, higher levels of growth were achieved than those observed in the control cultures, suggesting that the ligand **4-24** could be behaving as a siderophore under those conditions.

*4.3.4.2. Screening of the unsymmetrical ligand **4-24** against E. coli deficient in enterobactin synthesis*

The results obtained by growing *E. coli* BW25113 in the presence of **4-24** and iron demonstrated that iron sequestration by the ligand and subsequent iron starvation is unlikely to be the mechanism of action of **4-24**.

Further investigation was required to confirm that iron sequestration was not the mechanism of action. To achieve this, the unsymmetrical ligand **4-24** was screened against an *E. coli* mutant EntA$^-$. The mutant was deficient for the EntA protein, a key part of the enterobactin biosynthetic pathway[227]. EntA catalyses the final step in the biosynthesis of 2,3-dihydroxy benzoic acid in an NAD dependent reaction (**Scheme 4.5**)[228]. The protein is a member of the short chain oxidoreductase (SCOR) family. The protein exists as a tetramer, each subunit is composed of a central 7 strand β-sheet, with 7 α helices located around the central sheet[228].

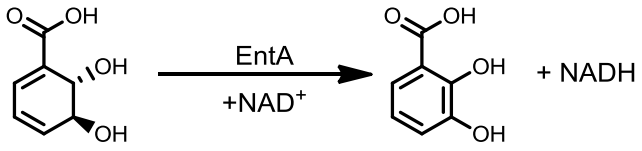

Scheme 4.5: NAD+ dependent biosynthesis of 2,3-dihydroxybenzoic acid from 2,3-dihydro 2,3-dihydroxybenzoic acid

Without this critical final step, *E. coli* is unable to synthesise enterobactin. Consequently it is deprived of its most efficient iron chelator. Additionally its ability to synthesise the alternative siderophore salmochelin S4 may also compromised as salmochelin S4 also contains the 2,3-dihydroxy benzoic acid moiety[64]. While the bacteria will still be able to scavenge iron through its mixed citrate/hydroxamate alternative siderophore aerobactin[62], its ability to obtain iron from its extracellular environment is significantly reduced.

The screening was performed as previously described, using the same concentration range as the wild type screening (**Figure 4.17**). The data indicated that against the mutant strain, inhibition was not observed, even at a concentration of 100 μM. In addition, it was observed that at most concentrations the unsymmetrical ligand **4-24** aided growth. Cultures that contained concentrations that were sub-lethal against the wild type strain, <30 μM, showed statistically significant growth above the level observed in the control.

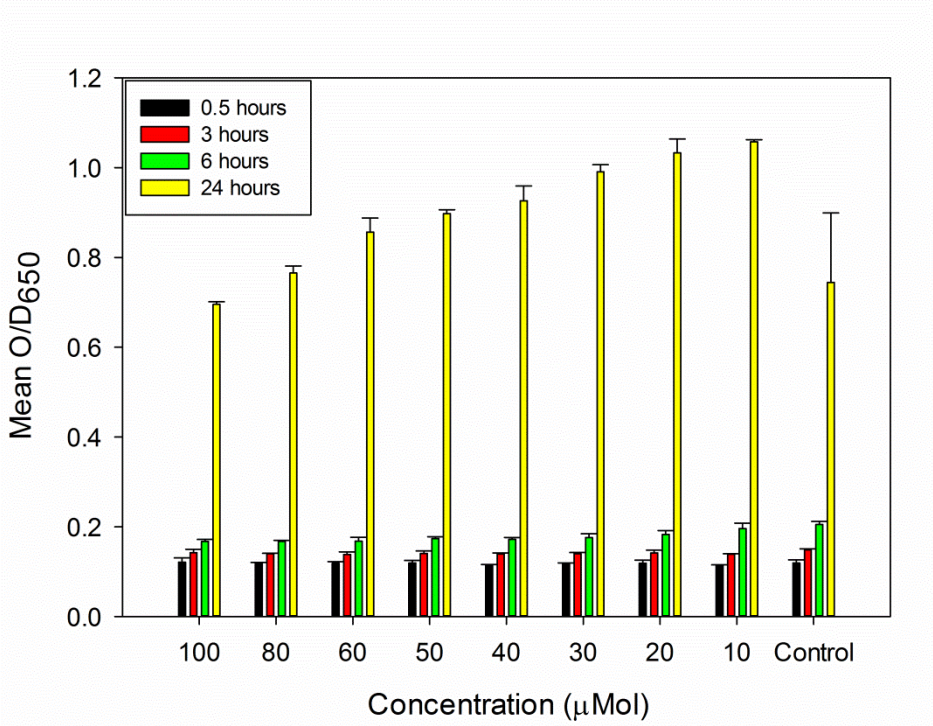

Figure 4.17: Mean O/D650 of EntA- E. coli BW25113 grown in M9 media in the presence of the unsymmetrical ligand 4-24. The experiments were performed in triplicate. Error bars represent ± one standard deviation from the mean. Control culture contains no ligand.

From the data it can be deduced that prevention of iron sequestration by bacteria is not the mechanism of action for the unsymmetrical ligand **4-24.** If that was the case then greater inhibition would have been observed in the absence of enterobactin, due to enterobactin's ability to remove iron from chelators with lower affinity[229-230]. The data suggests the opposite is true, and implies that the ligand **4-24** is gaining access to the cell and supplying iron, resulting in the observed increase in growth at sub-lethal concentrations. The reduced inhibition at higher concentrations could be due to ligand **4-24** forming complexes with extracellular iron and copper, present as trace elements in the buffer components. Complexation of metal ions would reduce the concentration of the free ligand within the cell and consequently it's antimicrobial effect. This is observed more easily in the absence of enterobactin as there is less competition for **4-24** when binding to these metal ions, and consequently the concentration of free ligand is reduced more than would be observed in the wild type screen (**Figure 4.18**).

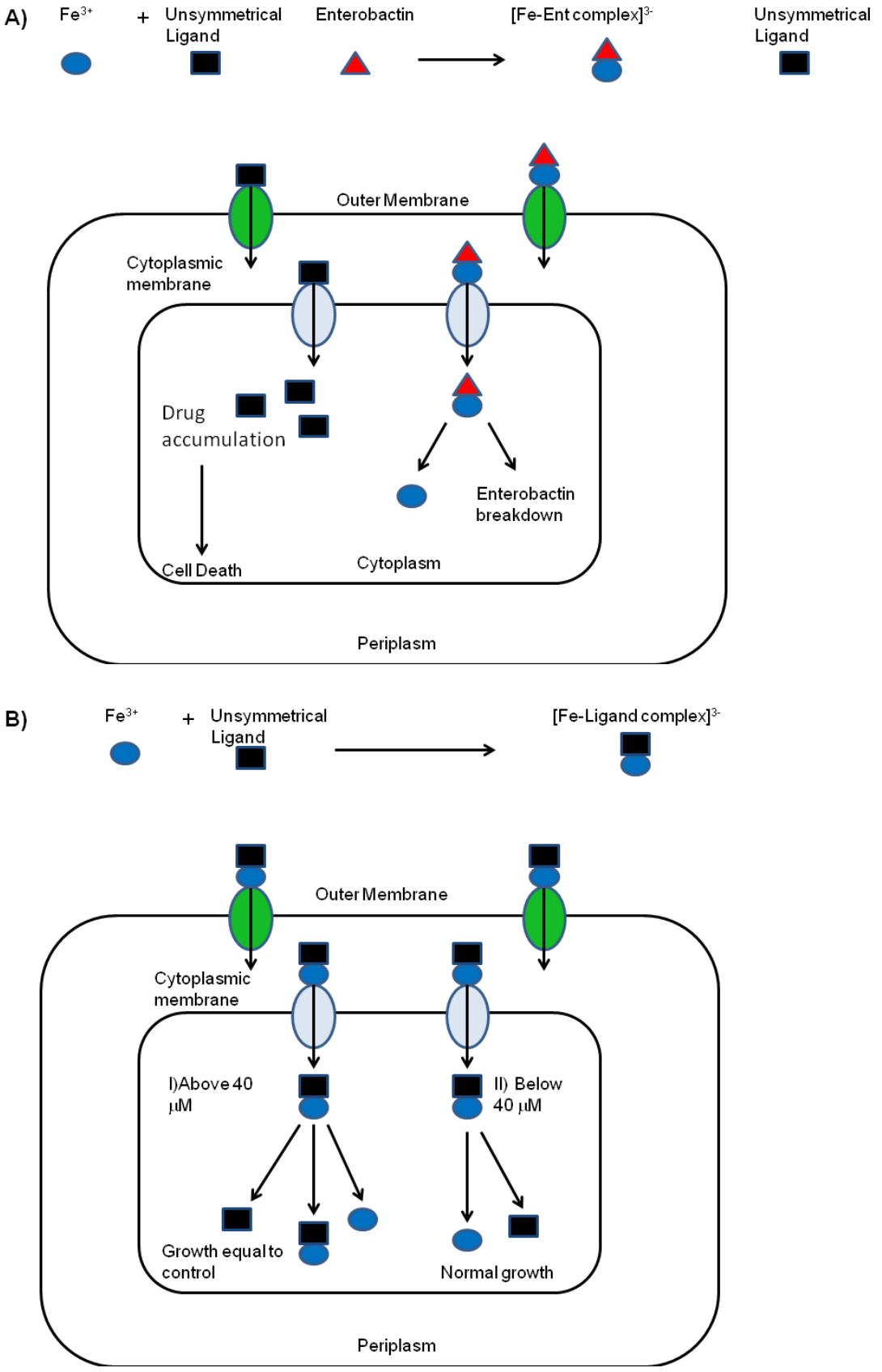

Figure 4.18: Schematic diagram of proposed explanation of the activity of **4-24** in the presence (A) and absence (B) of EntA. Bi) shows situation at concentrations above 40 μM Bii) shows the situation at concentrations below 40 μM

*4.3.4.3. Screening of unsymmetrical ligand **4-24** against TonB E. coli*

The results obtained in the previous assay indicated that in addition to possessing antimicrobial activity, the ligand **4-24** appeared to behave as a siderophore. To further investigate this possibility, the ligand **4-24** was screened against an *E. coli* mutant TonB^{-}. As TonB is essential for siderophore uptake in *E. coli*, its removal should result in a loss of activity if **4-24** is being actively transported as an iron complex through a siderophore transporter. The assay was performed as previously described, with an additional reading taken after 48 hours of growth (**Figure 4.19**).

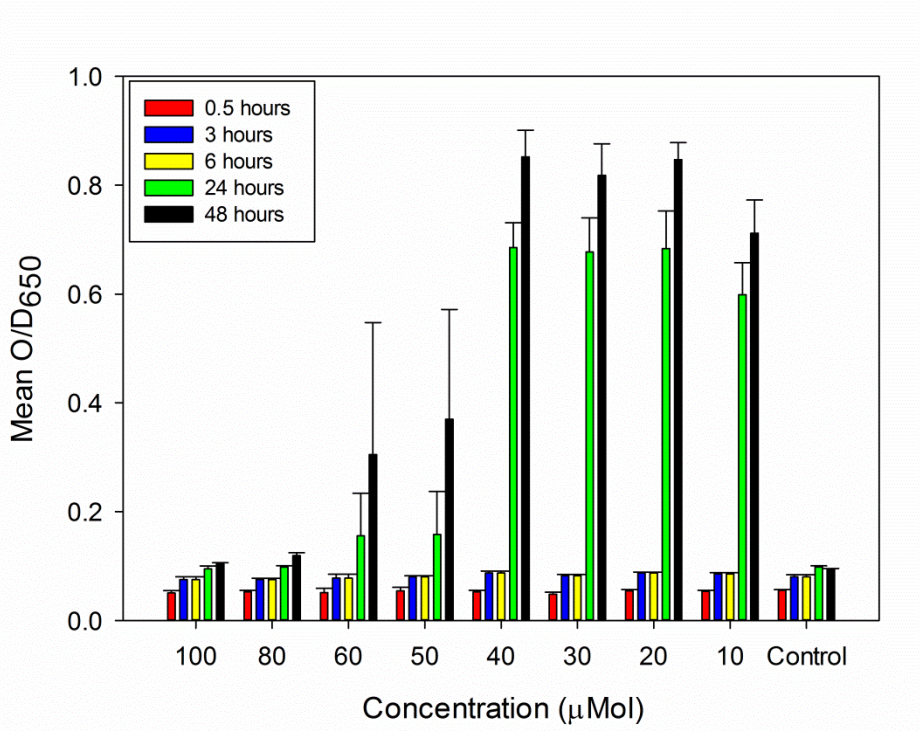

Figure 4.19: Growth of TonB- E. coli in the presence of unsymmetrical ligand 4-24. The experiments were performed in triplicate. Error bars represent ± one standard deviation from the mean. Control culture contains no ligand

The data observed demonstrates that the ligand **4-24** is not actively transported by a TonB dependent mechanism. However, the conclusion can also be drawn that the ligand does transport iron into the cells to allow growth, potentially through outer membrane porins as a 1:1 complex would be small enough (<600 Da) to pass through. The control culture shows minimal growth, as expected, due to the lack of siderophore-mediated iron

transport. Concentrations of **4-24** which were sub-lethal in the wild type screen show high levels of growth, suggesting that they are giving bacteria access to the iron required for growth. As the iron concentration in the media is a minimum of 3 μM due to trace amounts of iron in the buffer components, it is possible that this was complexed by **4-24** and transported via a porin into the cell. At concentrations above 40 μM, less growth is observed, suggesting that above this concentration some of the ligand may be still be transporting iron into the intracellular environment . However, as there is a sufficient concentration of non-complexed ligand, inhibition is observed. This explains the concentration dependence of activity observed for concentrations of 50 μM and above.

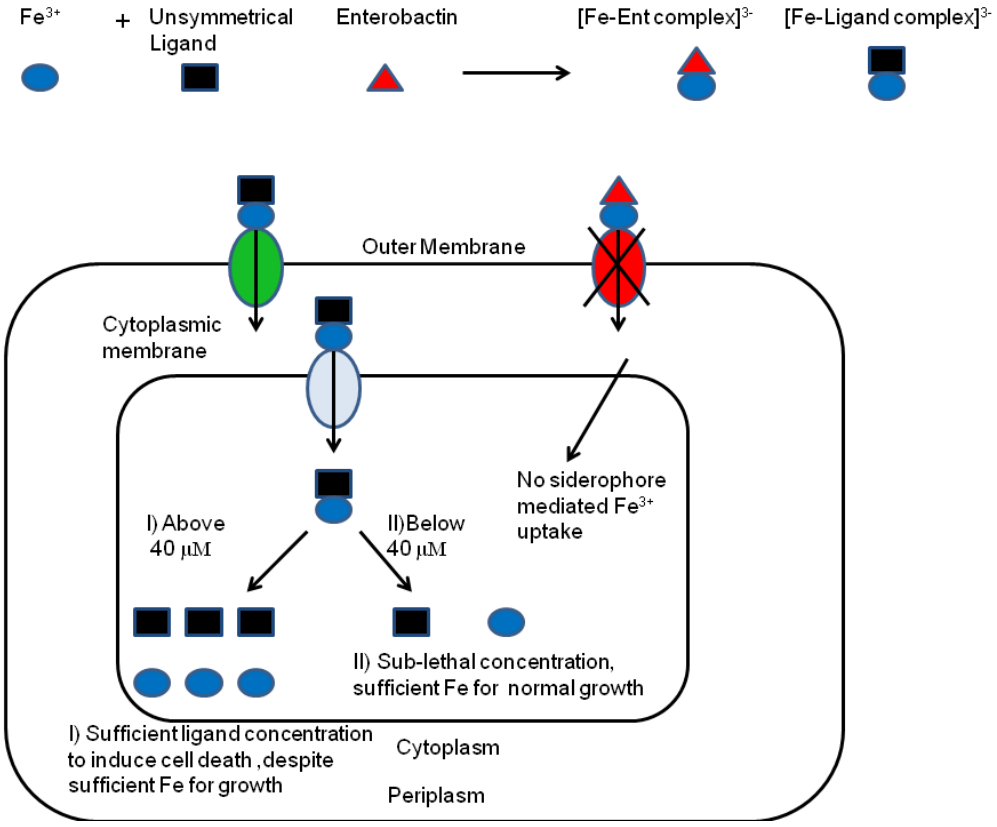

Figure 4.20: Schematic diagram of the proposed explanation of the activity of **4-24** in the absence of TonB

4.3.4.4. Screening of 4-LICAM and citrate against wild type E. coli BW25113

Screening against a TonB$^-$ mutant demonstrated that the ligand **4-24** was acting as a source of iron for *E. coli*, albeit not via active transport. It was

decided to compare its previously observed antimicrobial activity with two known iron chelators. The two iron chelators chosen were citric acid **1-26**, which is used as an exogenous siderophore by enteric bacteria[64], and 4-LICAM **4-3** (**Figure 4.21**)[231]. 4-LICAM was synthesised by D. J. Raines. The screening was performed as previously described using the same range of concentrations. For the citric acid **1-13** experiment, tri-sodium citrate was used.

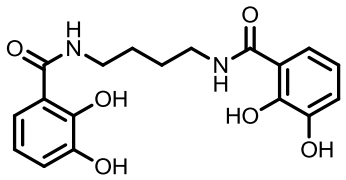

4-3

Figure 4.21: Structure of the tetradentate siderophore mimic 4-LICAM 4-3

The data obtained in the screen (**Figure 4.22**) yielded the expected result, that both citrate and 4-LICAM increased growth of *E. coli* BW25113 relative to a control with no iron chelator added. The 4-LICAM result is useful as it provides further evidence that it can function as a siderophore, following on from the work of Duhme-Klair *et al.* where they demonstrated that the 4-LICAM –Fe(III) complex can bind to a periplasmic binding protein[231]. The lack of antimicrobial activity demonstrated by the structurally similar 4-LICAM suggests that the antimicrobial effect observed when the unsymmetrical ligand **4-24** is added to cultures of *E. coli* is linked to the substitution of a secondary amine for one the amides in 4-LICAM.

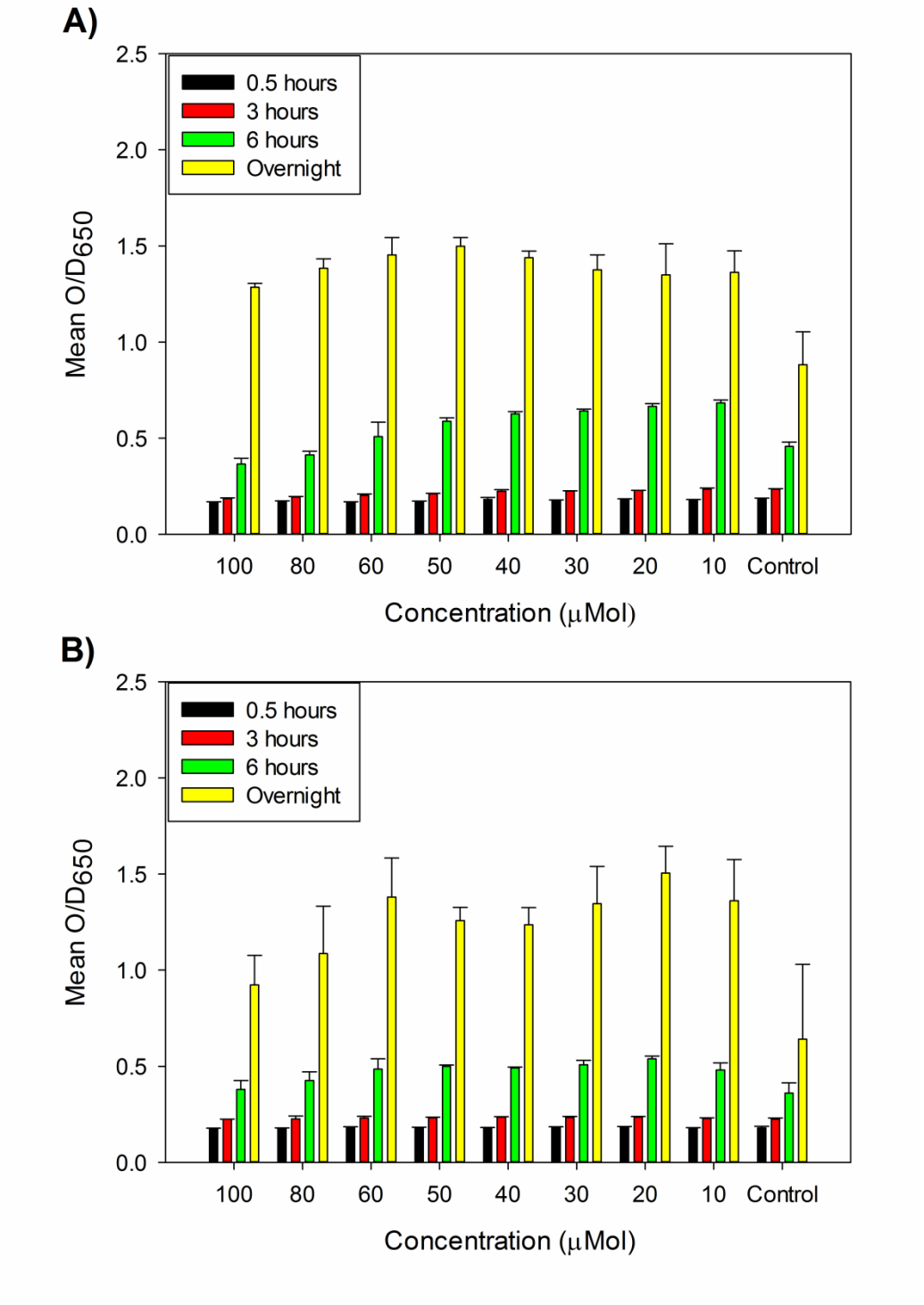

Figure 4.22: Growth of *E. coli* BW25113 in the presence of 4-LICAM **4-3** (top) and citric acid 1-26 (bottom). The experiments were performed in triplicate. Error bars represent ± one standard deviation from the mean. Control culture contains no ligand

4.3.5. Assessment of the stability of the unsymmetrical ligand 4-24

4.3.5.1. UV/vis analysis

To ascertain the suitability of the unsymmetrical ligand **4-24** as an antimicrobial compound, it was necessary to assess its stability in solution. The compound **4-24** was analysed in the same manner as the symmetrical bis-imine ligands **4-30−4-36**. A 2 mM stock solution was prepared and diluted to 80 μM. The ligand was initially analysed over a period of 1 hour, followed by a set of readings covering 8 hours (**Figure 4.23**). The UV spectra show minimal change over the course of 1 hour. On the 8 hour time scale, there is some evidence of a chemical change occurring. The most likely change is oxidation of the catechols to the corresponding quinones, as was observed with the symmetrical ligands.

From the UV data obtained it can be concluded that the unsymmetrical ligand **4-24** does not hydrolyse to individual catechol units in the same manner as the symmetrical bis-imine ligands, but that over time it is susceptible to oxidation. From the data, it is not possible to determine which exact species is responsible for the antimicrobial effect. It could be the ligand **4-24**, the corresponding quinone, or a partially oxidised semiquinone species.

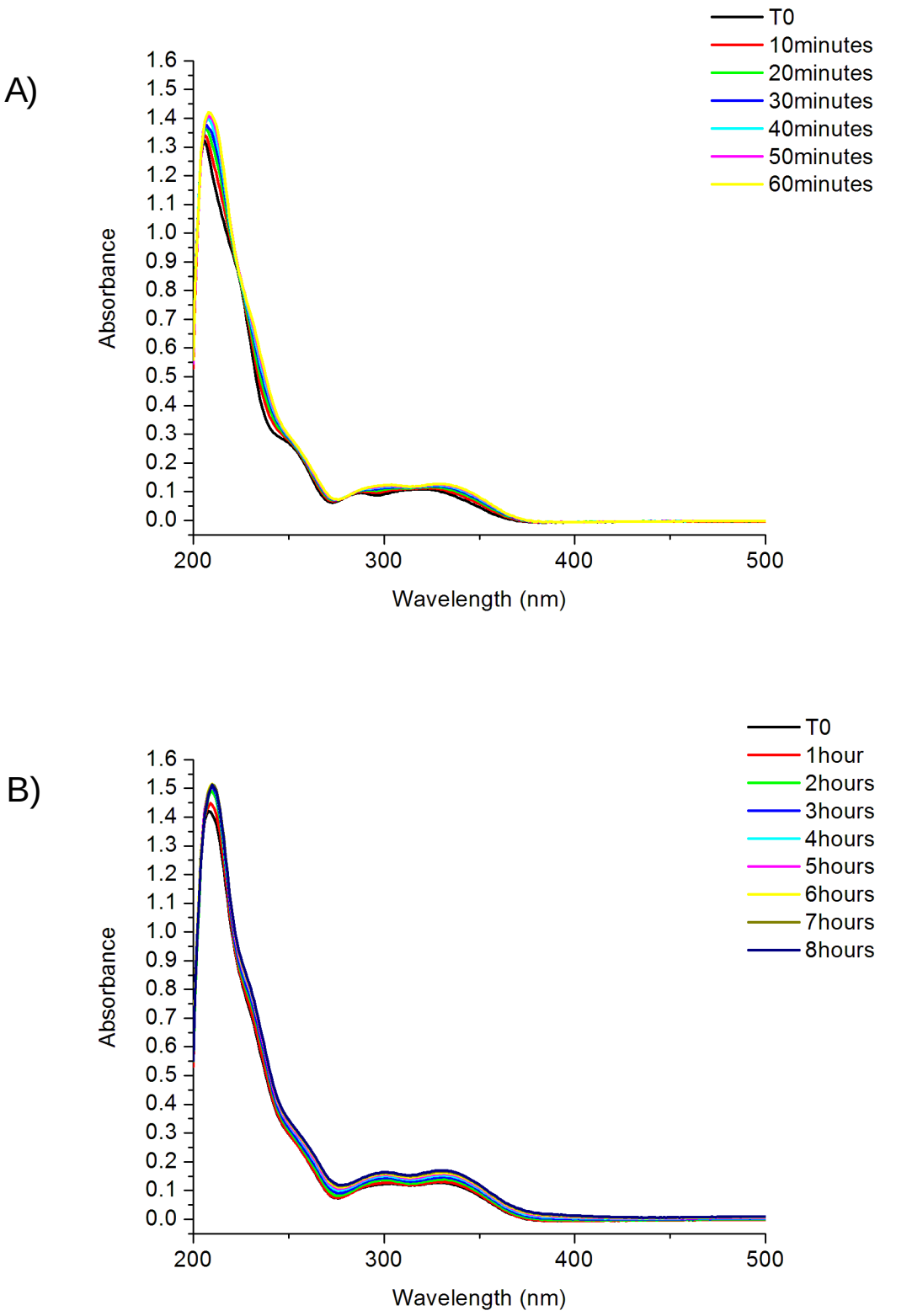

Figure 4.23: Changes in the UV spectra of 1mM unsymmetrical ligand **4-24** over **A)** 1 hour and **B)** over 8 hours in phosphate buffer (2:1 Na_2HPO_4: KH_2PO_4)

4.3.5.2. Electrochemical analysis

It was decided to undertake an electrochemical investigation on the ligand **4-24** in order to determine its redox potential, and to analyse its susceptibility to oxidation. The study was performed in MeCN using ferrocene as a standard and 0.1 M tetrabutylammonium hexafluorophosphate ([(*t*-Bu)$_4$N]PF$_6$) as a supporting electrolyte. Ferrocene was used because it exhibits reversible single electron transfer in a number of solvents and is therefore a suitable species to calibrate the reference electrode[232]. The electrochemical cell was set up using a Saturated Calamel Electrode (SCE) for the reference, a platinum disc for the working electrode, and platinum wire for the counter electrode. To determine the experimental set up for the calibration, the experiment was run using only the electrolyte. The parameters were set with a starting potential of zero, P1 = 1000 mV and P2 = -500 mV. The scan rate was set to 50 mV/S. The SCE was then calibrated using this set up with 2 mM ferrocene (**Figure 4.24**)

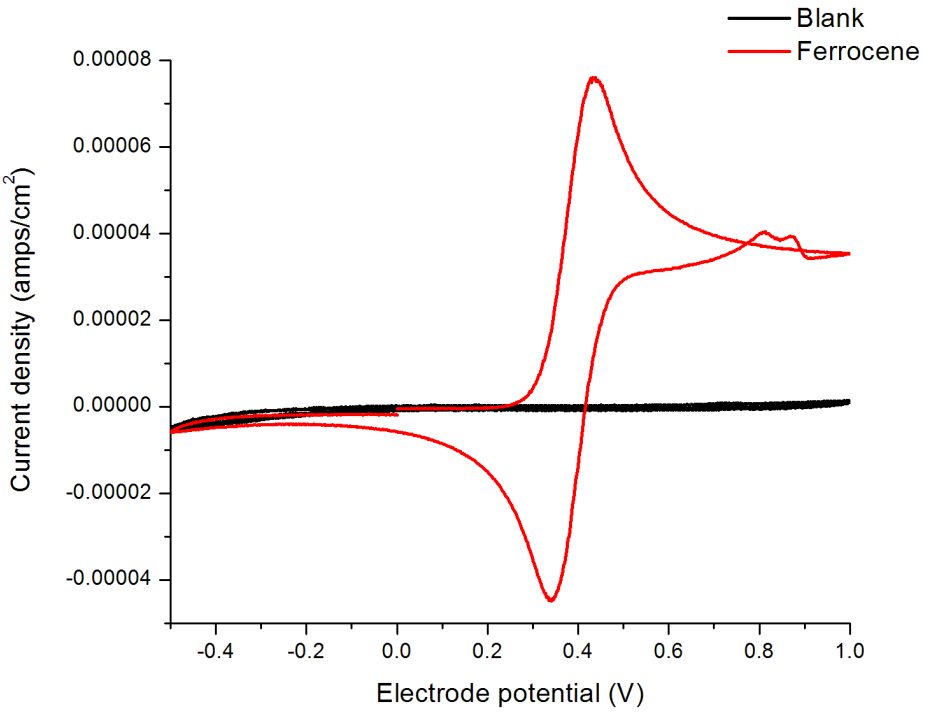

Figure 4.24: Cyclic voltammogram of 2 mM ferrocene, relative to a solution containing 0.1 M [(t-Bu)$_4$N]PF$_6$ as an electrolyte in MeCN

With the electrode calibrated, the parameters of the experiment were modified to identify a potential window where the ligand **4-24** could be oxidised. Initially, the ligand was analysed using a potential window starting at 1000 mV and scanning to −2000 mV at a concentration of 2 mM. No quantifiable change was observed. The potential window was changed to use more positive potentials, and the concentration of the ligand **4-24** solution increased to 10 mM. The final potential window utilised a potential range from 700-2500 mV (P_0 = 700 mV, P_1 = 2500 mV, P_2 = 700 mV) (**Figure 4.25**).

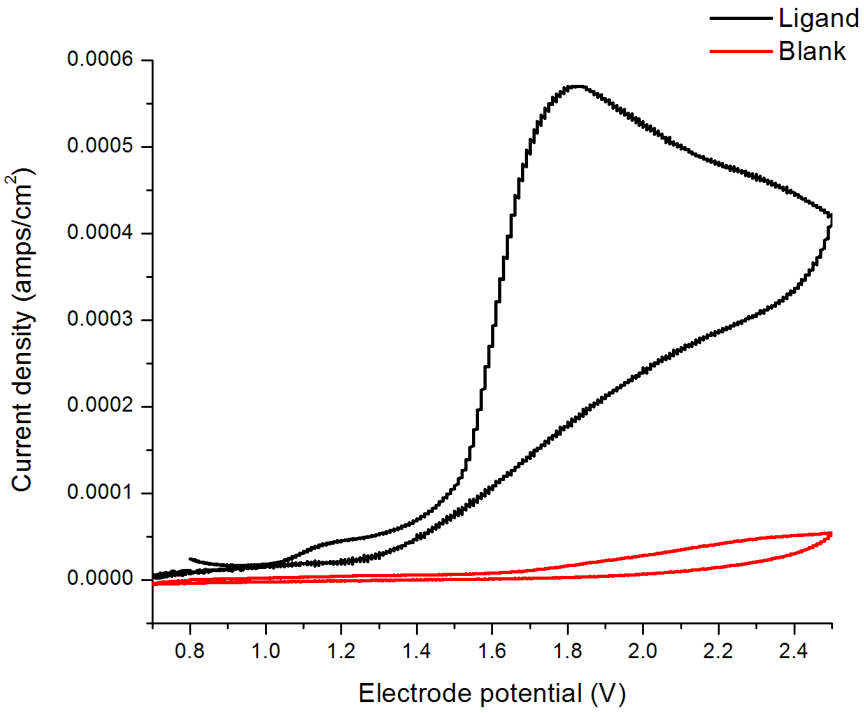

Figure 4.25: Cyclic voltammogram of 10 mM ligand **4-24** shown compared to a solution containing 0.1 M $[(t\text{-}Bu)_4N]PF_6$ as the electrolyte in MeCN

The cyclic voltammogram of ligand **4-24** indicated a single, irreversible oxidation at a potential of approximately 1.5 V. While the oxidation of the catechol groups appears irreversible, it is possible that diffusion effects prevented reduction back from the keto group to the alcohol. As MeCN is aprotic, protons removed from the hydroxyl groups may have diffused away by the time the electrode potential became less positive than the oxidation potential, thus preventing reduction. Additionally, the precipitation of a dark

brown solid, presumed to be the oxidised form of **4-24**, was observed upon completion of the experiment. Precipitation of the oxidised product is another potential explanation for why the oxidation appears irreversible. If the oxidised species is no longer in solution, it cannot be reduced back to its original state by the reversal of the electrode potential. Furthermore, as the resultant quinone can polymerise, it is possible the precipitated solid is an insoluble polymer.

4.3.5.3. Spectroelectrochemical analysis

To confirm that the transformation occurring under an applied potential was an oxidation, the ligand was also subjected to spectroelectrochemical analysis. The experiment was performed using the same solution of 0.1 M [(*t*-Bu)$_4$N]PF$_6$ in MeCN as the electrolyte. An electrochemical cell was set up in a quartz cuvette using an Ag/AgCl reference electrode, a platinum mesh for the working electrode, and platinum wire for the counter electrode. The reference electrode was calibrated using ferrocene as before. The first experiment was observed using photography, with the ligand concentration at 10 mM. The electrochemical cell was set up, and a working potential of 2V was passed through the solution. A photograph was taken every minute for the first 10 minutes, and every three minutes thereafter up to a time of 25 minutes (**Figure 4.26**). The test experiment shows the rapid oxidation of the ligand under the stated conditions. The solution darkens and in the later photograph timed at 5 minutes a small amount of precipitate can be seen beginning to form on the counter electrode. A control UV spectrum of the ligand **4-24** was taken using the 0.1 M [(*t*-Bu)$_4$N]PF$_6$ solution as the solvent, with readings taken every three minutes for thirty minutes (**Figure 4.28**). The UV/vis absorption experiment was then repeated with a working potential of 2 V across the electrochemical cell (**Figure 4.29**).

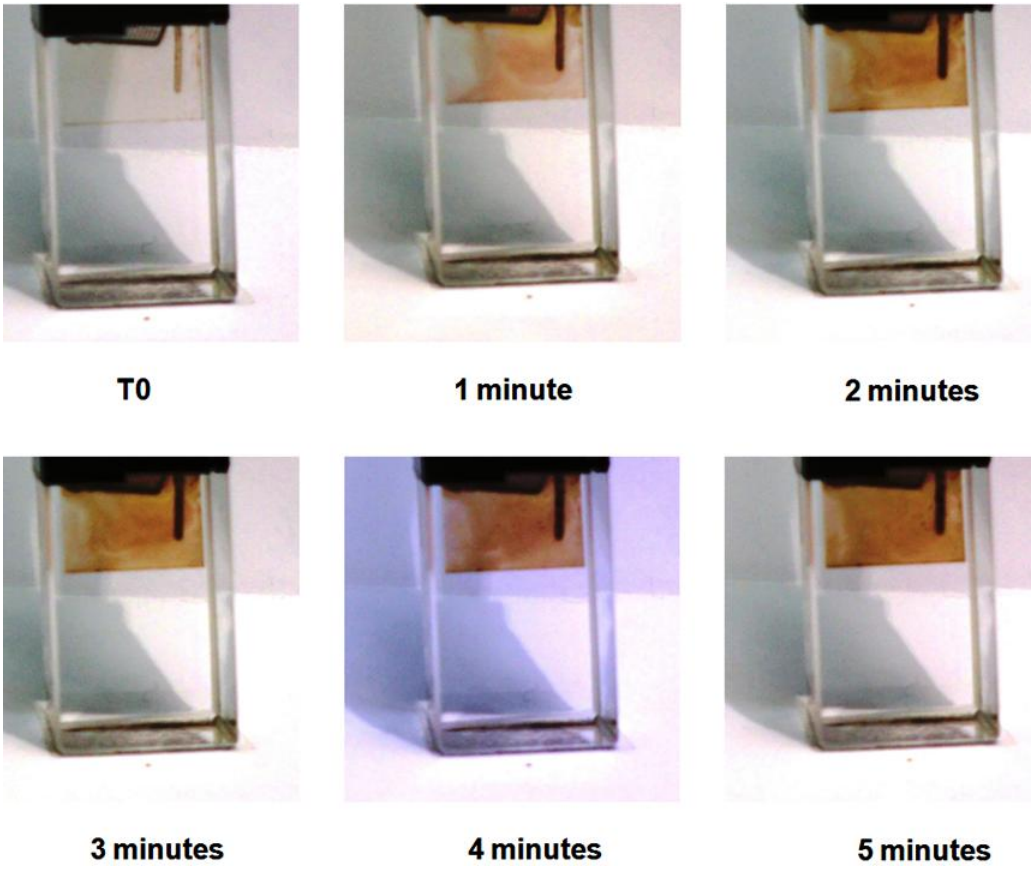

Figure 4.26: Oxidation of Ligand **4-24** *in situ* under a working potential of 2V relative to a Ag/AgCl electrode in 0.1 M $[(t\text{-Bu})_4N]PF_6$ in MeCN

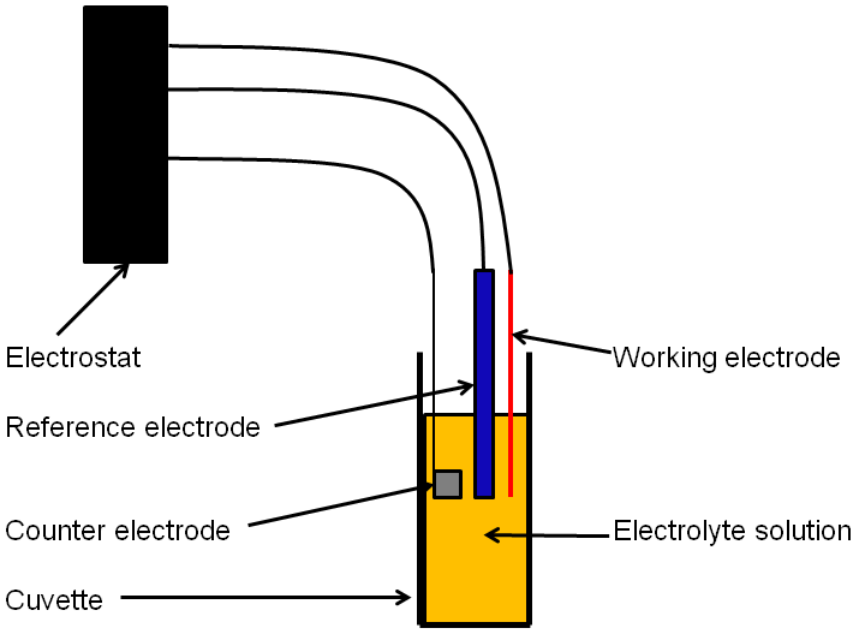

Figure 4.27: Schematic diagram of the experimental setup for the spectroelectrochemical analysis of **4-24**

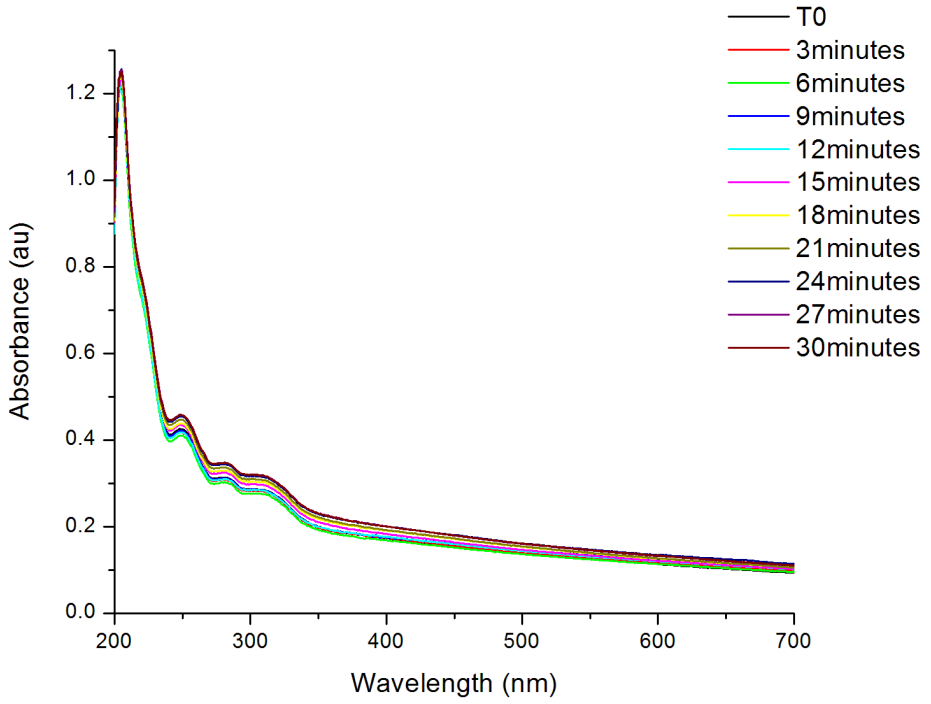

Figure 4.28: UV/vis spectrum of 10 mM **4-24** in 0.1 M $[(t\text{-Bu})_4N]PF_6$ in MeCN over 30 minutes

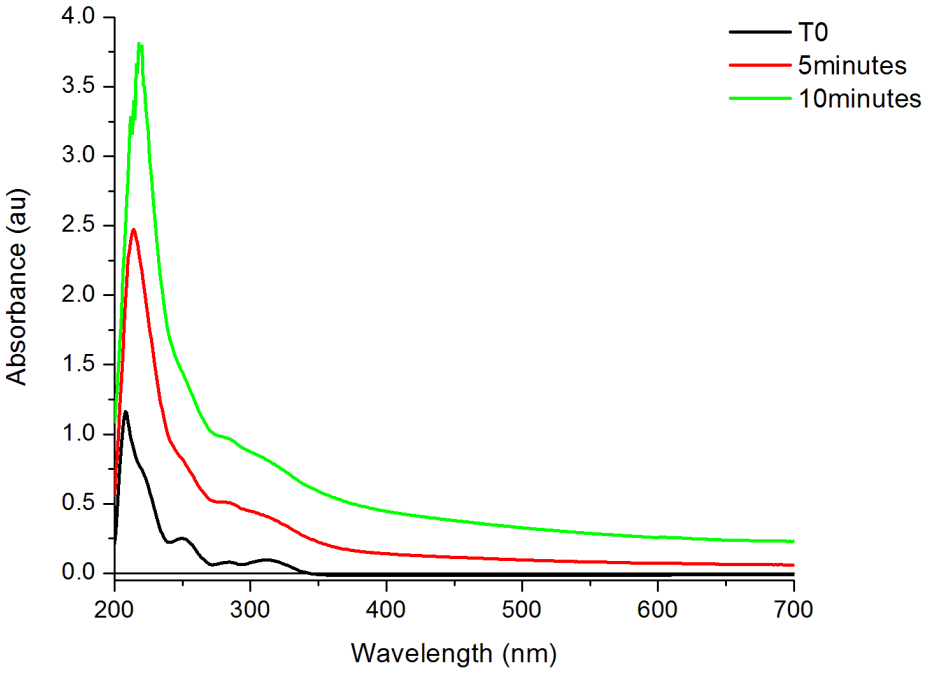

Figure 4.29: UV/vis spectrum of 10 mM **4-24** over time with a working potential of 2V applied in 0.1 M $[(t\text{-Bu})_4N]PF_6$ in MeCN

The UV/vis spectra measured confirmed the observation made when following the electrochemical process using photography. The ligand **4-24** is rapidly oxidised at a working potential of 2V. The increase in the baseline absorbance with time is due to scattering, caused by the precipitation of an unknown species. From these studies it can be concluded that the ligand is highly susceptible to oxidation, and will gradually oxidise over time, within the time frame of the biological assays.

4.4. Summary, conclusions and future work

In summary, three different types of compounds have been synthesised and characterised: an unsymmetrical bis-catechol ligand linked via an amide and a secondary amine; a set of bis-catecholimine ligands, and a set of benzyl protected bis-catecholimine compounds as precursors to bis-catecholamine ligands. The work on the protected bis-catecholimine compounds was not pursued further due to the instability of the target bis-catecholamine ligands.

The antimicrobial activity of the symmetrical bis-imine ligands was briefly analysed, but further screening was not pursued due to their susceptibility to hydrolysis when dissolved in phosphate buffer, with the smallest ligands **(4-30** and **4-31)** decomposing to their corresponding alkyl diamine and 2,3-dihydroxybenzaldehyde in under 2 hours. The dodecyl spacer containing ligand in the series **4-36** was not subjected to analysis due to its low solubility in the solvent systems used.

The unsymmetrical ligand **4-24** was assessed for antibacterial activity and showed promising results against wild type *E. coli*, with an MIC of <10 μM. Experiments to elucidate its mechanism of action were undertaken. The results indicated that there was an element of iron starvation, but that there is likely be an additional component, as evidenced by the compound retaining activity against *E. coli* in the presence of excess iron. Additional experiments, however, also demonstrated that the compound **4-24** is capable of acting as a siderophore, as in experiments against a TonB deficient strain the

compound aided growth of the bacteria at sub-lethal concentrations. Investigations into the stability of the compound have shown that the compound is unsuitable for use as an antimicrobial agent. UV/vis spectroscopy and electrochemistry have shown that the compound is susceptible to oxidation. Consequently, it cannot be said definitively whether **4-24** or one of its oxidation products is the active species.

For future work in this area, a key aspect is developing a reliable assay to give reproducible results for testing the efficacy of gallium nitrate against *E. coli.* Experiments could also be performed to determine if complexing the ligands with iron or gallium has a stabilising effect and prevents hydrolysis in buffer. If this is the case, the ligands could be complexed with gallium and rescreened to determine if the complexes have an antimicrobial effect. The same experiments could also be performed with the unsymmetrical ligand. If these experiments were successful, new synthetic work could be undertaken to prepare unsymmetrical bis-catechol ligands with varying linker lengths to examine the impact of linker link on the efficacy of the compounds. Additional work should also focus on the analysis of the oxidation products of **4-24**, specifically determining the identity of the products and assessing their stability and antimicrobial activity.

5. Studies into the bacterial uptake mechanism of glycosylated fluoroquinolones

5.1. Aims

The aim of the research in this chapter was to establish whether a set of glycosylated fluoroquinolones were capable of gaining access to their intracellular target via active transport. Additionally experiments were undertaken to establish whether or not the glycosylated fluoroquinolone retained the capacity to gain access to the cell through OMPs. The research contained in this chapter is published in the journal ChemBiochem[233].

5.2. Introduction

5.2.1. Overview

The key concept behind the Trojan horse strategy is smuggling a bactericidal moiety into the cell with a nutrient required for microbial growth. Iron is by no means the only nutrient required for microbial survival. Therefore, it stands to reason that siderophores are not the only means of potentially carrying bactericidal moieties into a bacterial cell using a required nutrient. While the majority of work in the literature on Trojan horses has focused on siderophore conjugates, there are alternatives which have been explored using alternative natural ligands There are several examples of using this approach to improve bioavailability of drugs in a mammalian system[234]. These include using glucose transport to aid the bioavailability of Non-steroidal anti-inflammatory drugs (NSAIDs)[235]. Other examples of utilising transporters to deliver drugs also include using peptides[236] and vitamin C[237]. The vitamin C conjugate used the NSAID diclofenac; the role of the vitamin C component is to target diclofenac to its site of action within the brain. The other two conjugates used indomethacin (glucose) and nabumetone (thiopeptide). The indomethacin conjugate enabled the uptake of the drug to the brain via glucose transport in rats[235], while the nabumetone conjugate was targeted towards the PepT1 transporter[236], a

transporter which has also been demonstrated to transport β-lactam antimicrobials[238].

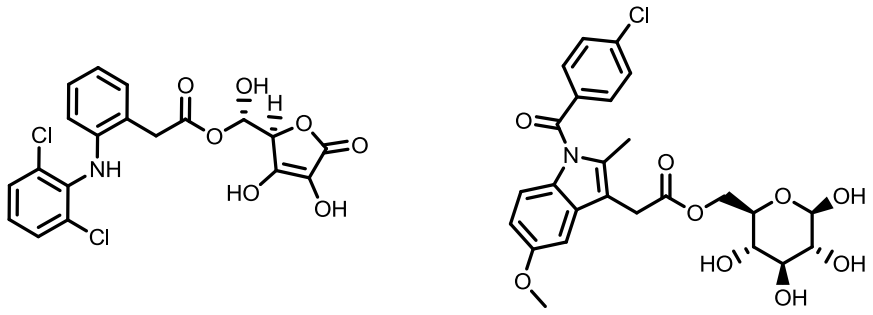

5-1 **5-2**

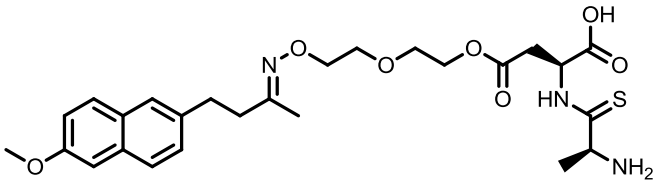

5-3

Figure 5.1: Structures of three examples of NSAIDs conjugated to natural ligands: vitamin C **5-1,** glucose **5-2** and a thiopeptide **5-3**

5.2.2. Sugar transport in bacteria

As carbohydrates are highly hydrophilic, they are incapable of passive diffusion through the hydrophobic inner membrane. The requirement of a carbon source for bacterial growth has led to the evolution of several mechanisms for carbohydrate transport in bacteria. Lactose passes through the inner membrane by proton coupled transport. The hexopyranose sugars glucose and galactose are transported via group translocation in addition to proton coupled transport (**Figure 5.2**)[239]. The group translocation is catalysed by phosphoenolpyruvate (PEP). This initiates a series of phophorylations, ultimately phosphorylating glucose to form glucose-6-phosphate (G6P) as glucose is transported through the IIC protein. This is known as the PEP phosphotransferase system (PEP-PTS)[240-241].

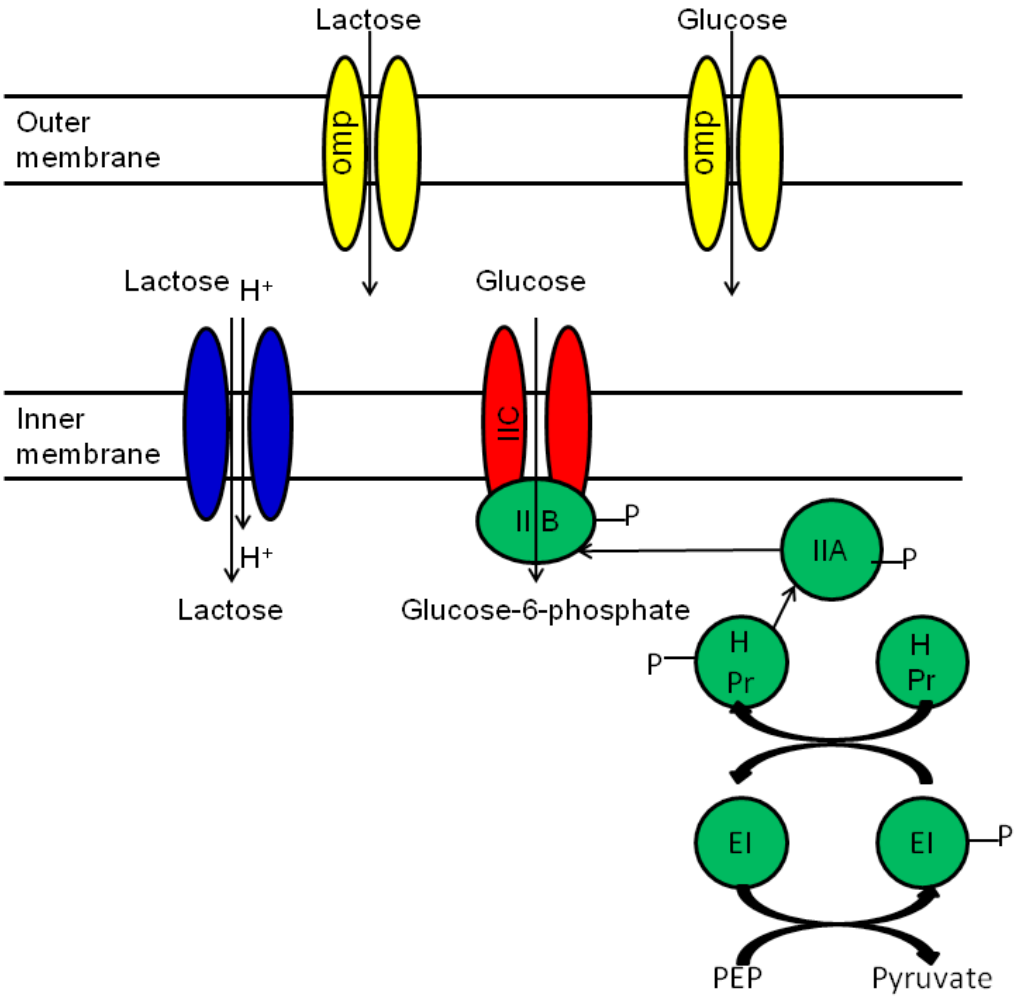

Figure 5.2: Schematic overview of lactose and glucose transport in *E. coli*

Galactose can also be taken up via proton coupled transport, in a similar fashion to lactose. The protein GalP transports galactose in *E. coli*[242] and exists in functional trimers in the outer membrane. Furthermore, bacteria can also obtain glucose using GalP[243], which is the closest analogue to the human glucose transporters (GLUTs)[244-245]. There are also two known galactose transporters; mglC and ytfT[246]. YtfT is a more recent discovery and has been found to be specific for galactofuranose[247]

5.2.3. Previous examples of carbohydrate-fluoroquinolone conjugates

Compared to siderophore based Trojan horses, carbohydrate based examples are extremely rare. Only two sets of carbohydrate based Trojan horses exist in the literature. These examples both use glucose and galactose as the carbohydrate component with norfloxacin and ciprofloxacin as the fluoroquinolone component.

5.2.3.1. Ciprofloxacin based carbohydrate conjugates

The first carbohydrate based Trojan horses were published by Jung *et al*. in 1999. Their intention was to target the sugar/H+ symporters and phosphotransferase (PTP) transporters. They utilised ciprofloxacin **1-18** as their antimicrobial moiety, with glucose and galactose as the carbohydrate component[248]. The proteins responsible for active transport of carbohydrates are highly specific[249], therefore the use of glucose and galactose should allow the conjugates to be actively transported by the target organism. They also experimented with linkers to determine the impact this had on activity.

The conjugates were tested for their antimicrobial activity using ciprofloxacin as a standard. It was found by Jung *et al.* that the conjugates with no linker **5-4** and **5-5,** displayed activity which was comparable to ciprofloxacin **1-18**. This was attributed to hydrolysis of the conjugates during incubation, resulting in the regeneration of ciprofloxacin. They observed that the conjugates **5-6−5-9**, which contained ethyl or propyl linkers, had significantly reduced activity relative to ciprofloxacin. From this observation they drew the conclusion that the conjugates **5-6−5-9,** containing an alkyl linker were stable under the assay conditions.

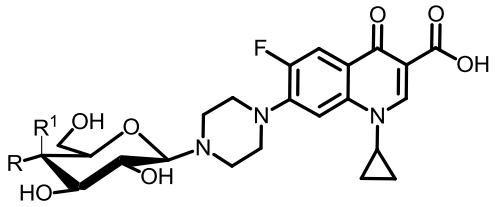

5-4: R = OH R^1 = H
5-5: R = H R^1 = OH

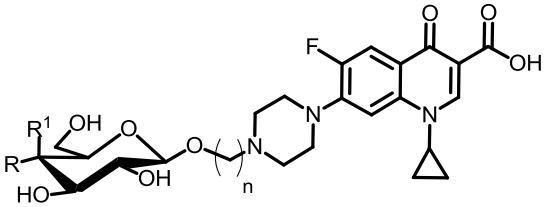

5-6: R = OH R^1 = H n = 2
5-7: R = H R^1 = OH n = 2
5-8: R = OH R^1 = H n = 3
5-9: R = H R^1 = OH n = 3

Figure 5.3: Examples of fluoroquinolone-carbohydrate conjugates prepared by Jung *et al*.[248]

This led to a further conclusion that the glucose conjugate **5-6** was being actively transported. The fact that the glucose conjugate **5-6** showed a higher level of activity than the corresponding galactose conjugate **5-7** against a variety of strains including *S. aureus* and *P. aeruginosa* was cited as evidence that the conjugates could be being differentially transported[248]. However, without screening of their conjugates against transport deficient mutants, this conclusion could not be confirmed.

5.2.3.2. Norfloxacin based carbohydrate conjugates

In 2005, Zsoldos-Mady *et al*. produced a new set of carbohydrate based Trojan horses. Their initial synthesis was similar to the work of Jung *et al.*, synthesising glycosyl amines utilising both glucose and galactose. The key difference was their use of norfloxacin **1-17** as the fluoroquinolone component instead of ciprofloxacin **1-18**. Following this, they synthesised new conjugates using carbamoyl and thiocarbamoyl linkers (**Figure 5.4**). They claimed that the compounds possess antimicrobial activity at a level below that of pefloxacin, however no specific data is given for screening of the efficacy of the compounds. There is also no experimental detail given for how the antimicrobial screening may have been performed[250].

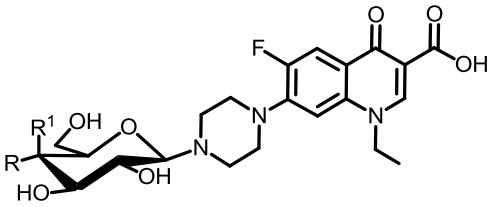

5-10: R = OH R^1 = H
5-11: R = H R^1 = OH

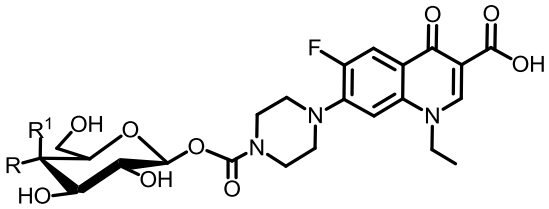

5-12: R = OH R^1 = H
5-13: R = H R^1 = OH

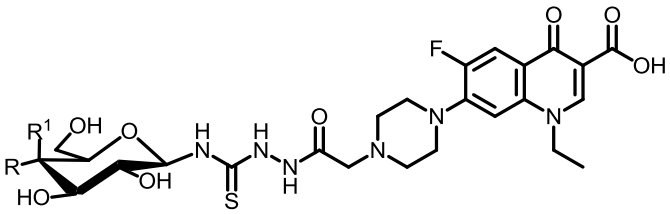

5-12: R = OH R^1 = H
5-13: R = H R^1 = OH

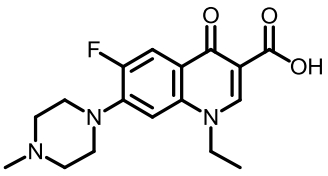

5-14

Figure 5.4: Examples of norfloxacin-carbohydrate conjugates prepared by Zsoldos-Mady *et al.* and their control compound pefloxacin **5-14**.

Given the available data from these two studies, it is clear that there is scope for further study of both the potential efficacy of carbohydrate-fluoroquinolone conjugates. Additionally further investigation is required to determine to what extent, if any, carbohydrate-fluoroquinolone conjugates are actively transported.

5.3. Results and discussion

5.3.1. Screening of compounds on glucose and galactose media against wild type *E. coli*

5.3.1.1. Glycosylated fluoroquinolones

Three compounds that had previously been prepared by S.J. Milner were used (**Figure 5.5**)[151]. All of the compounds contained ciprofloxacin as the active pharmacophore, with a sugar component conjugated via the piperazinyl nitrogen. The sugar components were glucose, galactose and lactose.

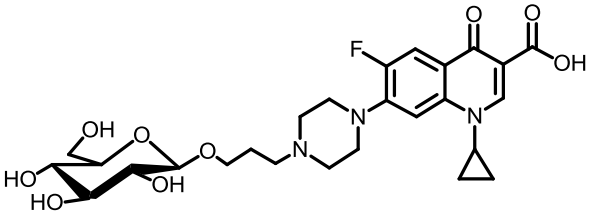

5-15
Glucose conjugate

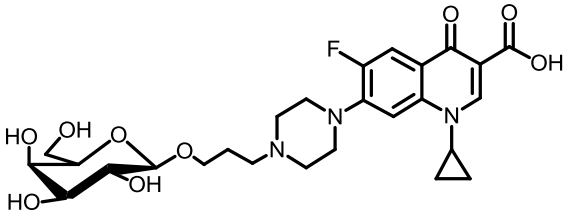

5-16
Galactose conjugate

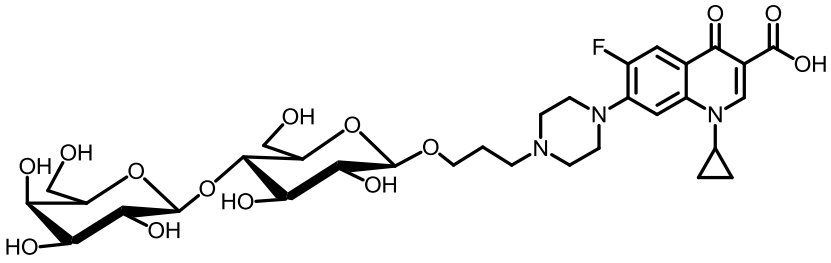

5-17
Lactose conjugate

Figure 5.5: Structures of the three sugar based Trojan horses with glucose **5-15,** galactose **5-16**, and lactose **5-17** as the carbohydrate components

5.3.1.2. Establishment of suitable growth conditions

In order to determine whether or not the glycosylated fluoroquinolones were being actively transported into the cells, as hypothesised by Jung *et al.*[248], it was necessary to establish a set of conditions where bacterial growth was dependent on a specific mono-saccharide, with the hypothesis that the conjugate with the selected mono-saccharide would be actively transported by specific transporters and thus have greater activity under the assay conditions than the conjugates not containing the selected monosaccharide. As glucose is the preferred carbon source of *E.coli*, it was decided to utilise galactose as the limiting carbon source. To establish galactose as the limiting carbon source conditions were established were it could be demonstrated that galactose transport was required for growth. To enable this, a mutant strain was selected with deletions in three galactose transport genes: YtfT, GalP and MglC[242, 246-247]. The galP and mglC genes both encode galactose transporters. YtfT is part of the *E.coli ytfQRTyjfF* operon which encodes a galactofuranose transporter.

Initially, growth of a double mutant with defects in GalP and MglC was grown in addition to a wild type strain (BW25113). These were grown overnight in M9 glucose, however no growth was observed, this was believed to be due to a problem with the stock culture. It was decided to test six different strains for viability. The BW25513 was used, in addition to: *galP::kan*, *mglC::kan*, Δ*mglC*. Δ*GalP*Δ*MglCytfT::kan*, and Δ*gal*PΔ*mgl*CΔ*ytf*T. Out of these strains, three contained kanamycin resistance genes ($GalP^-$, $MglC^-$, and $\Delta GalP^-\Delta MglC^-$YTFT). The six strains were grown in LB media for three days. Observation of the cultures confirmed growth in all six, confirming that all the strains were viable. The O/D_{650} of the wild type and $\Delta GalP^-\Delta MglC^-$ ΔYTFT strains were measured, and the cultures diluted into 12 cultures (3 wild type in glucose M9, 3 Δ*galP*Δ*mglC*Δ*ytfT* in glucose M9, 3 wild type in galactose M9, and 3 Δ*galP*Δ*mglC*Δ*ytfT* in galactose M9). The cultures were incubated at 37°C and their O/D_{650} measured every thirty minutes (**Figure 5.6**).

The data from this initial screen showed that under these conditions, where glucose was the carbon source the cultures grew with no problems However in the galactose media, no significant growth was observed during the time frame of the assay. However, the galactose cultures were left to incubate, and after 2 additional days at 37°C, growth was observed with the wild type strain. A further experiment using cultures grown in mannose, and gluconic acid lactone (in addition to glucose and galactose) was performed. The experiment was performed under the same conditions, mannose and gluconic acid lactone both yielded growth within 24 hours. The fact that these conditions gave rise to growth within 24 hours for mannose, gluconic acid lactone and glucose, but not galactose, suggests a prolonged lag phase in the bacterial growth cycle when galactose is the sole carbon source. As expression of galactose transporters is repressed in the presence of glucose[251-252], it is likely that after overnight growth in LB media the *E.coli* does not have any galactose transporters expressed. Consequently, the lag period is extended while the bacteria overcome the initial repression and expresses the required transporters to obtain galactose from the medium.

A)

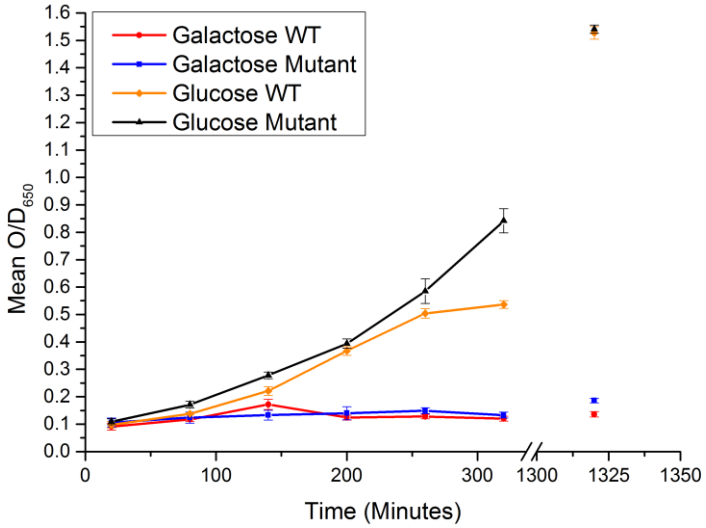

B)

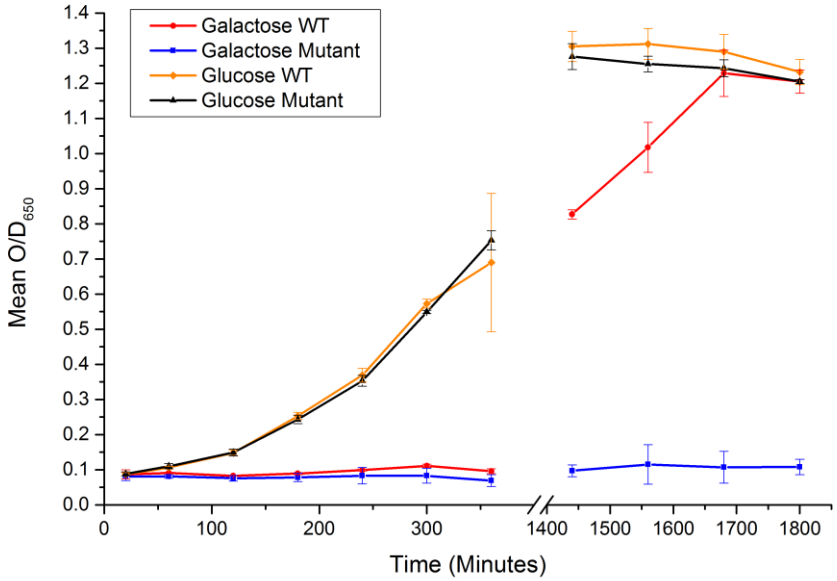

Figure 5.6: Growth data of wild type and ΔGalP⁻ΔMglC⁻ΔYtfT⁻ strains of *E. coli* grown in M9 glucose and M9 galactose with **A)** LB media pre-growth and **B)** M9 glycerol pre-growth. The experiments were run in triplicate. Error bars correspond to the standard deviation of the data.

While growth was observed in the *E. coli* cultures grown in M9 galactose, the prolonged lag phase was undesirable due to the length of time used for the zone of inhibition assays (**Figure 5.6**). Conditions were required

where the cells enter the log phase of growth and reach a sufficient O/D_{650} in side 24 hours. It was decided to investigate the effect of the initial growth media. A culture of wild type *E.coli* was prepared in LB media and incubated at 37°C overnight. The cells were washed by being centrifuged at 3500 rpm for 3 minutes, removing the supernatant and re-suspending the cells in M9 salts. This was repeated twice to remove as much of the LB media as possible. The cells were then resuspended in M9 containing either 0.2 % glucose or 0.2% glycerol. These cultures were then incubated overnight at 37°C. The O/D_{650} was measured for both cultures and were determined to be 1.43 for the M9 glycerol culture and 1.93 for the M9 glucose. The cultures were diluted to an approximate O/D_{650} of 0.1 in M9 with 0.2% galactose. The O/D_{650} after 7 hours was approximately 0.3 for both solutions. After 3 days the O/D_{650} was measured again and recorded as 0.958 for the culture pre-grown with glycerol and 0.974 for the culture grown with glucose.

Culture	Observed O/D_{650}	Actual O/D_{650}	Dilution required
Wild type 1	0.218	2.18	0.92 ml in 20 ml
Wild type 2	0.197	1.92	1.04 ml in 20 ml
Mutant strain 1	0.150	1.50	1.33 ml in 20 ml
Mutant strain 2	0.206	2.06	0.97 ml in 20 ml

Table 5.1: O/D650 data and dilutions for both wild type and mutant E. coli after overnight pre-growth in M9 glycerol

Based on these results it was decided to repeat the initial assay using M9 glycerol as the pre-growth media instead of LB. 4 Cultures were prepared (2 Wild type, 2 mutants) and incubated overnight at 37°C in M9 glycerol.

O/D_{650} measurements were recorded for all four cultures (**Table 5.1**) and the dilution required for an O/D_{650} of 0.1 was calculated.

The assay was then performed as before with O/D_{650} readings taken every hour. After growth overnight further readings were taken at 2 hour intervals. The data showed growth in both the wild type and mutant cultures grown with 0.2% glucose within the first 6 hours, with the cultures in stationary phase after overnight growth. Critically, while there was no observable growth in either of the cultures grown with 0.2% galactose in the first 6 hours, after overnight growth, the wild type strain was in log phase and after 30 hours had reached stationary phase. However no growth was observed with the mutant strain (**Figure 5.6**). This demonstrated that under the selected pre-growth conditions (M9 salts with 0.2% glycerol) that growth in galactose media was dependent on galactose transport. In addition to this it demonstrated that under these conditions, galactose transport was sufficiently up-regulated to allow growth after overnight incubation, unlike pre-growth in LB media.

5.3.1.3. Zone of inhibition assays

With the pre-growth conditions determined, the next step was to determine the activity of the compounds *in vitro*, and compare the results to the activity of ciprofloxacin **1-18**. Stock solutions of the compounds were prepared in 100 mM acetic acid, at a concentration of 3.02 mM (equivalent to 1 mg/mL of ciprofloxacin). A dilution series was then prepared using 1 in 5 dilutions down to a concentration of 0.965 μM. Initially, the compounds were screened against wild type *E. coli* on M9 agar, in order to establish rough MIC values. A wild type culture was grown overnight at 37°C in LB media, and then diluted to an O/D_{650} of approximately 0.1. The culture was then grown to an O/D_{650} of approximately 0.6 and inoculated into an agarose solution (4 ml culture in 100 ml of agar). This was added to the LB agar and left to set, 5 μL of each concentration of each compound was then spotted onto the agar, left to dry, and the plates incubated overnight at 37°C. After

incubation, the zones of inhibition around the antibiotic spots were measured and the data analysed (**Figure 5.7**)

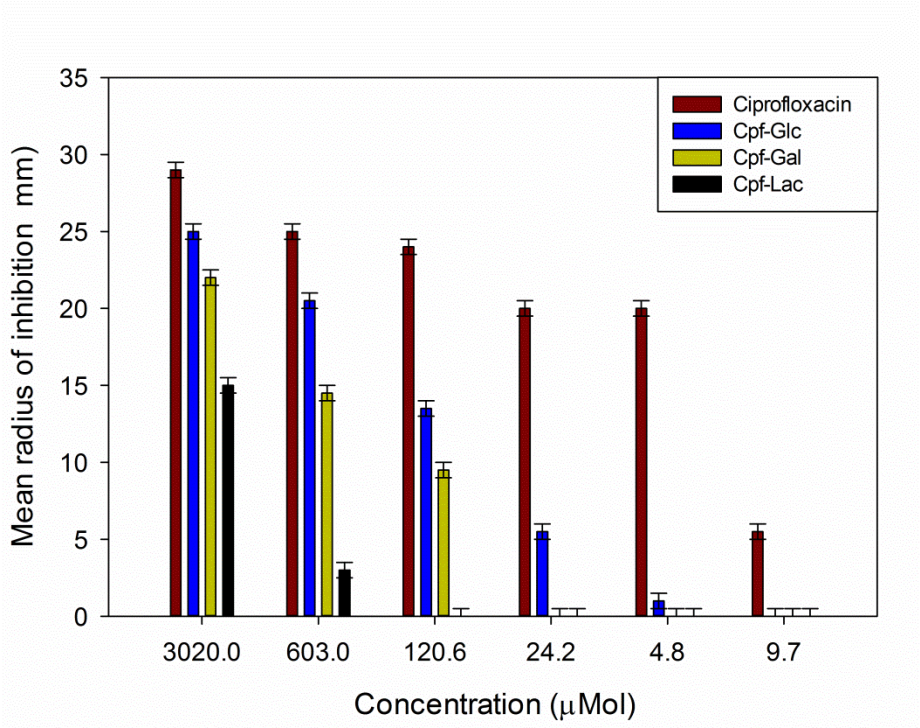

Figure 5.7: Mean zones of inhibition of ciprofloxacin **1-18** and the three glycosylated derivatives **5-15−17** against WT *E.coli* grown on LB media. The experiment was run as a single sample. Error bars correspond to plus or minus 0.5 mm.

The data, as expected, shows concentration dependency for all four compounds. The key trend across the compounds in the data set is the decrease in activity with increasing molecular weight, with the largest derivative, cpf-lac **5-16** showing an MIC somewhere between 0.12-0.6 mM. There is also a statistically significant difference between the activities of the cpf-glc **5-14** and cpf-gal **5-15** with MICs in the range of 0.96-4.8 μM and 0.024-0.12 mM respectively. As the molecular weight of these compounds is identical, it suggests there may be some kind of structure based recognition involved, thus supporting the conclusions of Jung *et al.* [248].

To test the hypothesis the compounds were screened again using the previously determined experimental conditions. M9 agar plates were prepared, half with 0.2% glucose, half with 0.2% galactose. The assay was performed using the same protocol as the LB agar assay, but using M9 glycerol as the pre-growth media. This resulted in slower bacterial growth, however a suitable O/D_{650} was reached and the culture inoculated into the top agar. The plates were incubated as before and the zones of inhibition measured (**Figure 5.8**).

The results of this assay show the same pattern of activity as previously observed with growth on LB media. However, the key finding is that the difference in activity between the cpf-glc and cpf –gal conjugates is negligible on both media. Taking into account experimental error the activity is approximately equal. While the cpf-gal conjugate has a slightly higher activity on the M9 galactose, approximately 15% more effective at 3 mM, the same can be also said for the other two conjugates and ciprofloxacin. Consequently the increase in activity on M9 galactose could be attributed to the conditions being less favourable for bacterial growth than M9 glucose. In addition to this, on both the glucose and the galactose media, cpf-glc is more effective than cpf-gal. If active transport was involved, it would be expected for this observation to be reversed in M9 galactose media. As this is not the case it must therefore be concluded that the tested conjugates were not being taken up by active transport.

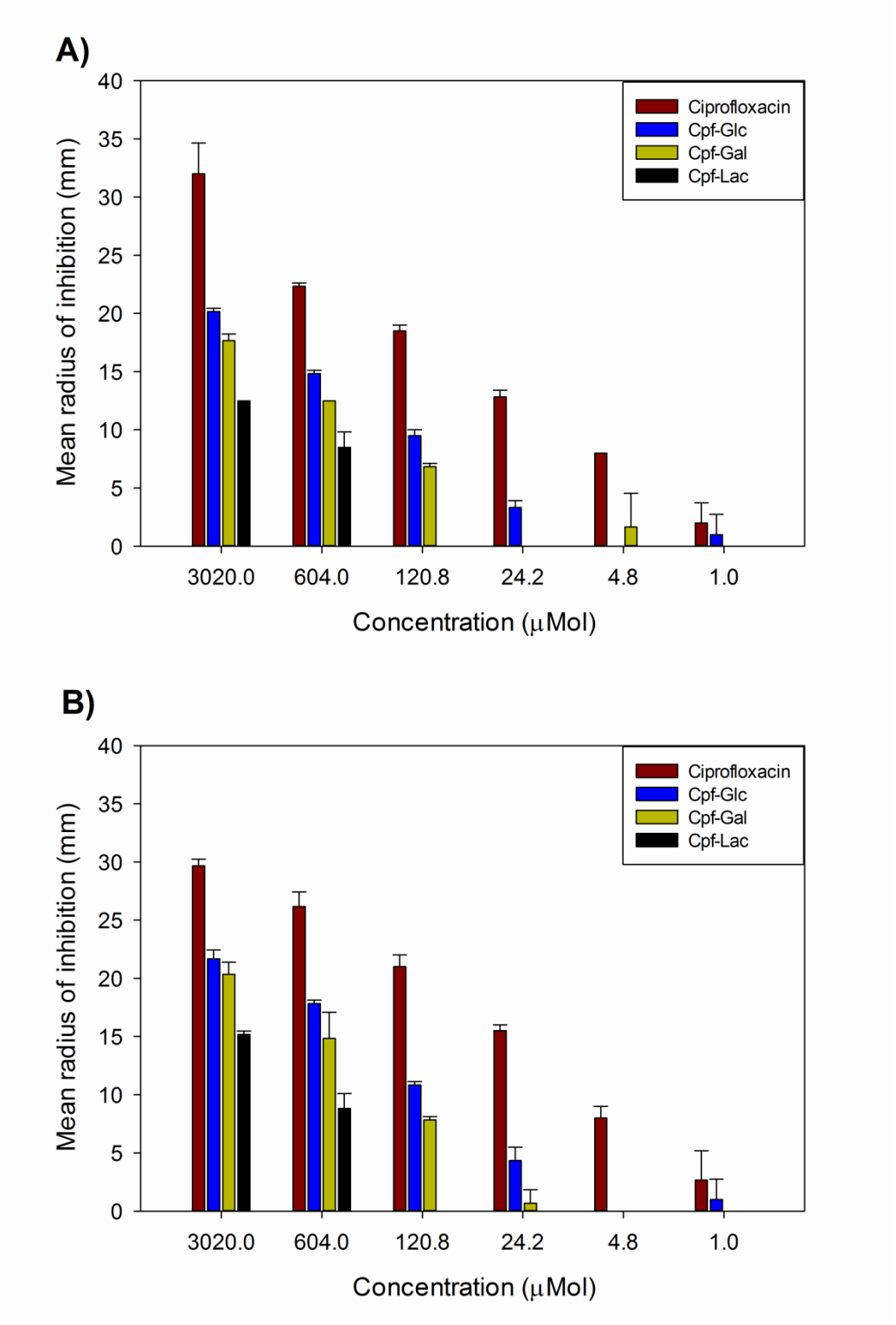

Figure 5.8: Mean zones of inhibition for ciprofloxacin and the glycosylated derivates against WT *E. coli* grown on **A)** M9 glucose and **B)** M9 galactose. The experiments were run in triplicate. Error bars correspond to the standard deviation of the data.

5.3.2. Activity of compounds against *E.coli* deficient in ompF

As the initial assays had suggested that the sugar transport systems were not responsible for the uptake of the conjugates in *E. coli*, further experiments were required to ascertain how the conjugates were gaining access to the bacterial cell. As it was well established in the literature that fluoroquinolones gain access to the cells via OMPs[253-256], this seemed a logical uptake mechanism to investigate. A new set of M9 agar plates were prepared, and cultures were set up using an *E. coli* strain deficient in ompF. OmpF is differentially expressed depending upon the environmental conditions[257], existing as a trimer of β-barrels (**Figure 5.9**) spanning the outer membrane.

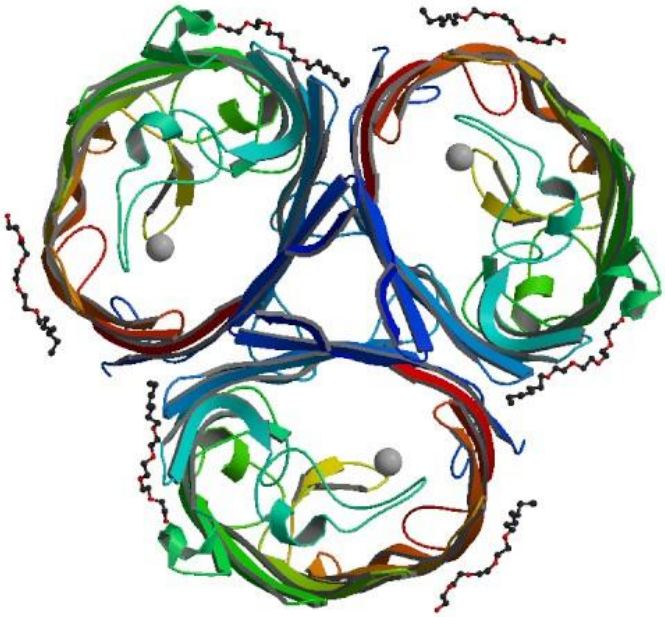

Figure 5.9: Top down crystal structure of ompF

For the assay against the ompF, the glucose concentration of the medium was increased from 0.2% to 0.5%, to replicate the conditions of a published procedure[117, 148]. The remaining aspects of the experiment were unchanged. The experiment was performed in triplicate using only the wild

type BW25113 *E.coli* strain and the OmpF$^-$ mutant. After overnight growth at 37°C the radii of inhibition were measured and the data plotted (**Figure 5.10**).

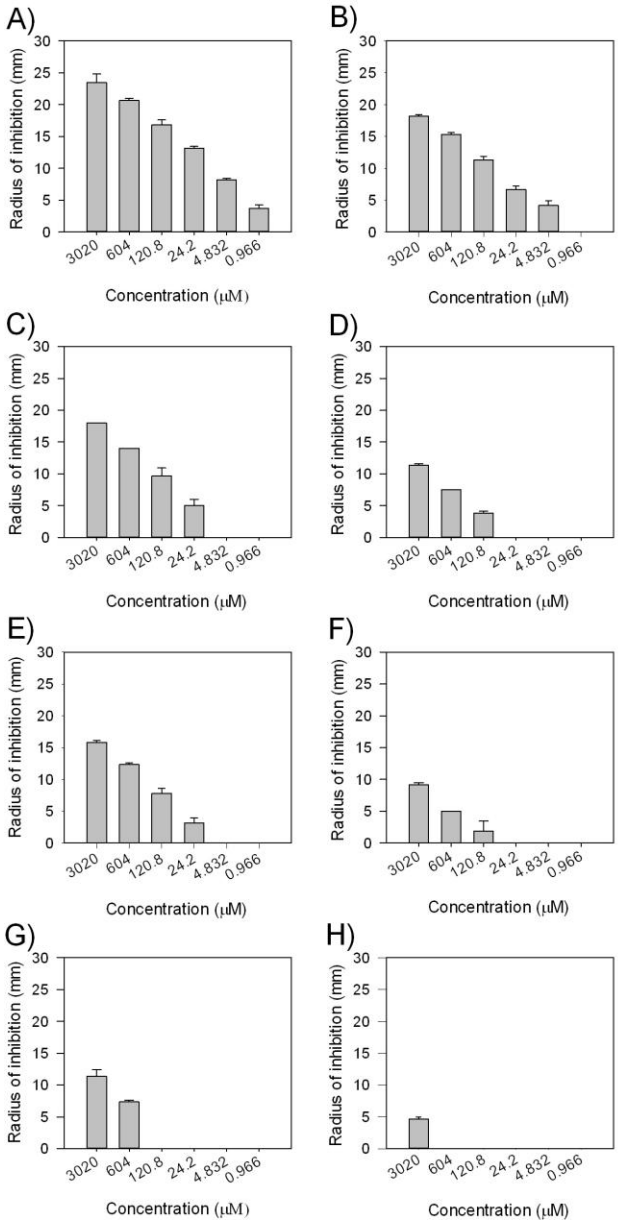

Figure 5.10: Zones of inhibition of ciprofloxacin and derivatives against wild type and OmpF$^-$ *E. coli*. A) Ciprofloxacin Vs WT B) Ciprofloxacin Vs ompF$^-$ C) Cpf-Glc Vs WT D) Cpf-Glc vs. OmpF$^-$ E) Cpf-Gal Vs WT F) Cpf-Gal vs. OmpF$^-$ G) Cpf-Lac Vs WT H) Cpf-Lac Vs OmpF$^-$. The experiments were run in triplicate. Error bars correspond to the standard deviation of the data.

This experimental run showed a clear decrease in activity with the removal of OmpF from the *E. coli*. While activity was not completely eliminated, presumably due to the continued presence of OmpC, there was a statistically significant reduction in activity for all three conjugates. In all cases the MIC was raised to an extent whereby a previously lethal concentration proved to be sub-lethal in the $OmpF^-$ mutant.

5.4. Conclusions and future work

In this section a set of growth conditions have been established where galactose transport was essential for bacterial growth. In addition to this the conditions also allow bacterial growth in a galactose medium to occur without a prolonged lag phase.

Experiments have been performed to determine to what extent, if any, the compounds synthesised by S.J. Milner are accessing bacterial cells by active transport via sugar uptake systems. The results obtained suggest that while the glycosylated conjugates retain their activity against *E.coli*, there is no significant variation in activity when the transport system required for the uptake of a specific carbon source is not present. Therefore it must be concluded that these conjugates are not entering the cell via active transport.

Further experiments have determined that the likely mode of entry into the cell is via the outer membrane porins. While preliminary experiments on a variety of mutants yielded inconclusive data, a further assay focusing purely on the $OmpF^-$ mutant showed a clear and significant reduction in activity, in agreement with the literature[49, 256, 258]. This demonstrates that despite the additional steric bulk associated with the glycosylated conjugates, they can still pass through the outer membrane and ultimately reach their target.

Potential future work in this area could be pursued by creating alternative glycosylated fluoroquinolones using monosaccharides such as xylose and arabinose to ascertain if conjugates containing these sugars could be actively transported. Another synthetic option would be to create

glycosylated fluoroquinolones with cleavable linkers, as previous research has shown that the added steric bulk of the sugar moiety reduces the ability of ciprofloxacin to bind to its target. Further screening work of mutants could also be undertaken to further substantiate the conclusion that glycosylated fluoroquinolones are still gaining access to the periplasm through porins, but aren't gaining access to the cytoplasm via active transport.

6. Conclusions and future work

6.1. Conclusions

An analogue of the *Bacillus* siderophore petrobactin has been synthesised and fully characterised. Attempts were also made to prepare a Trojan horse conjugate based on the analogue, using ciprofloxacin as the antimicrobial component. These attempts were unsuccessful as it was found the protected conjugates were unstable and decomposed when attempts were made to deprotect them to yield the final conjugate. This was due to the instability of the amide bond bound to the central citrate carboxylate group. When a glycine spacer was introduced, a similar process occurred. This was possibly due to cyclisation of the backbone, and subsequent release of the ciprofloxacin component.

A Trojan horse conjugate was prepared using the Ugi condensation, and several compounds were synthesised to form a set of building blocks for a library of potential Ugi conjugates. The synthesised Ugi conjugate was screened for activity against *Escherichia coli* on both nutrient rich and minimal media. The Ugi conjugate was also subjected to a DNA gyrase assay. The conjugate was found to be active against *E. coli* and was demonstrated to still be exerting its antimicrobial effect by inhibiting the activity of DNA gyrase. However, the activity of the conjugate was found to be lower than that of the parent antimicrobial ciprofloxacin. This observation can be attributed to the steric bulk of the siderophore component inhibiting the ability of ciprofloxacin to bind DNA gyrase. Additionally, the steric bulk of the siderophore component may have been inhibiting rather than aiding uptake. This would explain the difference in the MIC observed between the disc diffusion assay and the gyrase assay.

An asymmetric bis-catechol ligand and a series of bis-catecholimines were synthesised and fully characterised. The bis-imine ligands were subjected to preliminary screening against *E. coli* to ascertain if they

possessed antimicrobial activity. The initial screening showed promising results. However, stability studies determined that the compounds were unstable under the assay conditions. The asymmetric ligand also showed promising antibacterial activity however analysis by UV/vis spectrophotometry and electrochemistry demonstrated that the compound was susceptible to oxidation. Consequently the active species could not be identified.

A set of glycosylated fluoroquinolones previously synthesised within the group was screened against a variety of *E. coli* strains to ascertain their mechanism of uptake. The studies determined that the conjugates were not being actively transported; when bacteria were grown under conditions requiring a specific sugar, galactose, there was no statistically significant difference in inhibition between the conjugates. Additionally, further experiments against an OMP mutant showed a decrease in activity, demonstrating that the conjugates were gaining access to the cells via OMPs.

6.2. Future work

The primary focus of future work should be completing the synthesis of the petrobactin analogue-ciprofloxacin conjugate. This would require a new protecting group strategy to try and avoid the problems observed with the methods attempted in this thesis. Additionally further analogues could be prepared using alternative antimicrobials, backbone lengths and different catechol configurations.

The Ugi analogue has shown promise as a novel way of generating iron-chelator antimicrobial conjugates. With a new set of building blocks prepared, a series of Ugi conjugates could be prepared and deprotected, and then screened to ascertain their activity against bacterial species. Using longer linkers between functional groups could potentially reduce the steric hindrance which inhibits the binding of ciprofloxacin to DNA gyrase. Additionally Ugi conjugates should be synthesised with different iron binding

groups including carboxylates as well as catechols to generate a range of novel iron chelators. There is also scope to introduce alternative antimicrobials other than ciprofloxacin, providing they contain a functional group required for the Ugi condensation.

The bis-catecholate ligands showed promising activity, but are unstable in solution. Consequently, they are unsuitable for use as antimicrobials. Future work on this area should focus on the synthesis and analysis of the metal complexes of these ligands. Preparing complexes with gallium or an alternative antibacterial metal may provide a method of delivering antimicrobial metals into bacterial cells, as has previously been demonstrated using ferrioxamine. Additionally, complexation of the ligands with a metal ion may increase the stability of the ligands in solution, and therefore increase their suitability for use as antimicrobials.

The glycosylated fluoroquinolones examined in this thesis utilised the sugars glucose, galactose and lactose. Future work in the area could focus on alternative sugars, or labile linkers. Examination of alternative sugars such as xylose or arabinose may yield conjugates that can be actively transported, and this should be investigated.

7. Experimental

7.1. General Chemistry Procedures

7.1.1. Mass Spectrometry

Positive and negative ESI mass spectrometry (high and low resolution) was performed using a Thermo-Finnigan LCQ Spectrometer. LC-MS was performed using an Agilent 1200 series column using a H_2O:MeCN gradient starting from 9:1, up to 1:4 after 25 minutes and Bruker MicrOTOF. MS-MS experiments were performed using a Bruker MicrOTOF.

7.1.2. NMR

^{1}H NMR (399.785 MHz), ^{13}C NMR (100.535 MHz), and ^{19}F NMR (376.152 MHz) spectra were recorded on Jeol ECS 400 or Jeol ECX 400 NMR spectrometers in the stated deuterated solvents. Variable temperature NMR was performed using a Bruker AV500 NMR spectrometer. All resonances were reported in parts per million (ppm) using the residual solvent signal as a reference. Multiplets corresponding to multiple protons are reported as ranges, single proton multiplets are reported from the midpoint of the resonance. *J* values are reported in Hertz to one decimal place. All ^{13}C NMR spectra are proton de-coupled. Reference signals were as follows; 7.26 ppm and 77.16 ppm ($CDCl_3$), 3.31 ppm and 49.00 ppm (d_3-MeOD), 2.50 ppm and 39.53 ppm (d_6-DMSO). For ^{19}F NMR, fluorobenzene was used as a standard. Chemical shifts for multiplets are reported from the middle of the multiplet.

7.1.3. IR

IR spectra were recorded using a Thermo Nicolet Avatar FTIR spectrometer, using KBr discs. Discs were pressed under a pressure of 10 tonnes. Oils were analysed by dissolving in a specified anhydrous solvent and their solution spectra recorded using the same instrument. IR spectra were processed using OMNIC software.

7.1.4. UV

UV/vis absorption spectra were recorded using a Hitachi U-300 spectrophotometer in 1 cm quartz cuvettes. The data was processed using Origin pro 7.0 software.

7.1.5. Electrochemistry

Electrochemical experiments were performed using a Voltalab PST050, and the data collected using Voltamaster 4 software. Experiments were run in MeCN with 0.1 M tetrabutyl ammonium hexafluorophosphate ([(*t*-butyl)$_4$N]PF$_6$) as a supporting electrolyte at pH 7.0. Potentials were measured relative to a calomel electrode with a platinum disc as the working electrode and platinum wire as the counter electrode. 2 mM ferrocene was used as a standard to calibrate the electrode. Data was processed using Origin pro 7.0

7.1.6. Spectroelectrochemistry

Spectroelectrochemical experiments were performed using a Mom Technologies Compactstat.e and the data collected using IVIUM software, and a Hitachi U-300 UV spectrometer. Experiments were run in MeCN with 0.1 M [(*t*-butyl)$_4$N]PF$_6$ as a supporting electrolyte, in a quartz cuvette with a 1 mM path length. Potentials were measured relative to a Ag/AgCl electrode with a platinum mesh as the working electrode and platinum wire as the counter electrode. 2 mM ferrocene was used as a standard to calibrate the electrode. Data was processed using Origin pro 7.0

7.1.7. HPLC

HPLC was performed using Gilson HPLC apparatus (Gilson 234 auto-injector, Gilson 321 pump, Gilson 170 diode array detector) with an HPLC technology Alphasil5ODS column (length = 25 cm internal diameter = 4.6 mm) in an aqueous/MeCN system. Data was collected using Gilson Unipoint 3.0 software and tabulated using Origin pro 7.0.

7.1.8. Melting Points

Melting points were recorded using a Stuart Scientific SMP3 apparatus. These values are uncorrected and accurate to ±0.05 °C.

7.1.9. Chemical Reagents

All chemicals were purchased from Sigma Aldrich, Fischer Scientific or Alfa Aesar and were used as supplied unless otherwise stated. Chemicals were handled with appropriate safety measures according to toxicity and potential hazards.

7.1.10. Solvents

Solvents were supplied by Sigma Aldrich and Fischer scientific. Solvents were dried over 3 and 4 Å molecular sieves prior to use where appropriate. For all synthetic procedures deionised water was used. Dry THF DMF and MeCN were obtained using the departmental solvent stills (Prosolv MD 7 solvent purification system; solvents are passed through two columns of molecular sieves) and stored over 3 or 4 Å molecular sieves.

7.2. Chemical Synthesis

7.2.1. Synthesis of a petrobactin analogue and the ciprofloxacin conjugate of the petrobactin analogue

*7.2.1.1. Methyl-1-cyclopropyl-6-fluoro-4-oxo-7-(piperazin-1-yl)-1,4-dihydroquinoline-3-carboxylate(**2-20**)*[36]

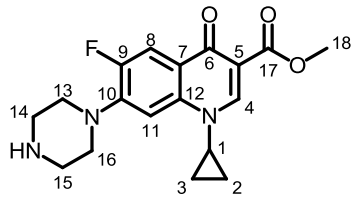

Molecular Formula: $C_{18}H_{20}FN_3O_3$
Molecular Weight: 345.368 g mol^{-1}

To a stirred solution of ciprofloxacin **1-18** (3.00 g, 8.68 mmol) in anhydrous MeOH (100 mL) in an ice bath at 0-5 °C was added thionyl chloride (13.1 mL, 181 mmol) dropwise. The resulting yellow solution was heated under reflux at 80 °C for 24 hours, and allowed to cool to room temperature. Excess solvent was removed *in vacuo*. The resultant solid residue was re-suspended in aqueous K_2CO_3 (0.05 g/mL, 200 mL) to yield a basic solution. The product was extracted from the solution with DCM (3 x 80 mL).The aqueous layer was diluted further with aqueous K_2CO_3 (0.05 g/mL, 100 mL), and re-extracted with DCM (3 x 40 mL). The organic layer was washed with H_2O (2 x 40 mL). The organic layer was dried over $MgSO_4$, filtered and concentrated *in vacuo*, yielding the product as a pale yellow solid.

Yield: 1.89 g, 63%

m.p: Decomposed 226-227 °C

R_f (4:1, DCM: MeOH): 0.40

m/z (ESI): 346.16 ($[M+H]^+$, 100%)

HRMS (ESI): Calc. for $C_{18}H_{21}FN_3O_3$= 346.1561. Found $[M+H]^+$ 346.1556, mean error= 1.2 ppm

^{1}H NMR (400 MHz, $CDCl_3$): δ_H 8.53 (1H, s, H**4**), 7.99 (1H, d, $^3J_{H-F}$ 13.6 Hz, H**8**), 7.25 (1H, d, $^4J_{H-F}$ 6.8 Hz, H**11**), 3.90 (3H, s, CH_3, H**18**), 3.42 (1H, m, CH, H**1**), 3.18-3.21 (4H, m, piperazine CH_2, H**14/15**), 3.05-3.07 (4H, m, piperazine CH_2, H**13/16**), 1.93 (1H, broad s, NH), 1.28 (2H, m, cyclopropyl ring, CH_2, H**2/3**), 1.11 (2H, m, cyclopropyl ring CH_2, H**2/3**).

^{13}C NMR (100 MHz, $CDCl_3$): δ_C 173.46 (C=O, C**6**), 166.70 (C=O, C5-C=O, C**17**), 153.59 (*ipso*-Ar C-F, d, $^1J_{C-F}$ 249.3 Hz, C**9**), 148.59 (C-H, C**4**), 145.26 (*ipso*-Ar C-C, d, $^2J_{C-F}$ = 10.68 Hz, C**10**), 138.22 (*ipso*-Ar C-C, C**5**), 122.99 (*ipso*-Ar, d, $^3J_{C-F}$ = 8.0 Hz, C**7**), 113.19 (C-H, d, $^2J_{C-F}$ = 24.0 Hz, C**8**), 109.95 (*ipso*-Ar, C**12**) 104.83 (Ar C-H, d, $^3J_{C-F}$ = 3.1 Hz C**11**), 51.97 (CH_3, C**18**), 50.94 (CH_2, C**13/14/15/16**), 50.89 (CH_2, C**13/14/15/16**), 45.71 (CH_2, C**13/14/15/16/**), 34.23(CH, C**1**), 7.65 (CH_2, C**2/3**).

^{19}F NMR ($CDCl_3$, 376 MHz, Fluorobenzene): δ_F -123.52 (dd, J_{H-F} = 12.6 Hz, 6.9 Hz, F**9**)

IR (KBr cm^{-1}): 3431.1 (N-H), 1724.0 (C=O), 1620.6 (C=O), 1270.7 (C-O)

*7.2.1.2. Methyl-7-[4-(2-([tert-butoxy)carbonyl]amino)acetyl)piperazine-1-yl]-1-cyclopropyl-6-fluoro-4-oxo-decahydroquinoline-3-carboxylate (**2-48**)[151]*

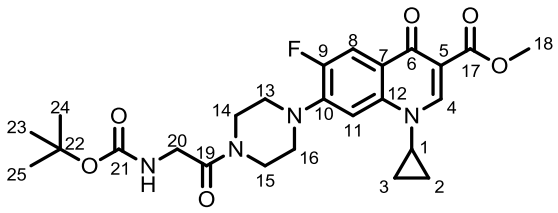

Molecular Formula: $C_{25}H_{31}FN_4O_6$
Molecular Weight: 502.223 g mol^{-1}

To a stirred solution of Methyl-1-cyclopropyl-6-fluoro-4-oxo-7-(piperazin-1-yl)-1,4-dihydroquinoline-3-carboxylate **2-20** (0.69 g, 1.99 mmol) in anhydrous DMF (60 mL) was added Boc-glycine **2-47** (0.35 g, 1.99 mmol), and EDC·HCl (0.38 g, 1.99 mmol). To the stirred solution was added DIPEA (0.35 mL, 2.01 mmol). The solution was briefly stirred, then HOBt·H_2O (0.27 g, 1.99 mmol) was added. The mixture was left to stir. After 24 hours, the solvent was removed *in vacuo*. The residue was diluted with deionised H_2O (60 mL) and extracted with DCM (3 x 110 mL). The organic layers were then washed with H_2O, CH_3SO_3H (0.05 M), $NaHCO_3$ (0.05 M), NaCl and H_2O (all 60 mL). The organic layer was dried over $MgSO_4$ and filtered. The organic layer was concentrated *in vacuo* to yield the product as a cream coloured solid. The crude product was triturated in diethyl ether and isolated by filtration as a white solid.

Yield: 0.47 g, 68%

m.p: 186-187 °C (lit 194-195 °C [151])

R_f (3:1, $CHCl_3$: MeOH): 0.60

m/z (ESI): 525.21 ($[M+Na]^+$, 38%), 503.23 ($[M+H]^+$, 100%).

HRMS (ESI): Calc. for $C_{25}H_{32}FN_4O_6$= 503.2300. Found $[M+H]^+$ 503.2303, mean error= -0.5 ppm. Calc. for $C_{25}H_{31}FN_4NaO_6$= 525.2120. Found $[M+Na]^+$ 525.2122, mean error= -0.6 ppm.

^{1}H NMR (400 MHz, $CDCl_3$): δ_H 8.49 (1H, s, H**4**), 7.96 (1H, d, $^3J_{H-F}$ =13.6 Hz, H**8**), 7.23 (1H, d, $^4J_{H-F}$ = 6.8 Hz, H**11**), 5.50 (1H, br s, N**H**), 4.01 (2H, d, $^3J_{H-H}$ = 4.57 Hz, H**20**), 3.91 (3H, s, H**18**), 3.85-3.87 (2H, m, H**14/15**), 3.61-3.64 (2H, m, H**14/15**), 3.42 (1H, m, H**1**), 3.22-3.27 (4H, m, H**13, 16**), 1.44 (9H, s, H**23, 24, 25**), 1.30-1.35 (2H, m, H**2/3**), 1.11-1.16 (2H, m, H**2/3**)

^{13}C NMR (100 MHz, $CDCl_3$): δ_C 172.23 (C=O, C**6**), 172.202 (C=O, C**19**), 167.13 (C=O, C**21**), 166.29 (C=O, C**17**), 154.65 (*ipso*-Ar, d, $^1J_{C-F}$ = 249 Hz, C**9**), 148.59 (CH, C**4**), 143.96 (*ipso*-Ar, d, $^2J_{C-F}$ = 10.7 Hz, C**10**), 138.01 (*ipso*-Ar, C**5**), 123.72 (*ipso*-Ar, d, $^3J_{C-F}$ = 6.9 Hz, C**7**), 113.53 (CH, d, $^2J_{C-F}$ = 23.0 Hz, C**8**), 110.18 (*ipso*-Ar, C**12**), 105.36 (CH, d, $^3J_{C-F}$ = 3.1 Hz, C**11**), 79.95 (4°C, C**23**), 52.18 (CH_3, C**18**), 50.16 (CH_2, C**14/15**), 49.73 (CH_2, C**14/15**), 44.40 (CH_2, C**20**), 42.29 (CH_2, C**13/16**), 41.86 (CH_2, C**13/16**), 34.66 (CH, C-**1**), 28.44 (CH_3, C**23/24/25**), 8.26 (CH_2, C**2, 3**)

^{19}F NMR (376 MHz, $CDCl_3$): δ_F -124.01 (dd, J_{H-F} = 12.6 Hz, 6. 9 Hz, F-**9**)

IR (KBr, cm^{-1}): 3427.2 (N-H), 1716.0 (C=O), 1653.3 (C=O), 1632.5 (C=O), 1495.6 (C-O), 1456.0 (C-O).

Spectral data consistent with literature values [151]

*7.2.1.3. Methyl-7-[4-(2-aminoacetyl)piperazin-1-yl]-1-cyclopropyl-6-fluoro-4-oxo-decahydroquinline-3-carboxylate hydrochloride salt (**2-49**)*[151]

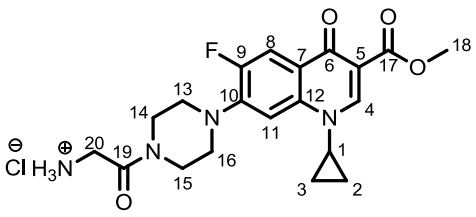

Molecular Formula: $C_{20}H_{24}ClFN_4O_4$ ($C_{20}H_{23}FN_4O_4$ as free amine)
Molecular Weight: 438.880 g mol^{-1} (402.419 g mol^{-1} as free amine)

Methyl-7-[4-(2-([*tert*-butoxy)carbonyl]amino)acetyl)piperazine-1-yl]-1-cyclopropyl-6-fluoro-4-oxo-decahydroquinoline-3-carboxylate **2-48** (0.39 g, 0.77 mmol) was dissolved in ice cold HCl (4 M in MeOH, 37 mL). The reaction was stirred overnight. After 18 hours, the solvent was removed *in vacuo*. The solid residue was redissolved in MeOH (20 mL) and concentrated *in vacuo* a second time to remove any residual HCl. The solid residue was resuspended in anhydrous MeOH (20 mL) and precipitated using Et_2O. The white precipitate was isolated by filtration and retained as the product.

Yield: 0.34 g, 98%

m.p: Dec. 230.0-230.5 °C

m/z (ESI): 425.16 ($[M+Na]^+$, 100%), 403.18 ($[M+H]^+$, 44%), 202.09 ($[M+2H]^{2+}$, 38%).

HRMS (ESI): Calc. for $C_{20}H_{24}FN_4O_4$= 403.1776. Found $[M+H]^+$ 403.1766, mean error= 2.7 ppm, Calc. for $C_{20}H_{23}FN_4NaO_4$ = 425.1596. Found $[M+H]^+$ 425.1577, mean error= 4.6 ppm.

^{1}H NMR (400 MHz, d_6-DMSO) δ_H 8.44 (1H, s, H**4**), 8.30 (2H, bs, NH_2), 7.75 (1H, d, $^3J_{H\text{-}F}$ =13.2 Hz, H**8**), 7.44 (1H, d, $^4J_{H\text{-}F}$ = 7.3 Hz, H**11**), 4.01 (2H, bs, H**20**), 3.71-3.74 (5H, m, H **14, 15, 18**), 3.61-3.66 (3H, m, CH, H**1**, CH_2, H**14,**

15), 3.23-3.30 (4H, m, H**13, 16**), 1.22-1.27 (2H, m, H**2/3**), 1.08-1.12 (2H, m, H**2/3**)

^{13}C NMR (100 MHz, d_6-DMSO): δ_C 172.25 (C=O, C**6**), 165.58 (C=O, C**21**), 165.40 (C=O, C**17**), 152.77 (*ipso*-Ar, d, C-F, $^1J_{C\text{-}F}$ = 247.0 Hz, C**9**), 148.94 (CH, C**4**), 143.98 (*ipso*-Ar, d, C-C, $^2J_{C\text{-}F}$ = 10.8 Hz, C**10**), 138.53 (*ipso*-Ar, C**5**), 122.57 (*ipso*-Ar, d, $^3J_{C\text{-}F}$ = 6.9 Hz, C**7**), 112.00 (*ipso*-Ar, C-H d, $^2J_{C\text{-}F}$ = 23.0 Hz, C**8**), 109.33 (*ipso*-Ar, C**12**), 106.97 (CH, d, $^3J_{C\text{-}F}$ = 3.1 Hz, C**11**), 51.37 (CH_3, C**18**), 49.55 (CH_2, C**14/15**), 49.51 (CH_2, C**14/15**), 43.89 (CH_2, C**20**), 41.24 (CH_2, C**13/16**), 39.32 (CH_2, C**13/16**), 34.76 (CH, C-**1**), 7.40 (CH_2, C**2/3**)

^{19}F NMR (376 MHz, d_6-DMSO): δ_F -124.69 (m, F-**9**)

IR (KBr, cm^{-1}): 3429.0 (N-H), 1725.4 (C=O), 1667.3 (C=O)

*7.2.1.4. 2-Hydroxy-4-methoxy-2-(2-methoxy-2-oxoethyl)-4-oxobutanoic acid(**2-21**)*[150]

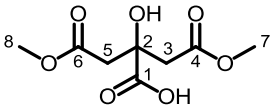

Molecular Formula: $C_8H_{12}O_7$
Molecular Weight: 220.177 g mol^{-1}

To a stirred solution of citric acid **1-26** (30.22 g, 0.157 mmol) in anhydrous MeOH (150 mL), was added concentrated H_2SO_4 (0.6 mL, 1.84 g/mL). The mixture was stirred under reflux for one hour. The mixture was then allowed to cool to room temperature. The mixture was diluted with deionised H_2O and neutralised using $Ca(OH)_2$. The resultant white precipitate was removed by filtration and discarded. The filtrate was reduced *in vacuo*, yielding a clear oil which solidified upon cooling. The white solid was broken down to a powder and dried under vacuum. The powder was re-suspended in deionised water

(100 mL), and the mixture was sonicated for 20 minutes. Any insoluble material was re-suspended in a further 100 mL of deionised water and sonicated as before. The insoluble material was removed by filtration. The filtrate was acidified to pH 0.0 using concentrated HCl (12 M), yielding a white precipitate. The precipitate was isolated by filtration and re-dissolved in aqueous $NaHCO_3$ (0.08 g/mL). The resulting solution was washed with $CHCl_3$ (3 x 40 mL). The organic layers were retained. The aqueous layer was re-acidified to pH 0.0 with concentrated HCl to yield a fine white precipitate. The precipitate was isolated by filtration and washed with $CHCl_3$ (1 x 20 mL) and then dried to yield the product. The organic layers were kept and concentrated under vacuum yielding a white solid which was dried on the vacuum line. The by-product in the $CHCl_3$ washes was found by ^{1}H NMR analysis to be 1,3,5-trimethyl citrate.

Yield: 10.70 g, 31%

m.p: 115-120 °C (lit 109-115 °C[259])

R_f (10:1:1, DCM: MeOH: HCOOH): 0.48

m/z (ESI): 243.04 ($[M+Na]^+$, 100%), 221.06 ($[M+H]^+$, 68.4%).

HRMS (ESI): Calc. for $C_8H_{13}O_7$ = 221.0656. Found 221.0654; mean error= 0.8 ppm Calc. for $C_8H_{12}NaO_7$ = 243.0475. Found 243.0472; mean error= 1.4 ppm.

^{1}H NMR (400 MHz, d_6-DMSO): δ_H 3.55 (6H, s, CH_3, H**7, 8**), 2.83 (2H, d, $^2J_{H\text{-}H}$ = 15.0 Hz, CH_2, H**3/5**), 2.72 (2H, d, $^2J_{H\text{-}H}$ = 15.0 Hz, CH_2, H**3/5**).

13C NMR (400 MHz, d_6-DMSO): δ_C 174.27(C=O, C**1**), 169.98 (C=O, C**4, 7**), 72.61 (4° C, C-OH, C**2**), 51.47 (CH_2, C**3, 6**), 42.71 (CH_3, C**5, 8**).

IR (KBr cm-1): 3474.1 (O-H), 1742.9 (C=O), 1634.1 (C=O)

^{1}H NMR data consistent with literature values [150]

*7.2.1.5. 1,2,3-Trimethyl 2-hydroxypropane-1,2,3-tricarboxylate(**2-22**)*[149]

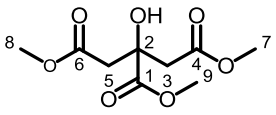

Molecular Formula: $C_9H_{14}O_7$

Molecular Weight: 234.203 g mol^{-1}

To a stirred solution of hydroxy-4-methoxy-2-(2-methoxy-2-oxoethyl)-4-oxobutanoic acid **2-21** (2.51 g, 11.4 mmol) in anhydrous MeOH (30 mL) was added H_2SO_4 (0.2 mL, 1.84 g/mL) and 2,2-dimethoxy propane (1.6 mL, 13 mmol). The initially white suspension became a clear solution upon stirring. The solution was stirred and heated under reflux for 7 hours. The solution was cooled to room temperature and the excess solvent removed *in vacuo*, yielding a white powder. This was further dried under vacuum. The product was recrystallised from a minimal amount of hot H_2O to produce a white crystalline solid which was isolated by filtration.

Yield: 21.60 g, 81%

m.p: 70.2-73.5 °C (lit 75-77 °C[260])

R_f (10:1:1, DCM: MeOH: HCOOH): 0.54

m/z (ESI): 257.06 ($[M+Na]^+$, 100%), 235.08 ($[M+H]^+$, 18.6%).

HRMS (ESI): Calc. for $C_9H_{15}O_7$= 235.0812. Found $[M+H]^+$ 235.0806 mean error= 2.6 ppm Calc. for $C_9H_{14}NaO_7$= 257.0632. Found [M+Na]+ 257.0630 mean error= 0.9 ppm.

^{1}H NMR (400 MHz, $CDCl_3$,): δ_H 3.83 (3H, s, CH_3, H**9**), 3.69 (6H, s, CH_3, H**7, 8**), 2.89 (2H, d, $^2J_{H\text{-}H}$ = 16.0 Hz, CH_2, H**3/5**), 2.78 (2H, d, $^2J_{H\text{-}H}$ = 16.0 Hz, CH_2, H**3/5**).

^{13}C NMR (100 MHz, $CDCl_3$): δ_C 173.82 (C=O, C**1**), 170.20 (C=O, C**4, 6**), 73.247 (4°-C, C**2**), 53.22 (CH_3, C**9**), 52.02 (CH_3, C**7, 8**), 43.05 (CH_2, C**3, 5**).

IR (KBr cm^{-1}): 3481.8 (O-H), 1756.7 (C=O), 1742.6 (C=O), 1722.1 (C=O)

Spectroscopic data is consistent with literature values[260]

*7.2.1.6. 3-Hydroxy-3-(methoxycarbonyl)pentanedioic acid (**2-24**)[149]*

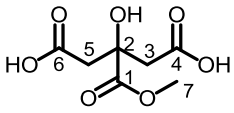

Molecular Formula: $C_7H_{10}O_7$
Molecular Weight: 206.150 g mol^{-1}

To a stirred solution of 1,2,3-trimethyl 2-hydroxypropane-1,2,3-tricarboxylate **2-22** (1.17 g, 5.0 mmol) in 70% MeOH (v/v in H_2O, 7.5 mL) was added an aqueous solution of 1 M NaOH (10 mL). The solution was then left to stir. After three hours the solvent was removed *in vacuo* to yield a white solid. This was re-dissolved in MeOH and desalted using a Dowex (50WX8-400) ion exchange column, using MeOH as the eluent. The solvent was removed *in vacuo* to yield a white solid which was recrystallised from hot acetone to yield the product as a white crystalline solid.

Yield: 0.54 g, 53%

m.p: 163.4-166.4 °C (lit 167 °C [149])

R_f (10:1:1, DCM: MeOH: HCOOH): 0.24

m/z (ESI): 229.03 ($[M+Na]^+$, 100%), 207.05 ($[M+H]^+$, 10.29%).

(ESI): Calc. for $C_7H_{11}O_7$= 207.0499 [M+H]+. Found 207.0494; mean error= 3.3 ppm, Calc. for $C_7H_{10}NaO_7$= 229.0319 [M+Na]+ Found 229.0319 mean error= 0.1 ppm.

^{1}H NMR (400 MHz, d_3-MeOD): δ_H 3.75 (3H, s, CH_3, H**7**), 2.74-2.93 (4H, m, CH_2, H**3,5**).

^{13}C NMR (100 MHz, d_3- MeOD): δ_C 176.32 (C=O, C**1**), 174.11 (C=O, C**4, 6**), 74.83 (4°C, C**2**), 53.23 (CH_3, C**7**), 44.29 (CH_2, C**3, 5**).

IR (KBr, cm-1): 3388.9 (O-H), 1747.7 (C=O), 1716.1 (C=O)

Spectroscopic data is consistent with literature values [149]

*7.2.1.7. 2-Tert-butyl 1,3-dimethyl 2-hydroxypropane-1,2,3-tricarboxylate (**2-23**)[152]*

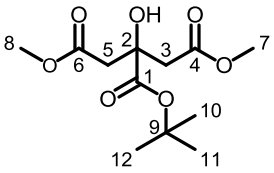

Molecular Formula: $C_{12}H_{20}O_7$
Molecular Weight: 276.283 g mol^{-1}

A solution of hydroxy-4-methoxy-2-(2-methoxy-2-oxoethyl)-4-oxobutanoic acid **2-21** (6.00 g, 27.2 mmol) in *tert*-butyl acetate (50 mL, 372 mmol) was prepared and sealed in a flask. The flask was purged of oxygen using a nitrogen balloon and a bleed needle. Concentrated perchloric acid (70%, 1 mL, 4.6 mmol) was added by syringe to the solution. The solution was left to stir for 3 days under a nitrogen atmosphere. After 3 days the solution was adjusted to pH 6 by the slow addition of a saturated solution of $NaHCO_3$. The organic layer was separated and retained. The aqueous layer was washed with diethyl ether (3 x 80 mL), the organic washes were combined, dried over $MgSO_4$ and filtered. The dried washes were then concentrated *in vacuo*, and then dried further using a vacuum line. The oil was re-dissolved in 60-80 pet. ether and rapidly stirred, insoluble material was filtered and the filtrate concentrated *in vacuo* to yield the product as pale yellow oil.

Yield: 3.69 g, 58%

R_f (10:1:1, DCM: MeOH: HCOOH): 0.45

m/z (ESI): 299.11 ([M+Na]+, 100%).

HRMS (ESI): Calc. for $C_{12}H_{20}NaO_7$= 299.1101. Found $[M+Na]^+$ 299.1106, mean error= -1.6 ppm

^{1}H NMR (400 MHz, $CDCl_3$,): δ_H 3.68 (6H, s, CH_3, H**7, 8**), 2.74-2.88 (4H, m, CH_2, H**3/5**), 1.49 (9H, s, CH_3, H**10, 11, 12**).

^{13}C NMR (100 MHz, $CDCl_3$): δ_C 172.76 (C=O, C**1**), 170.54 (C=O, C**4, 7**), 83.28 (4°C, C−O, C**9**), 72.97 (4°C, C−OH, C**2**), 51.67 (CH_3, C**5, 8**), 43.12 (CH_2, C**3, 6**), 27.43 (CH_3, C**10, 11, 12**).

IR ($CHCl_3$, cm^{-1}): 3500.0 (O-H), 1739.6 (C=O), 1221.2 (C-O), 1155.2 (C-O)

Spectroscopic data is consistent with literature values [152]

*7.2.1.8. 3-[(tert-Butoxy)carbonyl]-3-hydroxypentanedioic acid (**2-15**)*[152]

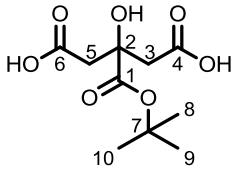

Molecular Formula: $C_{10}H_{16}O_7$
Molecular Weight: 248.230 g mol^{-1}

A solution of 2-*tert*-butyl-1,3-dimethyl-2-hydroxypropane-1,2,3-tricarboxylate **2-23** (1.00 g, 3.63 mmol) in MeOH (30 mL) was cooled in an ice bath to 0 °C. A cold solution of NaOH (2 M, 10 mL) was added. The solution was allowed to warm to room temperature and left to stir. After three hours, the mixture was acidified to pH 2 using HCl (2 M). The solution was extracted using EtOAc (3 x 60 mL). The organic washes were combined and dried over $MgSO_4$. The organic layer was filtered and concentrated *in vacuo* to yield pale oil, which solidified on the vacuum line to yield a white solid.

Yield: 2.49 g, 75%

m.p: 117.4-120.5 °C (lit 124 °C[152])

R_f (10:1:1, DCM: MeOH: HCOOH): 0.33

m/z (ESI): 271.08 ($[M+Na]^+$, 100%).

HRMS (ESI): Calc. for $C_{10}H_9NaO_7$= 271.0788. Found $[M+Na]^+$ 271.0790, mean error= -0.8 ppm

^{1}H NMR (400 MHz, d_3-MeOD): δ_H 2.86 (2H, d, $^2J_{H\text{-}H}$= 15.6 Hz, CH_2, H**3/5**), 2.71 (2H, d, $^2J_{H\text{-}H}$= 15.6 Hz, CH_2, H**3/5**), 1.48 (9H, s, CH_3, H**8, 9, 10**)

^{13}C NMR (100 MHz, d_3-MeOD): δ_C 173.80 (C=O, C**1**), 173.36 (C=O, C**4, 6**), 83.42 (4°-C, C-OH, C**2**), 74.34 (4°-C, $C(CH_3)_3$, C**9**), 44.15 (CH_2, C**3,6**), 28.04 CH_3 C**10, 11, 12**).

IR (KBr, cm-1): 3477.2 (O-H), 1735.5 (C=O) 1707.7 (C=O), 1186.7 (C-O).

Spectroscopic data consistent with literature values[152].

*7.2.1.9. 2,3-Bis(benzyloxy)benzaldehyde (**2-25**)[138]*

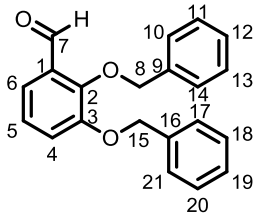

Molecular Formula: $C_{21}H_{18}O_3$
Molecular Weight: 318.366 g mol^{-1}

To a stirred solution of 2,3-dihydroxy benzaldehyde **2-18** (5.00 g, 36.2 mmol) and benzyl chloride (10 mL, 86.9 mmol) in anhydrous EtOH (80 mL), was added $K_2CO_{3(S)}$ (6.49 g, 46.9 mmol). The resulting suspension was refluxed at 80 °C. After 18 hours the suspension was cooled to room temperature and the solid formed removed by filtration. The solid was washed with acetone (3 x 10 mL) and then discarded; the acetone wash was added to the filtrate. The filtrate was concentrated *in vacuo* to yield a pale waxy solid. The solid was

re-crystallised from hot MeOH to yield a pale brown solid which was isolated by filtration and retained as the product.

Yield: 8.06 g, 70%

m.p: 92.1- 93.1 °C

R_f (10:1, $CHCl_3$: MeOH): 0.85

m/z (ESI): 341.12 ($[M+Na]^+$, 76.47%,), 336.16 ($[M+NH_4]^+$, 88.23%), 319.13 ($[M+H]^+$, 100%,).

HRMS (ESI): Calc. for $C_{21}H_{19}O_3$= 319.1332. Found $[M+H]^+$ 319.1329, mean error= -0.8 ppm. Calc. for $C_{21}H_{18}NaO_3$= 341.1150. Found $[M+Na]^+$ 341.1148, mean error= -0.7 ppm.

^{1}H NMR (400 MHz, $CDCl_3$): δ_H 10.28 (1H, s, CH, H**7**), 7.41-7.43 (11H, m, Ar, C-H, H**6, 10-14, 17-21**), 7.26 (1H, m, Ar, C-H, H**4**), 7.12 (1H, m, Ar, C-H, H**5**) 5.22 (2H, s, CH_2, H**8/15**), 5.20 (2H, s, CH_2, H**8/15**)

^{13}C NMR (100 MHz, $CDCl_3$): δ_C 190.18 (C=O, C**7**), 151.98 (*ipso*-Ar, C-O, C**2**), 150.52 (*ipso*-Ar, C-O, C**3**), 136.24 (*ipso*-Ar, C-C, C**9, 16**), 130.44 (*ipso*-Ar, C-C, C**1**), 129.90 (ipso-Ar, C-O, C**2/3**) 128.73-127.51(Ar. C-H, C**10-14, 17- 21**), 124.20 (Ar, C-H, C**5**), 119.84 (Ar, C-H, C**4**), 119.51 (Ar, C-H, C**6**) 76.40 (CH_2, C**8/15**), 71.20 (CH_2, C**8/15**)

IR (KBr cm^{-1}): 1699.4 (C=O), 1267.7 (C-O), 1247.0 (C-O).

*7.2.1.10. 2,3-Bis(benzyloxy)benzoic acid (**2-26**)[153]*

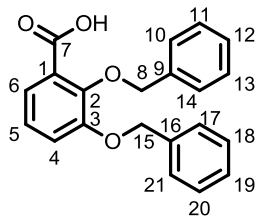

Molecular Formula: $C_{21}H_{18}O_4$

Molecular Weight: 334.365 g mol^{-1}

To a solution of 2,3-bis(benzyloxy)benzaldehyde **2-25** (3.61g, 11.3 mmol) in a 1:1 mixture of acetone (113 mL) and H_2O (113 mL) was prepared. $NaClO_2$ (1.30 g, 14.4 mmol) in H_2O (28 mL) and H_3NSO_3 (1.55 g, 16.0 mmol) in H_2O (28 mL) were added in alternating portions over 45 minutes. The solution was left to stir in an open flask. After 1 hour the volume of the solvent was reduced *in vacuo* by approximately 50% until a white precipitate was observed. The precipitate was isolated by filtration and retained as the product.

Yield: 3.40 g, 90%

m.p: 123.9-124.7 °C (Lit 124-124.5 °C[138])

R_f: (10:1, $CHCl_3$: MeOH): 0.57

m/z (ESI): 357.109 ($[M+Na]^+$, 84.2%), 352.15 ($[M+NH_4]^+$, 100%), 335.13 ($[M+H]^+$, 80.2%).

HRMS (ESI): Calc. for $C_{21}H_{19}O_4$= 335.1278. Found $[M+H]^+$ 335.1274, mean error= -3.5 ppm. Calc. for $C_{21}H_{22}NO_4$= 353.1543. Found $[M+Na]^+$ 352.1543, mean error= 1.6 ppm.

^{1}H NMR (400 MHz, $CDCl_3$): δ_H 11.44 (1H, s, COOH, H**7**), 7.75 (1H, dd, $^3J_{H\text{-}H}$ = 7.9 Hz, $^4J_{H\text{-}H}$ = 1.6 Hz, Ar C-H, H**6**), 7.42 (10H, m, Ar, C-H, H**10-14, 17-21**), 7.28 (1H,m, Ar, C-H, H**4**), 7.20 (1H, m, Ar, C-H, H**5**), 5.27 (2H,s, CH_2, H**8/15**), 5.21 (2H, s, CH_2, H**8/15**).

^{13}C NMR (100 MHz, $CDCl_3$): δ_C 165.36 (C=O, COOH, C**7**), 151.30 (*ipso* Ar, C-O, C**2**), 147.08 (*ipso* Ar, C-O, C**3**), 135.81 (*ipso* Ar, C-C, C**9/16**), 134.66 (*ipso*-Ar, C-C, C**9/16**) 129.25 -127.74 (Ar C-H, C**10-14, 17-21**), 124.98 (Ar, C-H, C**5**), 124.35 (Ar C-H, C**6**), 118.93 (Ar, C-H, C**4**), 77.04(CH_2, C**8, 15**), 71.46 (CH_2, C**8, 15**).

IR (KBr cm^{-1}): 1699.4 (C=O), 1267.7 (C-O), 1247.0 (C-O).

*7.2.1.11. 2,5-Dioxopyrrolidin-1-yl 2,3-bis(benzyloxy)benzoate (**2-27**)[153]*

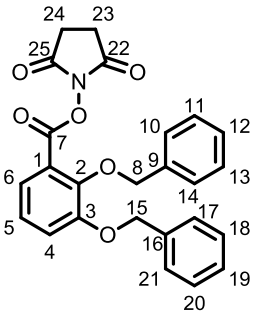

Molecular Formula: $C_{25}H_{21}NO_6$
Molecular Weight: 431.437 g mol^{-1}

To a stirred solution of 2,3-bis(benzyloxy)benzoic acid **2-26** (1.36 g, 4.07 mmol) in 1,4-dioxane (41 mL) was added NHS (0.49 g, 4.30 mmol). The solution was cooled to 0 °C in an ice bath. To the chilled solution, DCC (0.85 g, 4.12 mmol) was added. The ice bath was removed and the reaction allowed to return to room temperature and left to stir. After 24 hours the solid urea formed was removed by filtration. The filtrate was concentrated *in vacuo* to leave an oil. The product was crystallised from the oil by addition of iso-propanol. The crystals were then isolated by filtration and dried *in vacuo*.

Yield: 1.51 g, 86%

m.p: 95.6-98.2 °C (lit 112-114 °C [153])

R_f (10:1, $CHCl_3$: MeOH): 0.69

m/z (ESI): 454.13 ($[M+Na]^+$, 66.66%), 449.17 ($[M+NH_4]^+$, 100%), 432.14 ($[M+H]^+$, 21.79%).

HRMS (ESI): Calc. for $C_{25}H_{22}NO_6$ 432.1442. Found $[M+H]^+$ 432.1450, mean error= -1.7 ppm. Calc. for $C_{25}H_{21}NNaO_6$= 454.1261. Found $[M+Na]^+$ 454.1270, mean error= -2.1 ppm error.

^{1}H NMR (400 MHz, $CDCl_3$,): δ_H 7.61 (1H, m, Ar, C-H**,** H**6)**, 7.52-7.27 (11H, m, Ar, C-H, H**4, 10-14, 17-21**), 7.15 (1H, m, Ar, C-H**,** H**5**), 5.16 (4H, s, CH_2, H**8/15**), 2.88 (4H, s, CH_2, H**23, 24**).

^{13}C NMR (100 MHz, $CDCl_3$): δ_C 169.72 (C=O, C**7**), 161.08 (C=O, C**22/25**), 153.28 (*ipso*-Ar, C−O, C**2**), 150.1 (*ipso*-Ar-C−O, C**3**), 137.224 (*ipso*-Ar, C−C, C**9/16**), 136.46 (*ipso*-Ar, C−C, C**9/16**), 128.85-127.8 (Ar C-H, C**10-14, 17-21**), 124.45 (Ar, C−H, C**6**), 122.19 (Ar, C−H, C**5**), 121.19 (*ipso*-Ar, C-C ,C**1**), 120.25 (Ar, C−H, C**4**), 75.79 (CH_2, C**8/15**), 71.26 (CH_2, C**8/15**), 25.36 (CH_2, C**23, 24**).

IR (KBr, cm^{-1}): 1768.1 (C=O), 1739 (C=O), 1382.2 (N-O), 1262.1 (C-O), 1247.9 (C-O). `

*7.2.1.12. tert-Butyl N-(2-aminoethyl)carbamate (**2-31**)*[157-158]

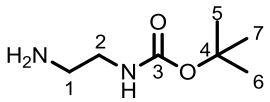

Molecular Formula: $C_7H_{16}N_2O_2$
Molecular Weight: 160.214 g mol^{-1}

1,2-Diaminoethane **2-19** (10 mL, 150 mmol) was dissolved in DCM (20 mL). To this stirred solution was added dropwise, a solution of di-*tert*-butyldicarbonate **2-30** (3.28 g, 15.0 mmol) in DCM (30 mL). The mixture was left to stir. After 20 hours, the solvent was removed *in vacuo*. The residue was taken up in NaCl: EtOAc (1:1). The aqueous layer was discarded, and the organic layer was washed with saturated $NaCO_3$ (3 x 30 mL). The

aqueous washes were discarded. The organic layer was retained and dried over $MgSO_4$ and filtered. The resulting filtrate was then concentrated *in vacuo*, yielding a pale yellow oil.

Yield: 1.96 g, 81%

R_f (10:1:0.1, $CHCl_3$: MeOH: NH_4OH): 0.55

m/z (ESI): 161.13 ($[M+H]^+$, 100%).

HRMS (ESI): Calc. for $C_7H_{17}N_2O_2$= 161.1285, Found $[M+H]^+$ 161.1287, mean error= -0.9

^{1}H NMR (400 MHz, $CDCl_3$): δ_H 4.92 (1H, Broad s, N**H**), 3.16-3.21 (2H, m, CH_2, H**2**), 2.80 (2H, t, $^3J_{H\text{-}H}$ = 6.0 Hz, CH_2, H**1**), 1.73 (2H, Broad s, NH_2), 1.43 (9H, s, CH_3, H**5, 6, 7**).

^{13}C NMR (100MHz, $CDCl_3$) δ_C 156.20 (**C**=O, C**3**), 79.17 (4°C, C**4**), 42.66 (CH_2, C**2**), 41.46 (**C**H_2, C**1**), 28.38 (CH_3, C**5, 6, 7**)

IR ($CHCl_3$, cm^{-1}): 3455.5 (N-H), 1706.8 (C=O), 1167.4 (C-O).

Spectroscopic data is consistent with literature values [157].

*7.2.1.13. tert-Butyl-N-(2-[[2,3-bis(benzyloxy)phenyl]formamido][261]ethyl)carbamate (**2-32**)*

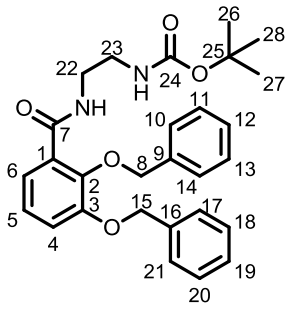

Molecular Formula: $C_{28}H_{32}N_2O_5$

Molecular Weight: 476.564 g mol^{-1}

To a stirred solution of 2,5-dioxopyrrolidin-1-yl 2,3-bis(benzyloxy)benzoate **2-27** (1.00 g, 2.32 mmol) in acetone (10 mL) was added a solution of *tert*-butyl N-(2-aminoethyl)carbamate **2-31** (0.40 g, 2.50 mmol) in H_2O (3.5 mL) and triethylamine (1 mL, 7.20 mmol). A cloudy mixture was observed, followed by the precipitation of a cream coloured solid. The mixture was left to stir. After 24 hours the solvent was removed *in vacuo* to yield a pale yellow solid. The solid was taken up in EtOAc (40 mL) and washed with HCl (0.1 M, 3 × 40 mL). The organic layer was then washed with H_2O (2 × 30 mL) until the aqueous washes were neutral. The organic layer was dried over $MgSO_4$ and filtered. The filtrate was concentrated *in vacuo* to yield the product as a white solid.

Yield: 1.10 g, 100%

m.p: 128.2-131.5 °C

R_f (10:1, $CHCl_3$: MeOH): 0.63

m/z (ESI): 499.22 ($[M+Na]^+$, 39.1%), 477.24 ($[M+H]^+$, 100%).

HRMS (ESI): Calc. for $C_{28}H_{33}N_2O_5$= 477.2384, Found $[M+H]^+$ 477.2393, mean error= -1.8 ppm

^{1}H NMR (400 MHz, $CDCl_3$): δ_H 7.99 (1H, m, NH_2), 7.61 (1H, m, Ar C-H, H**6** 7.28-7.63 (10H, m, Ar C-H, H**10-14, 17-21**), 7.06-7.07 (2H, m, Ar C-H, H**4, 5**) 5.0 (2H,s, CH_2, H**8/15**), 5.01 (1H, s, CH_2, H**8/15**), 3.25-3.29 (2H, m, CH_2, H**22**), 3.07-3.08 (2H, m, CH_2, H**23**), 1.32 (9H, s, CH_3, H**26, 27, 28**).

^{13}C NMR (100 MHz, $CDCl_3$): δ_C 166.11 (**C**=O, C**7**), 156.16 (C=O, C**24**), 151.82 (*ipso*-Ar, C-O, C**2**), 146.91 (*ipso*-Ar, C-O, C**3**), 136.48 (*ipso*-Ar, C-C, C**9/16**), 136.40 (*ipso*-Ar, C-C, C**9/16**), 128.99-127.27 (Ar C-H, C**10-14, 17-21**), 124.55 (Ar C-H, C**6**), 123.34 (Ar C-H, C**5**), 117.27 (Ar C-H, C**4**), 79.37 (4°C, C**25**) 76.61 (CH_2, C**8/15**), 71.44 (CH_2, C**8/15**), 41.04 (CH_2, C**23**), 39.72 (CH_2, C**22**), 28.49 (CH_3, C**26, 27, 28)**

IR (KBr cm^{-1}): 3350.7 (N-H), 3327.5 (N-H), 1685.5 (C=O), 1638.0 (C=O), 1217.3 (C-O).

*7.2.1.14. N-(4-aminobutyl)-2,3-bis(benzyloxy)benzamide hydrochloride (**2-40**)[161]*

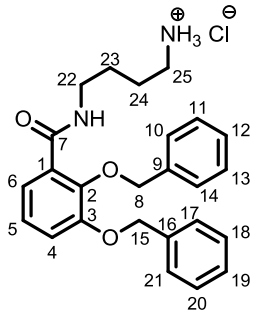

Molecular Formula: $C_{25}H_{29}ClN_2O_3$ ($C_{25}H_{28}N_2O_3$ as free amine)
Molecular Weight: 440.962 g mol^{-1} (404.501 g mol^{-1} as free amine)

2,3-bis(benzyloxy)benzoic acid **2-26 (**3.34 g, 10.0 mmol) was dissolved in anhydrous THF (15 mL). In a separate flask, 1,4-diaminobutane **2-39** (1.01 mL, 0.88 g, 10.0 mmol) was dissolved in anhydrous THF (20 mL). *N,N'*-carbonyldiimidazole (CDI) **2-37** (1.62 g, 10.0 mmol) was added to the benzoic acid solution, resulting in the evolution of CO_2. Once CO_2 evolution ceased, the benzoic acid solution was added dropwise to the diamine

solution over a period of 2 hours. Once addition was complete the solution was left to stir overnight. After stirring for 18 hours the excess solvent was removed *in vacuo* to yield a solid residue. This was redissolved in of $CHCl_3$ (150mL). The organic solution was then washed with saturated $NaHCO_3$ (100 mL), brine (100 mL), HCl (2 M, 100 mL) and brine (100 mL). The HCl and $NaHCO_3$ solutions were both also saturated with brine to aid separation. The organic layer was dried over $MgSO_4$ and filtered under gravity. The solution was then concentrated *in vacuo* to yield pale oil. EtOAc was added to the oil, producing the product as a white precipitate. This was isolated by filtration and retained as the product. Unreacted starting material was recovered by concentration of the filtrate *in vacuo*.

Yield: 2.38 g, 54%

m.p: 131-132 °C (Lit: 137 °C)[161]

m/z (ESI): 427.19 ($[M+Na]^+$ 3%), 405.22 ($[M+H)^+$ 100%].

HRMS (ESI): Calc. for $C_{25}H_{29}N_2O_3$= 405.2173, found $[M+H]^+$ 405.2178; mean error= 0.5 ppm

^{1}H NMR (400 MHz, $CDCl_3$): δ_H 8.33 (2H, br s, NH_2), 8.04 (1H, m, NH), 7.59-7.63 (1H, m, Ar C-H, H**6**), 7.33-7.45 (10H, m, Ar, C-H, H**10-14, 17-21**), 7.08-7.09 (2H, m, Ar C-H, H**4, 5**), 5.10 (s, 2H, CH_2, H**8/15**), 5.07 (2H, s, CH_2, H**8/15**), 3.18-3.23 (2H, m, CH_2, H**22**), 2.92-2.96 (2H, m, CH_2, H**25**), 1.68-1.75 (2H, m, CH_2, H**24**), 1.36-1.43 (2H, m, CH_2, H**23**).

^{13}C NMR (100 MHz, $CDCl_3$): δ_C 165.97 (C=O, C**7**), 152.01 (*ipso*-Ar, C-O, C**2**), 147.07 (*ipso*-Ar, C-O, C**3**), 137.13 (*ipso*-Ar, C-C, C**9/16**), 136.82 (*ipso*-Ar, C-C, C**9/16**), 129.14 (m, Ar, C-H, C**10-14, 17-21**), 124.59 (Ar, C-H, C**6**), 123.20 (Ar, C-H, C**5**), 117.2 (Ar, C-H, C**4**), 75.13 (CH_2), 70.19 (CH_2), 38.40 (CH_2, C**22**), 38.27 (CH_2, C**25**), 26.06 (CH_2, C**23/24**), 24.47 (CH_2, C**23/24**)

IR (KBr cm^{-1}): 3365.5 (NH), 1642.6 (C=O), 1264.7 (C-O)

Data consistent with literature values [161].

*7.2.1.15. Methyl3-[(4-[[2,3-bis(benzyloxy)phenyl]formamido]butyl)carbamoyl]-2-[[(4-[[2,3-bis(benzyloxy)phenyl]formamido]butyl)carbamoyl]methyl]-2-hydroxypropanoate (**2-41**)*

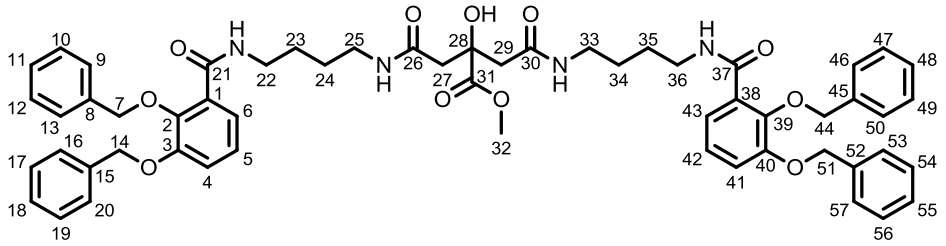

Molecular Formula: $C_{57}H_{62}N_4O_{11}$

Molecular Weight: 979.112 g mol^{-1}

3-hydroxy-3-(methoxycarbonyl)pentanedioic acid **2-24** (0.10 g, 0.50 mmol) and EDC·HCl (0.21 g, 1.10 mmol) were dissolved in anhydrous DMF (20 mL). DIPEA (0.35 mL, 1.99 mmol) was added and the solution was left to stir. After 15 minutes, $HOBt.H_2O$ (0.15 g, 1.11 mmol) was added and the solution left to stir. After 30 minutes *N*-(4-aminobutyl)-2,3-bis(benzyloxy)benzamide hydrochloride **2-40** (0.442 g, 1.00 mmol) and DIPEA (0.35 mL, 1.99 mmol) were added. The solution was left to stir. After 18 hours, the solvent was removed *in vacuo* yielding a dark oil. The oil was re-suspended in 80 mL of H_2O and extracted with DCM (3 × 100 mL). The organic layer was retained and washed with $MeHSO_3$ (0.05 M, 80 mL), $NaHCO_3$ (0.05 M, 80 mL), brine (80 mL) and H_2O (80 mL). The organic layer was dried over $MgSO_4$ and filtered. The filtrate was concentrated *in vacuo* to yield a yellow oil. This was purified using flash chromatography in 2:1 $CHCl_3$: MeCN. The appropriate fractions were concentrated *in vacuo* to yield a white foam.

Yield: 0.20 g, 41%

m.p: 129.5-131.0 °C

R_f (2:1, $CHCl_3$: MeCN): 0.43

m/z (ESI): 1001.43 ($[M+Na]^+$ 100%), 969.40 ($[M+H)^+$ 7%].

HRMS (ESI): Calc. for $C_{57}H_{62}N_4NaO_{11}$= 1001.4307, found $[M+Na]^+$ 1001.4318; mean error= -1.3 ppm

^{1}H NMR (400 MHz, $CDCl_3$): δ_H 8.01 (2H, t, $^3J_{H\text{-}H}$ = 5.7 Hz, N-H), 7.66-7.69 (2H, m, Ar C-H, H**6, 43**), 7.34-7.48 (20H, m, Ar, C-H, H**10-14, 17-21**), 7.13-7.16 (4H, m, Ar, C-H, H**4, 5, 41, 42**) 6.84 (2H, t, $^3J_{H\text{-}H}$ = 5.7 Hz, NH), 5.07 (2H, s, CH_2, H**7/14, 44/51**), 5.00 (2H, s, CH_2, H**7/14, 44/51**), 3.65 (3H, s, CH_3, H**32**), 3.05-3.22 (8H, m ,CH_2, H**23, 24, 33, 36**), 2.57-2.74 (m, 4H, CH_2, H**27, 29**), 1.25-1.42 (8H, m, CH_2, H**22, 25, 34, 35**)

^{13}C NMR (100 MHz, $CDCl_3$): δ_C 174.67 (C=O, C**26, 30**), 170.16 (C=O, **31**) 165.71 (**C**=O, C**7, 37**), 151.62 (*ipso*-Ar, C-O, C**3, 40**), 147.04 (*ipso*-Ar C-O, C**2, 39**), 136.61 (*ipso*-Ar, C-C, C**9, 16, 45, 52**), 131.14 (*ipso*-Ar, C-O), 128.42 (m, Ar C-H, C**10-14, 17-21**), 127.35 (ipso-Ar, C-C, C**1, 38**) 124.63 (Ar, C-H, C**6, 43**), 120.78 (Ar, C-H, C**5, 42**), 115.81 (Ar, C-H, C**4, 41**), 75.13 (CH_2, C**7/14, 44/51**), 70.19 (CH_2, C**7/14, 44/51**), 52.73 (CH_3, C**32**), 43.32 (CH_2, C**27, 29**) 38.40 (CH_2, C**22/25, 33/36**), 38.27 (CH_2, C**22/25, 33/36**), 26.06 (CH_2, C**23/24, 34/35**), 24.47 (CH_2, C**23/24, 34/35**)

IR (KBr cm^{-1}): 3379.9 (O-H), 3293.1 (N-H), 1649.6 (C=O) 1265.0 (C-O).

*7.2.1.16. 3-[(4-[[2,3-bis(benzyloxy)phenyl]formamido]butyl)carbamoyl]-2-[[(4-[[2,3-bis(benzyloxy)phenyl]formamido]butyl)carbamoyl]methyl]-2-hydroxypropanoic acid (**2-42**)*[164]

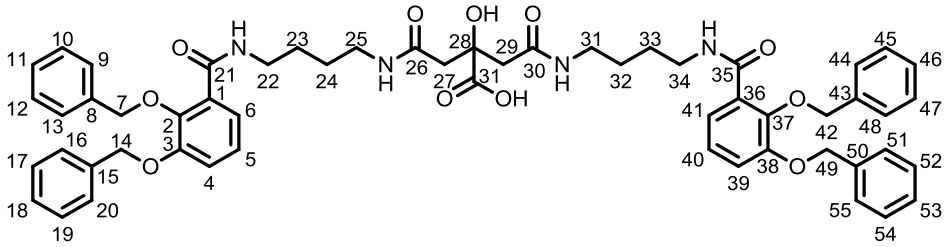

Molecular Formula: $C_{56}H_{60}N_4O_{11}$

Molecular Weight: 964.096 g mol^{-1}

To a stirred solution of methyl3-[(4-[[2,3-bis(benzyloxy)phenyl]formamido]butyl)carbamoyl]-2-[[(4-[[2,3-bis(benzyloxy)phenyl]formamido]butyl)carbamoyl]methyl]-2-hydroxypropanoate **2-41** 0.34 g (0.35 mmol) in 9:1 DCM: MeOH (10 mL) was added NaOH (2 M in MeOH, 0.52 mL). The solution was left to stir. After four hours, the solution was concentrated *in vacuo* to yield a yellow oil. The residue was redissolved in DCM (15 mL) and washed with aqueous HCl (0.1 M, 10 mL) and brine (10 mL). The organic layer was dried over $MgSO_4$ and filtered. The organic layer was concentrated *in vacuo* to yield the product as a pale yellow solid.

Yield: 0.28 g, 83%

m.p: 82.9- 83.9

m/z (ESI): 987.41 ($[M+Na]^+$ 100%), 965.43 ($[M+H)^+$ 100%].

HRMS (ESI): Calc. for $C_{56}H_{61}N_4O_{11}$= 965.4331, found $[M+H]^+$ 965.4293, mean error= 4.3 ppm, Calc. for $C_{56}H_{60}N_4NaO_{11}$= 987.4151, found $[M+Na]^+$ 987.4127; mean error= 2.7 ppm.

^{1}H NMR (400 MHz, $CDCl_3$): δ_H 8.11 (2H, t, $^{3}J_{H\text{-}H}$ = 5.9 Hz, N-H), 7.64-7.66 (2H, m, Ar C-H, H**6, 41**), 7.32-7.47 (20H, m, Ar, C-H, H**10-14, 17-21**), 7.12-7.13 (4H, m, Ar C-H, H**4, 5, 39, 40**), 5.14 (s, 2H, CH_2, H**7/14, 42/59**), 5.07 (s, 2H, CH_2, H**7/14, 42/59**), 3.12-3.29 (m, 8H, CH_2, H**22, 25, 31, 34**), 2.64-2.75 (m, 4H, CH_2, H**27, 29**), 1.36-1.43 (m, 8H, CH_2, H**23, 24, 32, 33**)

^{13}C NMR (100 MHz, $CDCl_3$): δ_C 181.78 (C=O, C**31**), 181.01 (C=O, C**26, 30**) 165.72 (C=O, C**7, 35**), 151.62 (*ipso*-Ar, C-O, C**3, 40**), 145.14 (*ipso*-Ar C-O, C**2, 37**), 136.97 (m, *ipso*-Ar C-C, **C9, 16**), 128.15 (m, Ar, C-H, C**10-14, 17-21**), 127.16 (*ipso*-Ar, C-C, C**1, 36**) 124.68 (Ar ,C-H, C**6**), 123.26 (Ar, C-H, C**5**), 117.17 (Ar, C-H, C**4**), 75.13 (CH_2, C**7/14, 42/49**), 70.19 (CH_2, C**7/14, 42/49**), 42.72 (CH_2, C**27, 29**) 38.40 (CH_2, C**22/25, 31/34**), 38.27 (CH_2, C**22/25, 31/34**), 26.06 (CH_2, C**23/24, 32/33**), 24.47 (CH_2, C**23/24, 32/33**)

IR (KBr, cm^{-1}): 3380.5 (O-H), 3276.7 (N-H), 1652.3 (C=O), 1265.2 (C-O)

*7.2.1.17. 2,3-bis(benzyloxy)-N-[4-(3-([(4-([2,3-bis(benzyloxy)phenyl]formamido)butyl)carbamoyl]methyl)-3-hydroxy-2,5-dioxopyrrolidin-1-yl)butyl]benzamide (**2-43**)*

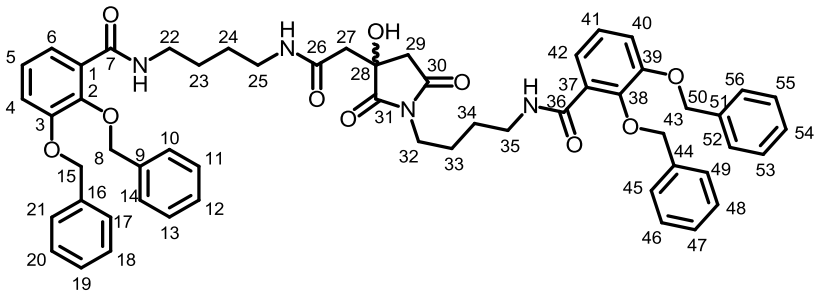

Molecular Formula: $C_{56}H_{58}N_4O_{10}$

Molecular Weight: 947.081 g mol^{-1}

2-43 was observed as a by-product in the synthesis of 3-[(4-[[2,3-bis(benzyloxy)phenyl]formamido]butyl)carbamoyl]-2-[[(4-[[2,3-bis(benzyloxy)phenyl]formamido]butyl)carbamoyl]methyl]-2-

hydroxypropanoic acid **2-42**. The compound was identified in the ESI mass spectrum. The compound was not isolated.

R_f (9:1, DCM: MeOH): 0.46

m/z (ESI): 947.42 ($[M+H]^+$, 100%)

*7.2.1.18. Methyl-6-(4-[3-[(4-[[2,3-bis(benzyloxy)phenyl]formamido]butyl)carbamoyl]-2-[[(4-[[2,3-bis(benzyloxy)phenyl]formamido]butyl)carbamoyl]methyl]-2-hydroxypropanoyl]piperazin-1-yl)-4-cyclopropyl-7-fluoro-1-oxo-1,4-dihydronaphthalene-2-carboxylate (**2-45**)*

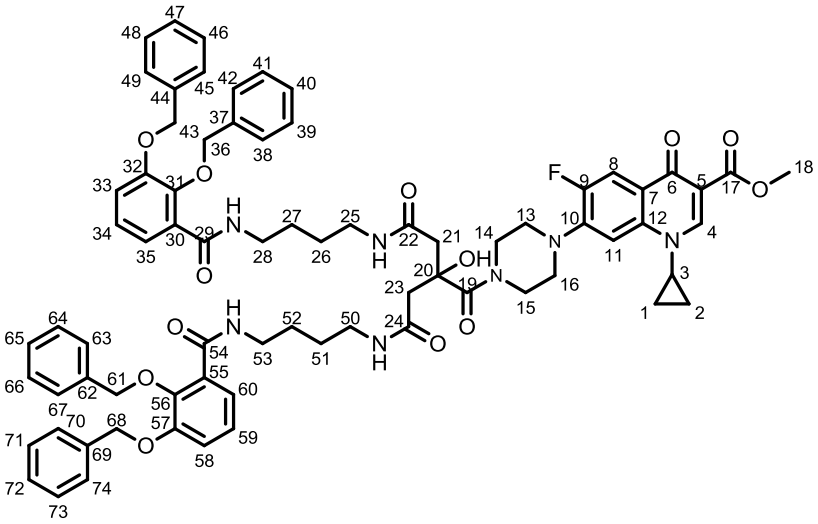

Molecular Formula: $C_{74}H_{78}FN_7O_{13}$

Molecular Weight: 1292.449 g mol^{-1}

To a stirred solution of 3-[(4-[[2,3-bis(benzyloxy)phenyl]formamido]butyl)carbamoyl]-2-[[(4-[[2,3-bis(benzyloxy)phenyl]formamido]butyl)carbamoyl]methyl]-2-hydroxypropanoic acid **2-42** (0.15 g, 0.155 mmol) and methyl-1-cyclopropyl-6-fluoro-4-oxo-7-(piperazin-1-yl)-1,4-dihydroquinoline-3-carboxylate **2-20** was added HBTU (0.066 g, 0.18 mmol) and DIPEA (0.03mL 0.15 mmol). The solution was stirred overnight. After 18 hours the solution was concentrated

in vacuo. The residue was dissolved in DCM (50 mL) and washed with HCl (0.05 M, 40 mL), $NaHCO_3$ (0.05 M, 40 mL), and brine (40 mL). The organic layer was dried over $MgSO_4$ and filtered. The filtrate was concentrated *in vacuo*. The product was purified by flash chromatography in 9:1 DCM: MeOH.

Yield: 0.13 g, 65%

R_f: (9:1, DCM: MeOH): 0.32

m/z (ESI): 1292.56($[M+H]^+$ 100%).

HRMS (ESI): Calc. for $C_{74}H_{79}FN_7O_{11}$= 1292.5714, found $[M+H]^+$ 1292.5662; mean error= 3.9 ppm

^{1}H NMR ($CDCl_3$, 400 MHz): δ_H 8.55 (1H, s, CH, H**4**), 7.96-8.10 (3H, m, Ar, C-H, **65** and NH), 7.65-7.67 (2H, m, Ar C-H, H**35, 60**), 7.34-7.47 (m, 21H, Ar, C-H, H**11, 38-42, 45-49, 63-67, 70-74**), 7.24-7.26 (2H, m, NH), 7.12-7.13 (4H, m, Ar C-H, H**34, 35, 58, 59**) 5.13 (2H, s, CH_2, H**36/43, 61/68**), 5.07 (2H, s, CH_2, H**36/43, 61/68**), 3.90 (3H, s, CH_3, H**18**), 3.76-3.84 (2H, m, CH_2, H**14/15**), 3.57-3.59 (2H, m, CH_2, H**14/15)** 3.10-3.26 (13H, m ,CH_2, H**13, 16, 25, 28, 50 ,53** CH, H**3**), 2.90 (2H, d, CH_2 $^4J_{H\text{-}H}$ = 14.4 Hz, H**21/23**), 2.58 (d, 2H, $^4J_{H\text{-}H}$ = 14.4 Hz, CH_2, H**21/23**),1.28-1.45 (10H, m, CH_2, H**1/2,25, 28, 50, 53**), 1.08-1.12 (2H, m, CH_2 , H**1/2**)

^{19}F NMR ($CDCl_3$, 376 MHz, Fluorobenzene): δ_F −123.58- 64- −123.64 (m, $J_{H\text{-}F}$ = 12.6 Hz, 6.9 Hz, F**9**)

IR (KBr cm^{-1}): 3379.9 (O-H) 1728.2 (C=O), 1621.3 (C=O), 1260.6 (C-O), 1211.6 (C-O).

*7.2.1.19. 7-(4-(3-[(4-([2,3-bis(benzyloxy)phenyl]formamido)butyl)carbamoyl]-2-([(4-([2,3-bis(benzyloxy)phenyl]formamido)butyl)carbamoyl]methyl)-2-hydroxypropanoyl)piperazin-1-yl)-1-cyclopropyl-6-fluoro-4-oxo-1,4-dihydroquinoline-3-carboxylic acid (**2-46**)– Attempted synthesis*

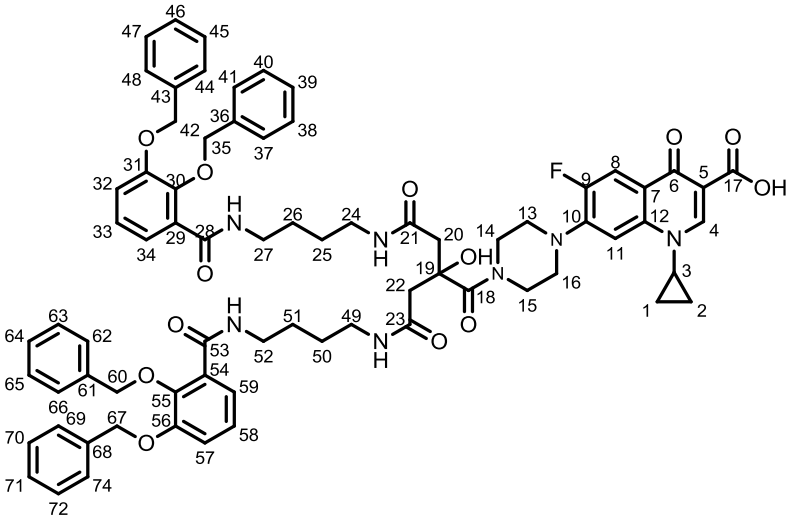

Molecular Formula: $C_{73}H_{76}FN_7O_{13}$

Molecular Weight: 1278.422 g mol^{-1}

Methyl-6-(4-[3-[(4-[[2,3-bis(benzyloxy)phenyl]formamido]butyl)carbamoyl]-2-[[(4-[[2,3-bis(benzyloxy)phenyl]formamido]butyl)carbamoyl]methyl]-2-hydroxypropanoyl]piperazin-1-yl)-4-cyclopropyl-7-fluoro-1-oxo-1,4-dihydronaphthalene-2-carboxylate (**2-45**)(0.11 g, 0.14 mmol) was dissolved in 9:1 DCM: MeOH (10 mL). NaOH (2 M in MeOH, 0.22 mL) was added and the solution left to stir.

After stirring overnight the solution was neutralised with HCl (1 mL) and the solvent removed *in vacuo*. The resultant residue was redissolved in DCM (30 mL) and washed with $NaHCO_3$ (0.05 M, 20 mL) and brine (10 mL). The organic layer was dried over $MgSO_4$ and filtered. The filtrate was concentrated *in vacuo* to yield a dark oil. Analysis of the residue indicated that the reaction was unsuccessful; as the compound appeared to have decomposed to **1-18** and **2-43**.

*7.2.1.20. Methyl 7-[4-(2-[3-[(4-[[2,3-bis(benzyloxy)phenyl]formamido]butyl)carbamoyl]-2-[[(4-[[2,3-bis(benzyloxy)phenyl]formamido]butyl)carbamoyl]methyl]-2-hydroxypropanamido]acetyl)piperazin-1-yl]-1-cyclopropyl-6-fluoro-4-oxo-1,4-dihydroquinoline-3-carboxylate (**2-51**)*

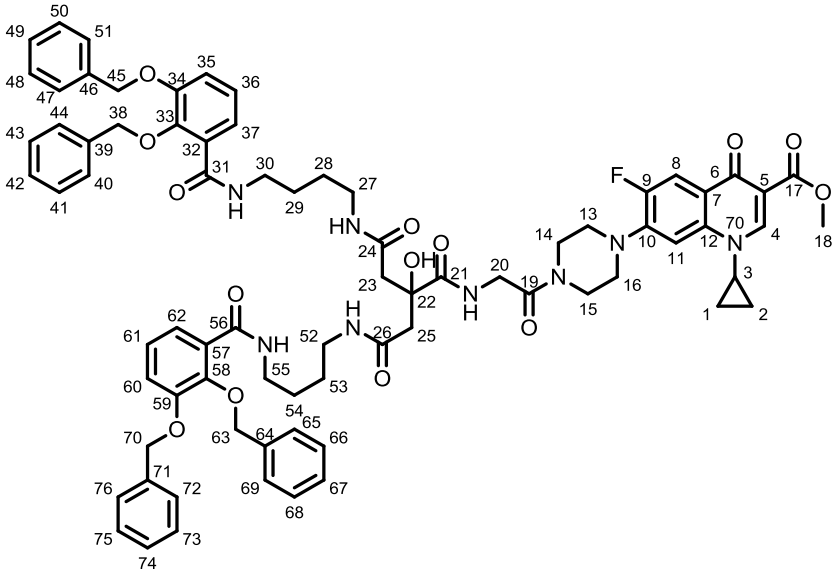

Molecular Formula: $C_{76}H_{81}FN_8O_{14}$

Molecular Weight: 1348.512 g mol^{-1}

of 3-[(4-[[2,3-bis(benzyloxy)phenyl]formamido]butyl)carbamoyl]-2-[[(4-[[2,3-bis(benzyloxy)phenyl]formamido]butyl)carbamoyl]methyl]-2-hydroxypropanoic acid **2-42** (0.19 g, 0.19 mmol) was dissolved in anhydrous DMF (20 mL). EDC·HCl (0.04 g, 2.10 mmol) and DIPEA (0.04 mL, 0.21 mmol) were added and the solution was stirred. After 15 minutes HOBt·H_2O (0.03 g, 2.20 mmol) was added. The solution was stirred for a further 15 minutes. Methyl-7-[4-(2-aminoacetyl)piperazin-1-yl]-1-cyclopropyl-6-fluoro-4-oxo-decahydroquinline-3-carboxylate hydrochloride salt **2-49 (**0.88 g, 0.2 mmol) was added followed by DIPEA (0.04 mL, 0.21 mmol). After 24 hours, the solvent was removed *in vacuo* to yield a dark oil. The oil was resuspended in H_2O and extracted with DCM (3 × 80 mL). The organic layer was washed with pyruvic acid (0.05 M, 40 mL), $NaHCO_3$ (0.05 M, 40 mL),

brine (40 mL) and H_2O (40 mL). The organic layer was dried over $MgSO_4$ and filtered. The filtrate was concentrated *in vacuo* to yield a yellow oil. The oil was purified by flash chromatography (10:1 DCM: MeOH) to give the product as a white solid

Yield: 0.12 g, 45%

R_f: (10:1, DCM: MeOH): 0.31

m/z (ESI): 1371.57 ($[M+Na]^+$, 23%), 697.28 ($[M+2Na]^{2+}$, 100%)

HRMS (ESI): Calc. for $C_{76}H_{81}FN_8NaO_{11}$= 1371.5748, found $[M+Na]^+$ 1371.5743, mean error= 0.0 ppm

^{1}H NMR ($CDCl_3$, 400 MHz): δ_H 8.54 (1H, s, CH, H**4**), 8.04 (1H, d, $^3J_{H\text{-}F}$ = 12.8 Hz, Ar C-H**8**), 7.96-8.00 (2H, m, N-H), 7.81 (1H, m, N-H) 7.63-7.66 (2H, m, Ar C-H, H**37, 62**), 7.33-7.47 (21H, m, Ar, C-H, H**11, 40-44, 47-51, 65-69, 72-76**), 7.26-7.28 (2H, m, NH) 7.09-7.13 (4H, m, Ar C-H, H**35, 36, 60, 61**) 5.13 (2H, s, CH_2, H**38/45, 63/70**), 5.07 (2H, s, CH_2, H**38/45, 63/70**), 4.06 (2H, d, $^3J_{H\text{-}H}$ = 4.2 Hz, CH_2, H**20**), 3.91 (s, 3H, CH_3, H**18**), 3.77-3.79 (2H, m, CH_2, H**14/15**), 3.56-3.58 (2H, m, CH_2, H**14/15**), 3.10-3.25 (13H, m ,CH_2, H **13, 16, 27, 30, 52, 55**, CH, H**3**), 2.75 (2H, d, CH_2 $^4J_{H\text{-}H}$ = 14.4 Hz, H**23/25**), 2.58 (2H, d, $^4J_{H\text{-}H}$ = 14.4 Hz, H**23/25**) CH_2, 1.26-1.43 (m, 10H, CH_2, H**1/2,28, 29, 53, 54**), 1.07-1.10 (2H, m, CH_2, H**1/2**)

^{19}F NMR ($CDCl_3$, 376 MHz, Fluorobenzene): δ_F −124.02-−123.94 (m, $J_{H\text{-}F}$ = 12.6 Hz, 6.9 Hz, F**9**)

IR (KBr cm^{-1}): 3386.4 (O-H), 1649.1 (C=O) 1263.8 (C-O), 1244.2 (C-O)

*7.2.1.21. 7-[4-(2-(3-[(4-([2,3-bis(benzyloxy)phenyl]formamido)butyl)carbamoyl]-2-([(4-([2,3-bis(benzyloxy)phenyl]formamido}butyl)carbamoyl]methyl)-2-hydroxypropanamido)acetyl)piperazin-1-yl]-1-cyclopropyl-6-fluoro-4-oxo-1,4-dihydroquinoline-3-carboxylic acid (**2-52**)- Attempted synthesis*

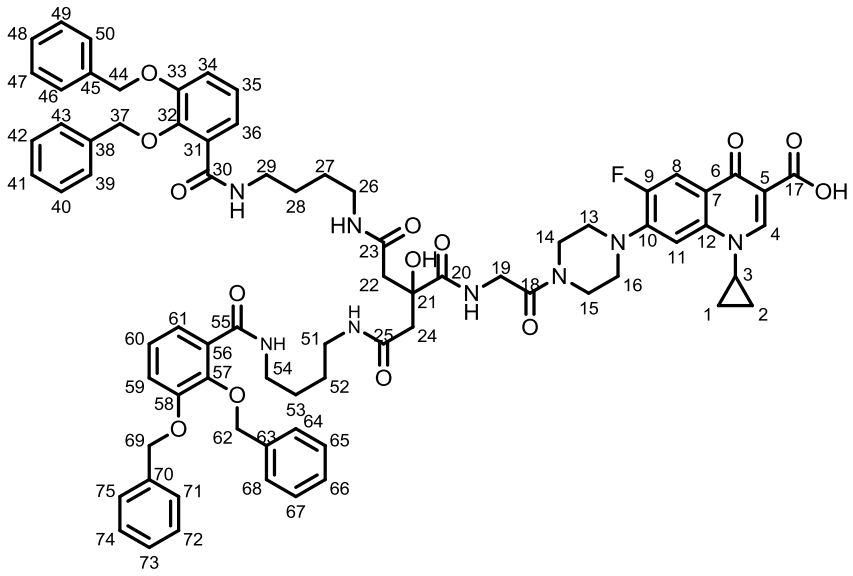

Molecular Formula: $C_{75}H_{79}FN_8O_{14}$

Molecular Weight: 1335.473g mol^{-1}

Methyl 7-[4-(2-[3-[(4-[[2,3-bis(benzyloxy)phenyl]formamido]butyl)carbamoyl]-2-[[(4-[[2,3-bis(benzyloxy)phenyl]formamido]butyl)carbamoyl]methyl]-2-hydroxypropanamido]acetyl)piperazin-1-yl]-1-cyclopropyl-6-fluoro-4-oxo-1,4-dihydroquinoline-3-carboxylate **2-51** (0.11 g, 0.14 mmol) was dissolved in 9:1 DCM: MeOH (10 mL). NaOH (2 M in MeOH, 0.22 mL) was added and the solution left to stir.

After stirring overnight the solution was adjusted to pH 5.5 using pyruvic acid (2 M). The solvent was removed *in vacuo*. The resultant residue was redissolved in DCM (20 mL) and washed with H_2O (10 mL) and brine (10 mL). The organic layer was dried over $MgSO_4$ and filtered. The filtrate was concentrated *in vacuo* to yield a dark oil. Analysis of the residue indicated

that the reaction was unsuccessful, and that the compound had decomposed to **2-49** and **2-43**.

*7.2.1.22. 3-([4-[(2,3-dihydroxyphenyl)formamido]butyl]carbamoyl)-2-[([4-[(2,3-dihydroxyphenyl)formamido]butyl]carbamoyl)methyl]-2-hydroxypropanoic acid (**2-44**)*

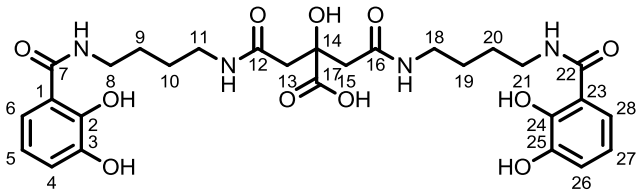

Molecular Formula: $C_{28}H_{36}N_4O_{11}$

Molecular Weight: 604.606 g mol^{-1}

3-[(4-[[2,3-Bis(benzyloxy)phenyl]formamido]butyl)carbamoyl]-2-[[(4-[[2,3-bis(benzyloxy)phenyl]formamido]butyl)carbamoyl]methyl]-2-hydroxypropanoic acid **2-42** (0.19 g, 0.20 mmol) was dissolved in 2:1 EtOH: toluene (15 mL). To the stirred solution was added a catalytic amount of palladium (10% on charcoal) was added. The flask was purged with N_2, and then placed under H_2. After 48 hours, the solution was filtered through a glass sinter to remove palladium. The solvent was removed *in vacuo* to yield the product as a yellow solid.

Yield: 0.024 g, 20%

m.p: 93.5-94.5 °C

m/z (ESI): 627.22 ($[M+Na]^+$, 45%), 605.24 ($[M+H]^+$, 100%).

HRMS (ESI): Calc. for $C_{28}H_{37}N_4O_{11}$= 605.2453 Found $[M+H]^+$ 605.2440, mean error= 1.4 ppm

^{1}H NMR (400 MHz, d_3-MeOD): δ_H 7.21 (2H, dd, $^3J_{H\text{-}H}$ = 6.4 Hz, $^4J_{H\text{-}H}$ = 1.6 Hz, Ar C-H, H**6, 28**), 6.92 (2H, dd, $^3J_{H\text{-}H}$ = 6.4 Hz , $^4J_{H\text{-}H}$ = 1.2 Hz, Ar C-H, H**4, 26**), 6.70 (2H, t, $^3J_{H\text{-}H}$ = 8 Hz. Ar C-H, H**5, 27**). 3.82 (4H, t, $^3J_{H\text{-}H}$ = 6.8 Hz, CH_2, H**8,**

21), 3.212 (4H, t, $^{3}J_{H\text{-}H}$ = 6.8 Hz, CH_2, H**11, 18**), 2.61-2.75 (m, 4H, CH_2, H**13, 15**), 1.54-1.67 (8H, m, CH_2, H**9, 10, 19, 20**).

^{13}C NMR (100 MHz, d_3-MeOD): δ_C 172.29 (C=O, C**7, 22**) , 150.96 (*ipso*-Ar, **C**-O, C**2, 3, 39, 40**), 147.98 (*ipso*-Ar **C**-C, C**1, 23**) 120.76 (Ar C-H, C**4, 6, 26, 28**), 119.15 (Ar C-H, C**5. 27**) 40.17 (CH_2, C**13, 15**), 40.02 (CH_2, C**8, 11, 18, 21**) 27.76 (CH_2, C**9, 10, 19, 20**).

IR (KBr cm^{-1}): 3356.2 (N-H), 1717.5 (C=O) 1640.32 (C=O), 1261.9 (C-O)

7.2.2. Synthesis of fluoroquinolone containing compounds using the Ugi 4CR

*7.2.2.1. Methyl-7-[4-[2([[2,3-bis(benzyloxy)phenyl]methylidene]amino)acetyl]piperazine-1-yl]-1-cyclopropyl-6-fluoro-4-oxo-1,4-dihydroquinoloine-3-carboxylate (**3-57**)*

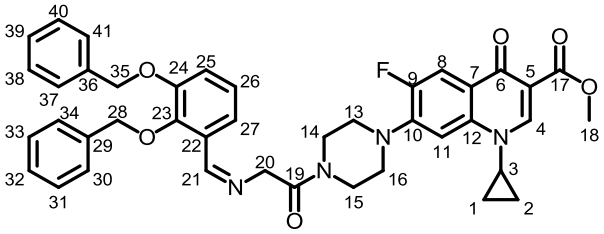

Molecular Formula: $C_{41}H_{39}N_4O_6F$

Molecular Weight: 702.770 g mol^{-1}

Methyl-7-[4-(2-aminoacetyl)piperazin-1-yl]-1-cyclopropyl-6-fluoro-4-oxo-decahydroquinline-3-carboxylate hydrochloride salt **2-49** (0.52 g, 1.18 mmol) was dissolved in anhydrous MeOH (20 mL). DIPEA (1.12 mL, 6.45 mmol) was added by syringe and the solution was stirred for 10 minutes. 2,3 bis(benzyloxy) benzaldehyde **2-25** (0.411 g, 1.29 mmol) was added. The solution was left to stir overnight. After 18 hours a white precipitate had formed. This was isolated by filtration and then dried *in vacuo* to yield the product.

Yield: 0.58 g, 71%

m.p: 177.5-180 °C

R_f: N/A, Decomposes during TLC

m/z(ESI): 725.27 ($[M+Na]^+$, 100 %), 702.29 ($[M+H]^+$, 14%).

HRMS (ESI): Calc. for $C_{41}H_{40}FN_4O_6$= 703.2926 Found $[M+H]^+$ 703.2907 mean error= 3.6 ppm. Calc. for $C_{41}H_{39}NaFN_4O_6$= 725.2746, Found $[M+Na]^+$ 725.2728 mean error= 2.6 ppm.

^{1}H NMR (400 MHz, $CDCl_3$): δ_H 8.59 (1H, s, C**H**=N, H**21**), 8.54 (1H, s, H**4**), 8.06 (1H, d, $^3J_{H\text{-}F}$ = 12.8 Hz, H**8**), 7.26 (14H, m, H), 5.15 (2H, s, CH_2 H**28/35**), 5.08 (2H, s, CH_2, H**28/35**), 4.43 (2H, s, CH_2, H**20**), 3.96-3.99 (2H, m, H**14/15**), 3.92 (3H, s, C**H**$_3$, H**18**), 3.85-3.87 (2H, m, C**H**$_2$, H**14/15**), 3.40 (1H, m, CH, H**30**), 3.30-3.32 (2H, m, CH_2, **13/16**), 3.20-3.22 (2H, m, CH_2, H**13/16**), 1.26-1.30 (2H, m, CH_2, H**1/2**), 1.14-1.11 (2H, m, CH_2, H**1/2**)

^{13}C NMR (100 MHz, $CDCl_3$): δ_C 173.10 (C=O, C**6**), 168.15 (C=O, C**19**), 166.44 (C=O, C**17**), 160.35 (C=N, C**21**), 153.43 (*ipso*-Ar, d, $^1J_{C\text{-}F}$ = 251.6 Hz, C**9**), 152.13 (*ipso*-Ar C-C, C**22**), 148.77 (*ipso*-Ar C-C, C**29/36**), 148.54 (CH, C**4**), 144.28 (*ipso*-Ar, d, $^2J_{C\text{-}F}$ = 10.7 Hz, C**10**), 138.06 (*ipso*-Ar, C**5**), 136.93-136.62 (*ipso*-Ar C-C, C**29/36**) 130.59, (*ipso*-Ar C-O, C**23/24**), 128.77-128.38 (Ar C-H, C**30, 31, 32, 33, 34, 37, 38, 39, 40, 41**), 127.61 (Ar C-H, C**26**), 124.27 (Ar C-H, C**27/25**), 123.57 (Ar C-H, C**27/25**), 123.53 (*ipso*-Ar, d, $^3J_{C\text{-}F}$ = 6.90 Hz, C**7**), 119.12 (CH, C**26**), 113.52 (CH, d, $^2J_{C\text{-}F}$ = 23.0 Hz, C-**8**), 110.21 (*ipso*-Ar, C**12**), 105.28(CH, d, $^3J_{C\text{-}F}$ = 3.1 Hz, C**11**), 76.12 (CH_2, C**28/35**), 71.11 (CH_2, C**28/35**), 64.51 (CH_2, C**20**), 52.18 (CH_3, C**18**), 50.89 (CH_2, C**14/15**), 49.57 (CH_2, C**14/15**), 46.07 (CH_2, C**13/16**), 41.76 (CH_2, C-**13/16**), 34.63 (CH, C**3**), 8.24 (CH_2, C**1/2**).

^{19}F NMR ($CDCl_3$, 376 MHz, Fluorobenzene): δ_F -123.76 (m, F**9**)

IR (KBr, cm^{-1}): 1722.0 (C=O), 1695.3 (C=O) 1650.4 (C=O), 1609.5 (C=N), 1495.1 (C-O), 1470.6 (C-O)

*7.2.2.2. Methyl-7-[4-(2-[1-[2,3-bis(benzyloxy)phenyl]-N-[[2,3-bis(benzyloxy)phenyl](cyclohexylcarbamoyl)methyl]formamido]acetyl) piperazine-1-yl]-1-cyclopropyl-6-fluoro-4-oxo-1,4-dihydroquinoline-3-carboxylate (**3-58**)*

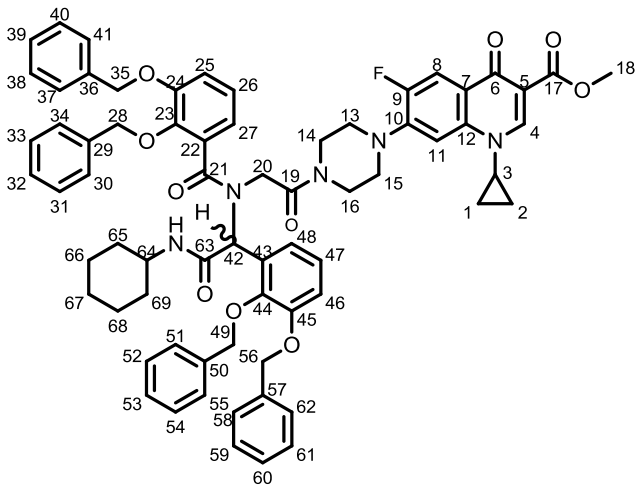

Molecular Formula: $C_{69}H_{68}N_5O_{10}F$

Molecular Weight: 1145.495 g mol^{-1}

Methyl-7-[4-[2([[2,3-bis(benzyloxy)phenyl]methylidene]amino)acetyl]piperazine-1-yl]-1-cyclopropyl-6-fluoro-4-oxo-1,4-dihydroquinoloine-3-carboxylate **3-57** (0.21 g, 0.3 mmol), 2,3-bis(benzyloxy)benzoic acid **2-26** (0.03 g, 0.3 mmol) and cyclohexyl isocyanide **3-54** (12.3 µl, 0.3 mmol), were combined in a microwave vial and suspended in anhydrous MeOH (2mL). The suspension was microwaved with stirring at 90 °C, 50 W for 60 minutes. The resultant solution was diluted with DCM, and then concentrated *in vacuo* to yield a pale yellow solid. The solid was redissolved in DCM (30 mL), and washed with HCl (1 M, 20 mL), saturated $NaHCO_3$ (20 mL) and brine (20 mL). The organic layer was dried over $MgSO_4$ and filtered. The filtrate was evaporated to dryness *in vacuo* to yield a yellow solid. The product was purified by flash chromatography in 12:1 DCM: MeOH

Yield: 0.13 g, 38%

m.p: 85.3-86.3 °C

R_f (12:1, DCM: MeOH): 0.23

m/z (ESI): 1168.5 ($[M+Na]^+$, 16%)1146.5, ($[M+H]^+$, 100%).

HRMS (ESI): Calc. for $C_{69}H_{69}N_5O_{10}F$= 1146.5023 Found $[M+H]^+$ 1146.5007, mean error= 1.7 ppm.

^{1} H NMR (d_6-DMSO, 500 MHz, 383 K): δ_H 8.40 (1H, s, H**4**), 7.78 (1H, d, $^3J_{H-F}$ = 10.8 Hz, H**8**), 6.80-7.46 (26H, m, Ar, C-H, H**25, 26, 27, 30-34, 37-41, 46, 47, 48, 51-55, 58-62**), .5.91 (1H, s, CH, H**42**), 5.01-5.16 (8H, m, CH_2, H**28, 35, 49, 56**), 4.05-4.09 (2H, m, CH_2, H**20**), 3.77 (3H, s, CH_3, H**18**), 3.57-3.66 (3H, m, CH_2 and CH, H**13/15, 64**), 3.29-3.33 (3H, m, CH_2 and CH, H**3, 13/15**), 2.89-3.01 (4H, m, CH_2, H**14, 16**), 1.54-1.79 (4H, m, CH_2, H**65, 69**), 1.19-1.31 (8H, m, CH_2 H**1/2, 66, 67, 68**), 1.05-1.10 (2H, m, CH_2, H**1/2**).

^{19}F NMR (376 MHz, d_6-DMSO): δ_F-124.58 (m, F**9**)

IR (KBr, cm^{-1}): 3433.0 (N-H), 1728.9 (C=O), 1621.7 (C=O), 1263.9 (C-O), 1229.5 (C-O)

*7.2.2.3. 6-[4-(2-[1-[2,3-bis(benzyloxy)phenyl]-N-[[2,3-bis(benzyloxy)phenyl](cyclohexylcarbamoyl)methyl]formamido]acetyl)piperazin-1-yl]-4-cyclopropyl-7-fluoro-1-oxo-1,4-dihydronaphthalene-2-carboxylic acid (**3-59**)[164]*

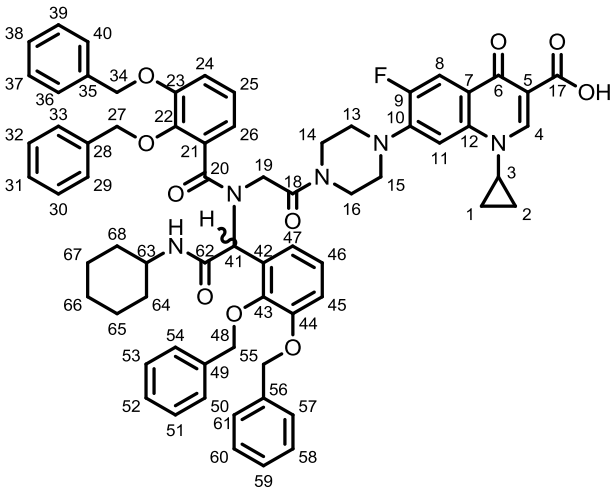

Molecular formula: $C_{68}H_{66}N_5O_{10}F$

Molecular weight: 1132.278 g mol^{-1}

To a stirred solution of methyl-7-[4-(2-[1-[3,4-bis(benzyloxy)phenyl]-N-[[3,4-bis(benzyloxy)phenyl](cyclohexylcarbamoyl)methyl]formamido]acetyl)piperazine-1-yl]-1-cyclopropyl-6-fluoro-4-oxo-1,4-dihydroquinoline-3-carboxylate **3-56** (0.20 g, 0.175 mmol) in 9:1 DCM: MeOH (4.5 mL) was added NaOH (2 M in MeOH, 0.5 mL). After four hours the solvent was removed *in vacuo*. The residue was redissolved in DCM (20 mL) and washed with HCl (0.1 M, 10 mL) and brine (10 mL). The organic layer was dried over $MgSO_4$ and filtered. The filtrate was evaporated to dryness *in vacuo* to yield the crude product. The crude product was purified using flash chromatography in 9:1:0.1 $CHCl_3$: MeOH: HCOOH and recovered as a white solid.

Yield: 0.12 g, 58%

m.p: 110.4-11.3 °C

R_f: (9:1:0.1, $CHCl_3$: MeOH: HCOOH): 0.54

m/z (ESI): 1154.46 ($[M+Na]^+$, 10%), 1132.48 ($[M+H]^+$, 100%).

HRMS (ESI): Calc. for $C_{68}H_{67}N_5O_{10}F$= 1132.4866 Found 1132.4846, mean error= 2.4 ppm. Calc. for $C_{68}H_{66}NaN_5O_{10}F$= 1154.4686 Found 1154.4670, mean error= 0.2 ppm.

^{1} H NMR (400 MHz, d_6-DMSO 353 K): δ_H 8.42 (1H, s, H**4**), 7.75 (1H, d, $^3J_{H-H}$ = 10.8 Hz, H**8**), 7.08-7.49 (26H, m, Ar, C-H, H**24, 25, 26, 29-33, 36-40, 45, 46, 47, 50-54, 57-61**), .5.91 (1H, s, CH, H**41**), 4.96-5.18 (8H, m, CH_2, H**27, 34, 48, 55**), 4.07-4.10 (2H, m, CH_2, H**19**), 3.58-3.65 (3H, m, CH_2 and CH, H**13/15, 63**), 3.30-3.34 (3H, m, CH_2 and CH, H**3, 13/15**), 3.08-3.18 (4H, m, CH_2, H**14, 16**), 1.60-1.84 (4H, m, CH_2, H**64, 68**), 1.25-1.30 (8H, m, CH_2 H**1/2, 65, 66, 67**), 0.99-1.01 (2H, m, CH_2, H**1/2**).

^{19}F NMR (376 MHz, d_6-DMSO): δ_F-123.69 (m, F**9**)

IR (KBr, cm^{-1}): 3432.9 (N-H), 1728.9 (C=O), 1621.7 (C=O)

7.2.2.4. 7-[4-(2-[N-[(cyclohexylcarbamoyl)(2,3-dihydroxyphenyl)methyl]-1-(2,3-dihydroxyphenyl)formamido]acetyl)piperazin-1-yl]-1-cyclopropyl-6-fluoro-4-oxo-1,4-dihydroquinoline-3-carboxylic acid ***3-1***

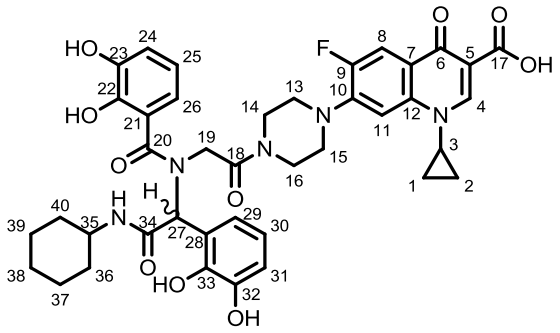

Molecular formula: $C_{40}H_{42}FN_5O_{10}$
Molecular weight: 771.787 g mol^{-1}

6-[4-(2-[1-[2,3-Bis(benzyloxy)phenyl]-N-[[2,3-bis(benzyloxy)phenyl](cyclohexylcarbamoyl)methyl]formamido]acetyl)piperazin-1-yl]-4-cyclopropyl-7-fluoro-1-oxo-1,4-dihydronaphthalene-2-carboxylic acid **3-58** (0.01 g, 0.1 mmol was

dissolved in 1:1 EtOH: Toluene (50 mL). To the stirred solution was added a catalytic amount of Pd black. The solution was stirred under H_2 at 50 bar. After 48 hours, the solution was filtered through a glass filter to remove the catalyst and the solvent removed *in vacuo* to yield the product as a yellow solid.

Yield: 0.08 g, 100%

m.p: 123.5-124.4

m/z (ESI): 794.28 ($[M+Na]^+$, 100%).

HRMS (ESI): Calc. for $C_{40}H_{43}N_5O_{10}F$= 772.2988 Found 772.3005, mean error= -1.5 ppm. Calc. for $C_{40}H_{42}NaN_5O_{10}F$= 794.2808 Found 794.2819, mean error= -1.3 ppm.

^{1} H NMR (500 MHz, d_6-DMSO): δ_H 8.82 (1H, s, Ar, C-H, H**4**), 7.93 (1H, m, Ar, C-H, H**26**), 7.64 (1H, m, Ar, C-H, H**24**), 6.51-6.77 (6H, m, Ar, C-H, H**8, 11, 25, 29, 30, 31**), 5.82 (s, 1H, CH, H**27**), 4.20-4.22 (2H, m, CH_2, H**19**), 3.85 (1H, m, CH, H**35**), 3.37-3.44 (4H, m, CH_2, H**13, 15**), 3.08-3.16 (2H, m, CH_2, H**13/16**), 2.84-2.92 (2H, m, CH_2, H**13/16**), 2.74 (1H, m, CH, H**3**), 1.18-1.37(14H, m, CH_2, H**1, 2, 36-40**)

^{13}C NMR: Compound not sufficiently soluble to obtain a ^{13}C NMR spectrum

^{19}F NMR (376 MHz, d_6-DMSO): δ_F -121.99 (m, F**9**)

IR (KBr, cm^{-1}): 3432.9 (N-H) 1729.0(C=O), 1628.7 (C=O), 1247.5 (C-O)

*7.2.2.5. 3,4-bis(benzyloxy)benzaldehyde (**3-65**)[138]*

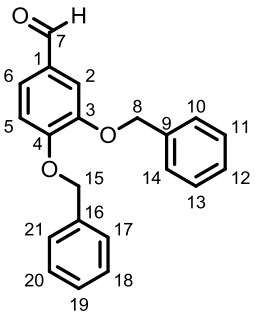

Molecular Formula: $C_{21}H_{18}N_2O_3$
Molecular Weight: 318.366 g mol^{-1}

3,4-Dihydroxybenzaldehyde **2-7** (0.55 g, 4 mmol) was dissolved in anhydrous EtOH (10 mL). To the stirred solution was added benzyl chloride (1.05 mL, 9.2 mmol). To the resultant yellow solution was added $K_2CO_{3(s)}$ (0.72 g, 5.2 mmol). The mixture was then heated under reflux. After 24 hours the solution was cooled to room temperature and filtered. The solid recovered was washed with acetone and any insoluble material discarded. The acetone washes were added to the filtrate which was then concentrated *in vacuo* to yield the crude product. The crude product was recrystallised from a minimal amount of hot MeOH to yield the product as a brown crystalline solid.

Yield: 0.79 g, 62%

m.p: 84.4-85.2 °C

R_f: (3:1, EtOAc: Pet Ether): 0.62

m/z (ESI): 341.11 ($[M+Na]^+$, 57%), 336.16 ($[M+NH_4]^+$, 42%), 319.13 ($[M+H]^+$, 100%).

HRMS (ESI): Calc. for $C_{21}H_{19}O_3$= 319.1329. Found $[M+H]^+$ 319.1331, mean error= -1.1 ppm. Calc. for $C_{21}H_{18}NaO_3$= 341.1148. Found $[M+Na]^+$ 319.1149 , mean error= -0.5 ppm.

^{1}H NMR (400 MHz, $CDCl_3$): δ_H 9.81 (1H, s, CHO, H**7**), 7.31-7.49 (12H, m, Ar, C-H, H**2, 6, 10-14, 17-21**), 7.02 (1H, d, $^{3}J_{H-H}$ = 8.2 Hz, Ar C-H, H**5**), 5.26 (2H, s, CH_2, H**8/15**), 5.21 (2H, s, CH_2, H**8/15**).

^{13}C NMR (100 MHz, d_6-DMSO): δ_C 191.33 (C=O, C**7**) 153.59 (*ipso*-Ar, C-O, C**4**), 148.44 (*ipso*-Ar, C-O, C**3**), 136.84 (*ipso*-Ar, C-C, C**9/16**), 136.50 (*ipso*-Ar, C-C, C**9/16**), 128.57 (Ar. C-H, Benzyl group, C**10-14, 17-21**), 126.24 (Ar, C-H, C**5**), 113.26 (Ar, C-H, C-**2/6**), 111.97 (Ar, C-H, C-**2/6**) 75.40 (CH_2, C-**8/15**), 70.52 (CH_2, C-**8/15**)

IR (KBr, cm^{-1}): 1676.1 (C=O), 1270.6 (C-O), 1264.1 (C-O)

*7.2.2.6. 3,4-bis(benzyloxy)benzoic acid(**3-66**)[153]*

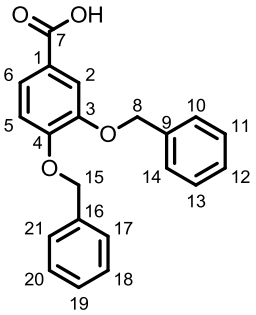

Molecular Formula: $C_{21}H_{18}O_4$
Molecular Weight: 334.365 g mol^{-1}

3, 4-Bis(benzyloxy)benzaldehyde **3-64** (0.30 g, 9.4 mmol) was dissolved in 10 mL 1:1 acetone: H_2O (10 mL). Sulfamic acid (0.13 g, 1.32 mmol) was dissolved in H_2O (4 mL) and sodium chlorite (0.11 g, 1.24 mmol) was dissolved in H_2O (4 mL). These two solutions were added to the benzaldehyde solution in alternating portions over 15 minutes. After two hours stirring the volume of solvent was reduced *in vacuo* by 50%. The resultant white precipitate was isolated by filtration and retained as the product.

Yield: 0.26 g, 84%

m.p: 180.2-181.0 °C

R_f: 0.24 (3:1, EtOAc: Pet Ether)

m/z (ESI): 357.11 ($[M+Na]^+$, 100%), 335.13 ($[M+H]^+$, 52%).

HRMS (ESI): Calc. for $C_{21}H_{19}O_4$= 335.1278. Found $[M+H]^+$ 535.1271, mean error= 1.8ppm. Calc. for $C_{21}H_{18}NaO_4$= 357.1097. Found $[M+Na]^+$ 357.1082, mean error= 3.9 ppm

^{1}H NMR (400 MHz, d_6-DMSO) δ_H 12.21 (br s, 1H, COOH, H**7**), 7.27-7.55 (12H, m, Ar, C-H, H**2, 6, 10-14, 17-21**), 7.15 (1H, d, $^3J_{H-H}$ = 9.2 Hz, Ar, C-H, H**5**), 5.22 (2H, s, CH_2, H**8/15**), 5.18 (2H, s, CH_2, H**8/15**).

^{13}C NMR (100 MHz, d_6-DMSO): δ_C 166.99 (C=O, C**7**), 152.12 (*ipso*-Ar, C-O, C**4**), 147.65 (*ipso*-Ar, C-O, C**3**), 137.06 (*ipso*-Ar, C-C, C**9/16**), 136.75 (*ipso*-Ar, C-C, C**9/16**), 127.99 (Ar C-H, C**10-14, 17-21**), 127.74 (*ipso*-Ar C-C, C**1** 123.52 (Ar C-H, C**6**), 123.30, (Ar C-H, C**2**) 114.61 (Ar C-H, C**5**) 70.03 (CH_2, C**8/15**), 69.90 (CH_2, C**8/15**)

IR (KBR, cm^{-1}) 3440.2 (OH), 1679.3 (C=O), 1275.5 (C-O) 1225.7 (C-O),

*7.2.2.7. Methyl 5-aminopentanoate hydrochloride salt (**3-72**)[201]*

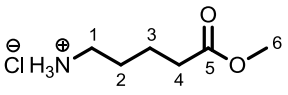

Molecular Formula: $C_6H_{13}NO_2$
Molecular Weight: 131.173 g mol^{-1}

5-Aminopentanoic acid **3-71** (2.00 g, 17 mmol) was dissolved in anhydrous MeOH (10 mL). The suspension was cooled to approximately 0 °C in an ice bath. Distilled thionyl chloride (3.7 mL, 51 mmol) was added by syringe. The solution was then stirred under reflux.

After 18 hours the reaction was cooled to room temperature and the excess solvent removed *in vacuo*. The resultant residue was resuspended in MeOH

and precipitated using Et_2O. The resultant white precipitate was filtered and the process repeated. The final product was isolated by filtration as a white solid.

Yield: 2.21 g, 99 %

m.p: 135-136.2 °C (lit 122-123 °C [201])

m/z (ESI): 132.10 ($[M+H]^+$, 100%).

HRMS (ESI): Calc. for $C_6H_{14}NO_2$= 132.1019. Found $[M+H]^+$ 132.1019, mean error= 0.0[ppm].

^{1}H NMR (400 MHz, MeOH-d3): δ_H 3.67 (3H, s, CH_3, H**6**), 2.92-2.96 (2H, m, CH_2, H**5**), 2.39-2.43 (2H, m, CH_2, H**2**), 1.68-1.72 (4H, m, CH_2, H**3/ 4**).

^{13}C NMR (100 MHz, MeOH-d3): δ_C 175.27 (C=O, C**5**), 52.13 (CH_3, C**6**), 40.40 (CH_2, C**1**), 33.92 (CH_2, C**2**), 27.91 (CH_2, **C3/4**), 22.70 (CH_2CH_2, **C3/4**)

IR (KBR, cm^{-1}): 3460.6 (N-H), 1736.7 (C=O), 1197.0 (C-O)

Methyl-5-[[2,3-bis(benzyloxy)phenyl]formamido]pentanoate(**3-74**)

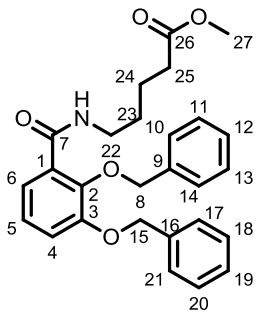

Molecular Formula: $C_{27}H_{29}NO_5$

Molecular Weight: 447.205 g mol^{-1}

2,3-Bis(benzyloxy) benzoic acid **2-26 (**2.00 g, 5.9 mmol), methyl-5-aminopentanoate hydrochloride salt **3-72** (1.00 g, 5.9 mmol) and HOBt·H_2O (0.81 g, 5.9 mmol) were dissolved in anhydrous DMF (15 mL). DIPEA (1.04 mL, 5.9 mmol) was added and the solution was stirred. After 30 minutes

stirring EDC.HCl (1.15 g, 5.9 mmol) was added to the solution followed by a further portion of DIPEA (1.04 mL, 5.9 mmol). The solution was left to stir.

After 24 hours the solvent was removed *in vacuo* to yield an orange solid. The residue was resuspended in H_2O (40 mL) and extracted with DCM (3 × 60 mL). The organic layer was then washed with H_2O, CH_3SO_3H (0.05 M), $NaHCO_3$ (0.05 M), brine and H_2O (all 50 mL). The organic layer was dried over $MgSO_4$ and filtered. The solvent was removed *in vacuo* to yield the product as a white solid

Yield: 2.19 g, 83%

m.p: 63.2-63.6 °C

R_f: (1:1, EtOAc: Pet ether): 0.33

m/z (ESI): 470.19 ($[M+Na]^+$, 100%), 448.21 ($[M+H]^+$, 18%).

HRMS (ESI): Calc. for $C_{27}H_{30}NO_5$= 448.2118. Found $[M+H]^+$ 448.2113, mean error= 1.2 ppm. Calc. for $C_{27}H_{29}NaNO_5$= 470.1938 Found $[M+Na]^+$ 470.1934, mean error= 1.0 ppm.

^{1}H NMR: (400 MHz, $CDCl_3$): δ_H 7.97 (1H, t, $^3J_{H\text{-}H}$ = 5.2 Hz, **H**), 7.75 (1H, m, H**6**) 7.33-7.49 (10H, m, Ar C-H, H**10-14, 17-21**), 7.15-7.16 (2H, m, Ar, C-H, H**4/5**), 5.16 (2H, s, CH_2, H**8/15**), 5.09 (2H, s, CH_2, H**8/15**), 3.65 (3H, s, CH_3, H**28**), 3.26-3.10 (2H, m, CH_2, H**22**) 2.25 (2H, t, $^3J_{H\text{-}H}$ = 7.3 Hz, CH_2, H**25**), 1.55 (2H, qn, $^3J_{H\text{-}H}$, 7.6 Hz, CH_2, H**24**), 1.37 (2H, qn, $^3J_{H\text{-}H}$ = 7.6 Hz, CH_2, H**23**).

^{13}C NMR: (100 MHz, $CDCl_3$) δ_C 174.20 (C=O, C**26**), 165.46 (C=O, C**7**), 152.08 (*ipso* Ar C-O, C**3**), 146.87 (*ipso* Ar, C-O, C**2**), 136.64 (*ipso* Ar, C-C, C**9, 16**), 128.34 (Ar C-H, C**10-14, 17-21**), 127.75 (*ipso*-Ar C-C, C**1**), 124.57 (Ar C-H, C**4**), 123.54 (Ar C-H, C**6**), 117.03 (Ar, C-H, **C**5), 76.12 (CH_2, C**8/15**), 71.16 (CH_2, C**8/15**), 51.30 (CH_3, C**27**), 38.93 (CH_2, C**22**), 33.26 (CH_2, C**25**) 28.39 (CH_2, C**23**), 21.92 (CH_2, H**24**).

IR (KBr, cm^{-1}): 3385.7(N-H), 1729.2 (C=O), 1654.8 (C=O), 1213.2 (C-O)

*7.2.2.8. 5-[(2,3-dihydroxyphenyl)formamido]pentanoic acid (**3-76**)*

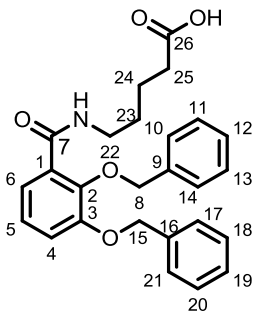

Molecular Formula: $C_{26}H_{27}NO_5$

Molecular Weight: 433.189 g mol^{-1}

Methyl-5-[[2,3-bis(benzyloxy)phenyl]formamido]pentanoate **3-74** (0.45 g, 1 mmol) was dissolved in9:1 DCM: MeOH (13.5 mL). NaOH (2 M in MeOH, 1.5 mL) was added and the solution was left to stir. After 18 hours the solvent was removed *in vacuo* to yield a dark oil.

The residue was dissolved in EtOAc (25 mL) and washed with HCl (1 M, 20 mL). The organic layer was separated and the aqueous layer washed with EtOAc (3 × 10 mL). The organic layers were combined and washed with brine (20 mL). The organic layer was dried over $MgSO_4$ and filtered. The filtrate was concentrated *in vacuo* to yield a pale oil. The product was purified using flash chromatography in 5:1:0.5 EtOAc: Pet ether (40-60): HCOOH.

Yield: 0.29 g, 68%

m.p: 70.3-71.0 °C

R_f (5:1:0.1, EtOAc: 40-60 pet ether: HCOOH): 0.43

***m/z* (ESI)**: 456.18 ($[M+Na]^+$, 100%), 434.19. ($[M+H]^+$, 96%).

HRMS (ESI): Calc. for $C_{26}H_{28}NO_5$= 434.1962. Found $[M+H]^+$ 434.1976, mean error= -2.7 ppm. Calc. for $C_{26}H_{27}NaNO_5$= 456.1781. Found $[M+Na]^+$ 456.1800, mean error= -3.2 ppm.

^{1}H NMR: (400 MHz, $CDCl_3$) δ_H 8.04 (1H, m, **H**), 7.74 (1H, m, H**6**) 7.34-7.49 (10H, m, Ar, C-H, H**10-14, 17-21**), 7.15-7.16 (2H, m, Ar, C-H, H**5**), 5.08 (2H, s, CH_2, H**8/15**), 5.12 (2H, s, CH_2, H**8/15**), 3.25-3.30 (2H, m, H**22**) 2.27-2.30 (2H, m, CH_2, H**25**), 1.51-1.58 (2H, m, CH_2, H**24**), 1.33-1.41 (2H, m, CH_2, H**23**).

^{13}C NMR: (100 MHz, $CDCl_3$) δ_C 174.18 (C=O, C**26**), 165.15 (C=O, C**7**), 151.82 (*ipso* Ar, C-O, C**3**), 146.87 (*ipso* Ar, C-O, C**2**), 136.53 (*ipso* Ar, C-C, **C9, 16**), 129.0 (*ipso*-Ar, C-C, C**1**), 128.34 (Ar, C-H, C**10-14, 17-21**), 124.57(Ar, C-H, **6**), 123.54 (Ar, C-H, C**4**), 116.95 (Ar, C-H, C**5**), 76.50 (CH_2, C**8/15**), 71.39 (CH_2, C**8/15**), 38.92 (CH_2, C**22**) 33.25 (CH_2, C**25**) 28.40 (CH_2, C**23**) 21.93 (CH_2, C**24**).

IR (KBr, cm^{-1}): 3385.7 (N-H) 1715.3 (C=O), 1237.4 (C-O)

*7.2.2.9. Methyl 6-[[2,3-bis(benzyloxy)phenyl]formamido]hexanoate(**3-75**)*

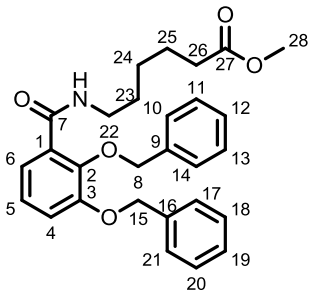

Molecular Formula: $C_{28}H_{31}NO_5$
Molecular Weight: 461.549 g mol^{-1}

2,3-Bis(benzyloxy)benzaldehyde **2-26** (0.33 g, 1 mmol), methyl-6-aminohexanoate hydrochloride **3-73** (0.18 g, 1 mmol) and HOBt·H_2O (0.17 g, 1 mmol) were dissolved in anhydrous DMF (50 mL). DIPEA (0.17 mL, 1 mmole) was added by syringe, followed by EDC·HCl (0.19 g, 1 mmol). The solution was left to stir.

After 36 hours the excess solvent was removed *in vacuo* leaving a yellow oil. This was resuspended in H_2O (40 mL) and extracted with DCM (2 × 50 mL).

The organic layer was then washed with H_2O (50 mL), CH_3SO_3H (0.05M, 50 mL), $NaHCO_3$ (0.05 M, 50 mL), brine (50 mL) and H_2O (50 mL). The organic layer was dried over $MgSO_4$ and filtered. The organic layer was then dried *in vacuo* to yield the product as colourless oil.

Yield: 0.43 g, 92%

R_f: (5:1, EtOAc: Pet ether (40-60)): 0.65

***m/z* (ESI)**: 484.21 ($[M+Na]^+$, 100%), 462.23 ($[M+H]^+$, 96%).

HRMS (ESI): Calc. for $C_{28}H_{32}NO_5$= 462.2275. Found $[M+H]^+$ 462.2268, mean error= 1.5 ppm. Calc. for $C_{28}H_{31}NaNO_5$= 484.2094. Found $[M+Na]^+$ 484.2092, mean error= 0.5 ppm.

^{1}H NMR: (400 MHz, $CDCl_3$) δ_H 7.95 (1H, m, **H**), 7.75(1H, m, H**6**) 7.24-7.40 (10H, m, Ar, C-H, H**10-14, 17-21**), 7.15-7.16 (2H, m, Ar, C-H, H**5, 6**), 5.16 (2H, s, CH_2, H**8/15**), 5.08 (2H, s, CH_2, H**8/15**), 3.66 (3H, s, CH_3, H**28**), 3.25-3.30 (2H, m, H**22**) 2.23 (2H, t, $^3J_{H-H}$ = 7.6 Hz , H**26**), 1.55 (2H, qn, $^3J_{H-H}$ = 7.6 Hz, CH_2, H**24**), 1.31-1.38 (2H, m, H**23**), 1.21-1.27 (2H, m, H**25**).

^{13}C NMR: (100 MHz, $CDCl_3$) δ_C 174.50 (C=O, C**27**) 165.42 (C=O, **C**OOH, C**7**), 152.05 (*ipso* Ar C-O, C**3**), 147.075 (*ipso* Ar, C-O, C**2**), 136.679 (*ipso* Ar, C-C, **C9, 16**), 128.977-127.91 (Ar, C-H, C**10-14, 17-21**), 124.57(Ar, C-H, C**5**), 123.54 (Ar, C-H, C**6**), 116.95 (Ar, C-H, C**4**), 76.50 (CH_2, C**8/15**), 71.39 (CH_2, C**8/15**), 51.62 (CH_3, C**28**), 39.22 (CH_2, C**22**), 33.59 (CH_2, C**26**), 28.64 (CH_2, C**25**), 26.20 (CH_2, C**23**) 24.25 (CH_2, C**24**).

IR ($CHCl_3$, 0.1 M, cm^{-1}): 3370.7 (N-H), 1738.4 (C=O), 1651.7(C=O), 1238.4 (C-O)

Spectroscopic data is consistent with literature values [262].

*7.2.2.10. 6-[(2,3-dihydroxyphenyl)formamido]hexanoic acid(**3-77**)*

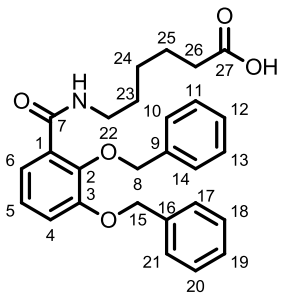

Molecular formula: $C_{27}H_{29}NO_5$

Molecular weight: 447.523 g mol^{-1}

Methyl 6-[[2,3-bis(benzyloxy)phenyl]formamido]hexanoate **3-75** (0.24 g, 05.2 mmol) was dissolved in 9:1 DCM: MeOH (10 mL). NaOH (2 M in MeOH, 0.75 mL) was added and the solution was left to stir. After 18 hours the solvent was removed *in vacuo* to yield a dark oil.

The residue was dissolved in EtOAc (30 mL) and washed with HCl (1 M, 20 mL). The organic layer was separated and the aqueous layer washed with EtOAc (2 × 20 mL). The organic layers were combined and washed with brine (20 mL). The organic layer was dried over $MgSO_4$ and filtered. The filtrate was concentrated *in vacuo* to yield a white solid

Yield: 0.17 g, 72 %

m.p: 71.4-72.4 °C (Lit: 74-76 °C [262])

m/z (ESI): 470.19 ($[M+Na]^+$, 100%), 448.21 ($[M+H]^+$, 21%).

HRMS (ESI): Calc. for $C_{27}H_{30}NO_5$= 448.2118. Found $[M+H]^+$ 448.2111, mean error= 1.8 ppm. Calc. for $C_{27}H_{29}NaNO_5$= 470.1938. Found $[M+Na]^+$ 470.1944, mean error= -0.3 ppm.

^{1}H NMR (400 MHz, $CDCl_3$): δ_H 8.01 (1H, t, $^3J_{H\text{-}H}$ = 5.2 Hz **H**), 7.74 (1H, m, H**6**) 7.36-7.49 (10H, m, Ar C-H, H**, 10-14, 17-21**), 7.15-7.17 (2H, m, Ar C-H, H**4, 5**), 5.16 (2H, s, CH_2, H**8/15**), 5.09 (2H, s, C**H**$_2$$C_6H_5$, H**8/15**), 3.26-3.30

(2H, m, CH_2, H**22**) 2.27 (2H, t, $^3J_{H-H}$=7.6 Hz , H**26**), 1.56 (2H, qn, $^3J_{H-H}$, 7.6 Hz, CH_2, H**24**), 1.31-1.38 (2H, m, H**23**), 1.21-1.28 (2H, m, H**25**)

^{13}C NMR (100 MHz, $CDCl_3$): δ_C 179.31 (C=O, C**27**), 165.58 (C=O, C**7**), 152.01 (*ipso*-Ar, C-O, C**3**), 147.08 (*ipso*-Ar C-O, C**2**), 136.65 (*ipso*-Ar C-C, C**9, 16**), 128.95- 127.88 (Ar C-H, C**10-14, 17-21**) 127.37 (*ipso*-Ar C-C, C**1**), 124.66 (Ar C-H, C**5**), 123.522 (Ar C-H, C**6**), 117.07 (Ar C-H, C**4**). 76.33 (CH_2, C**8/15**), 71.17 (CH_2, C**8/15**), 39.26 (CH_2, C**22**) 33.51 (CH_2, C**26**), 28.55 (CH_2, C**25**), 26.10 (CH_2, C**23**), 23.98 (CH_2, C**24**)

IR (KBr, cm^{-1}): 3340.7 (N-H), 1732.7 (C=O), 1616.5 (C=O), 1236.7 (C-O)

Spectroscopic data is consistent with literature values [262].

*7.2.2.11. 5-[4-[1-cyclopropyl-6-fluoro-3-(methoxycarbonyl)-4-oxo-1,4-dihydroquinolin-7-yl]piperazine-1-yl]5oxopentanoic acid (**3-78**)*

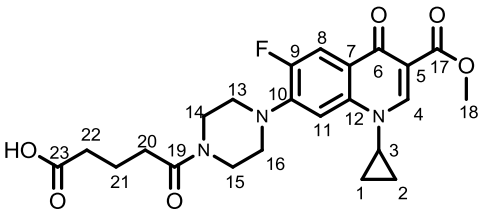

Molecular Formula: $C_{23}H_{26}FN_3O_6$

Molecular Weight: 459.468 g mol^{-1}

Methyl-1-cyclopropyl-6-fluoro-4-oxo-7-(piperazin-1-yl)-1,4-dihydroquinoline-3-carboxylate **2-20** (1.00 g, 2.9 mmol) was dissolved in $CHCl_3$ (30 mL). Glutaric anhydride **3-80** (0.37 g, 3.2 mmol) was added. The flask was purged with N_2 and the solution left to stir under N_2 overnight.

After 18 hours stirring a white precipitate was observed. The precipitate was isolated by filtration with suction. The isolated solid was then further dried *in vacuo* yielding the product as a white crystalline solid

Yield: 1.32 g, 99%

m.p: 220-221 °C

R_f (9:1:1, $CHCl_3$: MeOH: HCOOH): 0.23

m/z (ESI): 482.17 ($[M+Na]^+$, 8%), 460.18 ($[M+H]^+$, 100%).

HRMS (ESI): Calc. for $C_{23}H_{26}N_2FO_5$= 460.1878. Found $[M+H]^+$ 460.1872, mean error= 1.6 ppm. Calc. for $C_{23}H_{25}NaN_2FO_5$= 482.1698, found $[M+H]^+$ 482.1698, mean error= -0.4 ppm.

^{1}H NMR (400 MHz, d_6-DMSO): δ_H 8.42 (1H, s, H**4**), 7.73 (1H, d, $^3J_{H-F}$ = 13.4 Hz, H**8**), 7.43 (1H, d, $^4J_{H-F}$ = 7.3 Hz, H**11**), 3.72 (3H, s, CH_3, H**18**), 3.65 (5H, m, CH_2, H**14/15** & CH, H**3**), 3.19-3.24 (4H, m, CH_2, H**13/16**), 2.39 (2H, t, $^3J_{H-H}$ = 7.3 Hz, CH_2, H**22**), 2.27 (2H, t, $^3J_{H-H}$ = 7.3 Hz, CH_2, H**20**), 1.68-1.77 (2H, m, CH_2, H**21**), 1.22-1.27 (2H, m, CH_2 H**1/2**), 1.08-1.10 (2H, m, CH_2, H**1/2**)

^{13}C NMR (100 MHz, d_6-DMSO): δ_C 174.39 (C=O, C**23**), 171.59 (C=O, C**6**), 170.37 (C=O, C**19**), 164.98 (C=O, C**17**), 152.6 (*ipso*-Ar, $^1J_{H-F}$ =245.8 Hz, C**9**), 148.39 (C-H, C**4**), 143.67 (*ipso*-Ar, d, $^2J_{C-F}$ = 10.6 Hz, **C9**), 138.04 (*ipso*-Ar, C**12**), 122.1(*ipso*-Ar, d, $^3J_{C-F}$ = 6.90 Hz, C**7**), 111.58 (C-H, d, $^2J_{C-F}$ = 22 Hz, C**8**), 108.95 (*ipso*-Ar, C**5**), 106.67(C-H, C**11**), 51.34 (CH_3, C**18**), 49.69 (CH_2, C**16/13**), 44.70 (CH_2, C**14/15**), 40.74 (CH_2, C**14/15**), 34.83 (CH, C**3**), 33.04 (CH_2, C**20**), 31.48 (CH_2, C**22**), 20.28 (CH_2, C**21**), 7.60 (CH_2, C**1,** C**2**).

^{19}F NMR (376 MHz, $CDCl_3$) δ_F -124.43 (m, F-**9**)

IR (KBR, cm^{-1}): 3512.7 (C-O), 1716.3 (C=O), 1627.1 (C=O)

*7.2.2.12. 2,3-Bis(benzyloxy)-N-[4-([[2,3bis(benzyloxy)phenyl]methylidene]amino)butyl]benzamide (**3-81**)*

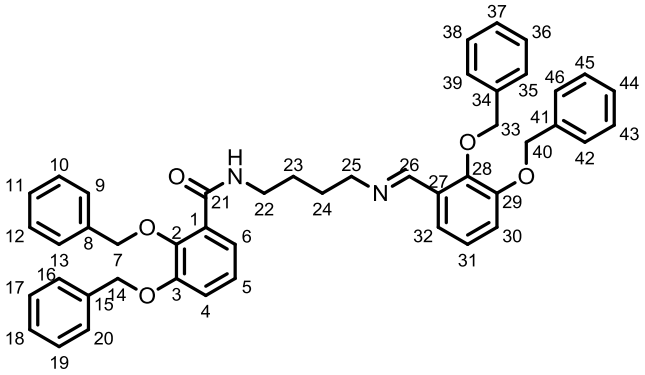

Molecular Formula: $C_{46}H_{44}N_2O_5$

Molecular Weight: 704.325 g mol^{-1}

N-(4-aminobutyl)-2,3-bis(benzyloxy)benzamide hydrochloride **2-40** (0.50 g, 1.10 mmol) and 2,3-bis(benzyloxy) benzaldehyde **2-25** (0.35 g, 1.1 mmol) was suspended in anhydrous EtOH (25 ml). DIPEA (0.38 mL, 2.20 mmol) was added by syringe. The reaction was left to stir for 18 hours. After 18 hours a white precipitate had formed. This was isolated by filtration and retained as the product.

Yield: 0.65g, 84%

m.p:111.4-112.3 °C

R_f: N/A, decomposes during TLC

m/z (ESI): 727.31 ($[M+Na]^+$, 8.3%), 705.33 ($[M+H]^+$, 100%).

HRMS (ESI): Calc. for $C_{46}H_{45}N_2O_5$= 705.3323 Found $[M+H]^+$ 705.3308, mean error= 2.7 ppm, Calc. for $C_{46}H_{44}N_2NaO_5$= 727.3142 Found $[M+Na]^+$ 727.3125 , mean error= 2.5 ppm.

^{1}H NMR (400 MHz, $CDCl_3$): δ_H 8.47 (1H, s, CH, H**26**), 7.94 (1H, m, N**H**) 7.77 (1H, dd, $^3J_{H-H}$ = 3.2 Hz, Ar, C-H, H**6**), 7.29-7.55 (21H, m, Ar, C-H, H**9-13, 16-**

20, 32, 35-39, 42-46), 7.15-7.16 (2H, m, Ar, C-H, H**4, 5**), 7.06-7.07 (2H, m, Ar, C-H, H**30, 31**), 5.16-5.17 (4H, m, CH_2, H**7/14, 33/40**), 5.09 (2H, s, CH_2, H**7/14, 33/40**), 3.42-3.45 (2H, m, CH_2, H**25**), 3.29-3.34 (2H, m, CH_2 H**22**), 1.55-1.62 (2H, m, CH_2, H**24**), 1.36-1.44 (2H, m, CH_2, H**23**).

^{13}C NMR (100 MHz, $CDCl_3$): δ_C 165.41 (C=O, C**21**), 157.55 (CH, C**26**), 152.27 (*ipso*-Ar, C-O, C**2**), 152.04 (*ipso*-Ar, C-O, C**3**), 148.38 (*ipso*-Ar, C-O, C**28**), 146.86 (*ipso*-Ar, C-O, C**29**), 136.93 (m, *ipso*-Ar, C-C, C**8, 15, 34, 41**), 130.71 (*ipso*-Ar, C-C, C**1, 27**), 128.81-127.55 (Ar C-H, C**9-13, 16-20, 35-39, 42-46**), 124.50 (Ar, C-H, C**5**), 124.42 (Ar, C-H, C**31**), 123.53 (Ar, C-H, C**6**) 119.41 (Ar, C-H, H**32**), 117.01(Ar, C-H, C**4**), 116.23 (Ar, C-H, C**30**), 76.49 (CH_2, C**7/33**), 76.11 (CH_2, C**7/33**), 71.38 (CH_2, C**14/40**), 71.10 (CH_2, C**14/40**), 61.42 (CH_2, C**25**) 39.64 (CH_2, C**22**), 28.43 (CH_2, C**24**), 27.19 (CH_2, C**23**)

IR (KBr, cm^{-1}): 1660.0 (C=N), 1655.0 (C=O) 1268.2(C-O)

7.2.3. Synthesis of bis-catecholate ligands

*7.2.3.1. N-(4-[[(2,3-dihydroxyphenyl)methyl]amino]butyl)-2,3-dihydroxybenzamide (**4-24**)*

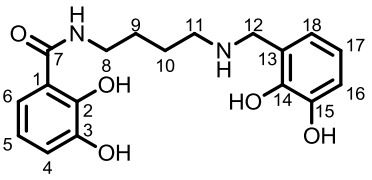

Molecular Formula: $C_{18}H_{22}N_2O_5$
Molecular Weight: 346.378 g mol^{-1}

2,3-Bis(benzyloxy)-*N*-[4-([[2,3bis(benzyloxy)phenyl]methylidene]amino)butyl]benzamide **3-80** (0.50 g 0.71 mmol), was suspended in 2:1 EtOH: Toluene (60 mL). A catalytic amount of Pd black was added to the solution. The mixture was stirred under hydrogen at 50 bar.

The reaction was monitored by TLC and ESI mass spectrometry. Once both techniques confirmed the completion of the reaction, the solution was passed through a glass filter to remove the Pd catalyst and the solution was concentrated *in vacuo* to yield a yellow residue. This was resuspended in anhydrous MeOH (10 mL) and passed through a micro-filter to remove any remaining Pd. The solution was concentrated *in vacuo* to yield the product:

Yield: 0.19 g, 79%

m.p: 92.6-93 °C

m/z(ESI): 347.16 ($[M+H]^+$, 100%).

HRMS (ESI): Calc. for $C_{18}H_{23}N_2O_5$= 347.1601. Found $[M+H]^+$ 347.1589 , mean error= 3.1ppm.

^{1}H NMR (400 MHz, d_6-DMSO): δ_H 7.25 (1H, m, Ar, C-H H**6**), 6.85 (1H, m, Ar, C-H, H**4**), 6.64 (1H, m, Ar, C-H, H**18**), 6.58 (1H, t, $^3J_{H\text{-}H}$=8.0 Hz, Ar, C-H,

H**5**), 6.52-6.53 (2H, m, Ar, C-H, H**16, 17**), 3.83 (2H, s, CH_2, H**12**), 3.26-3.29 (2H, m, CH_2, H**11**), 2.57-2.60 (2H, m, CH_2, H**8**), 1.54-1.55 (4H, m, CH_2, H**9,10**)

^{13}C NMR (100 MHz, d_6-DMSO): δ_C 169.59 (C=O, C**7**), 151.06 (*ipso*-Ar, C-O, C**2**) 148.54 (*ipso*-Ar, C-O, C**3**), 146.70 (*ipso*-Ar, C-O, C**14**), 146.2409 (*ipso*-Ar, C-O, C**15**), 123.21 (*ipso*-Ar, C-C, C**13**), 119.08-116.58 (Ar, C-H, C**4, 5, 6, 16, 17**), 115.03 (*ipso*-Ar, C-C, C**1**) 114.54 (Ar, C-H, C**18**), 50.36 (CH_2, C**12**) 47.63 (CH_2, C**11**), 39.58(CH_2, C**8**), 27.89 (CH_2, C**10**), 25.75 (CH_2, C**9**).

IR (KBr, cm^{-1}): 3384.3 (N-H), 1265.7 (C-O), 1224.3(C-O).

7.2.3.2. General procedure for the synthesis of bis-imine ligands [220]

2,3-Dihydroxybenzaldehyde **2-18 (**1.00 g, 7.24 mmol) was dissolved in 10 mL anhydrous MeOH (10 mL). The appropriate amine (3.62 mmol) was added by syringe. After 5 minutes stirring an orange/yellow (depending on the diamine) precipitate was formed. The mixture was allowed to stand for 30 minutes. The precipitate was isolated by filtration. The recovered solid was then stirred in ice cold MeOH and filtered to yield the product as an orange/yellow powder.

*7.2.3.3. 3-[(1E)-((2-[(E)-[(2,3-dihydroxyphenyl)methylidene]amino]ethyl)imino) methyl]benzene-1,2-diol (**4-30**)*

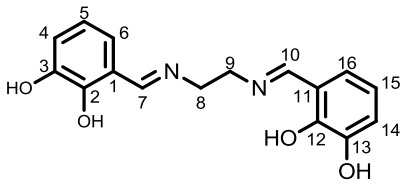

Molecular Formula: $C_{16}H_{16}N_2O_4$

Molecular Weight: 300.309 g mol^{-1}

Yield: 0.97 g, 89%

m.p: Decomposed at 188-189 °C

R_f: N/A, decomposes during TLC

m/z (ESI): 299.10 ($[M-H]^-$,100%).

HRMS (ESI): Calc. for $C_{16}H_{15}N_2O_4$= 299.1037, found $[M-H]^-$ 299.1039, Mean error= -0.6 ppm

^{1}H NMR (400 MHz, d_6-DMSO): δ_H 8.54 (2H, s, CH, H**7, 10**), 6.83-6.86 (4H, m, Ar, C-H, H**4, 6, 14, 16**), 6.64-6.68 (2H, m, Ar, C-H, **H5, 15**), 3.92 (4H, s, CH2, H**8, 9**),

^{13}C NMR (100 MHz, d_6-DMSO): δ_C 167.90 (CH, C**7, 10**), 151.76 (ipso-Ar, C-O, C**3, 13**), 146.46 (ipso-Ar, C-O, C**2, 12**), 122.35 (Ar-C, C-H, C**4, 14**), 118.57 (ipso-Ar, C-C, C**1, 11**), 118.23 (Ar-C, C-H, C**5, 15**) 118.14 (Ar-C, C**6, 16**), 58.18 (CH2, C**8, 9**)

(KBr, cm-1): 3452.44 (O-H), 3388.2 (O-H), 3254.2 (O-H), 1631.6 (C=N), 1200.1 (C-O)

*7.2.3.4. 3-[(1E)-([3-[(E)-[(2,3-dihydroxyphenyl)methylidene]amino]propyl]imino)methyl]benzene-1,2-diol (**4-31**)*

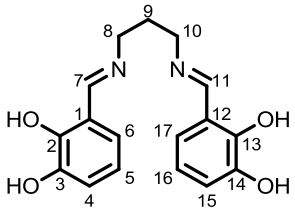

Molecular Formula: $C_{17}H_{18}N_2O_4$
Molecular Weight: 314.336 g mol^{-1}

Yield: 0.45 g, 90%

m.p: Decomposed at 156.4-157 °C

R_f: N/A, decomposes during TLC

m/z (ESI): 313.12 ([M-H]$^-$, 100%).

HRMS (ESI): Calc. for $C_{17}H_{17}N_2O_4$= 313.1194, found [M-H]$^-$ 313.1198, mean error= -1.1 ppm

^{1}H NMR (400 MHz, d_6-DMSO): δ_H 8.53 (2H, s, CH, H**7, 11**), 6.85-6.87 (4H, m, Ar, C-H, H**4, 6, 15, 17**), 6.63-6.67 (2H, m, Ar, C-H, H**5, 16**), 3.66-3.69 (4H, m, CH_2, H**8, 10**), 2.01 (2H, qn, $^3J_{H-H}$= 6.9 Hz, CH_2, H**9**

^{13}C NMR (100 MHz, d_6-DMSO): δ_C 167.18 (CH, C**7, 11**), 152.32 (*ipso*-Ar, C-O, C**3, 14**), 146.59 (*ipso*-Ar, C-O, C**2, 13**), 122.3 (Ar-C, C-H, **C4,15**), 118.45 (*ipso*-Ar, C-C, C**1, 12**), 118.02 (Ar-C, C-H, C**5, 16**) 117.92 (Ar-C, C**6, 17**), 58.18 (CH_2, C**8, 10**), 31.47 (CH_2, C**9**)

IR (KBr cm^{-1}): 3309.4 (O-H), 3007.0 (O-H), 1654.1 (C=N), 1224.3 (C-O)

*7.2.3.5. 3-[(1E)-([4-[(E)-[(2,3-dihydroxyphenyl)methylidene]amino]butyl]imino)methyl]benzene-1,2-diol (**4-32**)*

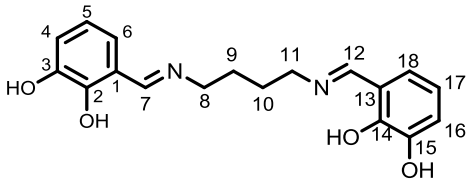

Molecular Formula: $C_{18}H_{20}N_2O_4$
Molecular Weight: 328.362g mol^{-1}

Yield: 0.58 g, 99%

m.p: Decomposed at 186.9-187.6 °C (lit decomposed at 205 °C [214])

R_f: N/A, decomposes during TLC

m/z (ESI): 327.14 ([M-H]$^-$, 100%).

HRMS (ESI): Calc. for $C_{18}H_{19}N_2O_4$= 327.1350, found [M-H]$^-$ 327.1354, mean error= -0.9 ppm

^{1}H NMR (400 MHz, d_6-DMSO): δ_H 8.51 (2H, s, CH, H**7, 12**), 6.81-6.85 (4H, m, Ar, C-H, H**4, 6, 16, 18**), 6.60-6.64 (2H, m, Ar, C-H, H**5, 17**), 3.63 (4H, br s, CH_2, H**8, 11**), 1.71 (4H, br s, CH_2, H**9, 10**)

^{13}C NMR (100 MHz, d_6-DMSO): δ_C 166.77 (CH, C**7, 11**), 152.26 (*ipso*-Ar, C-O, C**3, 15**), 146.78 (*ipso*-Ar, C-O, C**2, 14**), 122.22 (Ar-C, C-H, **C4,16**), 118.08 (*ipso*-Ar, C-C, C**1, 13**), 117.74 (Ar-C, C-H, C**5, 17**) 117.54 (Ar-C, C**6, 18**), 58.51 (CH_2, C**8, 11**), 27.88 (CH_2, C**9, 10**)

IR (KBr, cm^{-1}): 3213.6 (O-H), 1642.8 (C=N), 1236.0 (C-O)

*7.2.3.6. 3-[(1E)-([5-[(E)-[(2,3-dihydroxyphenyl)methylidene]amino]pentyl]imino)methyl]benzene-1,2-diol(**4-33**)*

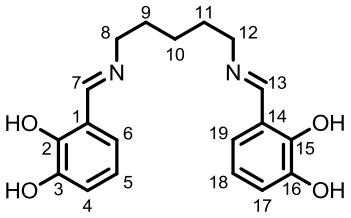

Molecular Formula: $C_{19}H_{22}N_2O_4$
Molecular Weight: 342.389 g mol^{-1}

Yield: 0.44 g, 72%

R_f: N/A, decomposes during TLC

m/z (ESI): 365.15.12 ($[M+Na]^+$ 18%), 343.16 ($[M+H]^+$100%), 172.08 ($[M+2H]^{2+}$ 89%).

HRMS (ESI): Calc. for $C_{19}H_{23}N_2O_4$= 343.1652, found $[M+H]^+$ 343.1662, mean error= -3.4 ppm, Calc. for $C_{19}H_{12}N_2NaO_4$= 365.1742, found $[M+Na]^+$ 365.1488, mean error= -4.5 ppm

^{1}H NMR (400 MHz, d_6-DMSO): δ_H 8.48 (2H, s, CH, H**7, 13**), 6.80-6.83 (4H, m, Ar, C-H, H**4, 6, 17, 19**), 6.58-6.62 (2H, m, Ar, C-H, H**5, 18**), 3.59 (4H, t,

$^{3}J_{H\text{-}H}$ = 6.8 Hz, CH_2, H**8, 12**), 1.69 (4H, qn, $^{3}J_{H\text{-}H}$ = 7.2 Hz , CH_2, H**9, 11**), 1.38-1.46 (2H, m, CH_2, H**10**)

^{13}C NMR (100 MHz, d_6-DMSO): δ_C 165.97 (CH, C**7, 13**), 152.93(*ipso*-Ar, C-O, C**3, 16**), 146.22 (*ipso*-Ar, C-O, C**2, 15**), 121.78 (Ar-C, C-H, **C4,17**), 117.54 (*ipso*-Ar, C-C, C**1, 14**), 117.18 (Ar-C, C-H, C**5, 18**) 116.96 (Ar-C, C**6, 19**), 56.52 (CH_2, C**8, 12**), 29.97(CH_2, C**9, 11**), 24.03 (CH_2, C**10**)

IR (KBr cm^{-1}): 3422.6 (O-H), 3299.7 (O-H), 1643.1 (C=N), 1235.2 (C-O)

*7.2.3.7. 3-[(1E)-([6-[(E)-[(2,3-dihydroxyphenyl)methylidene]amino]hexyl]imino)methyl]benzene-1,2-diol (**4-34**)*

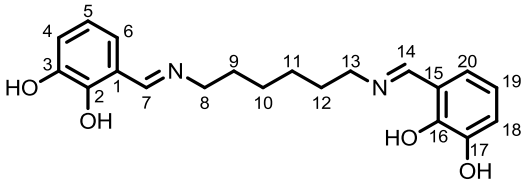

Molecular Formula: $C_{20}H_{24}N_2O_4$
Molecular Weight: 356.416 g mol^{-1}

Yield: 0.48, 75%

m.p: Decomposed at 149.5-150 °C

R_f: N/A, decomposes during TLC

m/z (ESI): 379.16 ($[M+Na]^+$ 5%), 357.18 ($[M+H]^+$ 54%), 179.09 ($[M+2H]^{2+}$ 100%).

HRMS (ESI): Calc. for $C_{19}H_{23}N_2O_4$= 357.1809 found $[M+H]^+$ 357.1802, mean error= 1.5 ppm.

^{1}H NMR (400 MHz, d_6-DMSO): δ_H 8.48 (2H, s, CH, H**7, 14**), 6.79-6.83 (4H, m, Ar, C-H, H**4, 6, 18, 20**), 6.57-6.61 (2H, m, Ar, C-H, H**5, 19**), 3.58 (4H, t,

$^{3}J_{H\text{-}H}$ = 6.8 Hz, CH_2, H**8, 13**), 1.63-1.66 (4H, m, CH_2, H**9, 12**), 1.39 (4H, br s, CH_2, H**10, 11**)

^{13}C NMR (100 MHz, d_6-DMSO): δ_C 165.57 (CH, C**7, 14**), 153.61 (*ipso*-Ar, C-O, C**3, 17**), 146.79 (*ipso*-Ar, C-O, C**2, 16**), 122.20 (Ar-C, C-H, **C4,18**), 117.91 (*ipso*-Ar, C-C, C**1, 15**), 117.54 (Ar-C, C-H, C**5, 19**) 117.32 (Ar-C, C**6, 20**), 55.56 (CH_2, C**8, 13**), 30.11(CH_2, C**9, 12**), 26.08 (CH_2, C**10, 11**)

IR (KBr, cm^{-1}): 3421.2 (O-H), 3259.9 (O-H), 1646.0 (C=N), 1208.5 (C-O)

*7.2.3.8. 3-[(1E)-([7-[(E)-[(2,3-dihydroxyphenyl)methylidene]amino]heptyl]imino)methyl]benzene-1,2-diol (**4-35**)*

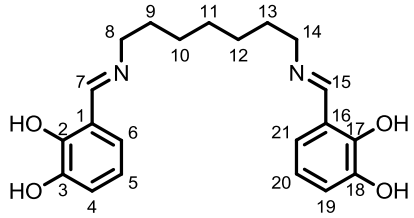

Molecular Formula: $C_{21}H_{26}N_2O_4$
Molecular Weight: 370.442 g mol^{-1}

Yield: 1.34 g, 100%

R_f: N/A, decomposes during TLC

m/z (ESI): 393.17($[M+Na]^+$, 100%).

HRMS (ESI): Calc. for $C_{21}H_{26}N_2NaO_4$= 393.1785. Found $[M+Na]^+$ 393.1774, mean error= 3.0 ppm

^{1}H NMR (400 MHz, d_6-DMSO): δ_H 8.47 (2H, s, CH, H**7, 15**), 6.79-6.83 (4H, m, Ar H, H**4, 6, 19, 21**), 6.57-6.61 (m, Ar, C-H, H**5, 20**), 3.57 (4H, t, $^{3}J_{H\text{-}H}$ =

6.6 Hz, CH_2, H**8, 14**), 1.60-1.64 (4H, m, CH_2, H**9, 13**), 1.35 (6H, br s, CH_2, H**10, 11, 12**)

^{13}C NMR (100 MHz, d_6-DMSO): δ_C 166.55 (CH, C**7, 15**), 153.76 (*ipso*-Ar, C-O, C**3, 18**), 146.84 (*ipso*-Ar, C-O, C**2, 17**), 122.23 (Ar-C, C-H, **C4,19**), 117.88 (*ipso*-Ar, C-C, C**1, 16**), 117.55 (Ar, C-H, C**5, 20**) 117.30 (Ar-C, C**6, 21**), 55.57 (CH_2, C**8, 14**), 30.17 (CH_2, C**9, 13**), 28.31 (CH_2, C**11**), 26.39 (CH_2, C**10, 12**)

IR (KBr cm^{-1}): 3333.5 (O-H), 1645.9 (C=N), 1240.9 (C-O)

*7.2.3.9. 3-[(1E)-([12-[(E)-[(2,3-dihydroxyphenyl)methylidene]amino]dodecyl]imino)methyl]benzene-1,2-diol(**4-36**)*

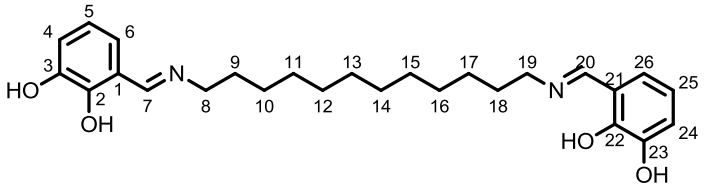

Molecular Formula: $C_{26}H_{36}N_2O_4$
Molecular Weight: 440.575 g mol^{-1}

Yield: 1.28 g, 80%

R_f: N/A, decomposes during TLC

m/z (ESI): 463.25 ($[M+Na]^+$, 11%), 441.23 ($[M+H]^+$, 100%).

HRMS (ESI): Calc. for $C_{26}H_{37}N_2O_4$= 441.2748. Found 441.2730, mean error= 4.1 ppm. Calc. for $C_{26}H_{36}N_2NaO_4$= 463.2567. Found 463.2563, mean error= 1.0 ppm

^{1}H NMR (400 MHz, d_6-DMSO): δ_H 8.48 (2H, s, CH, H**7, 20**), 6.78-6.83 (4H, m, Ar, C-H, H**4, 6, 24, 26**), 6.57-6.61 (m, Ar, C-H, H**5, 25**), 3.57 (4H, t, $^3J_{H-H}$ =

6.6 Hz, CH_2, H**8, 19**), 1.61 (4H, qn, $^3J_{H\text{-}H}$ = 6.9 Hz, CH_2, H**9, 18**), 1.24-1.34 (16H, m, CH_2, H**10, 11, 12, 13, 14, 15, 16, 17**)

^{13}C NMR (100 MHz, d_6-DMSO): δ_C 166.55 (CH, C**7, 20**), 153.76 (*ipso*-Ar, C-O, C**3, 23**), 146.84 (*ipso*-Ar, C-O, C**2, 22**), 122.23 (Ar-C, C-H, **C4,24**), 117.88 (*ipso*-Ar, C-C, C**1, 21**), 117.55 (Ar, C-H C**5, 25**) 117.30 (Ar-C, C**6, 26**), 55.57 (CH_2, C**8, 19**), 30.16 (CH_2, C**9, 18**), 28.31 (CH_2, C**13, 14**), 26.39 (CH_2, C**10-12, 15-17**)

IR (KBr, cm^{-1}): 3333.5 (O-H), 1650.2 (C=N), 1209.9 (C-O)

7.2.3.10. General procedure for the synthesis of benzyl protected bis-imines [220]

2,3-Bis(benzyloxy)benzaldehyde **2-25** (1.00 g, 3.14 mmol) was suspended in anhydrous MeOH (15 mL). The appropriate diamine (1.57 mmol) was added. The solution was left to stir. After stirring overnight, a white precipitate was formed. The precipitate was isolated by filtration as a white solid. The solid was stirred in hot MeOH to remove any impurities and filtered hot to give the product as a white solid.

*7.2.3.11. (E)-[[2,3-bis(benzyloxy)phenyl]methylidene]([2-[(E)-[[2,3-bis(benzyloxy)phenyl]methylidene]amino]ethyl])amine (**4-37**)*

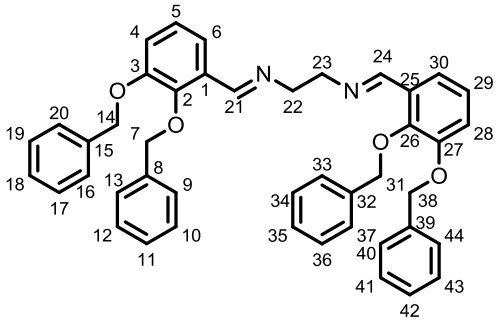

Molecular Formula: $C_{44}H_{40}N_2O_4$

Molecular Weight: 660.799 g mol^{-1}

Yield: 1.03 g, 100%

m.p: 138.8-139 °C

R_f: N/A, decomposes during TLC

m/z (ESI): 661.30 ($[M+H]^+$, 100%).

HRMS (ESI): Calc. for $C_{44}H_{40}N_2O_4$= 661.3044, found $[M+H]^+$ 661.3044, mean error= 2.5 ppm

^{1}H NMR (400 MHz, $CDCl_3$): δ_H 8.55 (2H, s, CH, H**21, 24**), 7.54-7.56 (2H, m, Ar, C-H, H**6, 30**), 7.30-7.47 (20H, m, Ar, C-H, H**9-13, 17-20, 33-37, 40-43**), 7.00-7.05 (4H, m, Ar, C-H, H**4, 5, 28, 29**), 5.14 (2H, s, CH_2, H**7/14, 31/38**) 4.99 (2H, s, CH_2, H**7/14, 31/38**), 3.85 (4H, s, CH_2, H**22, 23**),

^{13}C NMR (100 MHz, $CDCl_3$): δ_C 159.07 (CH, C**21, 24**), 152.28 (*ipso*-Ar, C-O, C**3, 27**), 148.71 (*ipso*-Ar, C-O, C**2, 26**), 137.23 (*ipso*-Ar, C-C, C**8/15, 32/39**), 137.00 (*ipso*-Ar, C-C, C**8/15, 32/39**), 130.77 (*ipso*-Ar, C-C, C**1, 25**), 128.8 (m, Ar, C-H, C**9-13, 16-20, 33-37, 40-44**), 124.42 (Ar, C-H, **C4,28**), 119.46 (Ar, C-H, C**6, 30**), 116.33 (Ar, C-H C**5, 29**), 75.95 (CH_2, C**7/14, 31/38**), 70.93 (CH_2, C**7/14, 31/38**), 61.89 (CH_2, C**22, 23**)

IR (KBr, cm^{-1}): 1641.8 (C=N), 1264.9 (C-O)

*7.2.3.12. (E)-[[2,3-bis(benzyloxy)phenyl]methylidene]([3-[(E)-[[2,3-bis(benzyloxy)phenyl]methylidene]amino]propyl])amine(**4-38**)*

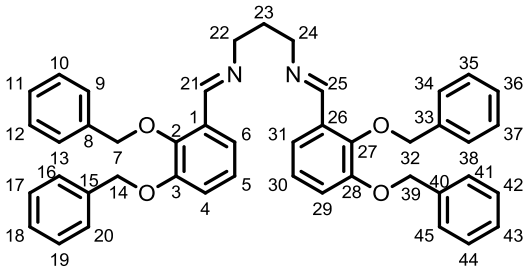

Molecular Formula: $C_{45}H_{42}N_2O_4$

Molecular Weight: 674.826 g mol^{-1}

Yield: 0.81 g, 76%

m.p: 93.4-93.6 °C

R_f: N/A, decomposes during TLC

^{1}H NMR (400 MHz, $CDCl_3$): δ_H 8.52 (2H, s, CH, H**21, 25**), 7.56 (2H, m, Ar, C-H, H**6, 31**), 7.37 (20H, m, Ar, C-H, H**9-13, 16-20, 34-38, 41-45**), 7.08 (4H, m, Ar, C-H, H**4, 5, 29, 30**) 5.17 (2H, s, CH_2, H**7/14, 32/39**), 5.09 (2H, s, CH_2, H**7/14, 32/39**), 3.52 (4H, m, CH_2, H**22, 24**), 1.65 (2H, m, CH_2, H**23**).

^{13}C NMR (100 MHz, $CDCl_3$): δ_C 157.52 (CH, C**21, 25**), 152.29 (*ipso*-Ar, C-O, C**3, 28**), 148.59 (*ipso*-Ar, C-O, C**2, 27**), 137.32 (*ipso*-Ar, C-C, C**8/15, 33/40**), 137.06 (*ipso*-Ar, C-C, C**8/15, 33/40**), 131.01 (*ipso*-Ar, C-C, C**1, 26**), 128.31 (m, Ar, C-H, C**9-13, 16-20, 34-38, 41-45**), 124.44 (Ar, C-H, **C4,29**), 119.46 (Ar, C-H, C**6, 31**), 116.23 (Ar, C-H C**5, 30**), 75.96 (CH_2, C**7/14, 32/39**), 70.93 (CH_2, C**7/14, 32/39**), 61.89 (CH_2, C**22, 24**), 28.40 (CH_2, C**23**).

IR (KBr cm^{-1}): 1641.6 (C=N), 1269.1 (C-O)

*7.2.3.13. (E)-[[2,3-bis(benzyloxy)phenyl]methylidene]([4-[(E)-[[2,3-bis(benzyloxy)phenyl]methylidene]amino]butyl])amine(**4-39**)*

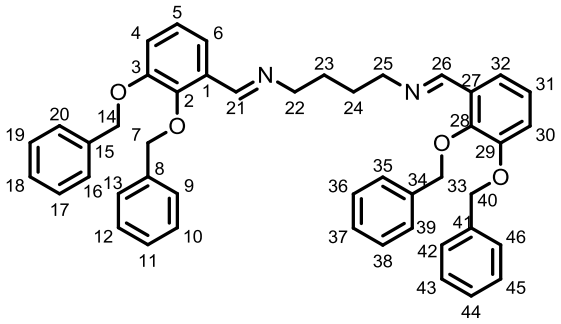

Molecular Formula: $C_{46}H_{44}N_2O_4$

Molecular Weight: 688.853 g mol^{-1}

Yield: 1.04 g, 96%

m.p: 129.5-130 °C

R_f: N/A, decomposes during TLC

m/z (ESI): 689.33 ($[M+H]^+$, 100%).

HRMS (ESI): Calc. for $C_{46}H_{45}N_2O_4$= 689.3374, found $[M+H]^+$ 689.3346, mean error= 4.5 ppm

^{1}H NMR (400 MHz, $CDCl_3$): δ_H 8.52 (2H, s, CH, H**21, 26**), 7.55-7.57 (2H, m, Ar, C-H, H**6, 32**), 7.31-7.50 (20H, m, Ar, C-H, H**9-13, 16-20, 35-39, 42-46**), 7.06-7.07 (4H, m, Ar, C-H, H**4, 5, 30, 31**) 5.17 (2H, s, CH_2, H**7/14, 33/40**), 5.09 (2H, s, CH_2, H**7/14, 33/40**), 3.55-3.56 (4H, m, CH_2, H**22, 25**), 1.68-1.70 (4H, m, CH_2, H**23, 24**).

^{13}C NMR (100 MHz, $CDCl_3$): δ_C 157.51 (CH, C**21, 26**), 152.29 (*ipso*-Ar, C-O, C**3, 29**), 148.59 (*ipso*-Ar, C-O, C**2, 28**), 137.32 (*ipso*-Ar, C-C, C**8/15, 33/40**), 137.06 (*ipso*-Ar, C-C, C**8/15, 34/41**), 131.01 (*ipso*-Ar, C-C, C**1, 27**), 128.31 (m, Ar, C-H, C**9-13, 16-20, 35-39, 42-46**), 124.44 (Ar, C-H, **C4,30**), 119.46 (Ar, C-H, C**6, 32**), 116.23 (Ar, C-H C**5, 31**), 75.96 (CH_2, C**7/14, 33/40**), 70.93 (CH_2, C**7/14, 33/40**), 61.87 (CH_2, C**22, 25**), 28.40 (CH_2, C**23, 24**).

IR (KBr cm^{-1}): 1644.9 (C=N), 1268.2 (C-O),

*7.2.3.14. (E)-[[2,3-bis(benzyloxy)phenyl]methylidene]([5-[(E)-[[2,3-bis(benzyloxy)phenyl]methylidene]amino]pentyl])amine (**4-40**)*

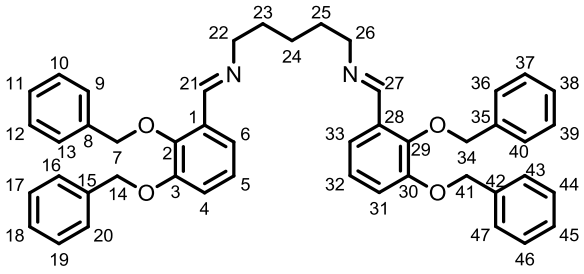

Molecular Formula: $C_{47}H_{46}N_2O_4$

Molecular Weight: 702.879 g mol^{-1}

Yield: 0.77 g, 70%

m.p: 83.9-84.7 °C

R_f : N/A, decomposes during TLC

m/z (ESI): 703.35 ($[M+H]^+$, 100%).

HRMS (ESI): Calc. for $C_{47}H_{47}N_2O_4$= 703.3530, found $[M+H]^+$ 703.3537, mean error= -0.4 ppm

^{1}H NMR (400 MHz, $CDCl_3$): δ_H 8.52 (2H, s, CH, H**21, 27**), 7.54-7.58 (2H, m, Ar, C-H, H**6, 33**), 7.32-7.50 (20H, m, Ar, C-H, H**9-13, 16-20, 36-40, 43-47**), 7.07-7.08 (4H, m, Ar, C-H, H**4, 5, 31, 32**) 5.17 (2H, s, CH_2, H**7/14, 34/41**), 5.09 (2H, s, CH_2, H**7/14, 34/41**), 3.52-3.55 (4H, m, CH_2, H**22, 26**), 1.66-1.73 (4H, m, CH_2, H**23, 25**), 1.36-1.43 (2H, m, CH_2, H**24**)

^{13}C NMR (100 MHz, $CDCl_3$): δ_C 157.51 (CH, C**21, 27**), 152.29 (*ipso*-Ar, C-O, C**3, 30**), 148.59 (*ipso*-Ar, C-O, C**2, 29**), 137.32 (*ipso*-Ar, C-C, C**8/15, 35/42**), 137.06 (*ipso*-Ar, C-C, C**8/15, 35/42**), 131.01 (*ipso*-Ar, C-C, C**1, 29**). 128.30 (m, Ar, C-H, C**9-13, 16-20, 37-41, 44-48**), 124.46 (Ar, C-H, **C4,31**), 119.46 (Ar, C-H, C**6, 33**), 116.18 (Ar, C-H C**5, 32**), 75.96 (CH_2, C**7/14, 34/41**), 70.93 (CH_2, C**7/14, 34/41**), 61.87 (CH_2, C**22, 26**) 30.61 (CH_2, C**23, 25**), 26.93 (CH_2, C**24**).

IR (KBr cm^{-1}): 1645.2 (C=N), 1272.2 (C-O)

*7.2.3.15. (E)-[[2,3-bis(benzyloxy)phenyl]methylidene]([6-[(E)-[[2,3-bis(benzyloxy)phenyl]methylidene]amino]hexyl])amine (**4-41**)*

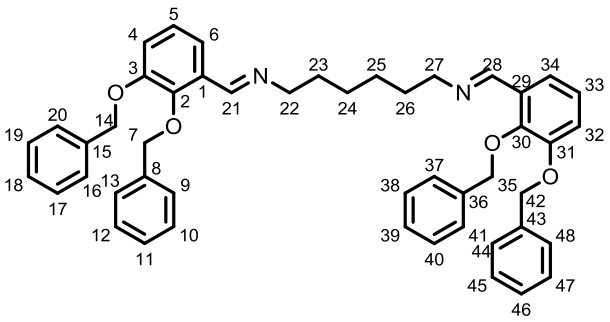

Molecular Formula: $C_{48}H_{48}N_2O_4$

Molecular Weight: 716.906 g mol^{-1}

Yield: 0.57 g, 51%

m.p: 94.0-94.3 °C

R_f : N/A, decomposes on TLC plate

m/z (ESI): 717.36 ($[M+H]^+$, 100%).

HRMS (ESI): Calc. for $C_{48}H_{49}N_2O_4$= 717.3687, found 717.3660, mean error= 3.1 ppm

^{1}H NMR: (400 MHz, $CDCl_3$): δ_H 8.52 (2H, s, CH, H**21, 28**), 7.54-7.58 (2H, m, Ar, C-H, H**6, 34**), 7.32-7.50 (20H, m, Ar, C-H, H**9-13, 17-20, 36-40, 43-47**), 7.07-7.09 (4H, m, Ar, C-H, H**4, 5, 31, 32**) 5.17 (2H, s, CH_2, H**7/14, 34/41**), 5.09 (2H, s, CH_2, H**7/14, 34/41**), 3.53 (4H, td, $^3J_{H\text{-}H}$ = 7.0 Hz, $^4J_{H\text{-}H}$ = 1.2 Hz, CH_2, H**22, 27**), 1.63-1.69 (4H, m, CH_2, H**23, 26**), 1.36-1.39 (4H, m, CH_2, H**24, 25**)

^{13}C NMR: (100 MHz, $CDCl_3$) δ_C 157.34 (CH, C**21, 28**), 152.29 (*ipso*-Ar, C-O, C**3, 31**), 148.59 (*ipso*-Ar, C-O, C**2, 30**), 137.32 (*ipso*-Ar, C-C, C**8/15, 36/45**), 137.06 (*ipso*-Ar, C-C, C**8/15, 36/45**), 131.01 (*ipso*-Ar, C-C, C**1, 29**). 128.30 (m, Ar, C-H, C**9-13, 16-20, 37-41, 44-48**), 124.46 (Ar, C-H, **C4,32**), 119.46 (Ar, C-H, C**6, 34**), 116.18 (Ar, C-H C**5, 33**), 75.96 (CH_2, C**7/14, 40/47**), 70.93

(CH_2, C**7/14, 40/47**), 61.87 (CH_2, C**22, 27**) 30.61 (CH_2, C**23, 26**), 26.93 (CH_2, C**24, 25**).

IR (KBr cm^{-1}): 1637.8 (C=N), 1269.1 (C-O).

*7.2.3.16. (E)-[[2,3-bis(benzyloxy)phenyl]methylidene]([7-[(E)-[[2,3-bis(benzyloxy)phenyl]methylidene]amino]heptyl])amine (**4-42**)*

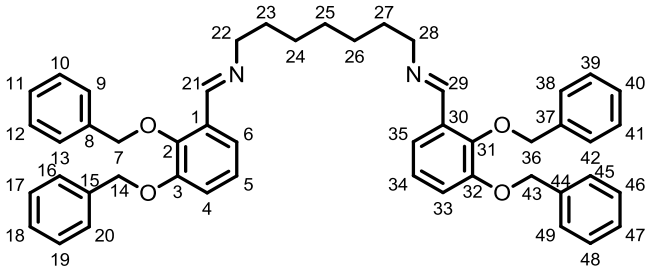

Molecular Formula: $C_{49}H_{50}N_2O_4$

Molecular Weight: 730.932 g mol^{-1}

Yield: 0.85 g, 74%

m.p: 85.4-86.2 °C

R_f: N/A, decomposes during TLC

m/z (ESI): 731.38 ($[M+H]^+$, 27%), 366.19 ($[M+2H]^{2+}$, 100%).

HRMS (ESI): Calc. for $C_{49}H_{52}N_2O_4$= 366.1958, found $[M+2H]^{2+}$ 366.1951, mean error= 2.6 ppm. Calc. for $C_{49}H_{52}N_2O_4$= 731.3843, found $[M+H]^+$ 731.3831, mean error= 2.0 ppm

^{1}H NMR: (400 MHz, $CDCl_3$): δ_H 8.52 (2H, s, CH, H**21, 29**), 7.54-7.59 (2H, m, Ar, C-H, H**6, 35**), 7.32-7.50 (20H, m, Ar, C-H, H**9-13, 17-20, 38-42, 45-49**), 7.06-7.08 (4H, m, Ar, C-H, H**4, 5, 33, 34**) 5.17 (2H, s, CH_2, H**7/14, 36/43**), 5.09 (2H, s, CH_2, H**7/14, 36/43**), 3.51-3.54 (4H, m, CH_2, H**22, 28**), 1.64-1.69 (4H, m, CH_2, H**23, 27**), 1.33-1.37 (6H, m, CH_2, H**24-26**)

^{13}C NMR: (100 MHz, $CDCl_3$) δ_C 157.30 (CH, C**21, 29**), 152.28 (*ipso*-Ar, C-O, C**3, 32**), 148.58 (*ipso*-Ar, C-O, C**2, 31**), 137.32 (*ipso*-Ar, C-C, C**8/15, 37/44**), 137.05 (*ipso*-Ar, C-C, C**8/15, 37/44**), 131.00 (*ipso*-Ar, C-C, C**1, 30**), 128.29 (m, Ar, C-H, C**9-13, 16-20, 38-42, 45-49**), 124.45 (Ar, C-H, **C4, 33**), 119.44 (Ar, C-H, C**6, 35**), 116.14 (Ar, C-H C**5, 34**), 75.93 (CH_2, C**7/14, 41/48**), 70.90 (CH_2, C**7/14, 41/48**), 61.91 (CH_2, C**22, 28**) 30.61 (CH_2, C**23, 27**), 29.03 (CH_2, C**25**), 27.02 (CH_2, C**24, 26**)

IR (KBr cm^{-1}): 1641.1 (C=N), 1270.4 (C-O)

*7.2.3.17. (E)-[[2,3-bis(benzyloxy)phenyl]methylidene]([12-[(E)-[[2,3-bis(benzyloxy)phenyl]methylidene]amino]dodecyl])amine (**4-43**)*

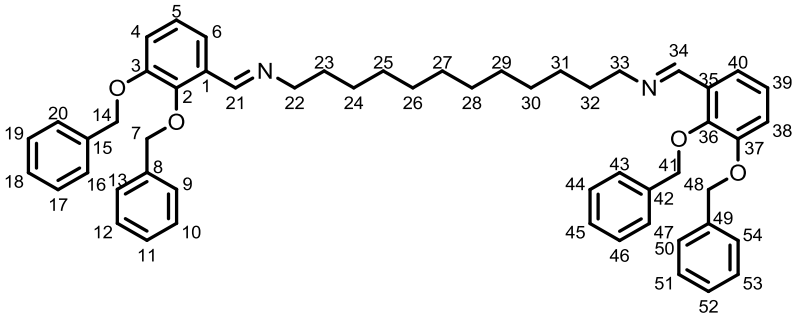

Molecular Formula: $C_{54}H_{60}N_2O_4$

Molecular Weight: 801.065 g mol^{-1}

Yield: 0.70 g, 56%

m.p:89.3-89.9 °C

R_f : N/A, decomposes on TLC plate

m/z (ESI): 801.46 ($[M+H]^+$, 11%), 401.23 ($[M+2H]^{2+}$, 100%).

HRMS (ESI): Calc. for $C_{54}H_{62}N_2O_4$= 401.2349, found $[M+2H]^+$ 401.2337, mean error= 4.9 ppm, Calc. for $C_{54}H_{61}N_2O_4$= 801.4626, found $[M+H]^+$ 801.4611, mean error= 2.2 ppm

^{1}H NMR: (400 MHz, $CDCl_3$): δ_H 8.53 (2H, s, CH, H**21, 34**), 7.56-7.58 (2H, m, Ar, C-H, H**6, 40**), 7.33-7.50 (20H, m, Ar, C-H, H**9-13, 17-20, 43-47, 50-54**), 7.07-7.09 (4H, m, Ar, C-H, H**4, 5, 38, 39**) 5.17 (2H, s, CH_2, H**7/14, 41/48**), 5.09 (2H, s, CH_2, H**7/14, 41/48**), 3.53 (4H, t, $^{3}J_{H-H}$ = 6.8 Hz, CH_2, H**22, 33**), 1.63-1.67 (4H, m, CH_2, H**23, 32**), 1.29-1.33 (16H, m, CH_2, H**24-31**)

^{13}C NMR: (100 MHz, $CDCl_3$) δ_C 157.27 (CH, C**21, 34**), 152.28 (*ipso*-Ar, C-O, C**3, 37**), 148.56 (*ipso*-Ar, C-O, C**2, 36**), 137.32 (*ipso*-Ar, C-C, C**8/15, 42/49**), 137.04 (*ipso*-Ar, C-C, C**8/15, 42/49**), 131.02 (*ipso*-Ar, C-C, C**1, 35**). 128.29 (m, Ar, C-H, C**9-13, 16-20, 43-47, 50-54**), 124.45 (Ar, C-H, **C4,38**), 119.44 (Ar, C-H, C**6, 40**), 116.12 (Ar, C-H C**5, 39**), 75.95 (CH_2, C**7/14, 41/48**), 70.89 (CH_2, C**7/14, 41/48**), 61.94 (CH_2, C**22, 33**), 30.62 (CH_2, C**23, 32**) 29.36 (CH_2, C**25-30**), 27.06 (CH_2, C**24, 31**)

IR (KBr, cm^{-1}): 1642.3 (C=N), 1268.2 (C-O)

7.3. Biological studies

7.3.1. Suppliers

All chemicals, reagents and media used in this project were purchased from: Acros Organics, Fermedium, Fischer Scientific, Invitrogen, Melford, New England Biolabs, Oxoid and Sigma Aldrich

7.3.2. Bacterial strains

See **Table 7.1** for details of the bacterial strains used.

Bacterial strain	Genotype	Source
BW25113	Wild type	Baba *et al.*, 2006 [263]
JW0588	BW25113 *entA::kan*	Baba *et al.*, 2006
BW25113	*ompF::kan*	Baba *et al.*, 2006
BW25113	*tonB::kan*	Baba *et al.*, 2006
BW25113	*galPmglCytfT::Δkan*	H. Neves and G.H. Thomas, unpublished data.

Table 7.1: List of *E. coli* strains utilised in biological assays

7.3.3. Media and antibiotics

All solutions and media were prepared using MilliQ deionised H_2O and sterilised by autoclave prior to use

7.3.3.1. Luria-Bertani (LB) media

LB media was prepared using 10 g tryptone, 5 g of yeast extract and 10 g NaCl per litre.

7.3.3.2. M9 minimal media

M9 minimal media was prepared using 6 g Na_2HPO_4, 3 g KH_2PO_4, 1 g NH_4Cl and 0.5 g NaCl per litre. After autoclaving, the solution was supplemented with a specified amount of carbon source (see individual experiments) and 1 mM $MgSO_4$[264]. The antibiotic kanamycin was also added where required.

7.3.4. Solid media

7.3.4.1. Nutrient agar

Nutrient agar was prepared by combining either LB or M9 minimal media with 1.5% (w/v) technical grade agar.

7.3.4.2. Top agar

Top agar was prepared using 0.7% (w/v) of agarose in MilliQ H_2O

7.3.4.3. Antibiotics

Kanamycin stock solutions were made in H_2O MilliQ at a concentration of 50 mg/mL and filter sterilized. The kanamycin was added where required to liquid cultures in a volume sufficient to give a concentration of 50 µg/mL.

7.3.5. Buffers and solutions

7.3.5.1. Agarose gel electrophoresis

TAE running buffer was prepared using 750 mL of H_2O, 48.4 g/L of Tris, 22.8 mL of glacial acetic acid, 200 mL of 29.2 g/L EDTA. The solution was made up to 1 L using H_2O. To produce a working concentration of TAE buffer the solution was diluted by 1 in 10 in H_2O. The agarose gels used were prepared using 1% (w/v) agarose in 1 x TAE buffer.

7.3.5.2. Stop buffer

The stop buffer for the DNA gyrase assay was prepared using 40% (w/v) of sucrose, 12.11 g/L Tris·HCl (pH 7.5), 0.29 g/L EDTA and 0.5 mg/mL of

bromophenol blue. This was used to terminate the assay in combination with a 24:1 solution of chloroform/ isoamyl alcohol.

7.3.5.3. DNA Gyrase assay buffer

The DNA gyrase assay buffer came pre-prepared in a kit from Inspiralis. The buffer contained 3.92 g/L Tris·HCl (pH 7.5), 1.79 g/L KCl, 0.38 g/L $MgCl_2$, 0.3 g/L dithiothreitol, 0.26 g/L spermidine, 0.5 g/L ATP, 6.5% (w/v) glycerol and 0.1 mg/mL BSA

7.3.6. Liquid culture assays

7.3.6.1. O/D_{650} measurements

Optical densities were recorded to 3 decimal places using a Jenway 6305 spectrophotometer in plastic cuvettes with a 1 cm path length, and are accurate to ±0.0005.

7.3.6.2. Determination of growth conditions fluoroquinolone uptake

Cultures of the wild type and galactose transport mutant strains were inoculated into 5 mL of M9 glycerol and incubated with shaking at 37 °C. The cultures were centrifuged, the supernatant was discarded and the pellet resuspended in M9 glucose and M9 galactose. This process was repeated. The O/D_{650} of the cultures was measured and the cultures diluted into 8 mL the appropriate media (one WT in M9 glucose, one WT in M9 galactose, one mutant in M9 glucose, one mutant in M9 galactose) in sterilins. The cultures were then incubated with shaking at 37 °C. O/D_{650} measurements were taken every hour for six hours, then every two hours after overnight growth.

7.3.6.3. Antimicrobial evaluation of iron chelators

Cultures of the required strains were inoculated into 20 mL of LB media and incubated overnight with shaking at 37 °C. The cultures were centrifuged, the supernatant was discarded and the pellet resuspended in M9 glucose. This process was repeated. The O/D_{650} of the cultures was measured and the culture diluted into 20 mL of M9 in sterilins to an

approximate O/D_{650} of 0.1. The cultures were inoculated with the compound to be evaluated using a range of concentrations from 100−10 μM. In experiments where iron was required one molar equivalent of iron was added to each culture (1:1 iron: ligand ratio) by adding an appropriate volume of aqueous $Fe(NO_3)_3$. The cultures were incubated with shaking at 37 °C for 24 hours with O/D_{650} measurements taken at 0.5 hours, 3 hours, 6 hours and 24 hours.

7.3.7. Zone of inhibition assays

*7.3.7.1. Screening of the Ugi conjugate **3-1***

Zone of inhibition assays were performed on solid media. Screening plates were prepared by melting M9 glucose or LB agar and pouring 100 mL molten agar into large screening plates. Cultures of *E. coli* BW25113 were pre-grown with shaking overnight 37 °C in LB media. After overnight growth the cultures were diluted into the appropriate media (M9 glucose or LB) at an O/D_{650} of 0.100. Cultures diluted into M9 were centrifuged and washed with M9 media to remove all traces of LB media. The cultures were grown with shaking at 37 °C to mid-log phase (O/D_{650} = 0.6). The cultures were inoculated into molten top agar at a concentration of 4% v/v. The inoculated top agar was poured onto the nutrient agar and allowed to set. 3 mM stock solutions of ciprofloxacin and the Ugi conjugate **3-1** were prepared in 0.1 M acetic acid and DMSO respectively. One in five dilutions series of both compounds were prepared using sterile H_2O. 3 μL of each concentration of each compound was applied to the agar plates using a micropipette and allowed to dry. The plates were incubated at 37 °C overnight to allow bacterial growth. After overnight growth the plates were examined and the zones of inhibition measured. The data was processed using Sigma-plot 12.0.

7.3.7.2. Screening of glycosylated fluoroquinolones

Zone of inhibition assays on the glycosylated fluoroquinolones were performed on solid media. Screening plates were prepared by melting M9 glucose or galactose and pouring 100 mL molten agar into large screening plates. Cultures of *E. coli* BW25113 were pre-grown with shaking overnight 37 °C in M9 glycerol. For the mutant studies BW25113 *ompf::kan* was used instead of the wild type. After overnight growth the cultures were diluted into the appropriate media (M9 glucose or M9 galactose) at an O/D_{650} of 0.100. The cultures were centrifuged and washed with M9 media to remove all traces of the pre-growth media. The cultures were grown with shaking at 37 °C to mid-log phase (O/D_{650} = 0.6). The cultures were inoculated into molten top agar at a concentration of 4% v/v. The inoculated top agar was poured onto the nutrient agar and allowed to set. 3 mM stock solutions of ciprofloxacin and the three fluoroquinolone conjugates were prepared in 0.1 M acetic acid. One in five dilutions series of each compound were prepared using sterile H_2O. 3 μL of each concentration of each compound was applied to the agar plates using a micropipette and allowed to dry. The plates were incubated at 37 °C overnight to allow bacterial growth. After overnight growth the plates were examined and the zones of inhibition measured. The data was processed using Sigma-plot 12.0.

7.3.8. DNA Gyrase assay

3 mM solutions of ciprofloxacin **1-18,** and the Ugi conjugate **3-1** were prepared in acetic acid and DMSO respectively. The antimicrobial compounds were combined with relaxed pBR322 DNA, DNA gyrase and running buffer (**6.3.5.3**) in H_2O at fixed proportions (**Table 7.2**). For ease of preparation a set of dilutions of the antimicrobial solutions were prepared with concentrations of 300, 30, 15 and 3 μM.

Antimicrobial concentration (µM) **[Solution concentration used]**	Volume of antimicrobial solution (µL)	Volume of H_2O (µL)
Positive control	0	21.5
Negative control	0	23.5
200 **[300 µM]**	20	1.5
150 **[300 µM]**	15	6.5
125 **[300 µM]**	12.5	9
100 **[300 µM]**	10	11.5
75 **[300 µM]**	7.5	14
50 **[300 µM]**	5	16.5
40 **[300 µM]**	4	17.5
30 **[300 µM]**	3	18.5
20 **[300 µM]**	2	19.5
10 **[300 µM]**	1	20.5
5 **[300 µM]**	0.5	21
1 **[30 µM]**	1	20.5
0.5 **[30 µM]**	0.5	21
0.25 **[15 µM]**	0.5	21
0.1 **[3 µM]**	1	20.5

Table 7.2: Volumes of antimicrobial solutions and H_2O added to each sample for the DNA gyrase assay.

The solutions were incubated at 37 °C for 30 minutes. The assay was stopped by the addition of 30 µL of 24:1 $CHCl_3$: isoamyl alcohol and 18 µL of stop buffer. 20 µL of each solution was loaded onto a 1% agarose gel. The gel was subjected to electrophoresis for 90 minutes at 80 volts. Upon completion of electrophoresis, the gel was stained using ethidium bromide overnight and photographed using a gel doc.

7.3.9. UV analysis of tetradentate ligands

Stock solutions of the ligands were prepared by dissolving in an aqueous buffer solution of Na_2HPO_4 (6 g/L) and KH_2PO_4 (3 g/L) at a concentration of 16 mM (equivalent to 5 mg/mL of ligand **4-30**). Samples were prepared by preparing a 1 in 20 dilution of the stock solution in the aqueous phosphate solution. A baseline was generated by running a scan of the aqueous phosphate buffer solution. Samples were then scanned relative to the phosphate buffer from 200-550 nm, and the data processed as described in **section 7.1.4.**

Appendix I: UV spectra of bis-catecholate imine ligands

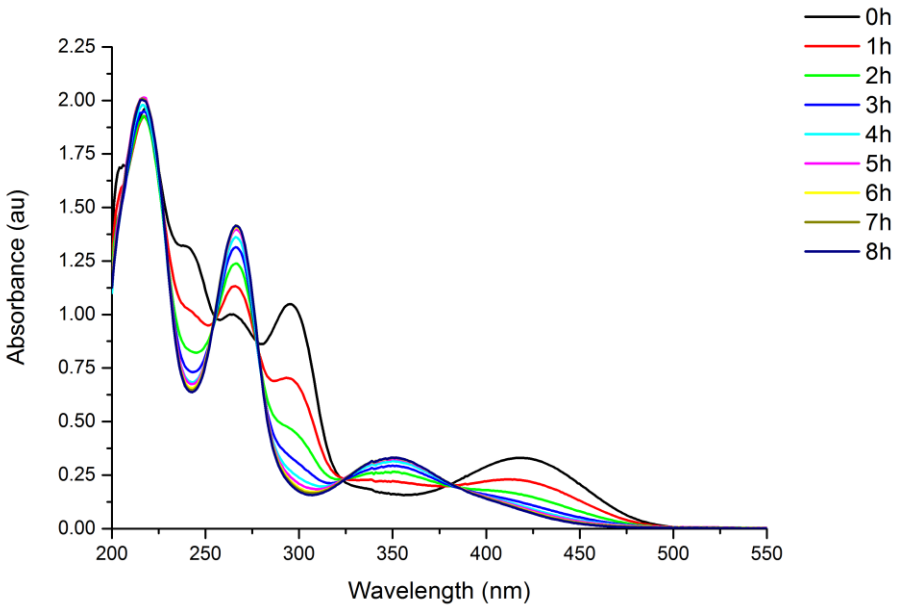

UV/Vis spectrum of the propyl bis-catecholimine ligand **4-30** over a period of 8 hours

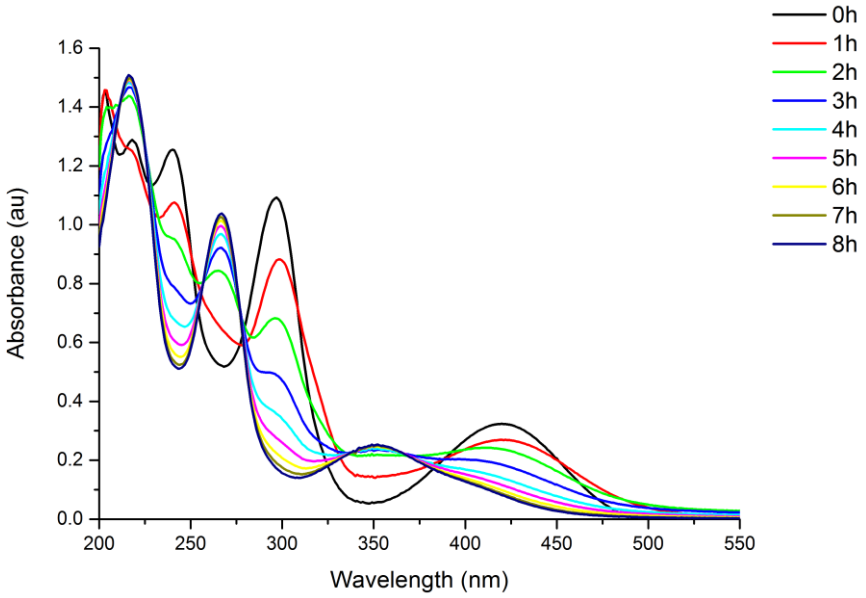

UV/Vis spectrum of the butyl bis-catecholimine ligand **4-31** over a period of 8 hours

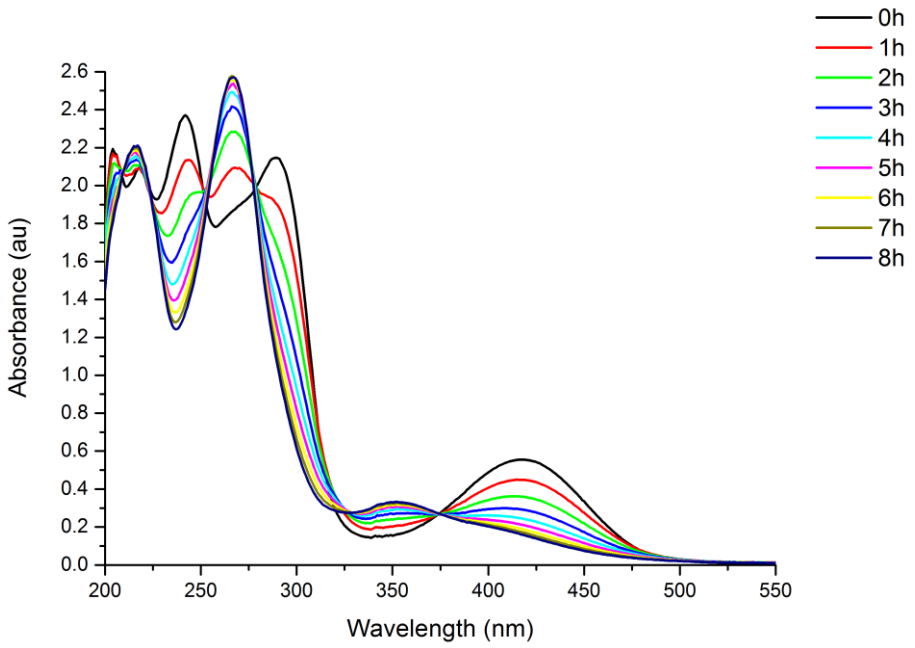

UV/Vis spectrum of the pentyl bis-catecholimine ligand **4-32** over a period of 8 hours

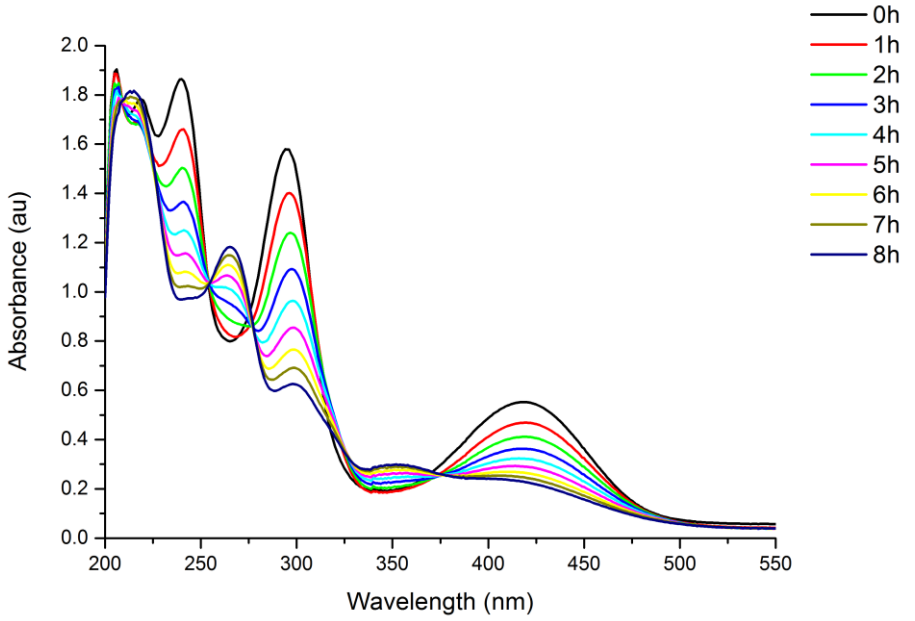

UV/Vis spectrum of the hexyl bis-catecholimine ligand **4-33** over a period of 8 hours

Appendix I: UV/vis spectra of bis-catecholate imine ligands

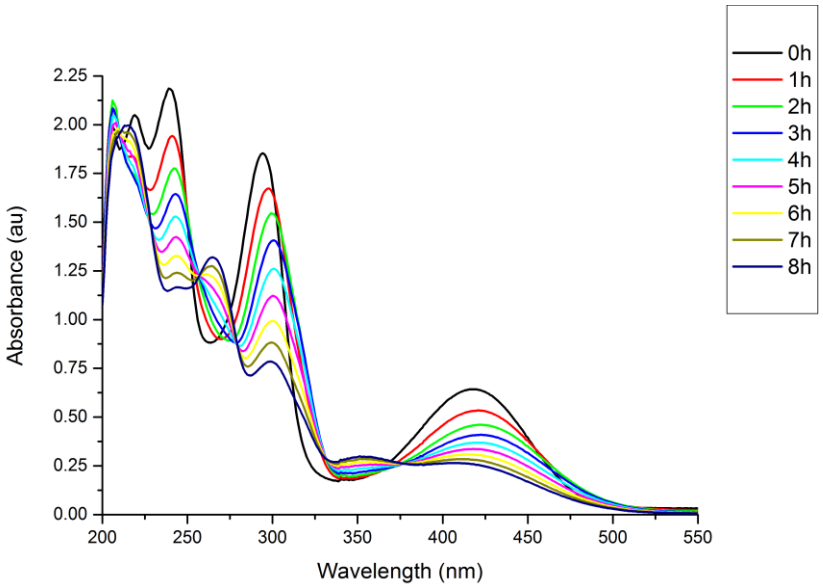

UV/Vis spectrum of the heptyl bis-catecholimine ligand **4-34** over a period of 8 hours

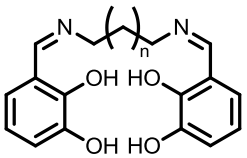

3-31 n = 1
3-32 n = 2
3-33 n = 3
3-34 n = 4
3-35 n = 5

General structure of the bis-catecholimine ligands

Glossary

Biological

ABC	ATP Binding Cassette
ADP	Adenosine Diphosphate
ATP	Adenosine Triphosphate
DNA	Deoxyribosenucleic acid
FDA	Food and Drug Administration
GLUT	Glucose Transporter Family
G6P	Glucose 6 Phosphate
MATE	Multi-drug and toxic compound Extrusion
MDR	Multi-drug resistant
MFS	Major Facilitator Superfamily
MIC	Minimum Inhibitory Concentration
MRSA	Multi-drug Resistant *Staphylococcus aureus*
NDM-1	New Delhi Metallo-β-lactamase
NSAID	Non-Steroidal Anti-Inflammatory Drug
OMP	Outer Membrane Porin
PBP	Penicillin Binding Protein
PerBP	Periplasmic Binding Protein
PEP	Phosphoenolpyruvate
PEP-PTS	Phosphoenolpyruvate-dependent sugar phosphotransferase system
P^i	Inorganic phosphate

pmf	Proton Motive Force
PRP	Pentapeptide Repeat Protein
QIDP	Qualified Infectious Disease Product
QNR	Quinolone resistance proteins
RND	Resistance Nodulation-Cell Division
SCOR	Short Chain Oxidoreductase
TMQR	Transferable Mechanisms of Quinolone Resistance

Chemistry

Acac	Acetylacetonate
Boc	*tert*-Butyloxycarbonyl
Boc_2O	Di-*tert*-butyl Dicarbonate
Boc-Gly-OH	Boc-protected glycine
CD_3OD	Deuterated methanol
$CDCL_3$	Deuterated chloroform
$CHCl_3$	Chloroform
Cpf	Ciprofloxacin
D_2O	Deuterated water
d_6-DMSO	Deuterated dimethyl sulfoxide
DCC	*N,N'*-Dicyclohexylcarbodiimide
DCE	1,2-Dichloroethane
DCM	Dichloromethane
DIPEA	*N,N'*-Diisopropylethylamine

DMF	Dimethylformamide
DMSO	Dimethyl sulfoxide
DPTA	Diethylenetriaminepentaacetic acid
EDC·HCl	1-Ethyl-3-(3'-dimethylaminopropyl)carbodiimide hydrochloride
Et_2O	Diethyl ether
EtOAc	Ethyl acetate
EtOH	Ethanol
$Ga(Acac)_3$	Gallium acetylacetonate
$Ga(NO_3)_3$	Gallium nitrate
H_2SO_4	Sulfuric acid
H_3PO_4	Phosphoric acid
HCl	Hydrochloric acid
HOBt·H_2O	*N*-Hydroxybenzotriazole hydrate
KBr	Potassium bromide
LICAM	Linear Catechol Amide
m.p.	Melting point
MCC	Multi-component condensation
MeCN	Acetonitrile
MeOH	Methanol
$MeSO_3H$	Methanesulfonic acid
$MgSO_4$	Magnesium Sulphate
Na_2CO_3	Sodium Carbonate

$NaHCO_3$	Sodium Hydrogen Carbonate
NaOH	Sodium Hydroxide
NHS	*N*-Hydroxy Succinimide
PhMe	Toluene
rt	Room Temperature
$SOCl_2$	Thionyl Chloride

Spectroscopy

4°-C	Quaternary carbon
^{1}H	Proton
^{13}C	Carbon
^{19}F	Fluorine
AU	Absorbance Units
Ar	Aromatic
br	Broad
Calc	Calculated
COSY	Correlation Spectroscopy
δ	Chemical Shift
d	Doublet
dd	Doublet of doublets
DEPT	Distortionless Enhancement of Polarisation Transfer
ESI	Electrospray Ionisation
HPLC	High-Performance Liquid Chromatography

HRMS	High Resolution Mass Spectrometry
HSQC	Gradient Heteronuclear Single Quantum Correlation
IR	Infra-red
J	Coupling constant
LC-MS	Liquid Chromatography- Mass Spectrometry
m	Medium
m	Multiplet
$[M+H]^+$	Protonated molecular ion
$[M+Na]^+$	Sodiated molecular ion
$[M+NH_4]^+$	Ammoniated molecular ion
MS	Mass Spectrometry
m/z	Mass to charge ratio
NMR	Nuclear Magnetic Resonance
ppm	Parts per million
q	Quartet
qn	Quintet
R_f	Retention Factor
S	Sharp
s	Singlet
t	Triplet
TLC	Thin Layer Chromatography
UV	Ultra violet

vis	Visible
w	Weak

Units

Å	Angstroms (1×10^{-10} m)
°C	Degrees Centigrade
$\mu A/cm^2$	Microamps per centimetre squared
µg/L	Micrograms per litre
µg/mL	Micrograms per millilitre
A	Amps
cm^{-1}	Wavenumbers
Da	Daltons
g	Grams
g mol^{-1}	Grams per mole
h	hours
Hz	Hertz
K	Degrees Kelvin
L	Litres
M	Molar
mg/L	Milligrams per litre
mg/mL	Milligrams per millilitre
mL	Millilitres
mol	Moles

w/v	Weight by volume

References

[1] S. C. Davies in *Annual report of the Chief Medical Officer: Infections and the rise of antibiotic resistance*, *Vol. 2* **2011**.

[2] Department of Health in *UK Five year antimicrobial resistance strategy 2013-2018*, *Vol.* **2013**.

[3] F. F. Barrett, R. F. McGehee and M. Finland, *N. Engl. J. Med.* **1968**, *279*, 441-448.

[4] A. MacGowan and E. Macnaughton, *Medicine* **2013**, *41*, 642-648.

[5] R. Laxminarayan and A. Malani in *Extending the Cure: Policy Responses to the Growing Threat of Antibiotic Resistance*, *Vol.* Resources for the Future, **2007**.

[6] L. A. Mitscher, *J. Nat. Prod.* **2008**, *71*, 497-509.

[7] D. King and N. Strynadka, *Protein Science* **2011**, *20*, 1484-1491.

[8] K. K. Karthikeyan, A. T. Mark, R. W. Timothy, B. Jay, B. Fafhana, B. Ravikumar, C. Uma, D. Michel, G. G. Christian, I. Seema, K. Padma, V. K. Anil, M. Sunil, M. Shazad, N. Tabassum, L. P. David, P. Andrew, P. Claire, P. Rachel, R. Bhargavi, R. Ujjwayini, B. S. Jayanta, S. Madhu, S. Elizabeth, A. T. Mandayam, T. Jane, U. Supriya, W. Marina, W. William, M. L. David and W. Neil, *Lancet Infect. Dis.* **2010**, *10*, 597-602.

[9] F. Baquero and J. Blazquez, *Trends Ecol. Evol.* **1997**, *12*, 482-487.

[10] A. G. McArthur, N. Waglechner, F. Nizam, A. Yan, M. A. Azad, A. J. Baylay, K. Bhullar, M. J. Canova, G. De Pascale, L. Ejim, L. Kalan, A. M. King, K. Koteva, M. Morar, M. R. Mulvey, J. S. O'Brien, A. C. Pawlowski, L. J. V. Piddock, P. Spanogiannopoulos, A. D. Sutherland, I. Tang, P. L. Taylor, M. Thaker, W. Wang, M. Yan, T. Yu and G. D. Wright, *Antimicrob. Agents Chemother.* **2013**, *57*, 3348-3357.

[11] L. Zhang, D. Kinkelaar, Y. Huang, Y. Li, X. Li and H. H. Wang, *Appl. Environ. Microbiol.* **2011**, *77*, 7134-7141.

[12] E. Toprak, A. Veres, J.-B. Michel, R. Chait, D. L. Hartl and R. Kishony, *Nat Genet* **2012**, *44*, 101-105.

[13] G. De Pascale and G. D. Wright, *ChemBioChem* **2010**, *11*, 1325-1334.

[14] S. B. Levy and B. Marshall, *Nat. Med.* **2004**, *10*, S122-S129.

[15] J. F. Fisher, S. O. Meroueh and S. Mobashery, *Chem. Rev.* **2005**, *105*, 395-424.

[16] R. E. W. Hancock, *Trends Microbiol.* **1997**, *5*, 37-42.

[17] C. de la Fuente-Núñez, F. Reffuveille, L. Fernández and R. E. W. Hancock, *Curr. Opin. Microbiol.* **2013**, *16*, 580-589.

[18] T.-F. C. Mah and G. A. O'Toole, *Trends Microbiol.* **2001**, *9*, 34-39.

[19] A. Kumar and H. P. Schweizer, *Advanced Drug Delivery Reviews* **2005**, *57*, 1486-1513.

[20] D. N. Wilson, *Nature Reviews Microbiology* **2014**, *12*, 35-48.

[21] I. Chopra and M. Roberts, *Microbiol. Mol. Biol. Rev.* **2001**, *65*, 232-260.

[22] K. Yokoyama, Y. Doi, K. Yamane, H. Kurokawa, N. Shibata, K. Shibayama, T. Yagi, H. Kato and Y. Arakawa, *The Lancet* **2003**, *362*, 1888-1893.

[23] M. G. Head, J. R. Fitchett, M. K. Cooke, F. B. Wurie, R. Atun, A. C. Hayward, A. Holmes, A. P. Johnson and N. Woodford, *J. Antimicrob. Chemother.* **2013**, *69*, 548-554.

[24] M. R. Barbachyn, D. K. Hutchinson, S. J. Brickner, M. H. Cynamon, J. O. Kilburn, S. P. Klemens, S. E. Glickman, K. C. Grega, S. K. Hendges, D. S. Toops, C. W. Ford and G. E. Zurenko, *J. Med. Chem.* **1996**, *39*, 680-685.

[25] S. J. Brickner, D. K. Hutchinson, M. R. Barbachyn, P. R. Manninen, D. A. Ulanowicz, S. A. Garmon, K. C. Grega, S. K. Hendges, D. S. Toops, C. W. Ford and G. E. Zurenko, *J. Med. Chem.* **1996**, *39*, 673-679.

[26] J. R. Colca, W. G. McDonald, D. J. Waldon, L. M. Thomasco, R. C. Gadwood, E. T. Lund, G. S. Cavey, W. R. Mathews, L. D. Adams, E. T. Cecil, J. D. Pearson, J. H. Bock, J. E. Mott, D. L. Shinabarger, L. Q. Xiong and A. S. Mankin, *J. Biol. Chem.* **2003**, *278*, 21972-21979.

[27] F. P. Tally and M. F. DeBruin, *J. Antimicrob. Chemother.* **2000**, *46*, 523-526.

[28] M. N. Thaker, W. Wang, P. Spanogiannopoulos, N. Waglechner, A. M. King, R. Medina and G. D. Wright, *Nat Biotech* **2013**, *31*, 922-927.

[29] M. S. Butler and M. A. Cooper, *J. Antibiot.* **2011**, *64*, 413-425.

[30] T. Shakya and G. D. Wright, *Antimicrob. Agents Chemother.* **2010**, *54*, 1909-1913.

[31] P. J. Stogios, P. Spanogiannopoulos, E. Evdokimova, O. Egorova, T. Shakya, N. Todorovic, A. Capretta, G. D. Wright and A. Savchenko, *Biochem. J.* **2013**, *454*, 191-200.

[32] G. G. Perron, S. Kryazhimskiy, D. P. Rice and A. Buckling, *Appl. Environ. Microbiol.* **2012**, *78*, 6137-6142.

[33] M. F. Gordeev, C. Hackbarth, M. R. Barbachyn, L. S. Banitt, J. R. Gage, G. W. Luehr, M. Gomez, J. Trias, S. E. Morin, G. E. Zurenko, C. N. Parker, J. M. Evans, R. J. White and D. V. Patel, *Bioorg. Med. Chem. Lett.* **2003**, *13*, 4213-4216.

[34] G. Y. Lesher, M. D. Gruett, E. J. Froelich, R. P. Brundage and J. H. Bailey, *Journal of Medicinal & Pharmaceutical Chemistry* **1962**, *5*, 1063-1065

[35] L. A. Mitscher, *Chem. Rev.* **2005**, *105*, 559-592.

[36] H. Koga, A. Itoh, S. Murayama, S. Suzue and T. Irikura, *J. Med. Chem.* **1980**, *23*, 1358-1363.

[37] S. T. Murphy, H. L. Case, E. Ellsworth, S. Hagen, M. Huband, T. Joannides, C. Limberakis, K. R. Marotti, A. M. Ottolini, M. Rauckhorst, J. Starr, M. Stier, C. Taylor, T. Zhu, A. Blaser, W. A. Denny, G. L. Lu, J. B. Smaill and F. Rivault, *Bioorg. Med. Chem. Lett.* **2007**, *17*, 2150-2155.

[38] R. Wise, J. M. Andrews and L. J. Edwards, *Antimicrob. Agents Chemother.* **1983**, *23*, 559-564.

[39] F. Van Bambeke, J. M. Michot, J. Van Eldere and P. M. Tulkens, *Clin. Microbiol. Infect.* **2005**, *11*, 256-280.

[40] D. M. Barnes, A. C. Christesen, K. M. Engstrom, A. R. Haight, M. C. Hsu, E. C. Lee, M. J. Peterson, D. J. Plata, P. S. Raje, E. J. Stoner, J. S. Tedrow and S. Wagaw, *Org. Process Res. Dev.* **2006**, *10*, 803-807.

[41] S. Lemaire, P. M. Tulkens and F. Van Bambeke, *Antimicrob. Agents Chemother.* **2011**, *55*, 649-658.

[42] K. Drlica and X. L. Zhao, *Microbiol. Mol. Biol. Rev.* **1997**, *61*, 377-392.

[43] J. Roca, *Trends Biochem.Sci.* **1995**, *20*, 156-160.

[44] L. L. Shen, L. A. Mitscher, P. N. Sharma, T. J. Odonnell, D. W. T. Chu, C. S. Cooper, T. Rosen and A. G. Pernet, *Biochemistry* **1989**, *28*, 3886-3894.

[45] I. Laponogov, M. K. Sohi, D. A. Veselkov, X.-S. Pan, R. Sawhney, A. W. Thompson, K. E. McAuley, L. M. Fisher and M. R. Sanderson, *Nat Struct Mol Biol* **2009**, *16*, 667-669.

[46] K. J. Aldred, S. A. McPherson, C. L. Turnbough, R. J. Kerns and N. Osheroff, *Nucleic Acids Res.* **2013**, *41*, 4628-4639.

[47] C. G. Noble, F. M. Barnard and A. Maxwell, *Antimicrob. Agents Chemother.* **2003**, *47*, 854-862.

[48] J. Ruiz, *J. Antimicrob. Chemother.* **2003**, *51*, 1109-1117.

[49] S. P. Cohen, L. M. McMurry, D. C. Hooper, J. S. Wolfson and S. B. Levy, *Antimicrob. Agents Chemother.* **1989**, *33*, 1318-1325.

[50] D. C. Hooper, J. S. Wolfson, K. S. Souza, E. Y. Ng, G. L. McHugh and M. N. Swartz, *Antimicrob. Agents Chemother.* **1989**, *33*, 283-290.

[51] K. Drlica and M. Malik, *Current Topics in Medicinal Chemistry* **2003**, *3*, 249-282.

[52] J. Ruiz, M. J. Pons and C. Gomes, *Int. J. Antimicrob. Agents* **2012**, *40*, 196-203.

[53] A. Fabrega, S. Madurga, E. Giralt and J. Vila, *Microb. Biotechnol.* **2009**, *2*, 40-61.

[54] E. Rimbara, N. Noguchi, T. Kawai and M. Sasatsu, *Helicobacter* **2012**, *17*, 36-42.

[55] K. Yokoyama, H. Kim, T. Mukai, M. Matsuoka, C. Nakajima and Y. Suzuki, *Antimicrob. Agents Chemother.* **2012**, *56*, 697-702.

[56] A. Robicsek, G. A. Jacoby and D. C. Hooper, *Lancet Infect. Dis.* **2006**, *6*, 629-640.

[57] M. W. Vetting, S. S. Hegde, M. Wang, G. A. Jacoby, D. C. Hooper and J. S. Blanchard, *J. Biol. Chem.* **2011**, *286*, 25265-25273.

[58] R. Martens, H. G. Wetzstein, F. Zadrazil, M. Capelari, P. Hoffmann and N. Schmeer, *Appl. Environ. Microbiol.* **1996**, *62*, 4206-4209.

[59] A. Robicsek, J. Strahilevitz, G. A. Jacoby, M. Macielag, D. Abbanat, C. H. Park, K. Bush and D. C. Hooper, *Nat. Med.* **2006**, *12*, 83-88.

[60] H. Drechsel and G. Jung, *J. Pept. Sci.* **1998**, *4*, 147-181.

[61] B. F. Matzanke, *Encyclopedia of Inorganic Chemistry* **1994**, *4*, 1915-1933.

[62] M. Miethke and M. A. Marahiel, *Microbiol. Mol. Biol. Rev.* **2007**, *71*, 413-415

[63] R. J. Abergel, A. M. Zawadzka and K. N. Raymond, *J. Am. Chem. Soc.* **2008**, *130*, 2124-2125.

[64] R. C. Hider and X. Kong, *Natural Product Reports* **2010**, *27*, 637-657.

[65] R. D. Perry, P. B. Balbo, H. A. Jones, J. D. Fetherston and E. DeMoll, *Microbiology-(UK)* **1999**, *145*, 1181-1190.

[66] S. Dhungana and A. L. Crumbliss, *Geomicrobiol. J.* **2005**, *22*, 87-98.

[67] T. Zhou, Y. M. Ma, X. L. Kong and R. C. Hider, *Dalton Trans.* **2012**, *41*, 6371-6389.

[68] K. Haselwandter, G. Häninger and M. Ganzera, *Biometals* **2011**, *24*, 153-157.

[69] J. B. Neilands, *J. Am. Chem. Soc.* **1952**, *74*, 4846-4847.

[70] O. Szabó and E. Farkas, *Inorganica Chimica Acta* **2011**, *376*, 500-508.

[71] M. J. Smith, J. N. Shoolery, B. Schwyn, I. Holden and J. B. Neilands, *J. Am. Chem. Soc.* **1985**, *107*, 1739-1743.

[72] W. Wagegg and V. Braun, *J. Bacteriol.* **1981**, *145*, 156-163.

[73] W. D. Linke, H. Diekmann and A. Crueger, *Arch Microbiol* **1972**, *85*, 44-50.

[74] K. Barbeau, G. P. Zhang, D. H. Live and A. Butler, *J. Am. Chem. Soc.* **2002**, *124*, 378-379.

[75] C. J. Carrano, H. Drechsel, D. Kaiser, G. Jung, B. Matzanke, G. Winkelmann, N. Rochel and A. M. Albrecht-Gary, *Inorg. Chem.* **1996**, *35*, 6429-6436.

[76] S. A. Amin, D. H. Green, F. C. Kupper and C. J. Carrano, *Inorg. Chem.* **2009**, *48*, 11451-11458.

[77] M. E. Cass, T. M. Garrett and K. N. Raymond, *J. Am. Chem. Soc.* **1989**, *111*, 1677-1682.

[78] S. A. Ong, T. Peterson and J. B. Neilands, *J. Biol. Chem.* **1979**, *254*, 1860-1865.

[79] T. Peterson and J. B. Nielands, *Tetrahedron Lett.* **1979**, *20*, 4805-4808.

[80] G. L. Griffiths, S. P. Sigel, S. M. Payne and J. B. Neilands, *J. Biol. Chem.* **1984**, *259*, 383-385.

[81] X. Y. Liang, D. J. Campopiano and P. J. Sadler, *Chem. Soc. Rev.* **2007**, *36*, 968-992.

[82] N. Noinaj, M. Guillier, Barnard, Travis J. and S. K. Buchanan, *Annu. Rev. Microbiol.* **2010**, *64*, 43-60.

[83] G. S. Moeck and J. W. Coulton, *Molecular Microbiology* **1998**, *28*, 675-681.

[84] A. D. Ferguson, E. Hofmann, J. W. Coulton, K. Diederichs and W. Welte, *Science* **1998**, *282*, 2215-2220.

[85] S. K. Buchanan, B. S. Smith, L. Venkatramani, D. Xia, L. Esser, M. Palnitkar, R. Chakraborty, D. van der Helm and J. Deisenhofer, *Nat. Struct. Biol.* **1999**, *6*, 56-63.

[86] W. W. Yue, S. Grizot and S. K. Buchanan, *Journal of Molecular Biology* **2003**, *332*, 353-368.

[87] C. H. Chatfield, B. J. Mulhern, D. M. Burnside and N. P. Cianciotto, *J. Bacteriol.* **2011**, *193*, 1563-1575.

[88] M. C. Clifton, C. Corrent and R. K. Strong, *Biometals* **2009**, *22*, 557-564.

[89] T. M. Hoette, R. J. Abergel, J. D. Xu, R. K. Strong and K. N. Raymond, *J. Am. Chem. Soc.* **2008**, *130*, 17584-17592.

[90] R. J. Abergel, M. K. Wilson, J. E. L. Arceneaux, T. M. Hoette, R. K. Strong, B. R. Byers and K. N. Raymond, *Proc. Natl. Acad. Sci. U. S. A.* **2006**, *103*, 18499-18503.

[91] B. Bister, D. Bischoff, G. J. Nicholson, M. Valdebenito, K. Schneider, G. Winkelmann, K. Hantke and R. D. Sussmuth, *Biometals* **2004**, *17*, 471-481.

[92] R. J. Abergel, E. G. Moore, R. K. Strong and K. N. Raymond, *J. Am. Chem. Soc.* **2006**, *128*, 10998-10999.

[93] S. Coyne, P. Courvalin and B. Perichon, *Antimicrob. Agents Chemother.* **2011**, *55*, 947-953.

[94] A. Speciale, R. Musumeci, G. Blandino, F. Caccamo, V. Siracusa and M. Renis, *Int. J. Antimicrob. Agents* **2000**, *14*, 151-156.

[95] G. Benz, T. Schroder, J. Kurz, C. Wunsche, W. Karl, G. Steffens, J. Pfitzner and D. Schmidt, *Angew. Chem.-Int. Edit. Engl.* **1982**, *21*, 527-528.

[96] W. Sackmann, P. Reusser, L. Neipp, F. Kradolfer and F. Gross, *Antibiot. Chemother.* **1962**, *12*, 34-45.

[97] L. Vertesy, W. Aretz, H. W. Fehlhaber and H. Kogler, *Helv. Chim. Acta* **1995**, *78*, 46-60.

[98] H. Bickel, P. Mertens, V. Prelog, J. Seibl and A. Walser, *Tetrahedron* **1966**, *22, Supplement 8*, 171-179.

[99] B. Kunze, W. Trowitzschkienast, G. Hofle and H. Reichenbach, *J. Antibiot.* **1992**, *45*, 147-150.

[100] B. Kunze, N. Bedorf, W. Kohl, G. Hofle and H. Reichenbach, *J. Antibiot.* **1989**, *42*, 14-17.

[101] E. M. Nolan and C. T. Walsh, *Biochemistry* **2008**, *47*, 9289-9299.

[102] R. Grinter, J. Milner and D. Walker, *FEMS Microbiol. Lett.* **2013**, *338*, 1-9.

[103] C. Ji, R. E. Juarez-Hernandez and M. J. Miller, *Future Med. Chem.* **2012**, *4*, 297-313.

[104] M. G. P. Page, *Ann. N.Y. Acad. Sci.* **2013**, *1277*, 115-126.

[105] H. Zahner, H. Diddens, W. Keller-Schierlein and H. U. Nageli, *Jpn J Antibiot* **1977**, *30 Suppl*, 201-206.

[106] N. A. Watanabe, T. Nagasu, K. Katsu and K. Kitoh, *Antimicrob. Agents Chemother.* **1987**, *31*, 497-504.

[107] M. Ghosh and M. J. Miller, *Bioorg. Med. Chem.* **1996**, *4*, 43-48.

[108] R. Schobert, A. Stangl and K. Hannemann, *Tetrahedron* **2006**, *62*, 7799-7808.

[109] S. Wittmann, M. Schnabelrauch, I. Scherlitz-Hofmann, U. Möllmann, D. Ankel-Fuchs and L. Heinisch, *Bioorg. Med. Chem.* **2002**, *10*, 1659-1670.

[110] L. Heinisch, S. Wittmann, T. Stoiber, A. Berg, D. Ankel-Fuchs and U. Möllmann, *J. Med. Chem.* **2002**, *45*, 3032-3040.

[111] U. Möllmann, L. Heinisch, A. Bauernfeind, T. Kohler and D. Ankel-Fuchs, *Biometals* **2009**, *22*, 615-624.

[112] C. Ji and M. J. Miller, *Bioorg. Med. Chem.* **2012**, *20*, 3828-3836.

[113] M. Ghosh, L. J. Lambert, P. W. Huber and M. J. Miller, *Bioorg. Med. Chem. Lett.* **1995**, *5*, 2337-2340.

[114] F. Rivault, C. Liebert, A. Burger, F. Hoegy, M. A. Abdallah, I. J. Schalk and G. L. A. Mislin, *Bioorg. Med. Chem. Lett.* **2007**, *17*, 640-644.

[115] T. A. Wencewicz, U. Möllmann, T. E. Long and M. J. Miller, *Biometals* **2009**, *22*, 633-648.

[116] S. Noël, V. Gasser, B. Pesset, F. Hoegy, D. Rognan, I. J. Schalk and G. L. A. Mislin, *Org. Biomol. Chem.* **2011**, *9*, 8288-8300.

[117] S. R. Md-Saleh, E. C. Chilvers, K. G. Kerr, S. J. Milner, A. M. Snelling, J. P. Weber, G. H. Thomas, A. K. Duhme-Klair and A. Routledge, *Bioorg. Med. Chem. Lett.* **2009**, *19*, 1496-1498.

[118] S. J. Milner, A. Seve, A. M. Snelling, G. H. Thomas, K. G. Kerr, A. Routledge and A. K. Duhme-Klair, *Org. Biomol. Chem.* **2013**, *11*, 3461-3468.

[119] M. J. Miller, A. J. Walz, H. Zhu, C. R. Wu, G. Moraski, U. Möllmann, E. M. Tristani, A. L. Crumbliss, M. T. Ferdig, L. Checkley, R. L. Edwards and H. I. Boshoff, *J. Am. Chem. Soc.* **2011**, *133*, 2076-2079.

[120] M. G. P. Page, C. Dantier and E. Desarbre, *Antimicrob. Agents Chemother.* **2010**, *54*, 2291-2302.

[121] K. Barbeau, E. L. Rue, K. W. Bruland and A. Butler, *Nature* **2001**, *413*, 409-413.

[122] R. J. Bergeron, G. F. Huang, R. E. Smith, N. Bharti, J. S. McManis and A. Butler, *Tetrahedron* **2003**, *59*, 2007-2014.

[123] A. T. Koppisch, C. C. Browder, A. L. Moe, J. T. Shelley, B. A. Kinke, L. E. Hersman, S. Iyer and C. E. Ruggiero, *Biometals* **2005**, *18*, 577-585.

[124] B. L. Garner, J. E. L. Arceneaux and B. R. Byers, *Curr. Microbiol.* **2004**, *49*, 89-94.

[125] M. K. Wilson, R. J. Abergel, K. N. Raymond, J. E. L. Arceneaux and B. R. Byers, *Biochem. Biophys. Res. Commun.* **2006**, *348*, 320-325.

[126] M. K. Wilson, R. J. Abergel, J. E. L. Arceneaux, K. N. Raymond and B. R. Byers, *Biometals* **2010**, *23*, 129-134.

[127] J. Y. Lee, K. D. Passalacqua, P. C. Hanna and D. H. Sherman, *PLoS One* **2011**, *6*, 1-11.

[128] G. P. Zhang, S. A. Amin, F. C. Kupper, P. D. Holt, C. J. Carrano and A. Butler, *Inorg. Chem.* **2009**, *48*, 11466-11473.

[129] W. R. Harris, C. J. Carrano, S. R. Cooper, S. R. Sofen, A. E. Avdeef, J. V. McArdle and K. N. Raymond, *J. Am. Chem. Soc.* **1979**, *101*, 6097-6104.

[130] S. Cendrowski, W. MacArthur and P. Hanna, *Molecular Microbiology* **2004**, *51*, 407-417.

[131] D. Oves-Costales, N. Kadi, M. J. Fogg, L. Song, K. S. Wilson and G. L. Challis, *J. Am. Chem. Soc.* **2007**, *129*, 8416-8417.

[132] D. Oves-Costales, N. Kadi, M. J. Fogg, L. J. Song, K. S. Wilson and G. L. Challis, *Chem. Commun.* **2008**, 4034-4036.

[133] A. T. Koppisch, K. Hotta, D. T. Fox, C. E. Ruggiero, C. Y. Kim, T. Sanchez, S. Iyer, C. C. Browder, P. J. Unkefer and C. J. Unkefer, *J. Org. Chem.* **2008**, *73*, 5759-5765.

[134] D. T. Fox, K. Hotta, C. Y. Kim and A. T. Koppisch, *Biochemistry* **2008**, *47*, 12251-12253.

[135] B. F. Pfleger, Y. C. Kim, T. D. Nusca, N. Maltseva, J. Y. Lee, C. M. Rath, J. B. Scaglione, B. K. Janes, E. C. Anderson, N. H. Bergman, P. C. Hanna, A. Joachimiak and D. H. Sherman, *Proc. Natl. Acad. Sci. U. S. A.* **2008**, *105*, 17133-17138.

[136] R. K. Pandey, G. G. Jarvis and P. S. Low, *Tetrahedron Lett.* **2012**, *53*, 1627-1629.

[137] R. A. Gardner, R. Kinkade, C. J. Wang and O. Phanstiel, *J. Org. Chem.* **2007**, *72*, 3158-3158.

[138] W. H. Rastetter, T. J. Erickson and M. C. Venuti, *J. Org. Chem.* **1981**, *46*, 3579-3590.

[139] M. J. Milewska, A. Chimiak and Z. Glowacki, *Journal Fur Praktische Chemie* **1987**, *329*, 447-456.

[140] A. Ghosh and M. J. Miller, *J. Org. Chem.* **1993**, *58*, 7652-7659.

[141] S. D. Dixon, B. K. Janes, A. Bourgis, P. E. Carlson Jr and P. C. Hanna, *Molecular Microbiology* **2012**, *84*, 370-382.

[142] A. M. Zawadzka, R. J. Abergel, R. Nichiporuk, U. N. Andersen and K. N. Raymond, *Biochemistry* **2009**, *48*, 3645-3657.

[143] A. M. Zawadzka, Y. Kim, N. Maltseva, R. Nichiporuk, Y. Fan, A. Joachimiak and K. N. Raymond, *Proc. Natl. Acad. Sci. U. S. A.* **2009**, *106*, 21854-21859.

[144] N. Bugdahn, F. Peuckert, A. G. Albrecht, M. Miethke, M. A. Marahiel and M. Oberthür, *Angew. Chem.-Int. Edit.* **2010**, *49*, 10210-10213.

[145] J. Y. Lee, B. K. Janes, K. D. Passalacqua, B. F. Pfleger, N. H. Bergman, H. C. Liu, K. Hakansson, R. V. Somu, C. C. Aldrich, S. Cendrowski, P. C. Hanna and D. H. Sherman, *J. Bacteriol.* **2007**, *189*, 1698-1710.

[146] B. F. Pfleger, J. Y. Lee, R. V. Somu, C. C. Aldrich, P. C. Hanna and D. H. Sherman, *Biochemistry* **2007**, *46*, 4147-4157.

[147] P. E. Carlson, S. D. Dixon, B. K. Janes, K. A. Carr, T. D. Nusca, E. C. Anderson, S. E. Keene, D. H. Sherman and P. C. Hanna, *Molecular Microbiology* **2010**, *75*, 900-909.

[148] S. R. Md-Saleh in *Siderophore-drug conjugates as novel antibacterial agents*, *Vol. MPhil* University of York, York, **2009**.

[149] K. Hirota, H. Kitagawa, M. Shimamura and S. Ohmori, *Chem. Lett.* **1980**, 191-194.

[150] H. Y. Guo, S. A. Naser, G. Ghobrial and O. Phanstiel, *J. Med. Chem.* **2002**, *45*, 2056-2063.

[151] S. J. Milner in *Siderophore-drug Conjugates as Novel Antimicrobial Agents*, *Vol. PhD* University of York, York, **2011**, p. 380.

[152] P. R. Deacon, M. F. Mahon, K. C. Molloy and P. C. Waterfield, *J. Chem. Soc.-Dalton Trans.* **1997**, 3705-3712.

[153] A. Chimiak and J. B. Neilands, *Struct. Bond.* **1984**, *58*, 89-96.

[154] B. Loev and C. R. Dawson, *Journal of the American Chemical Society* **1956**, *78*, 6095-6098.

[155] S. M. Cohen and K. N. Raymond, *Inorg. Chem.* **2000**, *39*, 3624-3631.

[156] R. J. Abergel, J. A. Warner, D. K. Shuh and K. N. Raymond, *J. Am. Chem. Soc.* **2006**, *128*, 8920-8931.

[157] J. Guy, K. Caron, S. Dufresne, S. W. Michnick, W. G. Skene and J. W. Keillor, *J. Am. Chem. Soc.* **2007**, *129*, 11969-11977.

[158] W. S. Saari, J. E. Schwering, P. A. Lyle, S. J. Smith and E. L. Engelhardt, *J. Med. Chem.* **1990**, *33*, 97-101.

[159] G. Han, M. Tamaki and V. Hruby, *J. Pept. Res.* **2001**, *58*, 338-341.

[160] B. Li, M. Berliner, R. Buzon, C. K. F. Chiu, S. T. Colgan, T. Kaneko, N. Keene, W. Kissel, T. Le, K. R. Leeman, B. Marquez, R. Morris, L. Newell, S. Wunderwald, M. Witt, J. Weaver, Z. J. Zhang and Z. L. Zhang, *J. Org. Chem.* **2006**, *71*, 9045-9050.

[161] A. K. Duhme, R. C. Hider and H. H. Khodr, *Chem. Ber.-Recl.* **1997**, *130*, 969-973.

[162] A. Lüttringhaus and H. W. Dirksen, *Angew. Chem.-Int. Edit. Engl.* **1964**, *3*, 260-269.

[163] N. A. M. Daud in *Novel developments for increased efficacy and longevity of existing clinically approved antibiotics Vol. MSc in Chemistry* York, York, **2012**.

[164] V. Theodorou, K. Skobridis, A. G. Tzakos and V. Ragoussis, *Tetrahedron Lett.* **2007**, *48*, 8230-8233.

[165] J. J. Gerschler, K. A. Wier and D. E. Hansen, *J. Org. Chem.* **2006**, *72*, 654-657.

[166] Q. X. H. Wang and O. Phanstiel, *J. Org. Chem.* **1998**, *63*, 1491-1495.

[167] J. M. Roosenberg and M. J. Miller, *J. Org. Chem.* **2000**, *65*, 4833-4838.

[168] R. J. Bergeron, M. G. Xin, R. E. Smith, M. Wollenweber, J. S. McManis, C. Ludin and K. A. Abboud, *Tetrahedron* **1997**, *53*, 427-434.

[169] M. J. Smith, *Tetrahedron Lett.* **1989**, *30*, 313-316.

[170] A. Dömling, W. Wang and K. Wang, *Chem. Rev.* **2012**, *112*, 3083-3135.

[171] A. Strecker, *Justus Leibigs Ann. Chem.* **1850**, *75*, 27-45.

[172] A. Dömling and I. Ugi, *Angew. Chem.-Int. Edit.* **2000**, *39*, 3169-3210.

[173] I. Ugi, *Angew. Chem.-Int. Edit.* **1959**, *71*, 386-386.

[174] G. A. Medeiros, W. A. da Silva, G. A. Bataglion, D. A. C. Ferreira, H. C. B. de Oliveira, M. N. Eberlin and B. A. D. Neto, *Chem. Commun.* **2014**, *50*, 338-340.

[175] S. Marcaccini and T. Torroba, *Nat. Protoc.* **2007**, *2*, 632-639.

[176] A. M. L. Hoel and J. Nielsen, *Tetrahedron Lett.* **1999**, *40*, 3941-3944.

[177] S. Kłossowski, B. Wiraszka, S. Berłożecki and R. Ostaszewski, *Org. Lett.* **2013**, *15*, 566-569.

[178] T. A. Keating and R. W. Armstrong, *J. Am. Chem. Soc.* **1995**, *117*, 7842-7843.

[179] A. Znabet, S. Blanken, E. Janssen, F. J. J. de Kanter, M. Helliwell, N. J. Turner, E. Ruijter and R. V. A. Orru, *Org. Biomol. Chem.* **2012**, *10*, 941-944.

[180] M. Sañudo, M. García-Valverde, S. Marcaccini and T. Torroba, *Tetrahedron* **2012**, *68*, 2621-2629.

[181] V. Kumar, M. P. Kaushik and A. Mazumdar, *Eur. J. Org. Chem.* **2008**, 1910-1916.

[182] J. C. Barrow, S. R. Stauffer, K. E. Rittle, P. L. Ngo, Z. Q. Yang, H. G. Selnick, S. L. Graham, S. Munshi, G. B. McGaughey, M. K. Holloway, A. J. Simon, E. A. Price, S. Sankaranarayanan, D. Colussi, K. Tugusheva, M. T. Lai, A. S. Espeseth, M. Xu, Q. Huang, A. Wolfe, B. Pietrak, P. Zuck, D. A. Levorse, D. Hazuda and J. P. Vacca, *J. Med. Chem.* **2008**, *51*, 6259-6262.

[183] G. Lesma, R. Cecchi, S. Crippa, P. Giovanelli, F. Meneghetti, M. Musolino, A. Sacchetti and A. Silvani, *Org. Biomol. Chem.* **2012**, *10*, 9004-9012.

[184] N. Narendra, T. M. Vishwanatha, G. Nagendra and V. V. Sureshbabu, *Tetrahedron* **2012**, *68*, 1992-2000.

[185] T. M. Vishwanatha, N. Narendra and V. V. Sureshbabu, *Tetrahedron Lett.* **2011**, *52*, 5620-5624.

[186] T.-F. Niu, C. Cai and L. Yi, *Helv. Chim. Acta* **2012**, *95*, 87-99.

[187] V. Y. Stolyarenko, A. A. Evdokimov and V. I. Shishkin, *Mendeleev Commun.* **2013**, *23*, 108-109.

[188] L. R. Odell, M. T. Nilsson, J. Gising, O. Lagerlund, D. Muthas, A. Nordqvist, A. Karlen and M. Larhed, *Bioorg. Med. Chem. Lett.* **2009**, *19*, 4790-4793.

[189] A. G. Zhdanko, A. V. Gulevich and V. G. Nenajdenko, *Tetrahedron* **2009**, *65*, 4692-4702.

[190] X. S. Fan, X. Y. Zhang, C. Bories, P. M. Loiseau and P. F. Torrence, *Bioorg. Chem.* **2007**, *35*, 121-136.

[191] C. C. Musonda, D. Taylor, J. Lehman, J. Gut, P. J. Rosenthal and K. Chibale, *Bioorg. Med. Chem. Lett.* **2004**, *14*, 3901-3905.

[192] A. V. Ivachtchenko, Y. A. Ivanenkov, V. M. Kysil, M. Y. Krasavin and A. P. Ilyin, *Russ. Chem. Rev.* **2010**, *79*, 787-817.

[193] A. d. F. S. Barreto, O. E. Vercillo, M. A. Birkett, J. C. Caulfield, L. A. Wessjohann and C. K. Z. Andrade, *Org. Biomol. Chem.* **2011**.

[194] A. d. F. S. Barreto, O. E. Vercillo and C. K. Z. Andrade, *J. Braz. Chem. Soc.* **2011**, *22*, 462-467.

[195] S. Santra and P. R. Andreana, *Org. Lett.* **2007**, *9*, 5035-5038.

[196] A. K. Duhme, R. C. Hider, M. J. Naldrett and R. N. Pau, *J. Biol. Inorg. Chem.* **1998**, *3*, 520-526.

[197] M. Albrecht and R. Fröhlich, *J. Am. Chem. Soc.* **1997**, *119*, 1656-1661.

[198] J. R. Pollack and J. B. Neilands, *Biochem. Biophys. Res. Commun.* **1970**, *38*, 989-992.

[199] A. Thieken and G. Winkelmann, *FEMS Microbiol. Lett.* **1992**, *94*, 37-42.

[200] H. Budzikiewicz, *Mini-Rev. Org. Chem.* **2005**, *2*, 119-124.

[201] L. Gros, S. O. Lorente, Jimenez, V. Yardley, L. Rattray, H. Wharton, S. Little, S. L. Croft, L. M. Ruiz-Perez, D. Gonzalez-Pacanowska and I. H. Gilbert, *J. Med. Chem.* **2006**, *49*, 6094-6103.

[202] M. Albrecht, J. A. Ingo and R. Fröhlich, *Chem. Commun.* **2005**, 157-165.

[203] A. K. Duhme, Z. Dauter, R. C. Hider and S. Pohl, *Inorg. Chem.* **1996**, *35*, 3059-3061.

[204] J. M. Lehn, A. Rigault, J. Siegel, J. Harrowfield, B. Chevrier and D. Moras, *Proc. Natl. Acad. Sci. U. S. A.* **1987**, *84*, 2565-2569.

[205] R. Kramer, J. M. Lehn, A. Decian and J. Fischer, *Angew. Chem.-Int. Edit. Engl.* **1993**, *32*, 703-706.

[206] F. L. Weitl and K. N. Raymond, *J. Am. Chem. Soc.* **1980**, *102*, 2289-2293.

[207] T. M. Dewey, J. Du Bois and K. N. Raymond, *Inorg. Chem.* **1993**, *32*, 1729-1738.

[208] A. K. Duhme, *J. Chem. Soc.-Dalton Trans.* **1997**, 773-778.

[209] E. J. Enemark and T. D. P. Stack, *Angew. Chem.-Int. Edit. Engl.* **1995**, *34*, 996-998.

[210] E. J. Enemark and T. D. P. Stack, *Inorg. Chem.* **1996**, *35*, 2719-2720.

[211] B. Kersting, M. Meyer, R. E. Powers and K. N. Raymond, *J. Am. Chem. Soc.* **1996**, *118*, 7221-7222.

[212] M. Meyer, B. Kersting, R. E. Powers and K. N. Raymond, *Inorg. Chem.* **1997**, *36*, 5179-5191.

[213] D. L. Caulder and K. N. Raymond, *Angew. Chem.-Int. Edit. Engl.* **1997**, *36*, 1440-1442.

[214] M. Albrecht, I. Janser, S. Kamptmann, P. Weis, B. Wibbeling and R. Fröhlich, *Dalton Trans.* **2004**, 37-43.

[215] M. Albrecht, I. Janser, A. Lutzen, M. Hapke, R. Frohlich and P. Weis, *Chem.-Eur. J.* **2005**, *11*, 5742-5748.

[216] I. Janser, M. Albrecht, K. Hunger, S. Burk and K. Rissanen, *Eur. J. Inorg. Chem.* **2006**, 244-251.

[217] T. B. Karpishin, T. D. P. Stack and K. N. Raymond, *J. Am. Chem. Soc.* **1993**, *115*, 6115-6125.

[218] Y. Y. Xie, M. S. Liu, P. P. Hu, X. L. Kong, D. H. Qiu, J. L. Xu, R. C. Hider and T. Zhou, *Medicinal Chemistry Research* **2013**, *22*, 2351-2359.

[219] D. H. Qiu, Z. L. Huang, T. Zhou, C. Shen and R. C. Hider, *FEMS Microbiol. Lett.* **2011**, *314*, 107-111.

[220] K. J. Winstanley and D. K. Smith, *J. Org. Chem.* **2007**, *72*, 2803-2815.

[221] Y. Kaneko, M. Thoendel, O. Olakanmi, B. E. Britigan and P. K. Singh, *J. Clin. Invest.* **2007**, *117*, 877-888.

[222] Genta Incorporated Inc in *Genta Presents Initial Clinical Data on Use of Gallium Compounds as Treatment for Serious Infections*, *Vol.* **2010**.

[223] L. C. S. Antunes, F. Imperi, F. Minandri and P. Visca, *Antimicrob. Agents Chemother.* **2012**, *56*, 5961-5970.

[224] E. Banin, A. Lozinski, K. M. Brady, E. Berenshtein, P. W. Butterfield, M. Moshe, M. Chevion and E. P. Greenberg, *Proc. Natl. Acad. Sci. U. S. A.* **2008**, *105*, 16761-16766.

[225] E. Bingham, B. Cohrssen and C. H. Powell, *Patty's toxicology*, 5th edition, John Wiley & Sons. New York, N.Y., **2001**, p. 174.

[226] A. B. Kelson, M. Carnevali and V. Truong-Le, *Current Opinion in Pharmacology* **2013**, *13*, 707-716.

[227] J. Liu, K. Duncan and C. T. Walsh, *J. Bacteriol.* **1989**, *171*, 791-798.

[228] J. A. Sundlov, J. A. Garringer, J. M. Carney, A. S. Reger, E. J. Drake, W. L. Duax and A. M. Gulick, *Acta Crystallogr. Sect. D-Biol. Crystallogr.* **2006**, *62*, 734-740.

[229] L. D. Loomis and K. N. Raymond, *Inorg. Chem.* **1991**, *30*, 906-911.

[230] W. R. Harris, C. J. Carrano and K. N. Raymond, *J. Am. Chem. Soc.* **1979**, *101*, 2213-2214.

[231] D. J. Raines, O. V. Moroz, K. S. Wilson and A. K. Duhme-Klair, *Angew. Chem.-Int. Edit.* **2013**, *52*, 4595-4598.

[232] N. Tsierkezos, *J. Solution Chem.* **2007**, *36*, 289-302.

[233] S. J. Milner, C. T. Carrick, K. G. Kerr, A. M. Snelling, G. H. Thomas, A.-K. Duhme-Klair and A. Routledge, *ChemBioChem* **2014**, *15*, 466-471.

[234] W. Kramer, *Biol. Chem.* **2011**, *392*, 77-94.

[235] M. Gynther, J. Ropponen, K. Laine, J. Leppanen, P. Haapakoski, L. Peura, T. Jarvinen and J. Rautio, *J. Med. Chem.* **2009**, *52*, 3348-3353.

[236] D. Foley, P. Bailey, M. Pieri and D. Meredith, *Org. Biomol. Chem.* **2009**, *7*, 1064-1067.

[237] A. Dalpiaz, B. Pavan, M. Scaglianti, F. Vitali, F. Bortolotti, C. Biondi, A. Scatturin and S. Manfredini, *Int. J. Pharm.* **2005**, *291*, 171-181.

[238] M. E. Ganapathy, M. Brandsch, P. D. Prasad, V. Ganapathy and F. H. Leibach, *J. Biol. Chem.* **1995**, *270*, 25672-25677.

[239] S. S. Dills, A. Apperson, M. R. Schmidt and M. H. Saier, *Microbiol. Rev.* **1980**, *44*, 385-418.

[240] P. W. Postma, J. W. Lengeler and G. R. Jacobson, *Microbiol. Rev.* **1993**, *57*, 543-594.

[241] M. L. Cai, D. C. Williams, G. S. Wang, B. R. Lee, A. Peterkofsky and G. M. Clore, *J. Biol. Chem.* **2003**, *278*, 25191-25206.

[242] A. J. S. Macpherson, M. C. Jones-Mortimer, P. Horne and P. J. F. Henderson, *J. Biol. Chem.* **1983**, *258*, 4390-4396.

[243] A. R. Walmsley, M. P. Barrett, F. Bringaud and G. W. Gould, *Trends Biochem.Sci.* **1998**, *23*, 476-481.

[244] H. J. Zheng, J. Taraska, A. J. Merz and T. Gonen, *Journal of Molecular Biology* **2010**, *396*, 593-601.

[245] X. H. Wu and H. H. Freeze, *Genomics* **2002**, *80*, 553-557.

[246] S. Harayama, J. Bollinger, T. Iino and G. L. Hazelbauer, *J. Bacteriol.* **1983**, *153*, 408-415.

[247] R. S. P. Horler, A. Müller, D. C. Williamson, J. R. Potts, K. S. Wilson and G. H. Thomas, *J. Biol. Chem.* **2009**, *284*, 31156-31163.

[248] M. E. Jung, E. C. Yang, B. T. Vu, M. Kiankarimi, E. Spyrou and J. Kaunitz, *J. Med. Chem.* **1999**, *42*, 3899-3909.

[249] P. J. F. Henderson, *J. Bioenerg. Biomembr.* **1990**, *22*, 525-569.

[250] V. Zsoldos-Mady, P. Sohar, J. Kovacs, I. Pinter and Z. Szakacs, *J. Carbohydr. Chem.* **2005**, *24*, 19-39.

[251] S. El Qaidi, F. Allemand, J. Oberto and J. Plumbridge, *Molecular Microbiology* **2009**, *71*, 146-157.

[252] S. Semsey, S. Krishna, K. Sneppen and S. Adhya, *Molecular Microbiology* **2007**, *65*, 465-476.

[253] G. A. Jacoby, *Clin. Infect. Dis.* **2005**, *41*, S120-S126.

[254] P. E. Klebba and S. M. C. Newton, *Curr. Opin. Microbiol.* **1998**, *1*, 238-247.

[255] F. Fernandes, P. Neves, P. Gameiro, L. M. S. Loura and M. Prieto, *Biochim. Biophys. Acta-Biomembr.* **2007**, *1768*, 2822-2830.

[256] L. J. V. Piddock, *J. Antimicrob. Chemother.* **1991**, *27*, 399-403.

[257] A. Basle, G. Rummel, P. Storici, J. P. Rosenbusch and T. Schirmer, *Journal of Molecular Biology* **2006**, *362*, 933-942.

[258] K. Hirai, H. Aoyama, T. Irikura, S. Iyobe and S. Mitsuhashi, *Antimicrob. Agents Chemother.* **1986**, *29*, 535-538.

[259] J.-H. Choi and D. U. Lee, *Bull. Korean Chem. Soc.* **2008**, *29*, 2051-2053.

[260] M. Miyazawa, T. Yamada and H. Utsunomiya, *Natural Product Research* **2003**, *17*, 319-323.

[261] S. R. Md-Saleh, E. C. Chilvers, K. G. Kerr, S. J. Milner, A. M. Snelling, J. P. Weber, G. H. Thomas, A.-K. Duhme-Klair and A. Routledge, *Bioorganic and Medicinal Chemistry Letters* **2009**, *19*, 1496-1498.

[262] P. Y. Ding, C. E. Schous and M. J. Miller, *Tetrahedron Lett.* **2008**, *49*, 2306-2310.

[263] T. Baba, T. Ara, M. Hasegawa, Y. Takai, Y. Okumura, M. Baba, K. A. Datsenko, M. Tomita, B. L. Wanner and H. Mori, *Mol. Syst. Biol.* **2006**, *2*, 1-11.

[264] F. C. Neidhardt, P. L. Bloch and D. F. Smith, *J. Bacteriol.* **1974**, *119*, 736-747.